

ZESZYTY NAUKOWE  
POLITECHNIKI RZESZOWSKIEJ

---

FOLIA SCIENTIARUM  
UNIVERSITATIS TECHNICAЕ RESOVIENSIS

---

NR 264

**BUDOWNICTWO  
I INŻYNIERIA ŚRODOWISKA**

Z. 52

Wydano za zgodą Rektora

Redaktor naczelny  
Wydawnictw Politechniki Rzeszowskiej  
Prof. dr hab. inż. Feliks STACHOWICZ

Komitet Redakcyjny

Ludomir LAUDAŃSKI  
Andrzej KOLEK  
Roman PETRUS  
Grzegorz PROKOPSKI  
Jan STANKIEWICZ  
Andrzej TOMCZYK

Redaktor serii

Grzegorz PROKOPSKI

Redaktor naukowy

Aleksander KOZŁOWSKI  
Leonard ZIEMIAŃSKI

Opiniodawcy

Magdaléna BÁLINTOVÁ, Zinoviy BLIKHARSKIJ, Bohdan DEMCHYNA, Pavol JUHÁS,  
Galyna KALDA, Aleksander KOZŁOWSKI, Stanisław KUŚ, Vincent KVOCÁK,  
Lech LICHOLAŁAI, Witold NIEMIEC, Vyacheslav PISARIEV, Grzegorz PROKOPSKI,  
Janusz RAK, Adam REICHHART, Myrosław SANYTSKY, Ingrid ŠENITKOVÁ,  
Nadezda STEVULOVA, Janusz TOMASZEK, Zuzana VRANAYOVÁ,  
Zenon WASZCZYSZYN, Szczepan WOLIŃSKI, Orest Voznyak, Leonard ZIEMIAŃSKI

Redaktor

Zdzisław PISAREK

ISBN

Oficyna Wydawnicza Politechniki Rzeszowskiej  
ul. W. Pola 2, 35-959 Rzeszów

# TABLE OF CONTENTS

Jacek ABRAMCZYK A mathematical model of free deformed corrugated flat sheet of rectilinear shell .....	5
Pavol BEKE, Vincent KVOČAK The effect of cross-section stiffness ratios on the resistance of joints composed of rectangular and circular hollow sections.....	17
Lidia BUDA-OŽÓG Changes of the resonant vibration frequencies for different concrete beams .....	25
Jakub DOLEJŠ, Ivan TUNEGA, Vaclav HATLMAN Experiments with high performance steel and composite members.....	33
Miron GOGOL Shaping of effective steel structures .....	43
Jiří JIRÁK, Jiří STUDNIČKA Research on steel bridges durability in Czech Republic.....	57
Pavol JUHÁS, Zuzana KOKORUĐOVÁ Effective using of higher strength structural steels in compression members .....	63
Ján KANÓCZ, Viktória BAJZECEROVÁ Investigation of timber - concrete composite beams under long term loading .....	71
Dušan KATUNSKÝ Structural Physical Problems Research of Industrial Production Hall Buildings .....	79
Yevhen KHARCHENKO, Taras PIDHAYNYI Mathematical modelling of transverse and torsion vibrations of compound metalwares.....	87
Rafał KLICH, Andrzej WOJNAR, Aleksander KOZŁOWSKI Initial stiffness of bolted joints used in steel thin walled structures .....	93
Stanisław KUŚ Development of funicular structures from plane to space .....	101
Andrzej J. MACHOWSKI, Izabela A. TYLEK Joint effect of steel frame equivalent geometrical imperfections.....	115
Mariusz MAŚLAK Moment redistribution in steel continuous beam according to limited plasticity concept .....	125
Karel MIKES, Ondrej JIRKA Semi – rigid joints of timber structures.....	135

Ivan D. PELESHKO, Vitalina V. YURCHENKO, Nikita A. BELIAEV Computer – aided design and optimization of steel structural systems .....	145
Zdzisław PISAREK Resistance and stiffness of the beam to column joints with angle flange cleats .....	155
Adam REICHHART Analysis of profiled sheet shells as a system of folds.....	165
Dmitrijs SERDJUKS, Karlins ROCENS, Rajmondas OZOLINSH Evaluation of cladding element`s prestressing for saddle – shaped cable roof.....	175
Slávka ŠIMKOVÁ Reinforced concrete members under the influence of elevated temperatures.....	185
Krystyna WRÓBEL, Wiesław KUBISZYN Influence of change in use conditions on an industrial building safety .....	193

Jacek ABRAMCZYK<sup>1</sup>

## A MATHEMATICAL MODEL OF FREE DEFORMED CORRUGATED FLAT SHEET OF RECTILINEAR SHELL

### ABSTRACT

The paper presents a mathematical model of a flat trapezoidal steel sheet deformed in a planned way during assembly work, to the directrices of the building shell. This model has been based on the results of the experimental tests concerning free deformations of flat sheets. The examined flat sheets were undergoing planned free bend or free twist deformations. The shells shaped with the help of a new method using this mathematical model are characterized by relatively free forms and relatively little effort resulting from free deformations of their sheets at their assembly. This method is more accurate than the methods used so far.

### 1. INTRODUCTION

The one-direction forming of a flat trapezoidal sheet leads to a wide range of its crosswise bending and twisting (Fig. 1) [1]. During shell assembly this sheet is fastened to the shell directrices and changes its shape from flat to a spatial one, thus undergoing its deformation (Fig. 2).



Fig. 1. Two free twisted sheets supported rectilinearly

Fig.2. Building shell made up of the flat sheets deformed in the planned way [2]

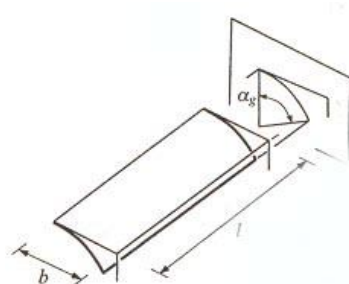


Fig. 3.a. Free bend deformation

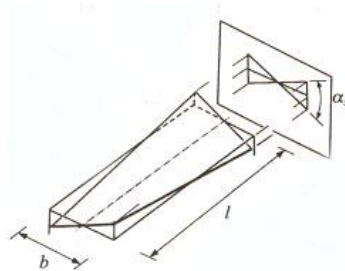


Fig. 3.b. Free twist deformation

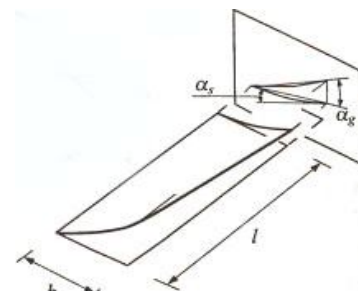


Fig. 3.c. Free bend-twist deformation

<sup>1</sup> MSc. Rzeszów University of Technology, Rzeszow, POLAND

Three basic free deformations of a flat sheet: free bend, free twist and free bend-twist were defined at the Rzeszów center (Fig. 3a, b, c) [2]. Flat sheets so deformed are applied in the construction of single and double curved rectilinear building shells. The shape of a flat profiled sheet changes readily from flat to spatial, therefore it is subject to deformation the kind and the value of which are accepted at the initial stage of the shell shaping process.

Suitable connecting technology of the adjacent sheets, along their longitudinal edges, makes it possible to shape the rectilinear shells [3, 4].

Experimental tests and theoretical analyses revealed that the range of permissible deformations only insignificantly decreases the diversity of the shell configurations. The range of the series of an infinite number of the available shell shapes of a deformed flat sheet results from the need to limit the effort of the deformed sheet and from the acceptance of the elastic range of its action in the shell. The building shells realized in the area of southern Poland confirm this recognition. Therefore, architectural forms of the designed shells can be original and almost unconstrained (Figs 4, 5).

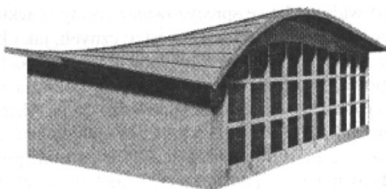


Fig. 4. Computer visualization of the conception of the shell corrugated roof

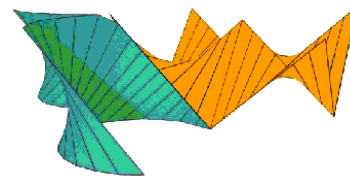


Fig. 5. Computer visualization of the structure made of shell sectors of ruled surfaces

It was assumed that the deformation resulting at the time of assembly and loading of the shell could not lead to the elastic depreciation of the local stability because of the lack of suitable experimental tests concerning supercritical capacity of the shell sheet. The created at the Rzeszów center new method of shell shaping assures the freedom of transversal strains of the free deformed sheets during assembly; hence the sheets are subject to free deformations. Therefore, their effort can be relatively small although the shell form can be almost free. The precision of assigning the supporting points of the sheet folds to the shell directrices plays a significant role in folded shell shaping because the assembled sheets should not be subjected to any useless additional transversal forces modifying the widths of their ends.

There exists interdependence between the lengths of the lines supporting both ends and the supporting conditions, as well as geometrical and physical properties of each sheet having the freedom of transversal strains during its assembly. This interdependence can be described with the help of mathematical functions. The space shape is not the only advantage of the free deformed sheet because such a deformed sheet retains its ability to carry loads.

The purpose of the experimental tests is a quantitative description of the shell shape of an intentionally deformed flat sheet. This description is performed with the help of a mathematical model of a shell sheet, in particular with the help of mathematical formulas. The way of applying this mathematical model or the description of shaping a shell lies outside the scope of this paper.

## 2. A QUALITATIVE MATHEMATICAL MODEL OF A FREE DEFORMED SHEET

Up till 1990s, light gauge steel shells had only been shaped in the form of cylindrical surfaces, hyperbolic-paraboloid ones or in the form of roof structures made up of insignificantly protruding hyperbolic paraboloid shell segments (Fig. 6) [5, 6]. It was at that time when a novel method of geometric and structural shaping was elaborated at the Rzeszów center by A. Reichhart. This method enables designing of the rectilinear shells of almost free forms because it is based on the possible to be obtained free deformations of a flat profiled sheet aided numerically. The available deformations were verified experimentally.

The nature of this method consists in its abandoning the ways of shell shaping used so far in favor of using the experimentally verified space shapes of a twisted flat sheet. A free deformed sheet assumes only one space configuration according to the supporting conditions. Only one mutual position of the transversal opposite edges of this space sheet corresponds to this configuration. A modification of the mutual position of the elements supporting the sheet ends results in changing the lengths of the supporting lines of this sheet and thus, the sheet shape, especially the sheet width, is also changed.

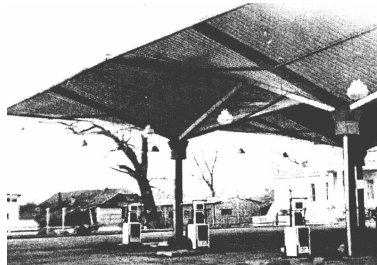


Fig. 6. The structure of insignificantly protruding hyperbolic paraboloid shell segments [6]

A sheet deformed on the experimental stand is called *an experimental sheet* and a deformed sheet of a building shell is called *a shell sheet*. The shell composed of two or three experimental sheets connected along their longitudinal edges is called *an experimental shell*. To get a free deformed flat sheet, the lengths of the lines supporting a single shell sheet ought to be precisely measured on the shell directrices on the basis of the experimental test results.

It is possible to determine the successive generatrices of the shell model corresponding to the longitudinal edges of the shell sheets on the basis of (Fig. 7):

- figure  $\Gamma$  composed of two curves  $e, f$  and the straight line  $t_0$  being directrices and generatrix of a ruled surface,
- structural condition describing the dependence of the mutual position of those edge generatrices of a shell sheet on the supporting conditions and the stiffness of the sheet.

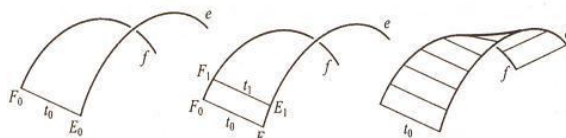


Fig. 7. Shell shaping with the help of the figure  $\Gamma$  and the structural condition

Structural condition is defined as the quality dependence of the positions of the rectilinear edge generatrices of the shell sheet in relation to the shell directrices, on the type of the flat sheet, the kind and the amount of deformation and its restrictions. The structural condition of the Reichhart's method

replaces the geometric one applied in problems connected with defining surfaces on the grounds of classical projection geometry. [7, 8].

The Reichhart's method sometimes proves not accurate enough which is visible in the already realized shells. This is because only geometric properties of the central sector of the right ruled paraboloid are used in creating geometric models of the shell sheet. Therefore, to make the description of the above dependence more precise, the following qualitative mathematical model of a shell sheet was proposed on the basis of the experimental test results and theoretical analyses. This model is constituted by:

- a generalized sector of the ruled surface,
- a formula composed of two equations (1) and (2) on the base of which the mutual position of two longitudinal opposite edge rulings of the above sector corresponding to the longitudinal sheet edges can be obtained.

$$b_e = b (1 + db_{ew} / 100), \text{ where: } db_{ew} = f_e(1, \alpha_{jed}, \varepsilon, \varphi, p_{st}, \kappa_e, \kappa_f) \quad (1)$$

$$b_f = b (1 + db_{fw} / 100), \text{ where: } db_{fw} = f_f(1, \alpha_{jed}, \varepsilon, \varphi, p_{st}, \kappa_e, \kappa_f) \quad (2)$$

The following was accepted:

- 1 - the value of the length of the flat sheet,
- $l$  - the length of the flat sheet,
- $\alpha_{jed}$  - the value of the measure of the unitary twist angle of the sheet,

- $\alpha_{jed}$  - the unitary twist angle of the (experimental or shell) sheet,  
 $\alpha$  - the twist angle of the (experimental or shell) sheet  
 $\varepsilon, \varphi$  - the values of the measures of the angles of the oblique cutting of the flat sheet ends  
 $\varepsilon, \varphi$  - the angles of the oblique cutting of the flat sheet ends  
 $p_{st}$  - the positive or negative position of the flat sheet  
 $\kappa_e, \kappa_f$  - the values of the curvatures of the shell directrices  $e$  and  $f$   
 $\kappa_e, \kappa_f$  - the curvatures of the shell directrices  $e$  and  $f$

The equations (1) and (2) describe the dependences of the end widths of the shell sheet on the factors whose influence could be essential.

The above model is based on the following assumptions:

- the lengths  $b_e$  and  $b_f$  of the supporting lines of the sheet ends (the widths of the sheet ends) describe the geometric shape of the shell sheet,
- the unitary twist angle  $\alpha_{jed}$  of the shell sheet, the curvatures  $\kappa_e$  and  $\kappa_f$  of the shell directrices  $e$  and  $f$  describe the supporting conditions of the shell sheet,
- the length  $l$  and the angles  $\varepsilon, \varphi$  of the oblique cutting of the flat sheet ends corresponding with the directrices and the positive or negative position  $p_{st}$  of the shell sheet and its type describe geometrical and physical properties of the shell sheet.

The main objective of the author's own experimental tests is a quantitative description of a shell sheet shape with the help of the discrete values of the significant factors, whereas the primary purpose of theoretical investigations is to build a mathematical quantitative model of a shell sheet reflecting the influence of the significant factors on the space shape of a shell sheet with the help of the functions  $f_e$  and  $f_f$ , where that space shape is described by the width increments  $db_{ew}$  and  $db_{fw}$ .

Since each modification of the supporting conditions results in a suitable change of the free deformed sheet shape, then the dependence of the relative increments  $db_{ew}$  and  $db_{fw}$  of the lengths of the supporting lines on the length  $l$ , the cutting angles  $\varepsilon, \varphi$ , the shape, the position  $p_{st}$  (positive or negative), the unitary twist angle  $\alpha_{jed}$  and the curvatures  $\kappa_e, \kappa_f$  of the  $e, f$  lines supporting the sheet ends is a functional one.

The following way of shell shaping based on the above mathematical model of a shell sheet can be applied. The  $e, f$  curves and the straight line  $t_0$  are assumed in the three dimensional Euclidean space (Fig. 8). These curves are directrices and the straight line is the

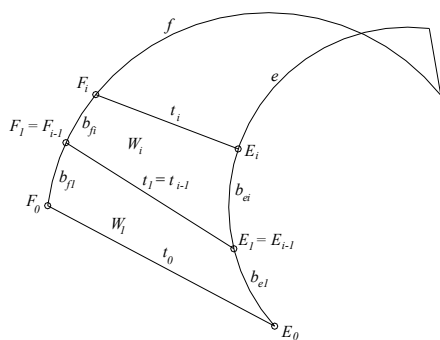


Fig. 8. Determination of rulings (border lines of the shell sheet models) creating the shell model

border ruling of the sector of the ruled surface being the model of the shell. The points  $E_i$  and  $F_i$  corresponding to each other are sought on the  $e$  and  $f$  so that the length values of the  $E_0E_1, F_0F_1$  and the values  $b_{e1}$  and  $b_{f1}$  calculated from the (1) and (2) are equal, where  $E_0 = e \cap t_0, F_0 = f \cap t_0$ . The obtained points  $E_1$  and  $F_1$  determine the ruling  $t_1$  being sought. The rulings  $t_0$  and  $t_1$  delimit the geometric model of a shell sheet. The remaining rulings  $t_i$  of the shell model corresponding to the borderlines of the successive sheets are determined in the same way. It is possible to obtain the geometric model of the single shell fold with the help of this mathematical model.

The effect of the substitution of the geometric condition by the structural condition is that the activities

connected with geometrical shaping and structural shaping have to be solved simultaneously with the steel shell shaping. Thus, it is impossible to divide these activities into two separate and succeeding parts as it is in the case of traditional methods of shaping the construction form.

If the differentiation between both ends of the deformed sheet is not important, the width increments  $db_{ew}$  and  $db_{fw}$  will be designated as  $db_w$ .



### 3. THE AUTHOR'S OWN INVESTIGATIONS INTO FREE BEND AND FREE TWIST DEFORMATIONS OF THE TRAPEZOIDAL SHEET

#### 3.1. Research methodology and measurement technique

The experimental sheets and experimental shells made up of two or three experimental rectangular sheets connected with one another along their longitudinal edges were used in the experimental tests. The deterministic and dynamic plan of the author's own research was accepted. The results of the research carried out at the Rzeszów center demonstrate that the dependences of the factors describing the space shape of a free deformed sheet on the factors describing the supporting conditions and geometric and physical properties of the flat sheet are nonlinear.

The author's research into the dependence of the space shape of the free deformed flat sheet on the cutting angles of the edges and the shape of this flat sheet was limited to a free twist deformation of this sheet supported rectilinearly on its ends.

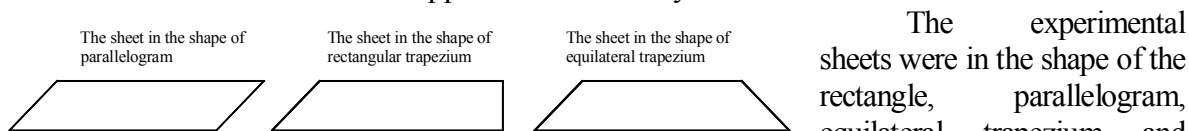


Fig. 9. Accepted shapes of the oblique cutting experimental sheets

The experimental sheets were in the shape of the rectangle, parallelogram, equilateral trapezium and rectangular trapezium (Fig. 9). Each new sheet shape under examination required cutting

the ends of a new flat rectangular sheet. The change of the sheet length required also transversal or oblique cutting of at least one of the sheet ends, hence it was rather inconvenient the modification of the twist angle was the least troublesome because it only required turning of the supporting elements of the experimental stand.

The author's experimental tests on the influence of the curvatures of the shell directrices on space shape of a shell sheet required modification of the experimental stand consisting in making new elements of different curvatures supporting the experimental sheet. The curvilinear supporting elements of an identical shape and only rectangular sheets were used in the case of the free bend and free bend-twist deformation.

In order to examine the space shape of the deformed experimental sheet, the centerlines of the upper shelves and the transversal measuring lines evenly distributed on the length of the experimental sheet were traced on the surface of the upper shelves. The central lines (axes) of the upper shelves made the family  $\{v(\alpha, j)\}$  and the measuring lines made the family  $\{u(\alpha, i)\}$  of the upper rectilinear surface of the experimental sheet (Fig. 10, 11) [9].

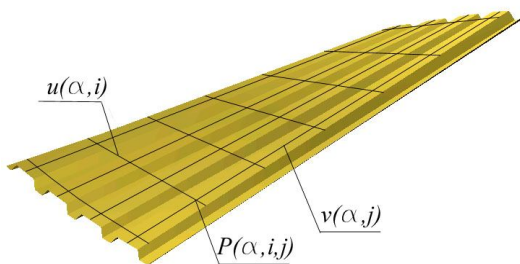


Fig. 10. Points and lines describing the shape of the deformed rectangular sheet



Fig. 11. An experimental free twisted trapezoidal sheet

In the case of the sheets in the shape of a rectangle and parallelogram all measuring lines are parallel to one another. However, in the case of the experimental flat sheet in the shape of an equilateral trapezium or rectangular trapezium all measuring lines intersect at one point. It is accepted that the measuring lines of the free deformed experimental sheets in the shape of a rectangle, parallelogram and equilateral trapezium are straight lines parallel to the same plane and their models are sectors of a ruled paraboloid. The longitudinal edges of each free twisted or free twisted and bent experimental sheet are curvilinear. Therefore, it was imperative to create a generalized geometric model of the experimental sheet having curvilinear longitudinal edges (Fig. 12) and next, the way of transforming this geometric model into the geometric model of the shell sheet having rectilinear longitudinal edges (Fig. 13).

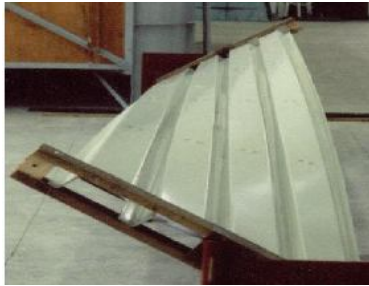


Fig. 12. A free twisted sheet with border bending of the longitudinal edges [2]



Fig. 13. The deformed shell sheets [2]

The following sector  $W_d$  of the ruled surface  $\omega_d$  was accepted as the geometric model of the experimental free deformed sheet  $A_d$  (Fig. 14). The rectilinear rulings  $v_{dj}$  of the first family  $\{v_{dj}\}$  of this model correspond to the axes of the upper shelves of the sheet, and the curvilinear generatrices  $u_{di}$  of the second family  $\{u_{di}\}$  correspond to the measuring lines of this sheet. Geometric properties of the generatrices  $u_{di}$  of the  $\{u_{di}\}$  are dependent on the supporting element shapes and geometric and physical properties of the deformed sheet. In the case of the general free deformation the supporting elements could be the arcs. In the case of the applied free twist deformation the supporting elements in the tests are rectilinear and the generatrices  $u_{di}$  of the second family  $\{u_{di}\}$  correspond to the measuring lines also are rectilinear (Fig. 15).

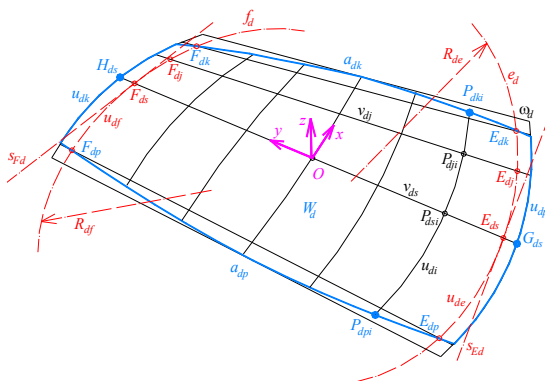


Fig. 14. Model  $W_d$  of the experimental sheet  $A_d$  supported by curvilinear elements bent in the adverse directories

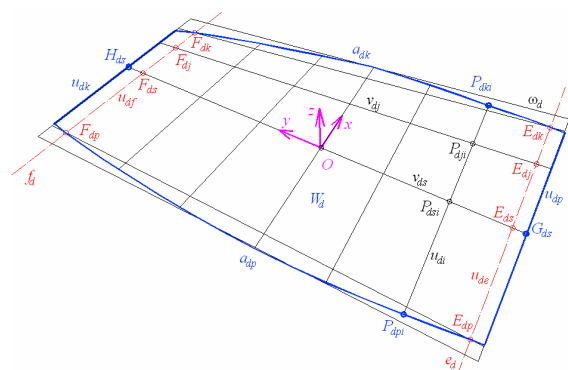


Fig. 15. Model  $W_d$  of the experimental free twisted sheet (shell)  $A_d$  supported by rectilinear elements

Regular sheet extension along the supporting lines observed during the tests, enables the points  $E_{dj}$  and  $F_{dj}$  of the segments  $u_{de}$  and  $u_{df}$  to be paired up as  $\{E_{dj}, F_{dj}\}$  determining the ruling  $v_{dj}$  of the first family  $\{v_{dj}\}$  of the surface  $\omega_d$ . The following way to obtain the



The following was applied in investigations:

- a relatively great number of values of the independent factors  $l$  and  $\alpha_{jed}$  (4 or 5 value levels) regularly arranged within the interval of the permissible values because the influence of these factors on the relative increments of the sheet widths is decisive and any change of the values of these factors is neither too high nor laborious,
- a relatively small number of values of the independent factors:  $\varepsilon$ ,  $\varphi$ , (2 or 3 value levels) arranged erratically within the interval of the permissible values adequately to the nonlinear nature of the changes of the relative increments of the sheet widths caused by the free deformation because the influence of these factors on the relative increments of the sheet widths is slight and any value changes of these factors are expensive and laborious.

The most important observations concerning the space shape of the free twisted experimental sheet supported rectilinearly on its ends are:

- the folds are deflected significantly in the surface of the sheet,
- the measuring lines are deflected insignificantly and they are accepted as straight lines,
- the middle fold of the experimental sheet remains rectilinear during free deformation and its axis is accepted as the axis of the free twist deformation.

The described in Section 3 way of transforming the geometric models of the free twisted, experimental sheets into the geometric models of the shell sheets makes it possible to calculate the infinite values of the relative width increments of the free twisted shell sheets and next, to obtain a substantial shape of the functions  $f_c$  and  $f_f$  from the formulas (1) and (2) by the method of least squares.

The simplifying assumptions are accepted:

- the shaped shell is made of the free deformed flat sheets that are not subject to the additional forces changing the widths of them transversal ends during assembly work,
- the geometric model of the shell sheet is contained in the neutral surface of this sheet,
- the neutral surface location is calculated on the base of the distances from the surfaces of the upper and lower shelves of the shell sheet (Fig. 17) in the same way as the distances of the neutral axis of the cross-section of the flat sheet from the planes of the upper and lower shelves,
- the measured in the neutral surface increments  $db_{wi}$  of the widths of the free deformed sheet are the same as the increments of the widths of the free twisted sheet and they ought to be calculated with the help of the formulas (4) and (5) described in the next section,
- the shell sheet high depends on the degree of the free deformation (on the value of the unitary angle of the twist) and can be calculated in the same way as the high of the free twisted sheet without taking the bend into consideration.

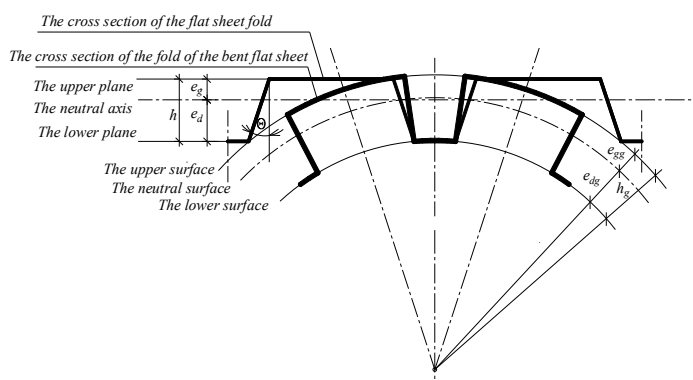


Fig. 17. Cross-section of the free bent experimental sheet

The above simplifications make possible to keep the satisfactory precision of the shell sheet shaping.

To define the influence of the above simplifications on the shaping precision the next experimental tests and theoretical analyzes related to the free bend and the free bend-twist deformations have to be carried out. These investigations lie outside of the scope of this paper.

### 3.2. The results of author’s own research on the free twist deformation of the flat trapezoidal sheet supported rectilinearly on its ends

The graphs present the variation of the width increments  $db_{wi}$  of each fold of the exemplifying free twisted experimental shell (before rectification of the longitudinal edges) crosswise (Fig. 18) and lengthwise (Fig. 19), where:  $n$  – the number of the fold,  $i$  – the number of the measured line,  $l = 6200$  [mm],  $\alpha_{jed} = 6,928$  [°].

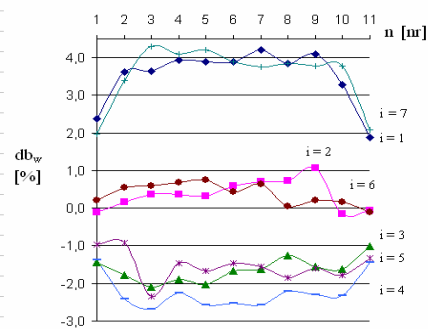


Fig. 18. The relative width increments  $db_w$  of the experimental shell along the measured lines (crosswise)

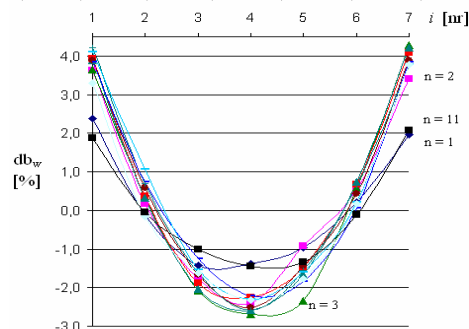


Fig. 19. The relative width increments  $db_w$  of the experimental shell lengthwise

The comparable values of the width increments  $db_{wi}$  of the internal folds make possible to average  $db_w$  for each measuring line. Exemplifying results of these simplifications are presented for the different kind of the experimental flat sheet shape (Fig. 20.a) and for the experimental shell composed of the 1, 2, 3 sheets (Fig. 20.b),  $l = 6200$  [mm],  $\alpha_{jed} = 6,928$  [°].

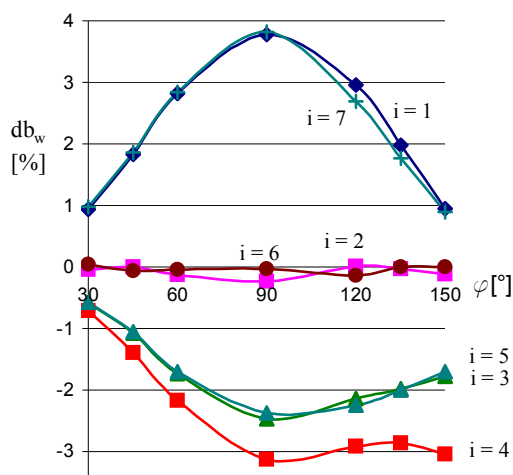


Fig. 20.a. The dependence between the relative width increments  $db_w$  and the shape of the oblique cutting 1 experimental sheet

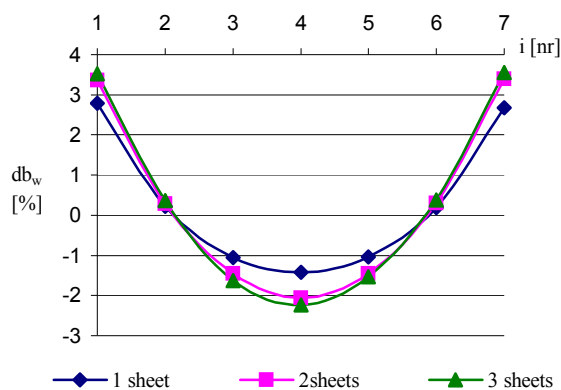


Fig. 20.b. The relative width increments  $db_w$  of the experimental shell composed of the 1, 2 and 3 sheets

The graphs (Fig. 21) present the dependence of the width increments  $db_w$  of the free twisted shell sheet end on the cutting angle of this end. It can be seen from these graphs that the cutting angle of the flat sheet significantly influences its space configuration after free twist. The character of the width changes of the free twisted sheet when changing its length  $l$  and unitary angle of twist  $\alpha_{jed}$ , is also curvilinear in nature.

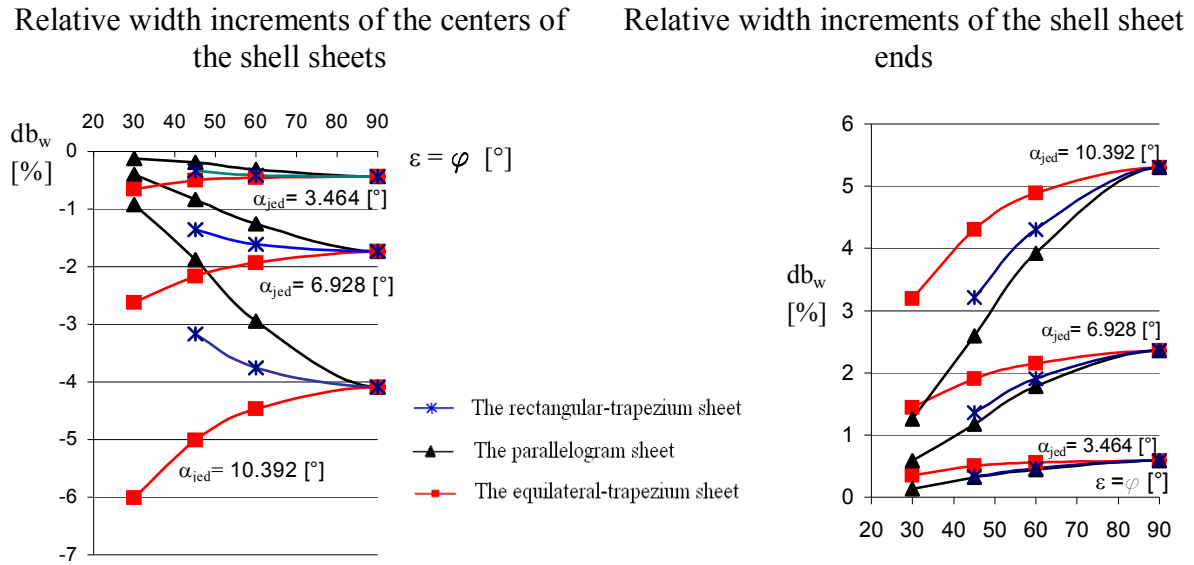


Fig. 21. The graphs of the dependences of the relative width increments of the centers and ends of the shell sheets  $l = 4900$  [mm] (after straightening the edges) on their cutting angles

The results of author's own research lead to the following conclusions.

1. The size of the cutting angle of the flat sheet end has a significant influence on the values of its width increments resulting from the free twist deformation and thus, on the space shape of the sheet.
2. The shape of the flat free twisted sheet during its assembly to the building shell also has an important influence on its width and space shape.
3. It is possible to create mathematical formulas based on polynomials of at least third degree describing satisfactorily the influence that is shown on the above graphs.

After the relative width increments of the adjacent folds of the experimental sheet had been compared, it was accepted that the allowable values of the rests being the result of subtraction of the calculated values (with the help of the  $f_e$  and  $f_f$  functions) and the measured values of the width increments ought to be located in the range of 0,8 – 1,1 %. However, the comparison of different experimental research results on the free twist deformation of the rectangular sheets of the same types and lengths and supporting conditions led to the assumption that the value of the root-mean-square error should be located in the range of 0,2 – 0,4 %. Mathematical functions (4) and (5) permit to calculate the  $db_w$  on both ends of the shell sheet along the shell directrices. The calculated value of the root-mean-square error of the above functions is 0,26 %.

$$f_e = b_1 \cdot \alpha_{jed}^2 \cdot (l^2 + b_2) \cdot (b_3 \cdot \varepsilon^2 + b_4 \cdot \varepsilon + b_5) \cdot (\varphi + b_6) \quad (4)$$

$$f_f = b_1 \cdot \alpha_{jed}^2 \cdot (l^2 + b_2) \cdot (b_3 \cdot \varphi^2 + b_4 \cdot \varphi + b_5) \cdot (\varepsilon + b_6) \quad (5)$$

where:  $b_1 = 0,0000300$   $b_4 = 0,79$   $l$  [m],  
 $b_2 = 1,00$   $b_5 = -1,3$   $\varepsilon$  [° / 10],  $\varphi$  [° / 10],  
 $b_3 = -0,042$   $b_6 = 24$   $\alpha_{jed}$  [°]

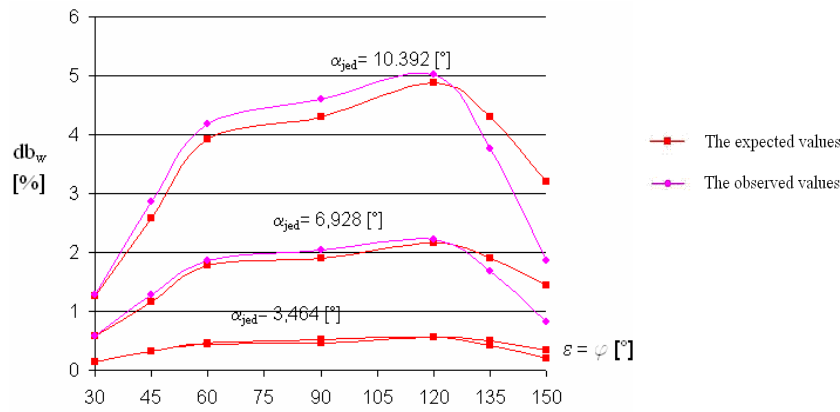


Fig. 22. Relative width increments of the shell sheets ( $l = 3,095$  m) calculated with the help of the formulas (4) and (5) and resulting from transforming the geometric models of the experimental sheets

The demonstration graph allows comparing the values of the width increments of the shell sheet calculated with the help of these functions (the expected values) as well as resulting from the transformation geometric models of the experimental sheets (the observed values of these increments) (Fig. 22).

#### 4. THE QUANTITATIVE MATHEMATICAL MODEL OF THE SHELL SHEET – CONCLUSIONS

The quantitative mathematical model of the shell sheet elaborated on the base of experimental research and theoretical analyses assumes that the following activities leading to creating the geometrical model  $W_{pi}$  of the shell  $A_{pi}$  sheet ought to be conducted (Fig. 23).

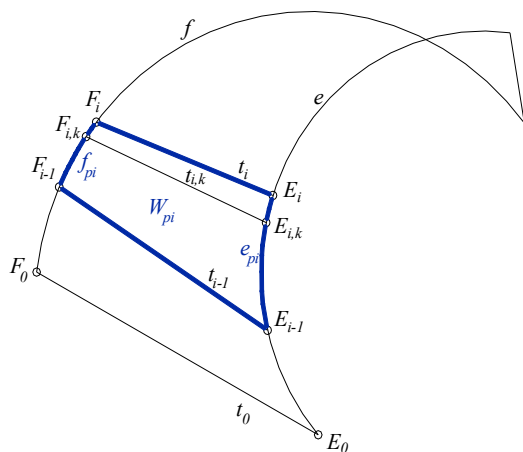


Fig. 23. The geometric model  $W_{pi}$  of the sheet of the building shell  $A_{pi}$

1. In the three-dimensional Euclidean space the curve  $e$  and  $f$  should be taken as the directing lines of the ruled surface  $\omega_p$ , in which the width increments of the shell sheet ends resulting from the free bend deformation are zero.
2. The qualitative mathematical model of the shell sheet and the way of determining the ruling  $t_i$  of the ruled surface  $\omega_p$ , described in Section 2, have to be used to obtain the model  $W_{pi}$  of the shell sheet.
3. The supporting lines of each shell sheet might be accepted as the straight lines and the free deformation of the shell sheet might be accepted as the free twist. Then, the values of increments  $db_w$  of the shell sheet  $A_{pi}$  resulting from the free twist deformation should be calculated with the help of functions (4) and (5).

4. The values  $e_{pi}$  and  $f_{pi}$  calculated from the formulas (1) and (2) ought to be accepted as the values of the lengths of the transversal curves  $e_{pi}$  and  $f_{pi}$  limiting the model  $W_{pi}$  and corresponding to the opposite transversal edges of the shell sheet  $A_{pi}$ . The curvatures  $\kappa_e$ ,  $\kappa_f$  of the shell directrices  $e$  and  $f$  ought to be accepted as equal zero.
5. The borderline of the model  $W_{pi}$ , which is made up of the  $e_{pi}$ ,  $f_{pi}$  and the segments:  $E_{i-1}F_{i-1}$ ,  $E_iF_i$  corresponding to the longitudinal rectilinear edges of the shell sheet should be built.

On the base of one point, for example  $E_{i,k}$  on the  $e_{pi}$  directrix, the ruling  $t_{i,k}$  of the  $W_{pi}$  can be determined in the following way: the point  $F_{i,k}$  corresponding to the accepted point  $E_{i,k}$

is found so that the proportion of the lengths of the curves  $E_{i-1}E_{i,k}$  and  $E_{i,k}E_i$  and the proportion of the lengths of the curves  $F_{i-1}F_{i,k}$  and  $F_{i,k}F_i$  are equal. This equality of the above proportions is an effect of the uniform extension of the opposite transversal shell sheet edges resulting from a free deformation. Finally, the ruling  $t_{i,k}$  passes through the points  $E_{i,k}$  and  $F_{i,k}$ .

To sum up, it should be stressed that the presented mathematical model is a great step towards making the process of shaping the corrugated steel shells more precise than by the methods used so far because with its help the points of fold assembly to the directrices can be found with a greater precision. Thus, the freedom of transversal strains of the assembled sheets is assured to such an extent that the shell sheets are not subjected to the action of useless, additional forces modifying their ends widths.

## REFERENCES

- [1] Abramczyk J.: Właściwości blachy fałdowej wykorzystywane w procesie kształtowania obiektów budowlanych, Materiały VII Sympozjum z cyklu: Nowe osiągnięcia techniki w budownictwie, "Kształtowanie konstrukcji. Konstrukcje z blach fałdowych. Konstrukcje ciągnowe." Oficyna PRz, Rzeszów 2005.
- [2] Reichhart A.: Geometrical and structural shaping of shells made of profiled metal sheets (in Polish), Oficyna Wyd. Politechniki Rzeszowskiej, Rzeszów 2002.
- [3] Abramczyk J.: Ruled Surfaces as the Models for Corrugated Building Shells, IASS 2004 Symposium Montpellier Shell and Spatial Structures for Models to Realization, September, Montpellier, France, pp. 280-281, 2004.
- [4] Abramczyk J.: A Mathematical – geometric model of the corrugated steel sheet of the building shell, Proc. Conference on Lightweight Structures in Civil Engineering, Local Seminar of IASS Polish Chapter, Warsaw 2007, pp. 98-101.
- [5] Davies J.M., Bryan E.R.: "Manual of stressed skin diaphragm design, Granada, London 1982.
- [6] Gioncu V., Petcu D. (1995) "Corrugated Hypar Structures" Proc. Inter. Conf. LSCE, Warsaw, pp. 637-644.
- [7] Januszewski B.: "Geometria wykreślna", Cz. 1, Skrypt PRz, Rzeszów 1990.
- [8] Polański S.: "Geometria powłok budowlanych", PWN, Warszawa 1986.
- [9] Reichhart A., Abramczyk J.: On the influence of oblique cutting of profiled steel sheet on its shell shape, Proc. Conference on Lightweight Structures in Civil Engineering, Local Seminar of IASS Polish Chapter, Warsaw 2006, pp. 172-175.



Pavol BEKE<sup>1</sup>  
Vincent KVOČÁK<sup>2</sup>

## THE EFFECT OF CROSS-SECTION STIFFNESS RATIOS ON THE RESISTANCE OF JOINT COMPOSED OF RECTANGULAR AND CIRCULAR HOLLOW SECTIONS

### ABSTRACT

The paper presented focuses on the comparison of the measurement results obtained in laboratory experiments on joints composed of rectangular and circular hollow sections. Special attention is paid to T-section joints that consist of single chord and brace members. The evaluation procedure monitors the resistances and deformations of such joints.

**KEYWORDS:** T-joints, circular hollow sections, rectangular hollow sections, vertical deformation, horizontal deformation

### 1. INTRODUCTION

The gradual increase in the production range of hollow sections has resulted in their more common application in various areas and types of construction. This type of section can find a number of applications in the construction industry, especially in structures where attractive general appearance of the whole structure is required.

From the point of view of a structural designer, the application of hollow section joints presents relatively effective utilization of the material. The distribution of the material and its mass in hollow section joints brings several advantages for various kinds of load. Their application is one of the best design solutions in members under compression, with respect to their buckling, as well as in members loaded in bending, with respect to their lateral-torsional buckling as well.

As far as strain is concerned, joints present the most exposed areas in structures composed of such types of section. Joints composed of rectangular hollow sections have recently received quite close attention [3], [6], [7]. Our experimental research programme concerns the hollow-section joints combined with other kinds of section.

The paper presents the results of the experimental programme that has been carried out at the Faculty of Civil Engineering of the Technical University in Košice. Great emphasis is placed on the joints composed of rectangular and circular hollow sections, such as T sections,

<sup>1</sup> Eng., Technical University in Kosice, Kosice, SLOVAK REPUBLIK

<sup>2</sup> Assoc. Prof. PhD. Eng., Technical University in Kosice, Kosice, SLOVAK REPUBLIK

while the chord members are of rectangular hollow sections and the brace members vary inspection in terms of their type and dimensions [1], [2], [4].



Figure. 1: Arrangement of the diagnostic apparatus on the specimens under observation

## 2. PREPARATION OF THE EXPERIMENT AND PERFORMED LABORATORY MEASUREMENTS

It is essential for the design of a joint to take into account a lot of factors that influence the stiffness of the joint, such as its geometry, the material used, stress application, etc [5].

As regards the geometry of joints, two kinds of joint were compared in our experiment. Of the two kinds, in the former kind of joint both chord and brace members were composed of rectangular hollow sections, whereas the latter kind of joint contained the chord member of rectangular hollow section, just like the former one, and the brace member of circular hollow section.

Another variable that can characterize the above-mentioned joints is a  $\beta$ -parameter. It is the ratio of the mean diameter or width of the brace members to that of the chord. Our effort was to cover as wide a range of  $\beta$ -parameters as possible. To this end, the constant section of RHS 140x140x4 was selected as the chord and, in the former type of joint, RHS 60x60x3, RHS120x120x3, and RHS140x140x4 were selected as the braces. In the latter type of joint, the chord remained identical and the brace members composed of CHS 60x4, CHS 100x4 and CHS 140x5. The  $\beta$ -parameter for the sections selected ranged in an interval from 0.429 to 1.00.

All models were made of steel S235 and a specimen of each model was taken to analyze its material characteristics. The yield strength in all specimens did not exceed the one declared by the steel manufacturer and it varied between 290 and 320 MPa.

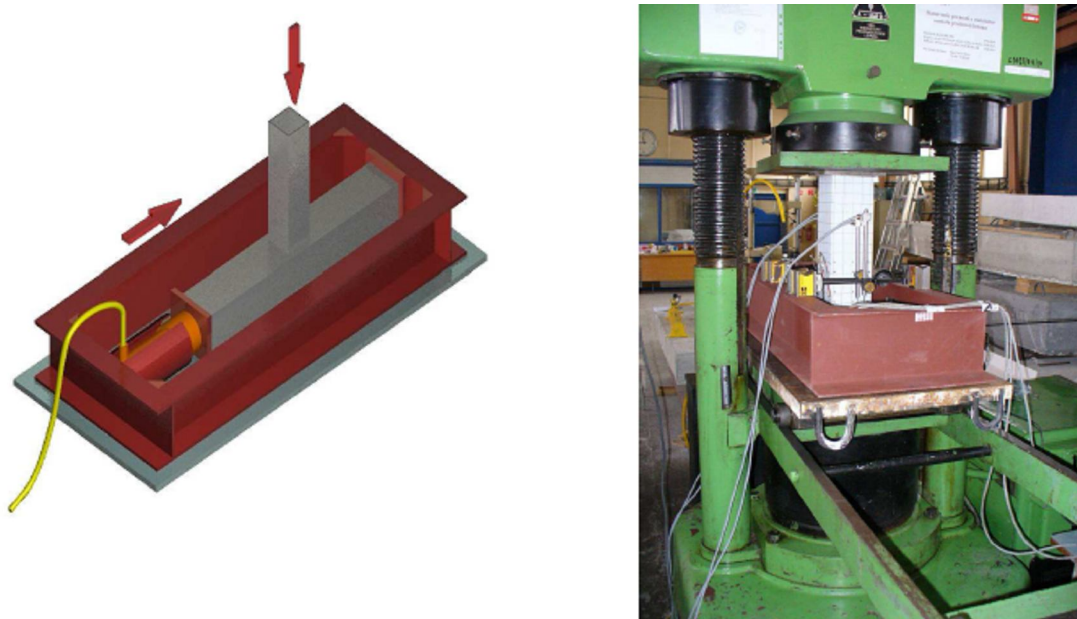


Figure 2: The loading test assembly

In order to simulate the real behaviour of the joint in a lattice structure, the chord member was assumed to act in horizontal compression, while the brace members were compressed in a vertical direction. Horizontal compression was actuated by means of an additional frame and pneumatic hand press. The numerical value of horizontal load remained constant during the whole loading period. Each specimen type was tested at three horizontal force levels: 68 kN, 115 kN and 192 kN. Vertical load imposed on the specimens by the main hydraulic press was gradually increased until the total failure of the specimen. With respect to the complexity of the task, the length of the brace member was designed so as to prevent buckling of the member.

Measurement points were then selected on the individual specimens. Strain gauges were used to measure stress in the specimens and inductive sensors to determine horizontal and vertical deformations in the specimens.

### 3. OBTAINED RESULTS

The types of joints selected were observed for both stress and deformation. In the following section of the paper, the attention will be directed to the deformation of the joints.

As can be seen from the figure below, deformation was measured mainly in the chord members, namely in the upper horizontal and vertical walls of the chord member section.

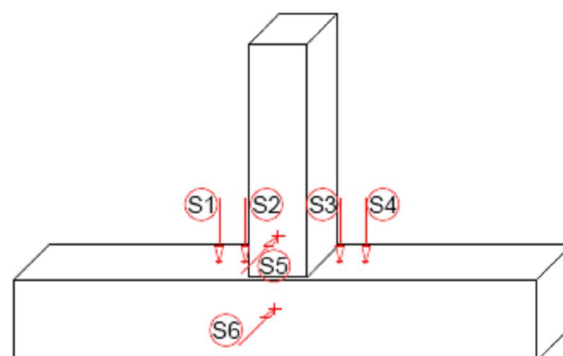


Figure 3: The geometrical arrangement of inductive sensors on a specimen

The behaviour of the individual joints and their deformation in both horizontal and vertical directions are shown in the following graphs.

In the first type of joint ( $\beta=1.0$ ), the stability of the vertical wall of the chord member section was crucial to the resistance of the joint. The numerical values of deformation in the selected measurement points on the specimen are shown in the deformation curves presented in Figure 4. Even at a relatively low horizontal load, the deformation of the vertical wall of the chord member section is significant. With the gradual increase of the horizontal load, the joint totally collapsed exactly due to the lateral buckling of the horizontal wall of the chord member.

When comparing the resistance of the used rectangular and circular hollow sections, the rectangular hollow sections demonstrated stronger resistance. As can be seen from the deformation curves in Figure 4, plastic deformation and the subsequent collapse of the specimen was observed in the joints with the brace members composed of circular hollow sections.

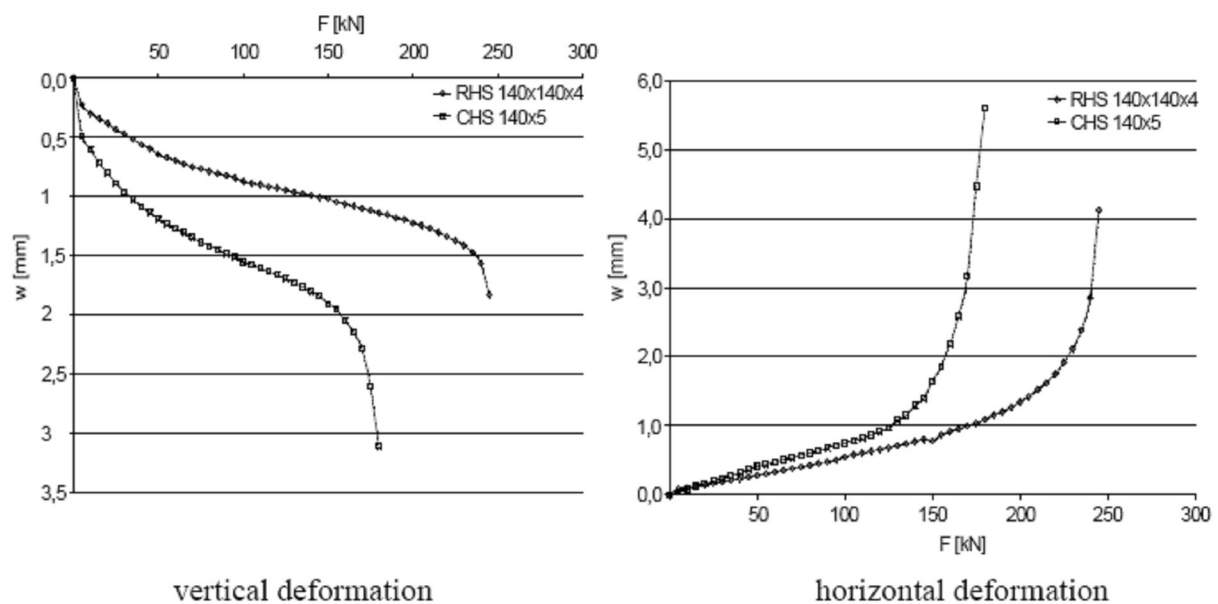


Figure 4: Comparison of experimental models with the brace members composed of RHS140x140x4 and CHS 140x5 – vertical and horizontal deformation curves.

In the case of joints with  $\beta=0.714$ , the overall resistance of the joint was affected by the lateral buckling of the vertical wall of the chord member. Even in this case, the overall resistance of the joint was affected by the loss of stability of the vertical wall, although the difference between the horizontal and vertical deformation was not as dramatic as in the first case.

When comparing the joints composed of the used rectangular and circular hollow section brace members, similarly, the rectangular sections seem to be stiffer. Here, unlike in the first case ( $\beta=1.0$ ), almost identical behaviour of both types of section can be observed at their elastic stage. However, the plastic deformation of the chord member occurs earlier in the joints with the circular hollow section brace members, as shown in Figure 5.

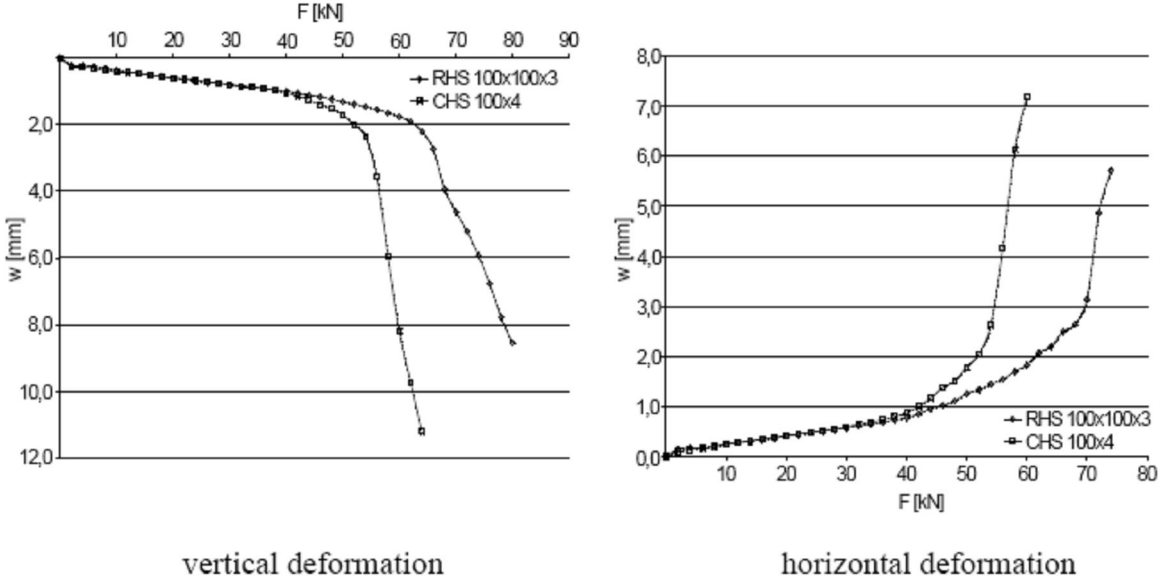


Figure 5: Comparison of experimental models with the brace members composed of RHS 100x100x3 and CHS 100x4 – vertical and horizontal deformation curves

In the third type of joint with the most slender brace members, the total stiffness of the joint was radically affected by the stiffness of the horizontal wall of the chord member. The difference between the horizontal and vertical deformation is the greatest of all. Equally, the greatest horizontal deformation occurred (Fig. 6).

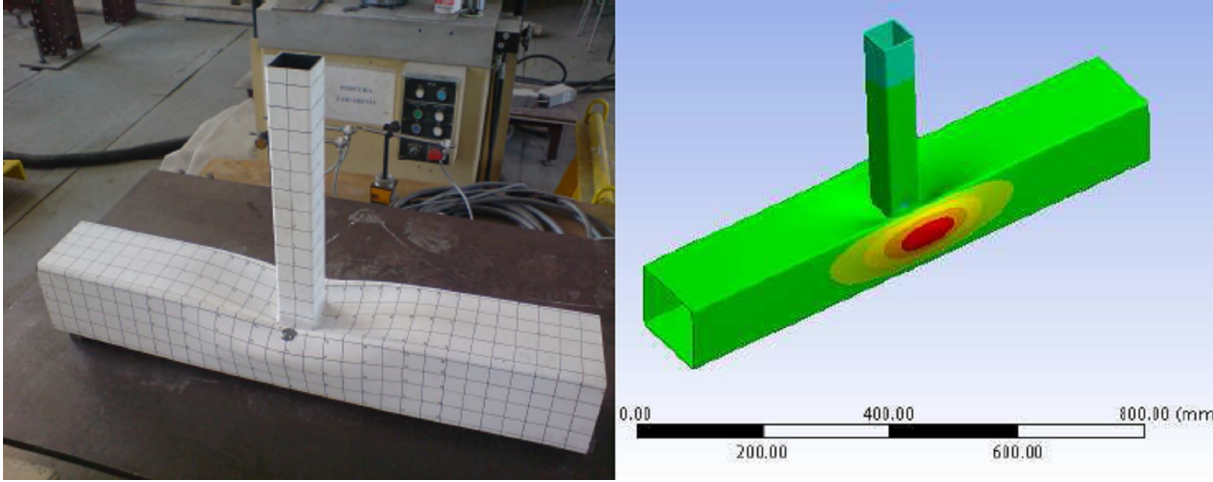


Figure 6: Comparison of the actual deformation of the specimen and the deformation modeled using the finite element method

As can be concluded from Figure 7, the application of rectangular or circular hollow sections is equivalent as far as the stiffness of the joint is concerned.

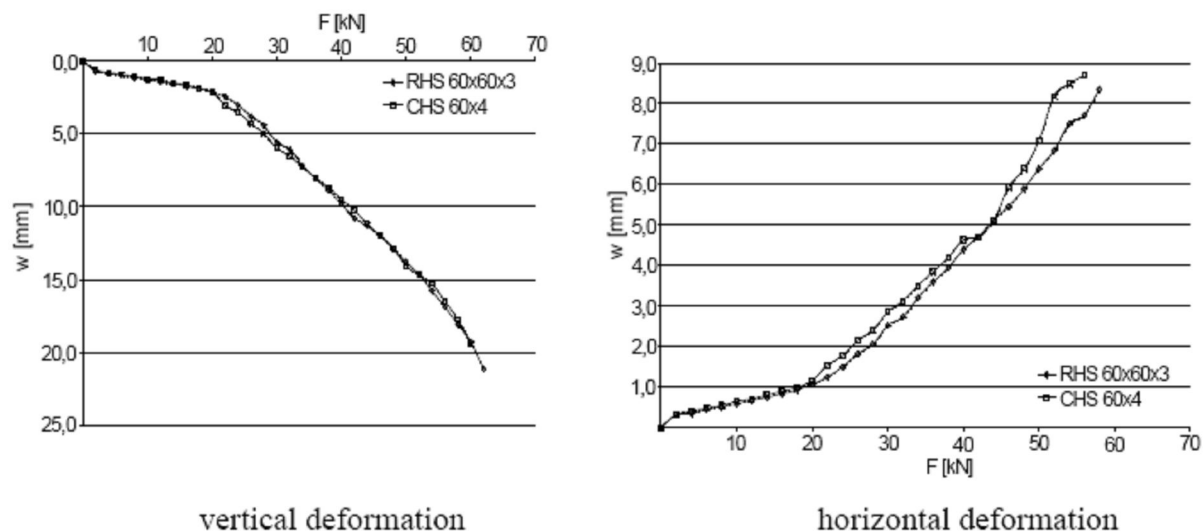


Figure 7: Comparison of experimental models with the brace members composed of RHS60x60x3 and CHS 60x4 – vertical and horizontal deformation curves

## CONCLUSION

The comparison of the results obtained in the experiments on the joints where the brace member is composed of various rectangular and circular hollow sections lead to the following conclusion:

- when the ratio  $\beta$  between the brace member and the chord member approaches one, the greater resistance is reached in the joints with the rectangular brace member, and failure occurs due to the lateral buckling of the vertical wall of the chord member;
- when the ratio  $\beta$  is considerably lower than one, failure occurs due to the deformation of the wall of chord member onto which the brace member is attached and, in terms of the resistance of the joint, the shape of the brace member plays no role.

The conclusions presented in this paper are only part of a number of results obtained in the experimental measurements. In the near future, the focus will be shifted towards joints composed of rectangular hollow sections in combination with rolled sections and the analysis and comparison of the experimental results with the results obtained using an appropriate finite calculation model.

*This work was funded by the project ITMS „26220120018“ “The Support to the Centre of Excellent Integrated Research into Progressive Building Structures, Materials and Technologies” and Grant VEGA No. 1/4220/07: “The Elastic-Plastic Behaviour and Bearing Capacity of Material Homogeneous and Combined Members under the Quasi-Static and Variable Load” of the grant agency VEGA of the Ministry of Education of the Slovak Republic and the Slovak Academy of Science.*

## BIBLIOGRAPHY:

- [1] STN 731403: Navrhovanie rúrok v oceľových konštrukciách, 1989
- [2] STN EN 1993-1-1: Design of steel structures, 2007

- [3] Packer J. A., Wardenier J., Kurobabne Y., Dutta D., Yeomans N.: Design Guide for Rectangular Hollow Section Joints under Predominantly Static Loading. Verlag TUV Rheiland, 1992
- [4] Beke P., Písomná práca k dizertačnej skúške – Analýza spojov uzavretých štvorcových prierezov, 2006
- [5] Kvočák V., Roth O., Hujdušová H.: Experimental investigation of end-plated joints. Zborník referátov 19.Česko-slovenská medzinárodná konferencia: Oceľové konštrukcie a mosty, 2000
- [6] Freitas, A. M. S., Mendes, F.C., Freitas, M. S. R.: Finite Elements Analyses of Welded T-Joints. In: Proceedings from 5th European Conference on Steel and Composite Structures, Eurosteel, 2008 Graz, 2008, pp.555 -560
- [7] Kindmann, R., Kraus, M., Vette, J.: On the Verification of Hollow Section Joint Resistances. In: Proceedings from 5th European Conference on Steel and Composite Structures, Eurosteel, 2008 Graz, 2008, pp.525 -530
- [8] Gizejowski, M. A., Barszcz, A. M., Kozłowski, A., Słęczka, L.: Modelling, Analysis and Design of Steel Semi-Continuous Frames. In: Progress in Steel, Composite and Aluminium Structures, Taylor & Francis Group, London, 2006, pp. 30-63, ISBN 0-415-40120-8





Lidia BUDA-OŻÓG<sup>1</sup>

## **CHANGES OF THE RESONANT VIBRATION FREQUENCIES FOR DIFFERENT CONCRETE BEAMS**

### **ABSTRACT**

This paper provides information about changes of resonant vibration frequencies for concrete and reinforced concrete (RC) beams. The objects of research were concrete beams of different dimensions and RC beams. The concrete beams were damaged by stage of cutting but RC beams were damaged by stage of static loading. After each stage of damage, the resonant vibration frequencies were determined. The parameters change their values while cutting or loading the beams due to cracking. On the basis of the obtained results from different beams, an effort was made to correlate the different dimension of beams, influence of reinforce and the damage of the tested beams with the changes of the modal parameters.

**KEYWORDS:** frequencies, beam, damage, concrete, reinforced concrete.

### **1. INTRODUCTION**

Development of non-destructive methods of diagnosing of the state of structure elements and building materials has been the subject of a large number of research works in recent years. The methods are particularly useful for diagnosing engineering constructions of particular importance, such as bridges, all kinds of containers, floating platforms, etc. where the occurrence of even the slightest damage is decisive of further operation. There are a few methods of detecting the damages of a structure. Visual inspection has been and still is the most common method used in detecting damage of a structure. However, conventional visual inspection can be costly and time consuming, especially when disassembly is necessary to provide access to the area under inspection. Non-destructive damage detection techniques such as ultrasonic, acoustic emission, x-ray inspection, etc. are "local" inspection approaches. Structural damage identification through changes in dynamic characteristics provides a "global" way to evaluate the structural state [3]. Therefore dynamics-based damage identification methods have been the subject of a considerable number of research projects in recent years (Deobeling 1996 [9], Vestroni and Capecchi 1996 [5,6], Ren and De Roeck 1998 [3,4]).

The article discusses methods of diagnosing the technical condition for different concrete and reinforced concrete (RC) beams, based on the changes of the resonant vibration frequencies. The concrete beams were damaged by stage of cutting but the RC beams were damaged by stage of static loading. After each stage of damage, the resonant vibration frequencies were determined.

<sup>1</sup> Ph.D. Eng., Rzeszow University of Technology, Rzeszow, POLAND

## 2. DESCRIPTION OF TEST BEAMS

The objects of research were 5 concrete beams marked CB1÷CB5 and 15 RC beams marked RB1÷RB15. The dimensions and reinforcement of the RC beams are shown in Fig. 1. One of the concrete beam (CB1) had the same dimensions as the RC beams. The dimensions of the rest of the concrete beams (CB2÷CB5) are shown in Fig. 2.

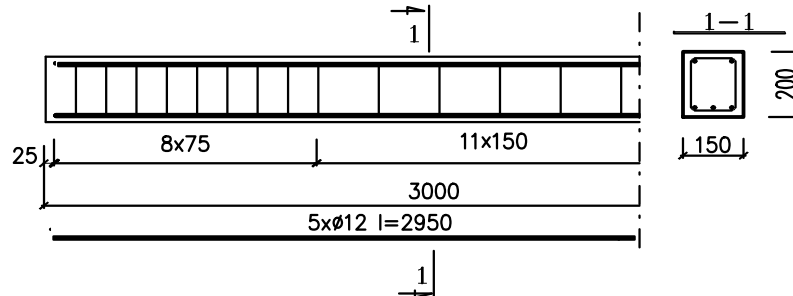


Fig. 1: Dimensions and reinforcement of beams RB1÷RB15

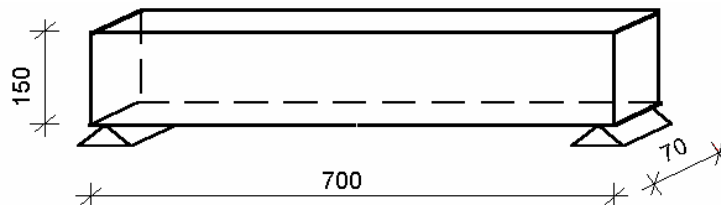


Fig. 2: Dimensions of concrete beams CB2÷CB5

The beams were made in stages. Each time the beams were made of the same class and recipe concrete. The properties of concrete: characteristic compressive strength of concrete ( $f_{ck}$ ) at 28 days and density ( $\rho$ ) for each beam are shown Tab.1.

Table 1. Characteristic compressive strength of concrete and density for beams

Number of beam	$f_{ck}$ [MPa]	$\rho$ [kg/m <sup>3</sup> ]
RB1, RB2, CB1	30,3	2187
RB3, RB4	30,0	2197
RB5, RB6	31,0	2211
RB7, RB8, RB13	30,1	2328
RB9, RB10, RB14	32,0	2264
RB11, RB12, RB15	29,7	2237
CB2, CB3, CB4, CB5	33,2	2175

## 3. TEST SETUP

Testing of concrete and reinforced concrete beams included both static and dynamic tests. The concrete beams were damaged by stage of cutting, while the RC beams were damaged by stage of loading. A series of step loaded static tests were aimed at producing successive damage to the beams. After each static load step (at the moment of displacement and strain stabilization), dynamic testing followed. Consequently, the dynamic characteristics of the test beams can be obtained for the reference state and each successive damage state.

### 3.1 Static Testing of RC beams

In the setup of static testing, the beams were simply supported at both sides with a cantilever of 0.1m for the beams RB1÷RB12. For the beams RB13÷RB15, the distances between supports were different and the dimension of the cantilever was changed from 0.1m to 0.5m. The change of distances between supports caused different damages in those beams. The all RC beam was loaded by two symmetric point loads at a distance of 1 m (four-point bending). Load was made by the steps from 1kN to failure of beam. While each load steps, displacements, strain, crack location and lengths were measured. After loading, at the moment of displacement and strain stabilization, the cracks were measured again. On the basis of crack location and lengths measured during load and unload steps and theory of flexure of reinforced concrete beam [1] describing the behavior of a beam cross section under increasing moment, four damage states were introduced for RB1-RB12 beams:

- D1 - no cracking was observed, the strains at this stage were very small, the stress distribution was linear.
- D2 - the stresses at the bottom of the beam cross-section reached the concrete tensile strength, cracking occurred. After cracking, the tensile force in the concrete was transferred to the steel. In the compression zone the stress distribution was linear. In this damage state cracks width of 0.1 – 0.3 mm under loading condition were observed. After unloading cracks width less than 0.1mm was visible.
- D3 - as the load was increased, the stress distribution in the compression zone became more markedly non-linear. This stage was observed, when some cracks closed while others were increased rapidly. For this damage state cracks width of 0.5 – 1.0 mm under loading condition were observed and 0.1 – 0.2 mm after unloading.
- D4 - failure of the beam, cracks width above 1.0 mm, evolution of cracks to compression zone with simultaneous crushing of concrete of the compression face.

Fig. 3 shows the crack pattern and damage for states number 2 and 4.

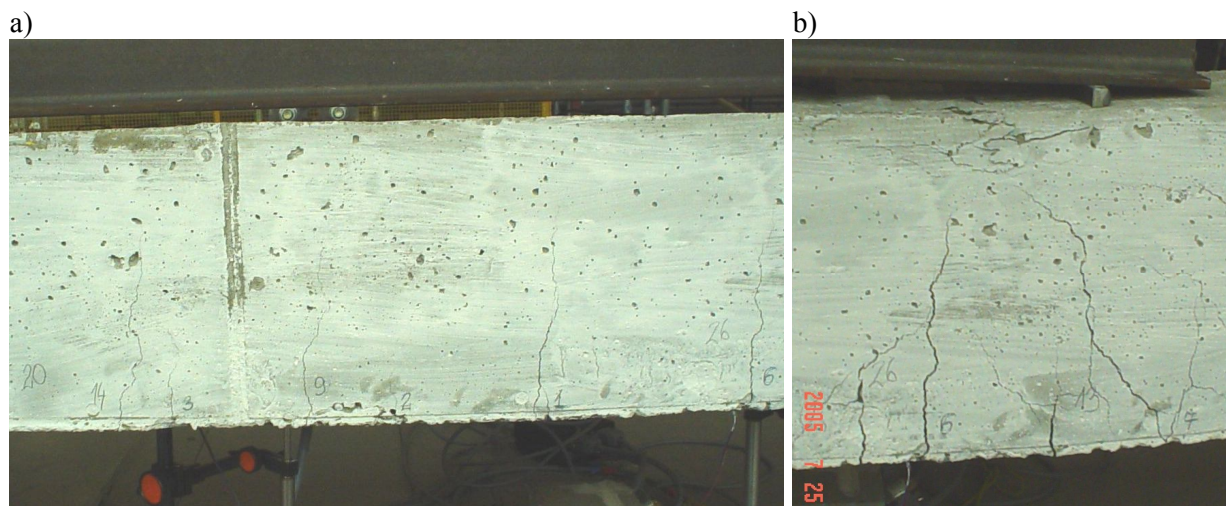


Fig. 3. Crack pattern and damage (RB1÷RB12): a) state 2, b) state 4, failure of the beam.

Analogously, on the basis of the progression of cracking, four damage states for RB13÷RB15 beam were introduced:

- DS1 - no cracking was observed,
- DS2 - flexural cracking width less than 0.3mm during loading, after unloading cracks were no visible,

- DS3 – inclined cracks width less than 0.3mm under loading condition. Flexural cracks less than 0.5mm during the loading.
- DS4 – failure of the beam, inclined cracks width above 1.0 mm, with simultaneous crushing of concrete of the compression zone. Fig. 4 shows the failure of the beam.

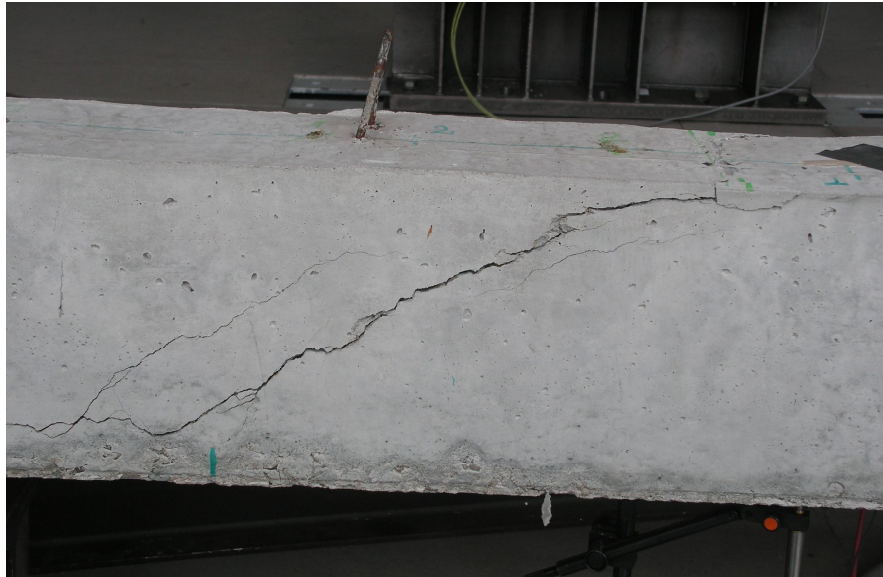


Fig. 4. Failure of RB13÷RB15.

### 3.2 Cutting of Concrete Beams

The concrete beams CB1÷CB5 were damaged by stage of cutting. The beam CB1 was cut in the middle of its length to the depth of 1, 4 and 6 cm. The beams CB2÷CB5 were cut in the middle of their length and within the distance of 17 cm from support. The changes of frequencies were determined for the following stages of cutting:

- P1- all beams cut in the middle of their length to the depth of 2 cm.
- P2- beams CB2, CB3 cut in the middle of their length to the depth of 4 cm, beams CB4, CB5- cut in the middle of their length to the depth of 2 cm and within the distance of 17 cm from support –2 cm deep
- P3- all beams-cut in the middle of their length to the depth of 4 cm, within the distance of 17 cm from support –2 cm deep
- P4 - all beams-cut in middle of their length to the depth of 4 cm, within the distance of 17 cm from support –4 cm deep.

### 3.3 Dynamic testing

Dynamic measurement was at first performed for the reference state of the test beams. This test result serves as a reference for further comparison of dynamic characteristics at different damage stages. After each static load step the beam is unloaded, and when the displacements and strains stabilized, dynamic parameters were measured. That way it was found out how they change, depending on damage. The setup of dynamic testing is shown in Fig. 5.

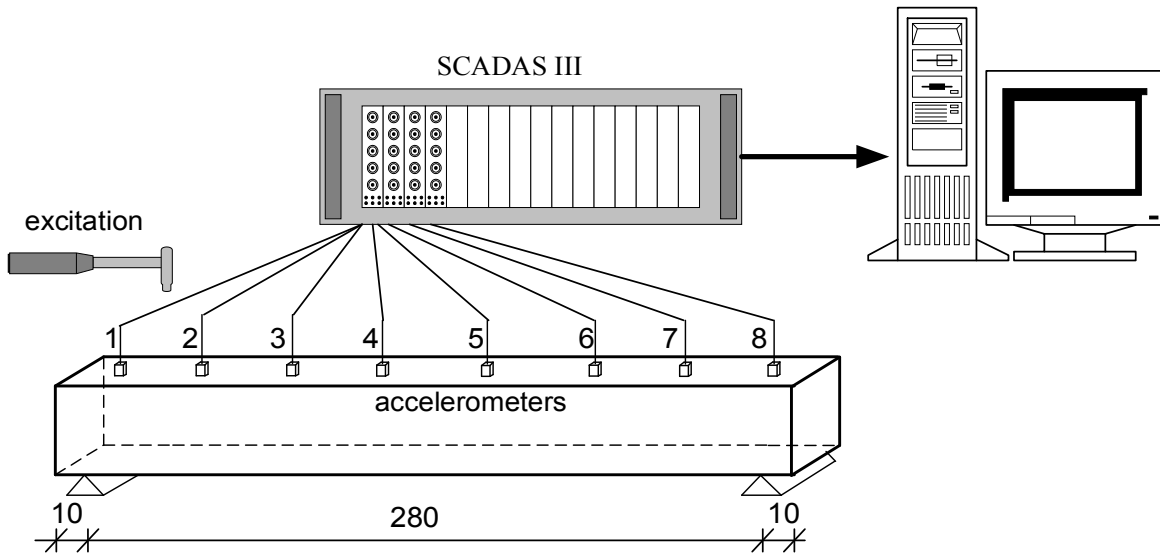


Fig. 5. Dynamic test setup

During dynamic testing each beam was excited by means of an impact hammer at three independent points on the beam. The response of beams to the impulse excitation was recorded by eight accelerometers. The data signal from each accelerometer was recorded by SCADAS III instrumentation recorder and it was processed by means of LMS CADA-X software from LMS Incorporated.

Frequency characteristics for each beam at each load and cut step were obtained. The natural frequencies are identified visually via the amplitude peaks of the frequency spectrum. The frequencies of RC beams and CB1 beam were selected from the whole range of frequency characteristics measured from 0 Hz to 500Hz, but for the beams CB2-CB5 the range of frequency characteristics were measured from 0 Hz to 7000Hz

The mean and standard deviation of the relative changes of frequencies with the respect to the reference state (undamaged state) for five identified frequencies and damage states for RB1÷RB12 beams are summarized in Tab. 2. The mean and standard deviation of the relative changes of frequencies for three identified frequencies and damage states for RB13÷RB15 beams are summarized in Tab. 3. The relative frequency changes of resonance frequencies given in this table were calculated from:

$$\Delta f_{(i)}^k = \frac{f_{r(i)} - f_{d(i)}^k}{f_{r(i)}} * 100\%$$

where:

- $f_{r(i)}$  - reference resonance frequency
- $f_{d(i)}^k$  - resonance frequency after damage
- $i$  - number of frequencies
- $k$  - number of damage states

Table 2: Decrease of selected frequencies depending on four damage states (mean  $\pm$  standard deviation) for RC beams (RB1÷RB12)

Damage states	Mean of relative change of frequencies $\pm$ standard deviation				
	frequency 1	frequency 2	frequency 3	frequency 4	frequency 5
	[%]	[%]	[%]	[%]	[%]
D1	0.6 $\pm$ 0.8	0.1 $\pm$ 0.4	0.2 $\pm$ 0.6	0.4 $\pm$ 0.8	0.3 $\pm$ 0.5
D2	8.8 $\pm$ 2.2	4.8 $\pm$ 2.5	2.1 $\pm$ 1.4	5.0 $\pm$ 1.6	7.7 $\pm$ 2.6
D3	14.5 $\pm$ 2.5	8.9 $\pm$ 2.3	4.1 $\pm$ 1.1	7.8 $\pm$ 1.4	13.3 $\pm$ 2.1
D4	25.1 $\pm$ 1.7	13.6 $\pm$ 1.4	7.9 $\pm$ 1.2	11.3 $\pm$ 3.3	19.2 $\pm$ 2.5

Table 3. Decrease of selected frequencies depending on four damage states (mean  $\pm$  standard deviation) for RC beams (RB13÷RB15)

Damage states	Mean of relative change of frequencies $\pm$ standard deviation		
	frequency 1	frequency 2	frequency 3
	[%]	[%]	[%]
DS1	0.9 $\pm$ 1.3	1.2 $\pm$ 0.7	1.3 $\pm$ 0.8
DS2	12.5 $\pm$ 2.5	12.3 $\pm$ 3.1	10.8 $\pm$ 3.8
DS3	16.4 $\pm$ 1.0	18.1 $\pm$ 1.2	16.9 $\pm$ 1.9
DS4	22.6 $\pm$ 3.7	23.3 $\pm$ 3.2	23.3 $\pm$ 3.2

Tab. 4 includes the changes of four selected frequencies for CB1 beams. The relative changes of the first and fifth frequencies depending on the states of cutting for CB2-CB5 beams are presented in Tables 5 and 6

Table 4. Decrease of selected frequencies depending on the stage of cutting for CB1 beam

Depth of cutting [cm]	Changes of frequencies			
	frequency 1	frequency 2	frequency 3	frequency 4
	[%]	[%]	[%]	[%]
1	2.7	1.0	1.0	3.7
4	5.5	1.0	1.6	3.7
6	8.3	4.2	4.4	6.3

Table 5. Decrease of the first selected frequencies depending on stage of cutting for the concrete beams (CB2÷CB5)

Number of beams	Changes of frequencies for stage of cutting			
	P1	P2	P3	P4
	[%]	[%]	[%]	[%]
CB2	4.7	11.2	16.4	17.2
CB3	3.4	10.3	13.0	15.1
CB4	7.7	9.7	19.2	20.3
CB5	6.9	8.7	19.5	23.8

Table 6. Decrease of the fifty selected frequencies depending on stage of cutting for the concrete beams (CB2÷CB5)

Number of beams	Changes of frequency for states of cutting			
	P1	P2	P3	P4
	[%]	[%]	[%]	[%]
CB2	2.7	7.7	8.3	9.9
CB3	2.4	7.2	8.2	10.4
CB4	3.1	3.2	9.1	10.8
CB5	3.3	3.4	9.3	11.8

#### 4 SUMMARY

The present paper describes a procedure of identification of damage through changes in dynamic characteristics of concrete and reinforced concrete (RC) beams. The obtained results show that changes of frequencies depend on slenderness ratio of a beam. Bigger changes are observed for beams with less slenderness ratio (beams RB13÷RB15 and CB2÷CB5) than for beams with more slenderness ratio (beams RB1÷RB12 and CB1). The number of identified frequencies in the range of frequencies measured from 0 Hz to 500Hz, depends on reinforcement of beams. For reinforced beams RB1÷RB12 five frequencies are identified but for the concrete beam CB1 (beam about the same dimensions as RB1÷RB12) only four ones. The obtained results for RC beams show that it is possible to identify the introduced damage stages on the basis of dynamic response of the structure. Big mean decreases of selected frequencies are observed after first cracks appear and at the moment of failure. For RC beams (RB1÷RB12) observed the changes are the biggest for the first and fifth frequencies, for the rest of resonance frequencies the decreases of frequencies are smaller but still visible to identify. For RC beams (RB13÷RB15) mean decreases of all selected frequencies are similar. The present experimental research and its estimation are an introduction to further research to be done on real reinforced concrete building constructions.

#### REFERENCES

- [1] J.G. MacGregor, J.K. Wight, Reinforced Concrete, Mechanics and Design, Pearson Prentice Hall, New Jersey 2005.
- [2] L.C. Hollaway, M.B. Leeming, Strengthening of reinforced concrete structures, Woodhead Publishing Ltd, Cambridge 2001.
- [3] W. Ren, G. De Roeck, Structural Damage Identification using Modal Data, *Journal of Structural Engineering*, **1**: 87-104, 2002.
- [4] J. Maeck, M. Abdel Wahab, G. De Roeck, Damage Detection in Reinforced Concrete Structures by Dynamic System Identification, *Proceedings ISMA 23, Noise and Vibration Engineering*, Leuven, Belgium, **9**: 939-946, 1998.
- [5] B. F. Vestroni, D. Capecchi, Damage Detection in Beam Structures Based on Frequency Measurements, *Journal of Engineering Mechanics*, **7**: 761-768, 2000.
- [6] B. F. Vestroni, D. Capecchi, Damage evaluation in cracked vibrating beams using experimental frequencies and finite element models, *Journal of Vibration and Control*, **2**: 69-86, 1996.
- [7] S.A. Neil, M.S. Williams, P.D. McFadden, Nonlinear Vibration Characteristics of Damaged Concrete Beams, *Journal of Structural Engineering*, **2**: 260-267, 2003.
- [8] S.S. Law, X.Q. Zhu, Nonlinear Characteristics of Damaged Concrete Structures under Vehicular Load, *Journal of Structural Engineering*, **8**: 1277-1285, 2005.

- [9] S.W. Deobeling, C.R Farrar, M.B. Prime, D.W. Sheritz, Damage identification and health monitoring of structural and mechanical systems from changes in their vibration characteristic: a literature review, Los Alamos Natl. Lab, 1996.



Jakub DOLEJŠ<sup>1</sup>  
Ivan TUNEGA<sup>2</sup>  
Václav HATLMAN<sup>3</sup>

## **EXPERIMENTS WITH HIGH PERFORMANCE STEEL AND COMPOSITE MEMBERS**

### **ABSTRACT**

It is generally known that reduction of total construction mass leads to a decrease of secondary costs as for example transport, assembly, disassembly etc. High performance materials can be effectively used in many types of common structures. Despite a good accessibility they are still not frequently used nowadays. The basic difficulty is a missing knowledge of their behaviour in structures.

**KEYWORDS:** steel, concrete, high strength, high performance, shear connection, long joint, bolt

### **1. GENERAL**

Research focused on high performance materials is running at CTU in Prague since 2003. Two main issues are studied: composite beams made of high performance concrete (since 2003) and higher steel I sections and connection of high strength steel tension members (started in 2007).

Ordinary design rules for composite steel-concrete beams with respect to specific material properties bring many questions. The main difficulties are caused by a special behaviour of connection studs in high performance concrete as well as a stress distribution along the high performance concrete cross section height. Results of experimental research with composite beams of real size made of steel S460 and concrete C70/85 are presented in submitted paper. Special attention is focused on shear connection and normal stress distribution. Possibility of partial connection has been studied.

Main issue of high strength steel research is investigation of long bolted joint of simple tension elements. This work is based on conclusions of research carried out at the University of Ljubljana [3]. Goal of CTU research is to verify or modify a design formula for long bolted joint given in [2] for normal strength steel. High strength steel has different mechanical properties, for example ductility and strain-hardening which can cause different response of structural member.

<sup>1</sup> Assistant Prof. Dr. Eng., Czech Technical University in Prague, Prague, CZECH REPUBLIC,

<sup>2</sup> Eng., Czech Technical University in Prague, Prague, CZECH REPUBLIC,

<sup>3</sup> Eng., Czech Technical University in Prague, Prague, CZECH REPUBLIC.

## 2. ARRANGEMENT OF EXPERIMENT WITH LONG BOLTED JOINT

### 2.1 Model

First experiments with long bolted tension joint of steel S960 plates have been carried out. Pilot specimen was tested in 2007. Arrangement of experiment was accomplished according to [2], parts for common grade steel with consideration of different mechanical properties of high strength steel. Main attention was paid to lower ductility and to manufacturing imperfections, which can strongly affect distribution of tension force among single bolts.

It was expected that both bearing resistance and net cross section resistance are higher than shear resistance of bolts. Specimen consisted of two plates connected with 10 M12 - 10.9 bolts without prestressing: Fig. 1. Spacing between bolts was considered in accordance with [2]. Fabrication of plates was prepared in common structural steel workshop to obtain response of common member.

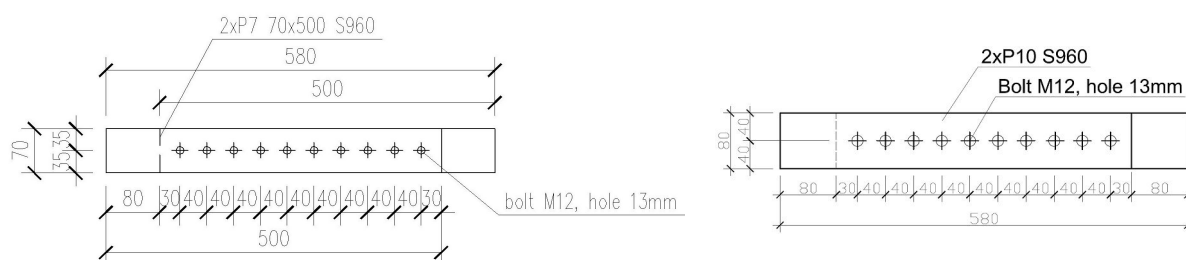


Fig. 1. Arrangement of pilot experiment (a) and common experiment (b)

Implicit method for measuring of force at each bolt position has been used by means of strain gauges placed on the plate surface. Strain gauges can record transferred force distribution by strain measuring in net cross sections. Strain gauges have been placed on both sides of each bolt hole to verify symmetry of loading. Based on this thesis it was designed a system of placement of strain gauges, which can help to describe flow of stress in net cross section. First strain gauge at each bolt was placed as close as possible to bolt head: Fig. 4. Strain gauges HBM 1-LY11-6/120 have been used for all samples.

### 2.2 Results of experiments

Tension tests of basic material have been carried out to obtain basic mechanical properties. Tension specimens have been made by the same industrial technology as main samples. Results are shown at Fig.2.

#### 2.2.1 Pilot experiment - sample S960-01

Pilot experiment was loaded by recommended step-by-step procedure. Maximal loading step was set on 50kN. Surface of plates was greased to minimize friction to obtain maximum force transferred by bolts. Expected maximum force was around 350kN for net cross section failure, actual force was  $F_{ext1} = 385\text{kN}$ . Failure was caused by net cross section collapse at first bolt: Fig. 3.

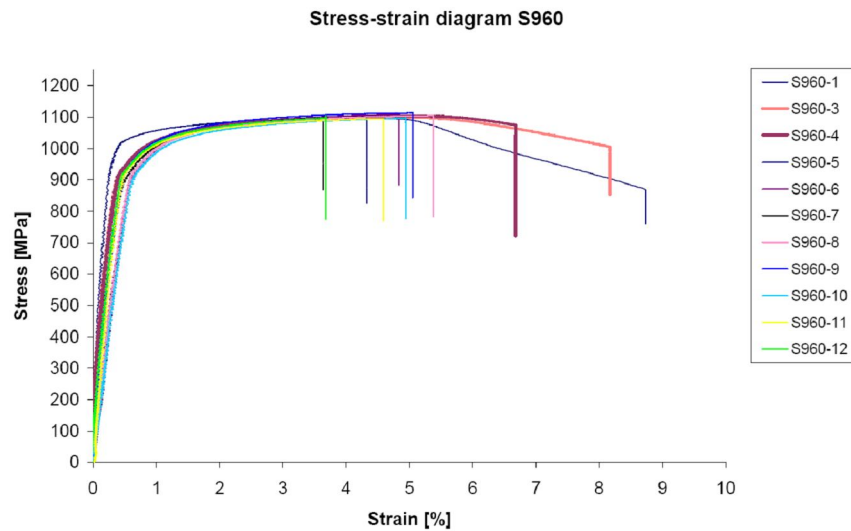


Fig. 2. Results of tension tests

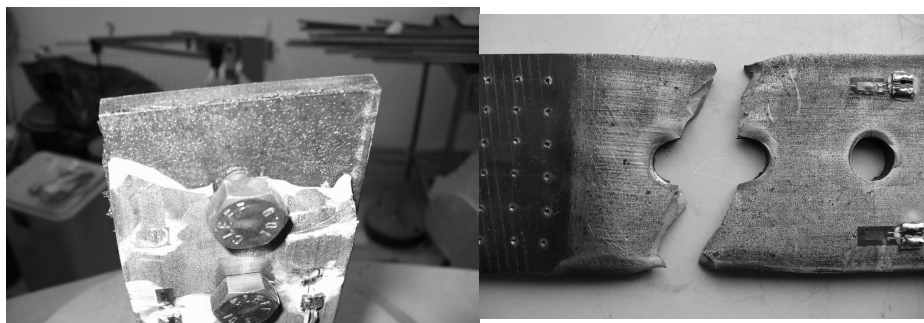


Fig. 3. Failure of tested plate S960-01

Special attention was paid on stress distribution in net cross section. Fig. 4 shows flow of stress in dependence on loading tension force. Level of stress at edges of hole and plate were extrapolated by bilinear curve. Maximum stress in plate was cut by value  $f_{u, nom} = 1099,44$  MPa. This value was achieved by material tension test.

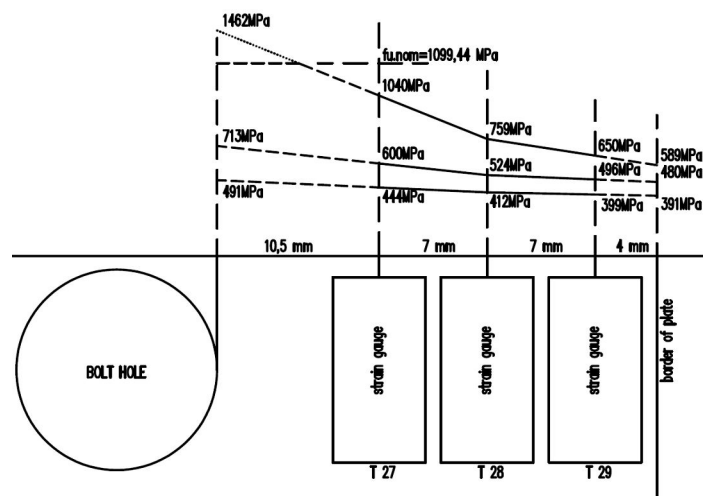


Fig. 4. Flow of stress in net cross section

Transfer of tension force by single bolts was investigated in next steps. For high strength steel with low ductility it was expected approximately linear flow of transfer.

### 2.2.2 Sample S960-02

Test of sample S960-02 was focused on verification of symmetry loading on plates in joint and distribution of tension force on single bolts. Strain gauges were set on both sides in the middle of both net section halves. This experiment was designed for shear collapse of bolts: Fig. 5. Loading step was 50kN and after 400kN it was modified to 25kN. Surface between plates was greased to minimize friction again. Expected maximum force was 520kN for bolt shear failure. Actual force was  $F_{ext2} = 525\text{kN}$



Fig. 5. Joint S960-02 after collapse

Fig. 6. shows that array of forces have not parabolic distribution. Possible explanation can be manufacturing imperfections of single holes which can cause more or less random loading at bolts. HSS have lower ductility in plastic range; therefore imperfections cannot be compensated by deformation of net cross section. These imperfections can affect force transfer by bolts. Symmetry of the joint seems to be satisfactory.

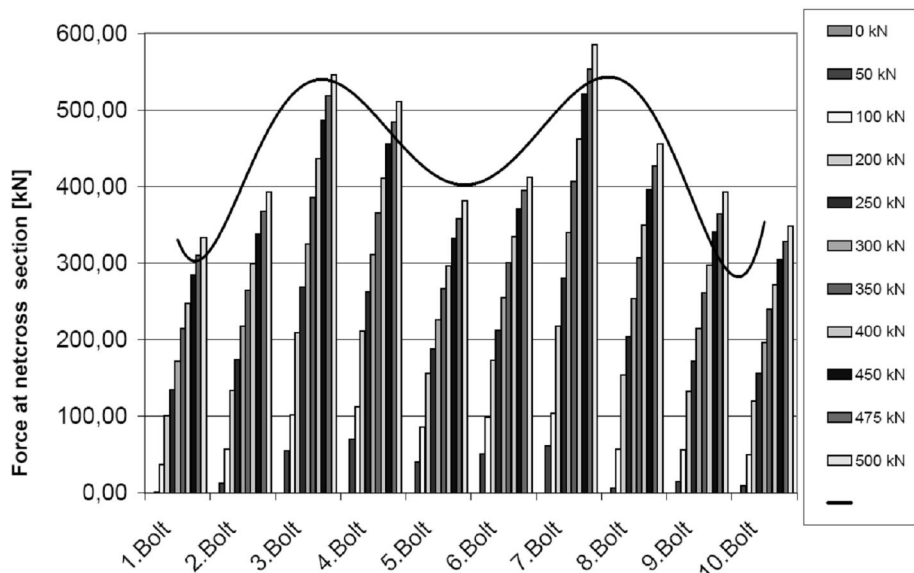


Fig. 6. Forces at net-cross section of sample S960-02

### 2.2.3 Sample S960-03

Experiment with S960-03 was focused on tension force distribution only. Results of the test are displayed at Fig. 7.

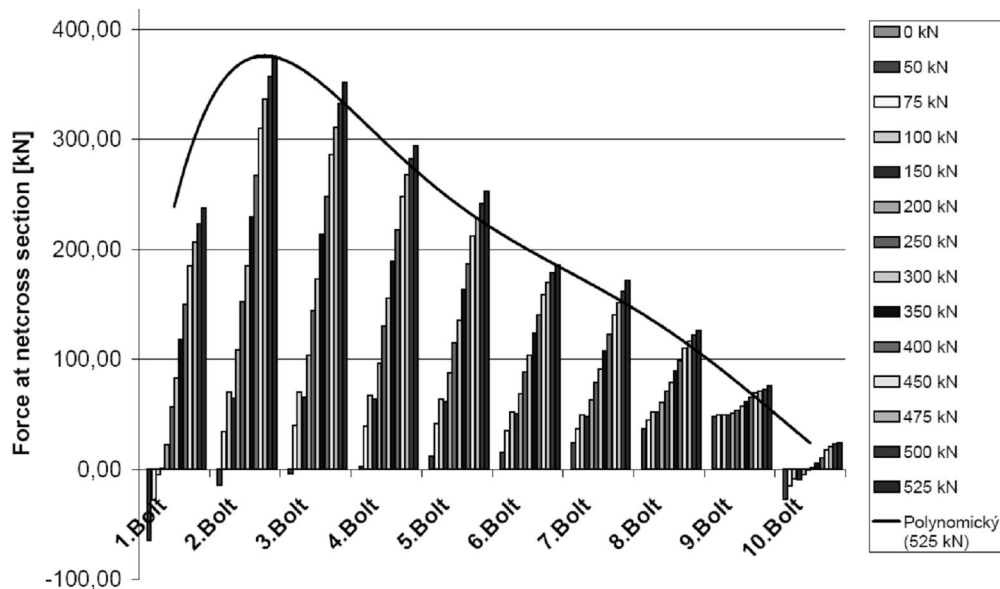


Fig. 7. Forces in net-cross section at S960-03

## 3. TESTS OF COMPOSITE BEAMS MADE OF HIGHER STRENGTH STEEL AND HIGH PERFORMANCE CONCRETE

Since new standard for composite members [8] has been issued it is possible to use steel grades S420 and S460 and concrete grades up to C60/75. It is obvious that structural design of members made of higher strength materials brings some difficulties and differences compared to elements compounded of common material grades. Standards also prescribe certain limitations for usage of high strength materials with partial shear connection.

### 3.1 Beams arrangement

Four four-point bending tests of simple supported beams have been carried out. The span of beams 1 and 2 was 4 800 mm, span of the beam 3 and 4 was 4 400 mm. Beams have been made of steel rolled members (HE260A, S 460) and concrete slabs 150 mm x 1000 mm (C 70/85). Shear connection has been provided by means of shear studs with nominal diameter  $d = 19$  mm and nominal tensile strength 450 MPa. Beams were loaded by means of two single loads symmetrically located in a distance 1000 mm: Fig. 8.

In the first case (beam 1) the arrangement was prepared to obtain a full connection between the steel beam and the concrete slab according to [8]. Shear studs were distributed uniformly in three rows along the whole beam length.

Beam 2 was considered as a partially connected beam. For the shear connection only one third of studs was used in one central row and uniform distances. The difference between two identical beams 1 and 2 was in a number of shear connectors only. Transverse reinforcement was 5 bars with 6 mm diameter per meter.

Beams 3 and 4 were considered as partially connected with similar shear connection degree as beam 2. Studs were distributed in accordance with the elastic shear force line: symmetrically at parts out of applied forces. One stud in the middle of the beam was used to restrain uplifting of the concrete slab only. Very important difference compared to beam 2 was in the degree of transverse reinforcement. Beam 3 and 4 was reinforced by 6,67 bars with 12 mm diameter per meter (1 transverse bar at each stud): Tab. 1.

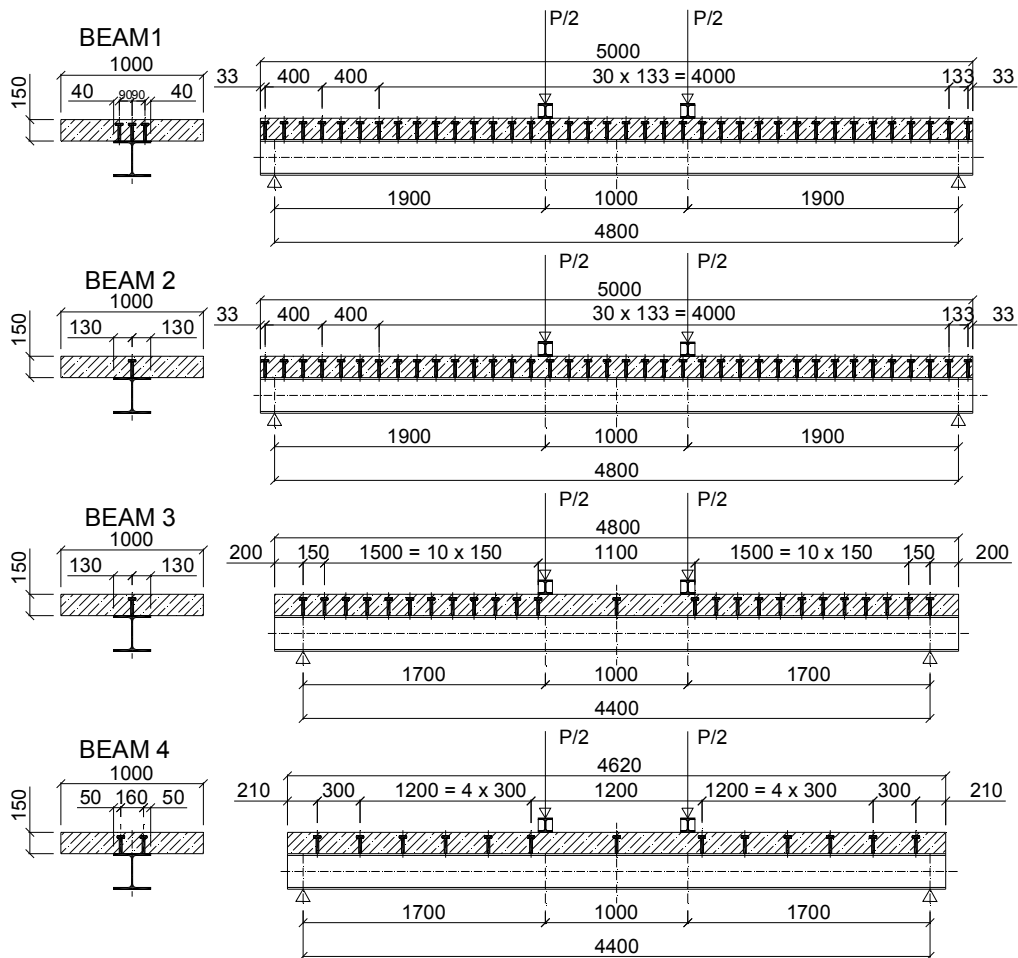


Fig. 8. Test arrangement and distribution of studs

### 3.2. Standard push-out tests

Experiments have been performed with the aim to determinate the load bearing capacity and ductility. Three samples have been made of steel rolled members (HE260A, S460) and concrete C 70/85. Shear connection has been provided by means of shear studs with nominal diameter  $d = 19$  mm and nominal tensile strength 450 MPa. Standard push-out tests according to [3] have been carried out: Fig. 9.

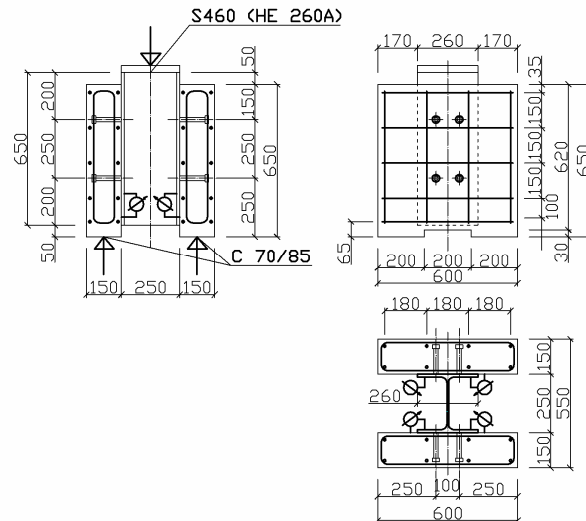


Fig. 9. Standard Push-Out Tests

For test evaluation of the tests the load-slip diagrams have been created for three samples: Fig. 10.

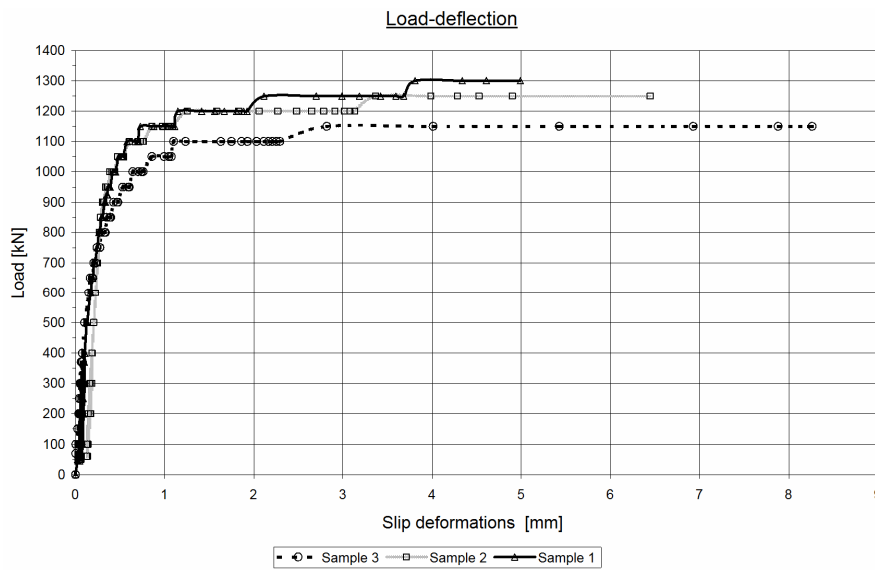


Fig. 10. Load-deflection: Studs Ø 19 mm

### 3.3 Headed shear studs Ø 19 [mm] in high strength concrete

The force from the connector is still transferred over the concrete wedge and base of the stud since there are friction forces acting in the joint between the wedge and concrete body [10]: Fig. 11.



Fig. 11. Deformations base of shear connector in high-strength concrete

### 3.4 Comparison of experiment and calculation

#### 3.4.1 Beam 1

The plastic stress distribution has been considered as a yield stress obtained from the material tests (494 MPa). Compression stress at the concrete top face has been considered by the value recommended in [6] as  $0,7 f_{c,exp} = 0,7 \cdot 77,7 \text{ MPa} = 54,4 \text{ MPa}$ .

It is obvious that almost whole steel cross section was in plastic stage at the failure load level. The bottom face of the steel beam achieved the yield stress at the load level about  $P = 650 \text{ kN}$  that is approximately 60 % of the failure load level. Top face of the concrete slab reached the stress value  $0,7 \cdot f_{c,exp}$  at the load level about  $P = 900 \text{ kN}$ . Because of a lack of measuring points the plastic deformation of the concrete slab is not too clear at the chart.

One can see the experiment agrees with the calculation very well. The difference in bending capacity is only about 2,5 % ( $M_{u,exp,1} = 1034 \text{ kNm}$ ,  $M_{u,theor,1} = 1010 \text{ kNm}$ ).

#### 3.4.2 Beam 2

Bottom flange of the steel member reached the yield stress ( $f_y = 497 \text{ MPa}$ ) approximately at the moment of the failure of the beam. Compression stress at the concrete top surface was about 42 MPa, that is less than  $0,7 f_{c,exp} = 54,4 \text{ MPa}$ .

Experiment has shown, that the actual load capacity is significantly less than the calculated capacity ( $M_{u,exp,2} = 617 \text{ kNm}$ ,  $M_{u,theor,2} = 755 \text{ kNm}$ ). The difference is approximately 22 % on the danger side. As an explanation we can say that the failure was caused by the cracked concrete along the shear studs line, not by the shear collapse of studs that had been assumed according to calculations. It is necessary to point out, that the minimum transverse reinforcement in accordance with [9] is obviously insufficient to carry the transverse tension caused by the compression of the concrete in longitudinal direction at line of shear studs.

#### 3.4.3 Beams 3 and 4

It was provided more measuring points at concrete part of the beam: Fig. 10. Bottom flange of the steel member reached in both cases the yield stress ( $\sigma_y = 495 \text{ MPa}$ ) approximately at the load level  $P = 700 \text{ kN}$ . Compression stress  $0,7 f_{c,exp,3} = 0,7 \cdot 70,5 \text{ MPa} = 49,4 \text{ MPa}$  was obtained at the same load level on the top face of the slab. Two neutral axes have been obtained due to partial shear connection.

The difference between calculated and experimental bending capacity is relatively small, about 8 % on safety side.



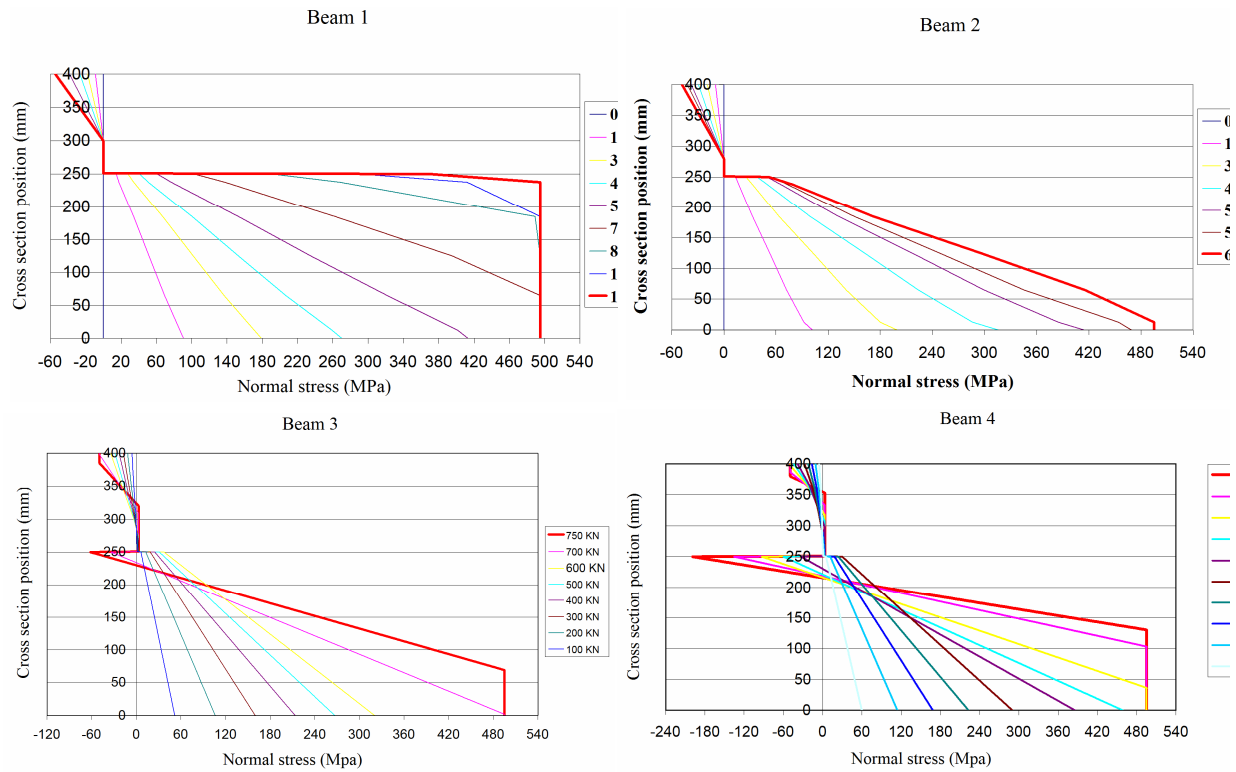


Fig. 12. Stress distribution at midspan

Table 1. Composite beams: Summary ( Steel S 460, Concrete C 70/85)

BEAMS		BEAM 1	BEAM 2	BEAM 3	BEAM 4
CONNECTION		full	partial	partial	partial
NUMBER OF SHEAR STUDS		114	38	25	25
TRANSVERSE REINFORCEMENT		5 R6/m	5 R6/m	6,67 R12/m	6,67 R12/m
SPAN	m	4,8	4,8	4,4	4,4
<b>CALCULATION</b>					
$f_y$	MPa	494	497	495	495
$f_c$	MPa	77,7	77,7	70,5	70,5
$M_{max,cal}$	kNm	1010	755	633	633
<b>EXPERIMENT</b>					
$P_{max,exp}$	kN	1088	649	803	802
$M_{max,exp}$	kNm	1034	617	683	682
$M_{max,exp}/M_{max,cal}$		<b>1,02</b>	<b>0,82</b>	<b>1,08</b>	<b>1,08</b>

#### 4. CONCLUSIONS

Long bolted joint:

- Results of experiments show that behaviour of high strength steel in long bolted joint can be different compared to normal grade steel. It seems that important role play production imperfections
- Additional experiments and theoretical study are necessary to find more exact explanation of high strength steel members' behaviour.

Composite beams:

- The compression stress limitation to  $0,7 f_{c,k}$  seems very realistic for full shear connection. The stress distribution achieved on a base of the experiment corresponded with this assumption very well.
- Load capacity of a beam with partial shear connection between the concrete slab and the steel member can match the theoretical value calculated according to [8] expressions for ductile connectors. Unexpected failure mode of partially connected beam can be obtained in case of insufficient transverse reinforcement of a concrete slab.

#### 5. ACKNOWLEDGEMENT

Authors convey their gratitude to project CEZ MSM VZ No. 6840770001 for financial support of this research.

#### 6. REFERENCES

- [1] Standard: Eurocode 3: Design of steel structures – Part 1.1: General rules and rules for buildings. CEN 2005.
- [2] Standard: Eurocode 3: Design of steel structures – Part 1.8: Design of joints. CEN 2005.
- [3] Može P., Beg D., Lopatič J.: Bolted Connections Made of High Strength Steel S960, ECCS TS 10, Paris 2005.
- [4] Kulak G.L., Fisher J.W., Struik J.H.A: Guide to Design Criteria for Bolted and Riveted Joints, Second Edition, John Wiley & Sons, 1973.
- [5] Collin P., Bernt J.: Eurocode for High Strength Steel and Applications in Construction, CEN /TC250/ SC3.
- [6] Institut of Steel Construction, RWTH Aachen: Use of high strength steel S 460. Part 6, Composite Beams Made of High Strength Steel and High Strength Concrete. Institute of Steel Construction, ECSC Steel RTD Programme, 2000.
- [7] Nethercot, David A.: Composite construction, London EC4P 4EE, 2003
- [8] Standard: EN 1994-1-1: Design of composite steel and concrete structures. Part 1.1: General rules and rules for buildings. CEN Brussels 2004.
- [9] EN 1992-1-1: Design of concrete structures. Part 1.1: General rules and rules for buildings. CEN Brussels 2004
- [10]Feldmann, M., Heger, J., Hechler, O., Rauscher, S., Wäschenbach, D., The use of shear connectors in high performance concrete, Proceedings of Stability and Ductility of Steel Structures, Lisboa, 2006.
- [11]Pierre-Claude Aitcin: Vysokohodnotný beton (High – Performance concrete), Praha, 2005 (In Czech).

Miron GOGOL<sup>1</sup>

## **SHAPING OF EFFECTIVE STEEL STRUCTURES**

### **ABSTRACT**

On the basis of the performed design of metal combined structures, it is shown, that logical, rational conception in the process of design is the most rational method of stress regulation. Such method requires no additional material charges. It is underlined, that the problem of structural design, in that number of combined, above all is a problem of their rational shape. There is developed generalized mathematical model of calculation of the combined structures on the basis of energy approach taking into account the deformed state of stiff beam. Idea of calculation method: at first on the basis of decomposition method system is divided on two subsystems - main and secondary. Further, using the synthesis of the system, its stress- deformation state is calculated. The algorithm of regulation of the stress- deformation state of the system is represented. The efficiency of such regulation and examples of introductions of such rational structures is shown. Result can be applied to industrial and civil engineering.

**KEYWORDS:** model, method, equal stress state, efforts regulation, “combined” structures, efficiency.

### **1. INTRODUCTION**

Modern trends of design discuss strong the problem of efficiency increase of steel structures [1]. One of methods of solution this problem is the use of regulation of the stress- deformation state of “combined” steel structures in the process of design. The most often used types of steel structures there are floors and coverings (beams, girders, “combined” structures, stays, etc.). In industrial buildings roof consume to 36-56% of the general volume of works [2], [3]. Market demands presently and in a future probably will use buildings of small spans up to 30-36 m [4], [5].

Beams due to their technological advantages (continuous cross section, simplicity act.) and reliability are the most widely used [1-5]. At the same time their demerits is substantial unevenness of stress along the beam, that gives ineffective use of material. Partial correction of these demerits is achieved in beams on stiff intermediate supports, but difference between support and span moments also lowers their efficiency, though they are lighter to 10-12% [2-4]. Additional demerit of such beams is sensitiveness to supports set and necessity of extreme span reduction (to 20%).

---

<sup>1</sup> Prof. PhD. Eng. Lviv Polytechnic National University, Lviv, UKRAINE,

In the steel beams the best way to perform efforts regulation is to transform them in continuous steel beams [12-14], with substantial reduction of bending moments. This principle is used in the “combined” structures (sub diagonal beams, beams-girders, stays and hanging systems). Using pre tension of stiff beam in such structures it is possible to make them work as continuous beams on stiff supports. [1-4]. Such structure has also the substantial failings, as we said before. Therefore previous tension of the structural systems is ineffective. Without previous tension of stiffness beam the “combined” structures work, as elastic beams. That gives possibility of regulating of supports pliability (system of pendant) to attain the set correlation of supporting and span moments, up to tensions equalizing in main beam cross sections. Thus the untraditional calculation method of SDS regulation is the most rational. Increase of stiffness of sub diagonal beams is done by sloping [19-21].

Thus idea of stress deformation state (SDS) regulation of the system lies in such choice of geometrical parameters and descriptions of elements of the system, rational choice of structural shape, character of fixings on resistances, which will allow in its deformed state to get the desired distributing of efforts. In the process of increase of the external loading there is expected rational redistribution of internal efforts between elements with the result of the stress deformation state similar, as from action of previous tension. Regulation potential, that is covered in such “combined” systems by the rational stress deformation state of structure already in the stage of design for structures, creates rational scientific base of a new generation. The problem of calculation of building structures, in that number of steel “combined”, above all is a problem of their rational design. Method [15] which allows simultaneously with the decision of rational design develops in the given work, to structure stress deformation state. Sequence of calculation: [6-14] at first on the basis of decomposition system is divided on two subsystems - main and secondary. Further, using the synthesis of the system, its stress- deformation state is calculated. The power criterion of [17], and also requirement of stress deformation state come forward as criteria of rationality: stress equality, bending moment equality, maximal inflexibility, or minimum mass of structure.

The unique calculation model of the combined systems is presented as a beam on elastic supports [12], in which a beam means the stiffness beam, and resilient supports - system of springs (Fig.1)

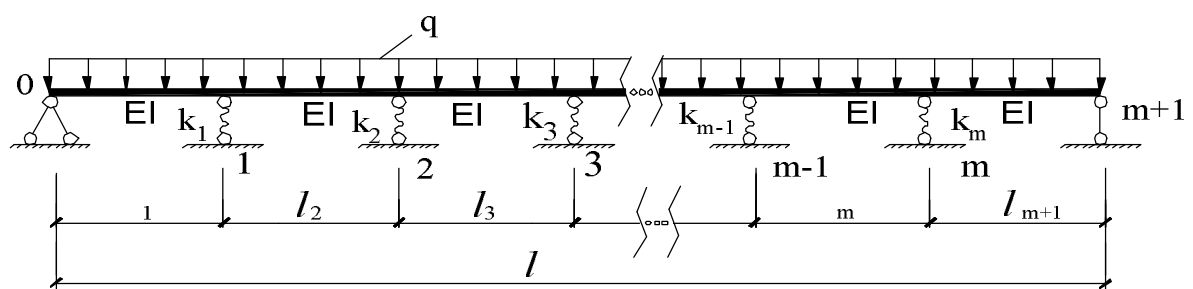


Fig.1. Chart of the generalized calculation model

The wide class of the “combined” steel structures of mass application is selected in which it is efficient to regulate the stress deformation state ( SDS) by calculation method (tab. 1) and for which it is possible to adopt a calculation chart in the type of beam on elastic intermediate supports.

For resilient supports it is suggested to use the Winkler model, after which reaction of elastic springs "R" is proportional to the size of its settling

$$R_i = K_i \Delta_i \quad (i = \overline{1, m}), \quad (1)$$

where  $K_i$  - stiffness coefficient for spring "i".

The calculation model differs from the real structure. In order to make it correct, it is necessary to use principle of compatibility, that is, that the points of contact of stiffness beam with elastic springs moved under loading on the same value, as knots points of suspension system of structure.

Opposing on classic theoretical pre-conditions for the record of mathematical model of the generalized calculation task for the "combined" structure we will use energy principles of structural mechanics. Then complete potential energy of the "e" system will be

$$\varepsilon = U + \Pi = \int_0^l \left( \frac{1}{2} E J_x \left( \frac{d^2 v_x}{dx^2} \right)^2 - v_x q \right) dx + \frac{1}{2} \sum_{i=1}^m K_i V_i^2, \quad (2)$$

where:  $v_x$  - function of beam bandings in all points on its length;  $E$  - deformation module to material of beam;  $K_i$  - is a stiffness coefficient of resilient support "i";  $I_x$  - is inertia moment of the beam;  $V_i$  - is a value of settling of resilient support "i".

These equalization describes the deformation state of the generalized calculation model at any values of "q" and "Ki" ( $i = \overline{1, m}$ ). According to energy variation principle of Lagrange the deformed system state will be actual, when infinitely small change of functions  $v_x$  - its variation  $\delta v_x$  - gives the infinitely small change of the total system energy  $\delta \varepsilon$ . This principle of condition of equilibrium of the system is written down

$$\delta \varepsilon (v_x) = 0. \quad (3)$$

Equalizations (2) and (3) give mathematical model for the generalized calculation (Fig.1).

## 2. ENERGY VARIATION METHOD

The energy variation method for salvation of mathematical model consists in the following. Equilibrium of the system, on the basis of dependence (2), after Dirikhlet theorem it is possible to estimate as minimum of "ε",

$$\delta \varepsilon = 0; \quad \delta^2 \varepsilon > 0 \Rightarrow \varepsilon = \varepsilon_{\min}, \quad \text{equilibrium of contact.}$$

If the case of stable equilibrium is chosen, ( $\delta^2 \varepsilon > 0$ ), minimum of potential energy of the system.

For this purpose the unknown function of  $v_x$  was set by a row

$$v_x = \sum_{i=1}^n \varphi_i a_{\varphi_i}; \quad (4)$$

where  $\varphi_i$  - functions which satisfy maximum and edge conditions and does not conflict with the kinematics of the system, that on Fig.1;

$a_{\varphi_i}$  - Unknown numbers due to which a row (4) satisfies the  $v_x$  function.

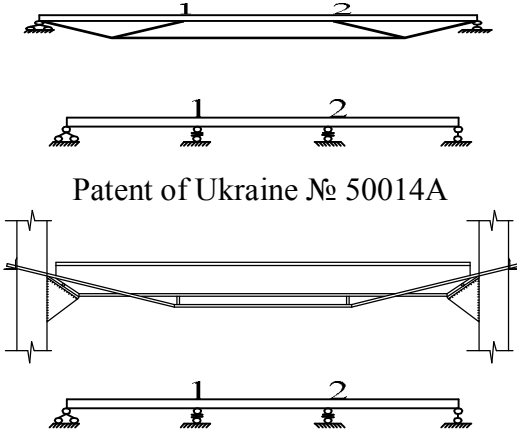
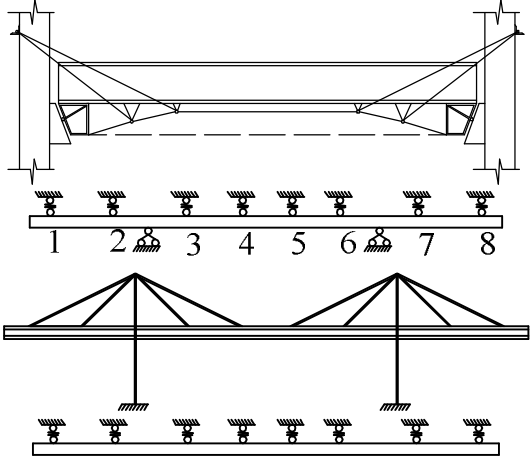
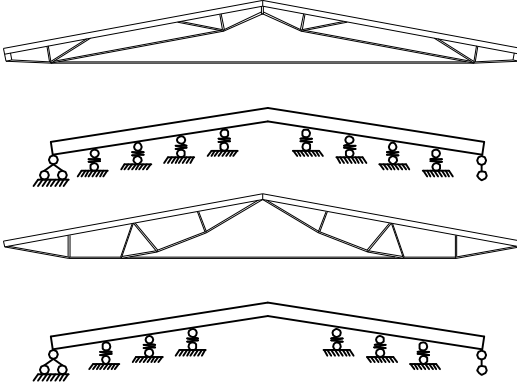
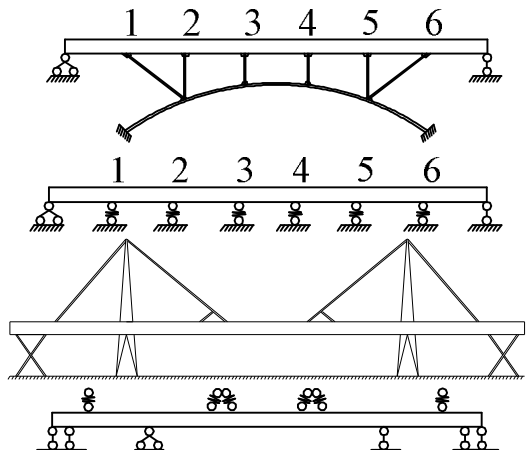
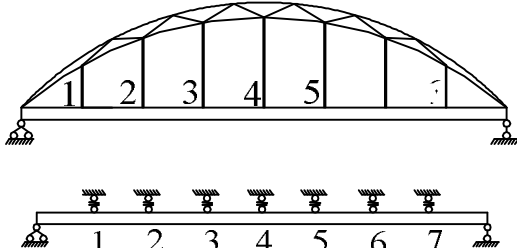
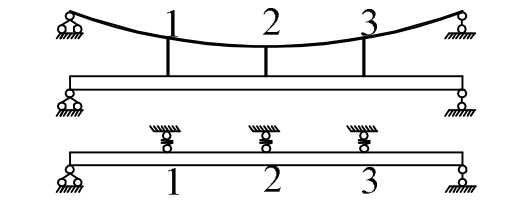
Every member of row (4) was given as a function  $\overline{\varphi}_i (i = \overline{1, n})$ , multiplied on other number such, that

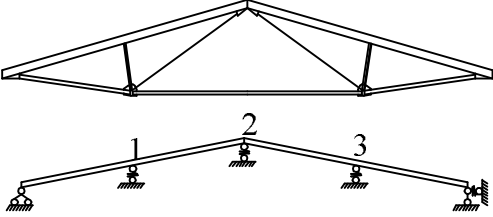
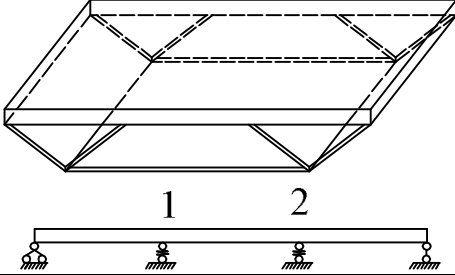
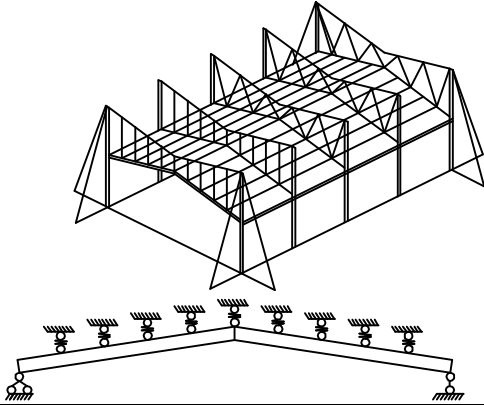
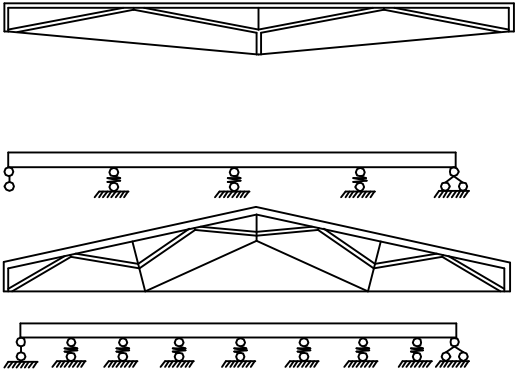
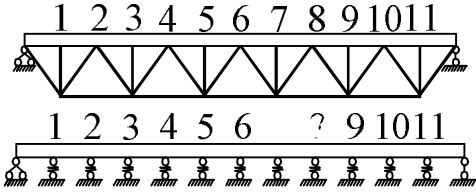
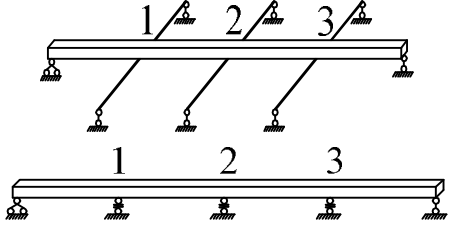
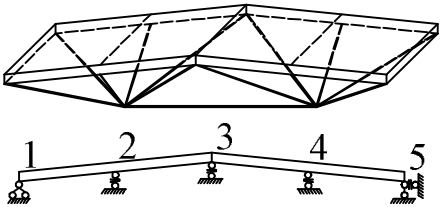
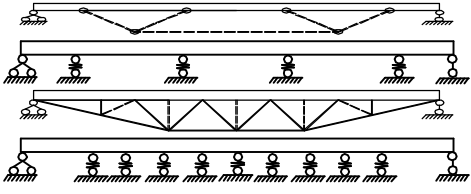
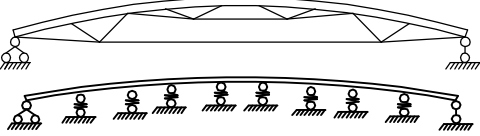
$$\varphi_i a_{\varphi_i} = \overline{\varphi}_i a_i, \quad (i = \overline{1, n}). \tag{5}$$

Thus in place of row (5), a row was got

$$v_x = \sum_{i=1}^n \overline{\varphi}_i a_i, \tag{6}$$

Table 1. Combined structures for the rational design.

Structural and calculation scheme	Structural and calculation scheme
<p>1. Sub diagonal systems Patent of Ukraine № 48841A</p>  <p>Patent of Ukraine № 50014A</p>	<p>2. Stay systems Patent of Ukraine № 46983A</p> 
<p>3. Large span stay systems</p> 	<p>4. Bridge structures</p> 
<p>5. Suspended coverage</p> 	<p>6. The combined systems with stiff struts</p> 

Structural and calculation scheme	Structural and calculation scheme
<p>7. Steel concrete structures</p> 	<p>8. Block girder</p> 
<p>9. Suspended stay roof</p> 	<p>10. Steel wood systems</p> 
<p>11. girder structures</p> 	<p>12. crossed systems</p> 
<p>13. Panel - stay systems</p> 	<p>14. Strengthening of structures</p> 
<p>15. Arch – sub diagonal systems</p> 	

On the basis of classic method of moving, set on superposition principle by the elementary numbers values  $a_i (i = \overline{1, n})$ , are gain functions  $\bar{\varphi}_i (i = \overline{1, n})$  which approximate the function of  $v_x$  and have the continuous first derivatives.

After a substitution approximated by a row (5) the  $v_x$  function in a formula (1) got value of “ $\varepsilon$ ” as a function which is named a functional

$$\varepsilon = \varepsilon (a_1, a_2, a_3, \dots, a_n, P), \quad (7)$$

On the basis of laws of variation condition (3) is presented

$$\delta\varepsilon = \frac{\partial\varepsilon}{\partial a_1} \delta a_1 + \frac{\partial\varepsilon}{\partial a_2} \delta a_2 + \dots + \frac{\partial\varepsilon}{\partial a_n} \delta a_n = 0 \quad (8)$$

At independent variations  $\delta a_i$  ( $i = \overline{1, n}$ ) equalization (8) can be self-possessed only on terms

$$\left. \begin{array}{l} \frac{\partial\varepsilon}{\partial a_1} = \frac{\partial U}{\partial a_1} + \frac{\partial \Pi}{\partial a_1} = 0 \\ \frac{\partial\varepsilon}{\partial a_2} = \frac{\partial U}{\partial a_2} + \frac{\partial \Pi}{\partial a_2} = 0 \\ \dots\dots\dots \\ \frac{\partial\varepsilon}{\partial a_n} = \frac{\partial U}{\partial a_n} + \frac{\partial \Pi}{\partial a_n} = 0 \end{array} \right\} \quad (9)$$

From the equalizations system (9) all unknown parameters  $a_i$  ( $i = \overline{1, n}$ ) were determined. Potential energy of deformation “U” is measured, as known by work of “A”, which is executed during translation of the system from the deformed state in initial, non deformed, that

$$U = A = \frac{1}{2} (P_1 \Delta_1 + P_2 \Delta_2 + \dots + P_n \Delta_n) = \frac{1}{2} (\vec{P})^T \vec{\Delta} \Rightarrow U = \frac{1}{2} (\vec{\Delta})^T \vec{P}, \quad (10)$$

where  $P_i$  and  $\Delta_i$  - accordingly the generalized forces, enclosed to the system in the points of “i”, and proper moving of these points.

### 3. CALCULATION OF THE DEFORMED STATE OF STIFFNESS BEAM

If on the stiffness beam “i” points impose the proper copulas, then, using principles of superposition, we are able to put down

$$P_i = r_{i1} \Delta_1 + r_{i2} \Delta_2 + \dots + r_{in} \Delta_n \Rightarrow \vec{P} = \begin{bmatrix} r_{11} & r_{12} & \cdot & \cdot & \cdot & r_{1n} \\ r_{21} & r_{22} & & & & r_{2n} \\ \cdot & \cdot & \cdot & \cdot & \cdot & \cdot \\ \cdot & \cdot & \cdot & \cdot & \cdot & \cdot \\ \cdot & \cdot & \cdot & \cdot & \cdot & \cdot \\ r_{n1} & r_{n2} & \cdot & \cdot & \cdot & r_{nn} \end{bmatrix} \cdot \begin{bmatrix} \Delta_1 \\ \Delta_2 \\ \cdot \\ \cdot \\ \cdot \\ \Delta_n \end{bmatrix} = R \vec{\Delta} \quad (11)$$





classic method if we replace unknown parameters  $a_i$  ( $i = \overline{1, n}$ ) to unknown  $z_i$  ( $i = \overline{1, n}$ ) of displacement classic method. A difference between the presented and classic method lie, at moving of the linear ties put on resilient supports, that is  $a_i$  ( $i = 4, 8, 12, \dots, n-2$ ), in the values of proper supports reactions  $r_{ii}$  ( $i = 4, 8, 12, \dots, n-2$ ). Values of Winkler coefficient «K» are added for the proper reactive efforts.

Reactive effort taking into account the support resiliency in the imposed tie will be

$$r_{ii} = \frac{12EI}{(0,5l_j)^3} + \frac{12EI}{(0,5l_{ju})^3} + K_i;$$

#### 4. SYNTHESIS OF THE SYSTEM AND ITS STRESS DEFORMATION STATE

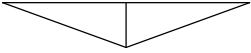
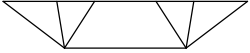





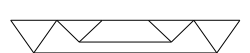

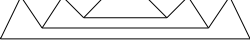
After reactive efforts in the system ties we found unknown parameters  $a_i$  ( $i = \overline{1, n}$ ). Consequently, in a matrix form the equalization (18) looks

$$R\vec{A} + \vec{R}_q = 0 \quad (19)$$

where the  $R$  - co diagonal matrix of system stiffness;  $A$  - vector of system points displacement "i" ( $i = \overline{1, n}$ );  $\vec{R}_q$  - vector of reactions in artificial supports from the external loading.

Thus, a vector  $\vec{A}$  gave the deformed state of beam and values of settling of resilient supports  $a_k$  ( $K = \overline{1, m}$ ). In the vector of settling indexes "a<sub>i</sub>" will be for resilient supports  $a_i$  ( $i=4, 8, 12, \dots, n-2$ ). Then after a formula (1), putting at "a" in place of "Δ", the vertical reactions  $R_{iq}$  were defined ( $i=4, 8, 12, \dots, n-2$ ) all resilient supports.

Table 2. Types of rational light sub diagonal girders with stress deformation and state regulation.

№	Combined system scheme	Range of use, Spans values, m	№	Combined system scheme	Range of use, Spans values, m
1		6,9,12	6		12,18,24,30
2		9,12,18	7		18,24,30,36, 42
3		12,18,24	8		9,12,18,24
4		12,18,24	9		45
5		9,12,18	10		63

Consequently, after a cross section method and equilibrium principle, normal efforts in the elements of stiffness beam reinforcement were found - elements of strut frame, which, as it said, are the statically determined systems. Effort in them was determined from equalizations of equilibrium of efforts projections on co-ordinate axes. In the improved combined systems calculation method where taken into accounts the deformed state of

stiffness beam unlike a traditional method: at first we determine deflections, and on their basis - effort. On that basis we offered [19-21] and patented a row of effective new light low element sub diagonal constructions by spans 9-63 m and rational range of their use. (Tab. 2). Efficiency comparison of a new construction [21] is executed with a typical girder (Tab. 3). Economy of material comparably with a typical girder by span 18 m achieves up to 27% with considerable simplification of producing technology.

Efficiency of the use of low elements sub diagonal girder (beam-girder) it is comparative with most used girders «Molodechno» is presented in Tab. 4. The steel economy comes up from 21% at span 12 m at the amount of elements 5 against 6, to 2% at span 30 m at an amount element 6 against 22. Also steel consumption for one bearing structure of roof with span 18 m at external loading near  $4,0 \text{ kN/m}^2$  (Tab. 5).

Table 3. Technical – economics indexes for 1 unit

№	Indexes	Measure	Typical girder L=18M	beam-girder L=18M	correlation
1	Structure mass	kg	3000	2189	73%
2	Labor time of production	hour	59	14,5	24,5
3	Cost of production and transporting	grn.	1350	560	42
4	Labor time of erecting	hour	6,0	6,3	105
5	Cost of erecting	grn.	520	550	106
6	Cost of erected structure	grn.	7536,6	5198,3	69
7	Economical effect	grn.		2338,3	

Table 4. Efficiency of combined structures

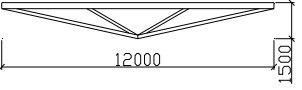
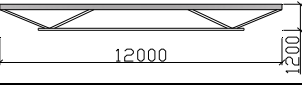
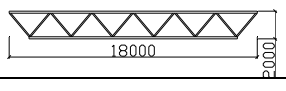
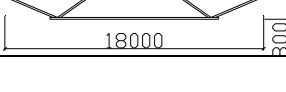
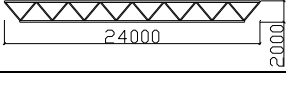
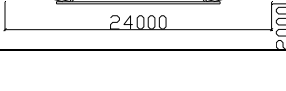
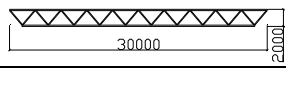
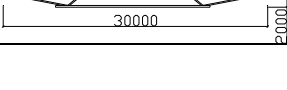
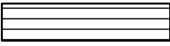
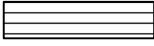
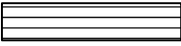
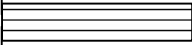
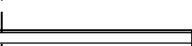

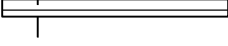


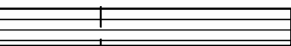


N	Girders scheme		Girder nods quantity		Mass of girder, kg		%
	«Molodjezno»	low element combined sub diagonal girders – «beam – girder»	typical	beam – girder	typical	beam – girder	
1			5	6	780	615	78,8
2			14	6	1310	1098	83,8
3			18	6	2035	1868	91,8
4			22	6	2513	2461	97,9

Table 5. Steel consumption indexes for one bearing structure of roof by span 18m at external loading near  $4,0 \text{ kN/m}^2$

Girder mass, kg		Structure type	Girder depth, m
903		beam-girder with parallel chords with effort	2,30
870		girder with perforated upper chords with	2,98
1050		Tube girder	2,30
1162 (reduced)		Reinforced concrete girder beam with double	2,30
1190		girder made of cubed welded tubes, angles	2,30
1205		girder with chords made of double T and angles	2,30
1310		girder made of cubed welded tubes, angles	2,30
1340		girder made of T and framing of single angles	2,30
1350		girder made of T and framing of double angles	2,30
1385		girder made of T and framing of T	2,30
1485		girder made of bars of paired angles	2,30
1500		girder made of single angles	2,30

As we can see from the table, the mass of beam-girder is less comparing to units with depth of 2,3 m. The mass of beam-girder is 3,8% higher comparing to girder with perforated upper chord with much less labor time. Efficiency of such regulation method (structure cost is to 15% lower comparing to typical ones) and given examples of inculcation of such structures: experimental factory, Lviv, business center "Pidzamze" Lviv, sanatorium "Zeneva" Truskavez and others. (Fig. 2-7).



Fig.2. Erection of low element sub diagonal girder with span  $L=12$  m. Sanatorium "Zeneva" Truskavez, 2004.



Fig.3. Appearance of beam-girder under construction  $L=18$  m. Sanatorium "Zeneva" Truskavez, 2007.



Fig.4. Light combined girders of floors with effort regulation.  $L=12$  m. business center "Pidzamze" Lviv, 2007.



Fig.5. Truss beam-girder  $L=12\text{m}$ . Experimental research factory, Lviv, 2004.



Fig.6. Beam-girder of floor



Fig.7. Beam-girder as composed cast in place reinforced concrete floor

## 5. CONCLUSIONS.

1. As result of stress deformation state (SDS), by means of calculation method is develop the combined structures of new generation.
2. Generalized method of the combined steel structure analysis is improved on the basis of energy variation principle (Lagrange principle) taking into account the deformed state of stiffness beam.
3. Universal design and analysis model of combined systems is based on - sub diagonal and stay systems as a beam on resilient elastic supports, in which a beam is considered as the stiffness beam, and resilient supports – as system of reinforcement.

4. Such method enables to define the deformed state of stiffness beam, which is taken into account at determination of efforts in the combined system. System, which provides equal safety of all units with the maximal economy of steel up to 17%.
5. On the base of the improved method of “combined” steel structures analysis, taking into account the deformed state of stiffness beam, the regulation method of stress deformation state (SDS) of the “combined” structures is developed. Rational shape and stiffness of elements cross sections is determined. It provides possibility of SDS regulation in the stiffness beam on its length to obtain equal tensions in main cross sections.
6. The solution of reverse task rational design, allows simultaneously solve direct of calculation of structure SDS.
7. The efficiency of SDS regulation method of the combined structure is appraised, due to which the economy of material comparably with the standard is up to 27% with considerable simplification of technology.
8. On the basis of analysis researches and study of influence of the stiffness beam deformed state on the combined steel structures, recommendations for the structural improvement and the new structural forms of the combined systems with mass less to 20%, are protected by the patents of Ukraine on inventions (Patents of Ukraine: № 50014, № 46383, № 48841)
9. The structural forms of the light sub- diagonal girders are applied with spans from 9 to 63 m on the basis of calculation method SDS. It is expedient to apply in place of typical structures of floors and roofs. An application of the combined structures with a general calculation scheme is extended (with the stiffness beam on resilient supports) on large-spans girder systems, light metal-wood structures, stay, hangings and arch - stay systems, composed structures, bridge systems, strengthening. An album and practical recommendations are the methods of design and SDS regulation. The results of research are inculcated in practice of building and educational process. The combined systems are applied in the process of design of such objects: factory of experimental mechanical tests, Lviv, 2004; a sanatorium of «Geneva» Truskavets, 2004; business-center of «Pidzamche», Lviv, 2007; cement factory in Mykolaiv, 2007; «Al'ba» Ltd, Shchirets', 2006; firm «VEEM», Lviv. 2007.

## REFERENCES

- [1] Shen Z.Y., Li G.Q., Zhang Q.L. Advances in steel structures. Fourth international Conference 13-15 June 2005 in Shanghai, China, 2005.
- [2] Пермяков В.О., Нілов О.Р., Шимановський О.В., Белов І.Д., Лавритенко Л.І., Володимирський В.О. Металеві конструкції.- К.: Видавництво «Сталь», 2008.
- [3] Брудка Я., Лубински М. Легкие стальные конструкции. Пер. с польск. М., Стройиздат, 1974.
- [4] Lubinski M., Filipowicz A., Zoltowski W. Konstrukcje metalowe. Czesc 1.- Warszawa: «Arkady», 2003.
- [5] Lubinski M., Zoltowski W. Konstrukcje metalowe. Czesc 2.- Warszawa: «Arkady», 2004.
- [6] Гоголь М.В. Особливості регулювання напружено-деформованого стану комбінованих сталевих конструкцій / М.В. Гоголь, М.Р. Більський // Промислове будівництво та інженерні споруди. – 2009.- № 1
- [7] Гоголь М.В. Проектування і розрахунок раціональних комбінованих металевих конструкцій / М.В. Гоголь // Металеві конструкції. – 2008. – Том 14. - № 4.
- [8] Пермяков В.А., Гоголь М. В., Пелешко И. Д. Комбинированные металлические конструкции с регулированием и их оптимизация // Наука и инновации в современном строительстве. Междунар. научн.-практ. конф. Сакт-Петербургский государственный архитектурно-строительный университет. Санкт-Петербург, 17-19 окт. 2007 г.- Санкт-Петербург.- 2007.

- [9] Гоголь М.В., Пелешко І.Д., Більський М.Р. Регулювання зусиль у стержневих металевих конструкціях // Будівельні металеві конструкції: сьогодення та перспективи розвитку. V Міжнар. наук.-техн. конф. УкрНДІпроектстальконструкція. К., 19-22 верес. 2006 р.- К., В-во „Сталь”.- 2006
- [10] Гоголь М.В., Більський М.Р., Пелешко І.Д. Проектування і розрахунок комбінованих металевих конструкцій з регулюванням зусиль // Современные строительные конструкции из металла и древесины. Сб.науч.трудов ОГАСА. Часть 1. – ОДЕСА, 2006.
- [11] Gogol Myron, Peleshko Ivan, Bilskyj Mykhajlo.Gajda Olexij. New constructive forms and their reliability // Quality and Reliability in Bulding industry. IV International Scientific Conference. 17-19 Oct.. 2006.- Levoca, Slovakia. Technical University of Kosice, 2006.
- [12] Гоголь М.В. Узагальнений метод розрахунку металевих конструкцій з регулюванням зусиль // Вісник НУ “Львівська політехніка”.Теорія і практика будівництва. 2002. - №462.
- [13] Гоголь М.В. Особливості розрахунку будівельних конструкцій із регулюванням зусиль // Будівельні конструкції. – Київ: НДІБК. – 2003. – Випуск 59. – Книга 1.
- [14] Пермяков В.О.,Гоголь М.В. Проблема регулювання напружено-деформованого стану плоских стержневих металевих конструкцій // Вісник НУ “Львівська політехніка”.Теорія і практика будівництва. 2004.
- [15] Пермяков В.А. Совершенствование стальных стержневых конструкций на основе решения обобщенной задачи оптимального проектирования: Дис... докт. техн. наук: 05.23.01. – К., 1993.
- [16] Проектування раціональних комбінованих металевих конструкцій / Укл.: В.О. Пермяков, М.В. Гоголь, І.Д. Пелешко, М.Р. Більський, Б.С. Чайка // За ред. проф. В.О. Пермякова. – Львів: Видавництво Національного університету „Львівська політехніка”, 2005.
- [17] Баженов В.А., Гранат С.Я., Шишов О.В. Будівельна механіка.-К., 1999.
- [18] Рекомендації з проектування раціональних металевих несучих конструкцій перекриття та покриття / Укл.: В.О. Пермяков, М.В. Гоголь. – Львів: Видавництво Національного університету „Львівська політехніка”, 2006.
- [19] Пат. 50014 А Україна, МКИ 7 Е04С3/10 В66С17/00. Балкова конструкція: Пат.50014 А Україна, МКИ 7 Е04С3/10 В66С17/00 Гоголь М.В.,Гайда О. М.(Україна) - № 99127148; Заявл. 28.12.99; Опубл. 15.10.02.
- [20] Пат. 46983 А Україна, МКИ 7 Е04С3/10. Прогінна конструкція: Пат.46983 А Україна, МКИ 7 Е04С3/10 Гоголь М.В.,Гайда О. М.,Чайка Б.С.(Україна) - № 2001031714; Заявл. 14.03.01; Опубл. 17.06.02.
- [21] Пат. 48841 А Україна, МКИ 7 Е04С3/08. Шпренгельна балка: Пат. 48841 А Україна, МКИ 7 Е04С3/08 Гоголь М.В., Чайка Б.С., Гайда О.М., Надала І.В.(Україна) - № 2001128874; Заявл. 21.12.01; Опубл. 15.08. 02.



Jiří JIRÁK<sup>1</sup>  
Jiří STUDNIČKA<sup>2</sup>

## **RESEARCH ON STEEL BRIDGES DURABILITY IN CZECH REPUBLIC**

### **ABSTRACT**

The paper summarizes the results of a research project carried out to evaluate the condition of steel and steel-concrete road bridges in different stages of service life. The behaviour and failure mechanisms were observed on different lifetime bridges in order to provide the resume of a condition, frequent failures and rising causes on steel bridges in Czech Republic. The custom in failure detection applies the visual way for the most part. The new bridge inspection guide was developed that will improve the field work in practice.

**KEYWORDS:** steelwork, steel bridge, service life, durability, reliability, failure,

### **1. INTRODUCTION**

#### **1.1. The field of interest**

Generally, the main aim of provided research was to contribute to increase in durability and reliability in bridge structures during the presumed service life equally with increase in economical perspective of design. The steel bridges reliability is provided by technically perfect design and assembling works as well as quality of inspection and maintenance during the service life. It is evident, although the best effort in design and assembling processes, the failures on bridge structures are developed during the service life. There have been selected and assumed the failures of steel and steel – concrete bridge on purpose of the research.

The total number of bridges in the Czech Republic reaches approximately 16 thousand and only 2 percents need early reconstruction to prevent a serious failure. Although small portion of the total number has a steel or steel-concrete superstructure, the developed results are fruitful through the half of presumed service life passed.

The Bridge structures of different age and various systems made of steel are still in service in the Czech Republic at the time. The knowledge of remaining service lifetime is an important input for decision making whether new structure is to be designed or if the existing one is to be reconstructed and maintained. According to standards, the durability of bridge structure is supposed to be 100 years.

---

<sup>1</sup> Eng., Czech Technical University in Prague, Prague, CZECH REPUBLIC

<sup>2</sup> Prof., PhD., Eng., DSc., Czech Technical University in Prague, Prague, CZECH REPUBLIC

## 1.2. Inspection scope and research method

An increase in the durability of existing bridges should be achieved by periodic bridge inspections and maintenance. The system of basic inspections in specified ordinary or extraordinary terms was developed. The Bridge Management System is centralized and achieves more effectively in maintenance in time. The first stage, inspections are performed in a visual way. The structural details are included. In the second stage, diagnostic investigation of defective bridge structure usually confirms the initial inspection results by smart technologies. The research attempts to improve the visual failure detection and defect causes assessment and creates a tool for a simple initial inspection. The evaluation of condition of the Czech Republic's bridges was carried out additionally.

The project was solved through the large amount of steel and steel-concrete bridges inspection. There were inspected the bridges in different age and various systems made of steel on highways and road all level. In spite of structural system, the investigation was provided on girder and truss bridges. The Bridge Management System was employed to select the bridges for inspections. Within the scope of the research project, in total 135 steel bridges in various stages of service life and of different structural systems made of steel were examined and described in detail. The large documentation including failure photo was obtained during the inspection. The particular description of the bridge failure was aimed to load-carrying members as the most important measure in evaluation of the condition. Failure causes and consequent advices on bridge design are determined apart. The condition of bridge facilities was taken into account only as necessary to meet road safety requirements. The number of examined bridges provides a statistically sufficient sample for analysis, as it includes bridges in all stages of service life and using various static systems. The research results were developed in analyses of failure documentation.

## 2. FAILURE CLASIFICATION IN TYPICAL CASES

### 2.1. Failure classification

While some defect has developed including bearing, connections and splices, expansion joints, deck insulation, improper details etc., the final consequence of incurred failure is the affected part corrosion. The corrosion causes arise usually from two sources:

- corrosion developed as the primary result of protective coating defect, in most cases the localized surface [1]
- corrosion developed as the secondary result of different failure in progress.

### 2.2 Low - class failure

A primary corrosion is discovered quite rarely, usually only on almost new or replaced structures. It should be eliminated by local protective coating maintenance. Figure 1 shows example of an ordinary corrosion defect in low level on bridge in the Karlstejn village. The shown structure was assembled in 1997. The protective coating layer was probably applied in insufficient thickness. The chalking of color coating is well-developed too [1].

### 2.3. Serious - class failure

The result of concurring defective action ordinary provides the higher degree corrosion of structural member. Because the corrosion cause is not obvious, maintenance is much more difficult. The one of frequent points of failure of short span beam bridges is the

connection between main girders and intermediate or bottom bridge deck. The left figure 2 shows exposed detail of a bridge in the city of Melnik after complete reconstruction in 2003. Unfortunately after 3 years, the repaired connection is contaminated again. The bridge in Melnik, assembled in 1938, was the first fully welded bridge in the former Czechoslovakia. The right figure 2 shows local corrosion of a short span bridge connection detail in the Zatec - assembled in 1901.



Fig.1. Defects of protective coating

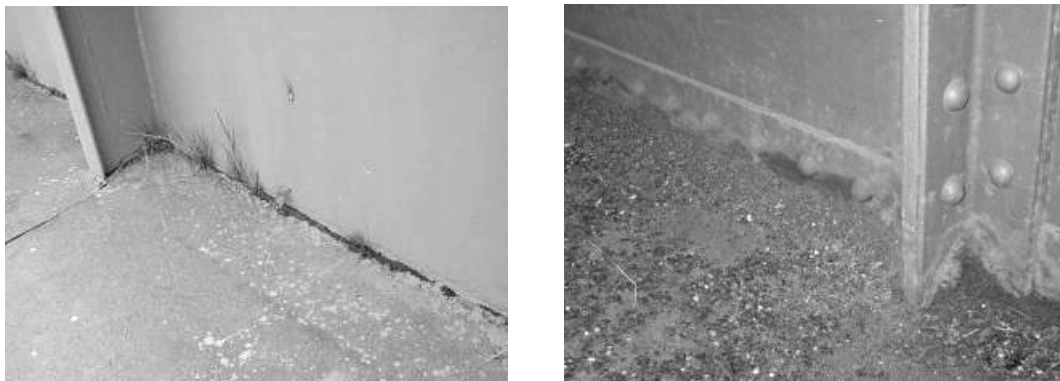


Fig.2. Deeply exposed details of corroded deck connection

Another frequent point of failure of short span bridges is found where reinforced concrete deck slab rests on the bottom flange of the main girders and where there are no shear connections between; indicate the heavy dead load of pavement assembled in maintenance [2]. Usually it is decided to artificially decrease the service load carrying capacity of the bridge. Usually the bridge is declared to be operational in only one direction at the time.

Generally, the most of appearing failures were developed in places, where dirt or water was being trapped. The design and particular details should recognize the requirements of the durability and facilitate whatever maintenance necessary. To maximise the service life of protective coatings, any features that would trap water or dirt should be avoided, and adequate access for the proper application and maintenance of protective coatings should be ensured. Access for maintenance should either be provided or be possible with the minimum of temporary works. It is possible that replacement of bearings will be necessary within the service life. The figure 3 shows the permanent formwork corrosion of a bridge in the city of

Budyne assembled in 1914. The composite action between deck slab and steel girders is excluded. Similarly, the defect of the deck slab insulation causes the formwork corrosion. Suitable drainage could have prevented such failure.



Fig.3. Deck slab corrosion

As the aggressive water flows through, it causes the main girders and concrete deck slab corrosion. The deck slab has been severely eroded and the concrete reinforcement corrosion is proceeding, see figure 3 left. The figure 4 left shows a bearing on a composite bridge in the city of Melnik built in 1993. The deck slab was cast in permanent formwork on the main girders. The cross beam is not included and so the bearing replacement will be difficult. The pitting corrosion started on trapezoid formwork plate. Also trapped dirt and water have participated on the corrosion of the bearing. The figure 4 right shows the A bearing failure caused by trapped dirt and so the fitting detail should be designed in a different way. Within the scope of the research project, only a few bridges made of tubosider and box girders system were inspected, but no serious defects were discovered.



Fig.4. Improper bearing details

### 3. CONDITION OF STEEL BRIDGES DURING THE SERVICE LIFE

#### 3.1. Generally

On the basis of the research results, the state of steel bridges in the Czech Republic could be assessed as satisfactory. Certainly, there are several exceptions. Occasional existence of severely damaged structures confirms the governmental statistics. Sample of bridges used in this article were sorted by age.

### 3.2. Bridges exceeding presumed service life

The truss bridges are the most frequently used systems made of steel in this category of service life stage. Generally, the bridges were erected before the 1<sup>st</sup> world war. Used technology is corresponding to the time of assembly. Splices are joined by rivets etc. The truss bridge in a village Haje is the one of the oldest bridges in the Czech Republic - erected in 1872, see figure 5 right. However the corrosion of the splices and bearing is developed, its condition is acceptable.



Fig.5. Bridge in Jablonec erected in 1883 (left), Bridge in Haje erected in 1872 (right)

### 3.3. Bridges between 50 and 100 years of service life

The bridges in this category were erected between the world wars. The different condition of the bridges closely depends on maintenance applied. The older bridges in this category were constructed in times, when usage of steel for bridge construction was restricted by the government.

Many various examples of bridges in different condition can be found. The truss Bailey bridge near the village of Rusalka represents a badly damaged structure without any maintenance applied, see figure 6 left. This temporary bridge was erected in 1948. The support members are deeply corroded due to soil and dirt refilling and no application of protective coating. The bridge needs to be overhauled immediately. Its load capacity was limited.

### 3.4. Bridges under 50 years of service life

Bridges in this category of service life were assembled very rarely, only on special occasion, because the different preferences of steel application in the former socialistic Czechoslovakia. The defects are developed more frequently than one would assume, as bridges lacked maintenance in those time. In particular, the deck slab insulation of the older bridges is not waterproof, there are no protective coatings on the steel members and generally, the right procedure of construction method was not followed precisely. The figure 6 right shows the consequent condition of a bridge near Kokovice that was assembled in 1961. Its steel structure is free of any protection against corrosion and the plate formwork as well. The bridge is heavily loaded by a thick pavement crust.

Steel bridges after 20 years of service life are generally in a very good condition. In the time of their erection, constructions were again considered from the economical point of view and proper assembling procedures were strictly followed. Bridges less than 10 years old were inspected only occasionally, when another older bridge was located nearby. No serious defects were found after this short time of service.



Fig.6. Bridge in Rusalka erected in 1948 (left), Bridge in Kokovice erected in 1961 (right)

#### 4. FAILURE CAUSES

The failure cause on steel and steel-concrete bridges is obvious and can be discovered simply, or the failure cause is complex and cannot be discovered apart. In general the failure causes can be classified as follows:

- deficiency design (incorrect numerical model in behaviour, composite action, bearing, detailing, etc.)
- inappropriate material (in spite of the fatigue, steel surface, waterproof insulation etc.)
- incorrect assembling ( incorrect or insufficient details in fatigue, inappropriate corrosive protection, the lack in technology of assembling works, denied movement in dilatation or bearing etc.)
- the lack in inspection (late or not provided, unprofessionally)
- un-sufficient maintenance (late maintenance, long – term lack in maintenance etc.)
- incorrect maintenance or reconstruction (overloading as consequence of incorrect reconstruction of pavement)
- traffic overloading

#### 5. CONCLUSIONS

Generally, the structural condition of the steel bridges is sufficient and deeply depends on provided maintenance. The research project on steel bridges offers the improvement in design costs and in inspection method. The condition of majority structures confirms that the presumed durability 100 years is well-achieved for bridges made of steel or steel-concrete.

#### ACKNOWLEDGEMENT

Research of the steel bridge durability and the bridge failure assessment has been performed at the Czech Technical University in Prague with support of grant GACR 103-08-H066.

#### REFERENCES

- [1] Hare C. H.: *Protective Coatings for Bridge Steel*, NCHRP Synthetics of Highway Practice 136, TRB, Washington, 1987.
- [2] Radomski W.: *Bridge Rehabilitation*, Imperial College Press, 2002.

Pavol JUHÁS<sup>1</sup>  
Zuzana KOKORUĐOVÁ<sup>2</sup>

## EFFECTIVE USING OF HIGHER STRENGTH STRUCTURAL STEELS IN COMPRESSION MEMBERS

### ABSTRACT

The chosen results of numerical analysis of middle and higher strength structural steels using in compression members are presented in the paper. The homogeneous cross-sections of the members with web slenderness  $\beta_w = 40, 48, 60, 80, 120$ ; member length  $L = 3,0; 4,0; 5,0$  and  $6,0$  m and structural steels S235, S275, S355, S420 and S460 are assumed. The full reference plastic load  $N_{pl}$ , local post-critical load  $N_{ul}$  and global buckling load  $N_{u,y}$  and  $N_{u,z}$  for all members by actual Slovak Standard STN EN 73 1401:1998 and by new European standards EN 1993-1-1:2005 and EN 1993-1-1:2006 for the design of steel structures, taking account the geometrical optimization determined. The obtained numerical results are compared and analyzed from the economical point of view.

**KEYWORD:** compressed steel member, homogeneous cross-section, yield stress, elastic-plastic loading, post-critical behavior, local and global buckling, load-carrying capacity.

### 1. INTRODUCTION

The overall economy of steel structures depends on their final prices, but these prices are affected by more actual economic relations, interests and conditions. Therefore, the economy and efficiency of steel structures is characterized and analyzed only by equivalent technical parameters in the paper.

The continuous effort to achieve more efficiency of steel structures has guide to decrease their weight. Generally, it is accepted that the weight decreasing of steel structures could be achieved mainly by their geometrical and material optimization, using the thin-walled cross-sections and the higher strength steels.

From the geometrical point of view the design of the member cross-sections is very important. For the optimization of the welded I cross-sections, the dominant factor is the partition of the total section area ( $A$ ) to the web area ( $A_w$ ) and the flanges ( $2A_f$ ), which is characterize by the ratio  $\gamma = A_w / A$ . In the case of simple elastic design of member I cross-sections the optimal ratio of sections areas  $\gamma \approx 0,5$ .

<sup>1</sup> Prof. DSc. Eng., Technical University in Košice, Košice, SLOVAK REPUBLIC,

<sup>2</sup> Assistant Prof. PhD. Eng., Technical University in Košice, Košice, SLOVAK REPUBLIC.

Follow on the provided ideal-numerical optimizing analysis, it is expressly to design the member I cross-sections with local stability flanges and adequate web thickness, due to there favorable post-critical behavior which is allowed by the current codes regulations. Such design is fitting to the ratio of the cross-section's area  $\gamma < 0,5$ , in dependence on the web slenderness  $\beta_w$  ( $\beta_w = d / t_w$ ,  $d$  is the depth and  $t_w$  is the web thickness of the cross-section) and the utilizing rate of the post-critical elastic plastic load-carrying capacity.

The utilizing of the higher strength steels look reasonable at the members subjected mostly to bending, if their lateral buckling is secured. At the same time, it is necessary to point out that in the case of bended members the lateral buckling is usually secured constructively.

The load-carrying capacity of compressed members, which are the subject of this paper, is affected first of all by there global stability. The global stability of compressed members does not depend on the strength, therefore the using of more expensive higher strength steels is not so clear as in case of the bended members. The global stability and related buckling load-carrying capacity of the compressed members seriously depends on their bending and torsion rigidity. Therefore, the efficiency of higher strength steels applying is substantially influenced also by their geometrical - shaping optimization [1-6].

This paper concentrating on the effective applying of the higher strength steels on the compressed members taking in consideration their shaping and material optimization. The presented considerations, proposals and conclusions are mainly based on the results of the realized numerical study [7]. At the same time they are applying the valid calculation related methods used for the design of steel structures according to the actual Slovak Standard STN 73 1301:1998, and new European Standards EN 1993-1-1:2005 and EN 1993-1-5:2006. The results of the realized numerical study in this manner enable also a liable comparison of the so far valid calculation methods in the actual Slovak Standard and European Standards, which after on, beginning from 2010 will be used in Slovak Republic as transformed standards STN EN 1993-1-1:2005 and STN EN 1993-1-5:2006.

## 2. NUMERICAL STUDY

With accordance to the purpose of this paper, for the proposal of this numerical study were used an chosen groups of the welded compressed members joint supported on both sides with different I cross-sections, but suitable related geometrical sizes according to the figure 1, and table 1 (A, B, C, D, E). The cross-sections of all members have had the same sectional area  $A = 11520 \text{ mm}^2$ , section depth  $h = 512 \text{ mm}$ , web depth  $d = 480 \text{ mm}$  and the thickness of the flanges  $t_f = 16 \text{ mm}$ . Only the web thickness  $t_w$  was varying ( $t_w = 4, 6, 8, 10, 12 \text{ mm}$ ) and thereby also the flange's width  $b$  ( $b = 180, 210, 240, 270$  and  $300 \text{ mm}$ ), the sectional area of the web  $A_w$  and sectional area of the flanges  $A_f$ .

Table 1. Geometrical dimensions and characteristics of the member cross-sections

Test members	A	h	b	t <sub>f</sub>	d	t <sub>w</sub>	A <sub>f</sub>	A <sub>w</sub>	$\beta_w$	$\beta_f$	$\gamma$
	(mm <sup>2</sup> )	(mm)				(mm <sup>2</sup> )					
A(1,2,3,4,5)	11520	512	180	16	480	12	2880	5760	40	5,25	0,500
B(1,2,3,4,5)			210			10	3360	4800	48	6,25	0,417
C(1,2,3,4,5)			240			8	3840	3840	60	7,25	0,333
D(1,2,3,4,5)			270			6	4320	2880	80	8,25	0,250
E(1,2,3,4,5)			300			4	4800	1920	120	9,25	0,167



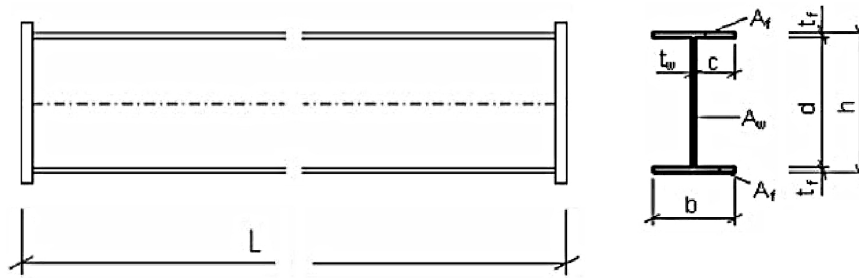


Figure 1. The considered compressed members and their geometrical dimension

According used variation a different web slenderness  $\beta_w$  (from 40 to 120) and different ratios of sectional areas  $\gamma$  (from 0,500 to 0,167) were achieved for the individual cross-sections. The web slenderness  $\beta_w$  were adjusted in order to show the markedly impact of the local stability and on the load-carrying capacity of the analyzed compressed members. On the other hand, the slenderness of the compressed flanges  $\beta_f$  was adjusted locally stable. From the point of view of the cross-section material of all groups were considered structural steels S235 (1), S275 (2), S355 (3), S420 (4) and S460 (5). For the individual geometrical cross-section groups (A,B,C,D,E) and material cross-section groups (1,2,3,4,5) finally were adjusted 4 different lengths of members L (L = 3, 4, 5 and 6 m), table 2.

Table 2. Member's material and geometrical characteristics

Members	$f_y$	L	$\lambda_y$	$\lambda_z$
	(MPa)	(m)		
AS(1,2,3,4,5)	235,275,355,420,460	3,4,5,6	from 12,21 to 29,69	from 162,01 to 35,71
BS(1,2,3,4,5)				
CS(1,2,3,4,5)				
DS(1,2,3,4,5)				
ES(1,2,3,4,5)				

By the intential modification of the web thicknesses their slenderness  $\beta_w$  are increased, but at the same time, by the relative regrouping of the web area with the flanges and the increasing of the flange's area, the rigidity of the cross-sections in increased by both axes (y, z), nevertheless, the global buckling load-carrying capacity of the members is increased, especially the load-carrying capacity at the more weak rigidity plane (z). By the increasing of the strength, respectively increasing of the steel yield strength, the local and global buckling load-carrying capacity of the members is increased, with dependence on the member's length L and related stable impacts; these are characterized by their slenderness  $\lambda_y$  and  $\lambda_z$ , table 2.

The applying of the intential modification, a total set of 100 compressed members with various geometrical dimensions and strength characteristics were achieved. This enables, with accordance of the main goal, the complex analysis of the compressed steel member design efficiency.

For such set of compressed steel members, sequentially were calculated according to the methods of considered standards the following theoretical loads, [7]:

- plastic load  $N_{pl}$ , provided the full compactness of the cross-sections and members,
- local elastic load-carrying capacity, taking in consideration the impacts of buckling and post-critical behavior of the slenderness webs in the elastic stage,

- global buckling load-carrying capacity  $N_{u,y}$  related to the axes y-y and  $N_{u,z}$  related to the axes z-z, taking in consideration the impacts of local buckling and the global buckling of members in the elastic stage.

In table 3 are mentioned the members limit loads  $N_{pl}$  and  $N_{ul}$ , calculated by Slovak Standard STN 73 1401:1998 (STN, STN (1)) and European Standard EN 1993-1-5:2006(EN).

Table 3. Limit loads  $N_{pl}$  and  $N_{ul}$  for the considered compressed members

Members	$N_{pl}$ [kN]		$N_{ul}$ [kN]		$N_{pl,STN}/N_{pl,STN(1)}$	$N_{pl,EN}/N_{ul,EN}$	$N_{ul,STN(1)}/N_{ul,EN}$
	STN	STN(1), EN	STN(1)	EN			
AS1	2461,1	2707,2	2707,2	2707,2	0,909	1,000	1,000
AS2			2551,6	2567,3		1,054	0,994
AS3			2449,4	2481,8		1,091	0,987
AS4			2406,4	2436,3		1,111	0,988
AS5			2429,5	2447,5		1,106	0,993
BS1	2754,8	3168,0	3070,8	3063,9	0,870	1,034	1,002
BS2			2913,8	2945,3		1,076	0,989
BS3			2816,9	2858,9		1,108	0,985
BS4			2786,2	2821,2		1,123	0,988
BS5			2828,8	2849,0		1,112	0,993
CS1	3408,0	4089,6	3772,9	3808,2	0,833	1,074	0,991
CS2			3620,5	3679,8		1,111	0,984
CS3			3540,3	3599,3		1,136	0,984
CS4			3539,1	3583,3		1,141	0,988
CS5			3624,4	3648,5		1,121	0,993
DS1	3870,7	4838,4	4324,8	4390,0	0,800	1,102	0,985
DS2			4181,4	4260,7		1,136	0,981
DS3			4119,5	4190,7		1,155	0,983
DS4			4145,9	4196,7		1,153	0,988
DS5			4268,6	4295,6		1,126	0,994
ES1	4239,4	5299,2	4658,0	4740,1	0,800	1,118	0,983
ES2			4522,1	4612,6		1,149	0,980
ES3			4472,9	4551,1		1,164	0,983
ES4			4517,7	4572,3		1,159	0,988
ES5			4664,2	4692,9		1,129	0,994

In STN 73 1401:1998 the different reliability partial factors  $\gamma_{M,0}$  and  $\gamma_{M,1}$  for individual structural steels are applied ( $\gamma_{M,0} = \gamma_{M,1} \neq 1,0$ ). By EN 1993-1-1:2005 the different reliability partial factors  $\gamma_{M,0} = \gamma_{M,1} = 1,0$ . Because of the different reliability partial coefficients  $\gamma_{M,0}$  and  $\gamma_{M,1}$ , for comparison the value of  $\gamma_{M,0} = \gamma_{M,1} = 1,0$  are also considered uniform, these are applied also in the new transformed standard STN EN 1993-1-1:2006.

The relative values  $N_{pl,STN}/N_{pl,STN(1)}$  show only the differences coming out by applying a different material coefficients  $\gamma_{M,0}$ . These can be considerable, especially when using the higher strength steels. The relative values  $N_{pl,EN}/N_{ul,EN}$  characterizing the unfavorable buckling effect of the web through the slenderness  $\beta_w$ , but also the favorable effect of partition the cross-section area to web and flanges through ratio  $\gamma$ . Even, the favorable effect of the partition of the cross-section area to web and flanges predominates in the case of higher slenderness webs  $\beta_w$ .

Based on the obtained results, it is possible to assign a cross-section characterized by the web slenderness  $\beta_w$  and ratio  $\gamma$  for each steel grade. This cross-section responds with the maximum value of ratio  $N_{pl,EN}/N_{ul,EN}$  and also with the minimum local load-carrying capacity  $N_{ul,EN}$ . By the steel strength increasing, the ratio  $N_{pl,EN}/N_{ul,EN}$  is also increasing, but not significantly. For example the value of this ratio for S235 is 1,111, and for S460 is 1,164.

The practical equality of the local stability and load-carrying capacity calculation of the thin-walled compressed steel members according to the standard STN 73 1401:1998 and standard EN 1993-1-5:2006, stems from the relative values  $N_{ul,STN(1)}/N_{ul,EN}$ , and in case of using the an equal material reliability coefficients  $\gamma_{M,1} = 1,0$ . The appeared differences are not more then 2%. In table 4 are mentioned the members global buckling load-carrying capacity  $N_{u,y}$  and  $N_{u,z}$  in dependent of the length L, calculated by standard EN 1993-1-1:2005.

Table 4. Global buckling loads  $N_{u,y,EN}$  and  $N_{u,z,EN}$  of the considered compressed members

Members	L = 3,0 m		L = 4,0 m		L = 5,0 m		L = 6,0 m	
	$N_{u,y,EN}$	$N_{u,z,EN}$	$N_{u,y,EN}$	$N_{u,z,EN}$	$N_{u,y,EN}$	$N_{u,z,EN}$	$N_{u,y,EN}$	$N_{u,z,EN}$
	[kN]							
AS1	2676,11	1675,31	2667,01	1235,21	2616,98	905,87	2565,87	679,59
AS2	2567,28	1933,15	2567,28	1584,54	2529,80	1257,14	2485,18	989,79
AS3	2481,76	2067,49	2481,76	1813,55	2460,27	1545,85	2420,40	1289,87
AS4	2436,27	2152,49	2436,27	1959,35	2425,09	1750,62	2388,09	1534,04
AS5	2447,53	2240,70	2447,53	2080,77	2441,09	1909,26	2404,94	1726,96
BS1	3063,86	1823,08	3040,13	1313,84	2979,24	950,85	2916,70	708,19
BS2	2945,35	2146,26	2940,56	1722,24	2886,89	1341,22	2832,18	1042,83
BS3	2858,89	2326,84	2858,89	2009,59	2819,15	1682,07	2769,91	1380,65
BS4	2821,21	2446,84	2821,21	2202,45	2793,00	1939,09	2746,85	1671,68
BS5	2849,02	2566,79	2849,02	2362,87	2825,36	2142,97	2779,81	1911,02
CS1	3808,16	2071,05	3750,30	1442,09	3666,67	1024,71	3579,96	755,79
CS2	3679,83	2522,90	3646,98	1951,08	3572,65	1476,52	3496,19	1127,76
CS3	3599,29	2803,66	3583,62	2350,66	3515,41	1905,96	3445,64	1524,53
CS4	3583,28	3001,18	3577,67	2641,87	3512,43	2261,54	3445,93	1894,71
CS5	3648,52	3189,76	3646,26	2885,26	3580,75	2556,52	3514,04	2219,39
DS1	4390,01	2238,51	4300,28	1526,95	4197,21	1073,99	4089,55	787,89
DS2	4260,68	2789,48	4200,29	2103,24	4107,96	1564,28	4012,35	1182,79
DS3	4190,69	3155,69	4149,77	2586,69	4064,15	2052,27	3975,99	1615,83
DS4	4196,74	3421,54	4166,37	2958,43	4083,55	2479,50	3998,54	2037,50
DS5	4295,57	3669,71	4267,24	3271,99	4183,22	2845,91	4097,05	2422,25
ES1	4740,13	2330,14	4629,15	1573,00	4513,68	1100,86	4392,57	805,50
ES2	4612,63	2938,96	4533,37	2185,51	4429,44	1611,20	4321,38	1212,24
ES3	4551,10	3358,44	4492,46	2716,78	4395,50	2130,30	4295,27	1663,88
ES4	4572,27	3668,03	4524,19	3137,22	4429,82	2597,53	4332,56	2112,49
ES5	4692,87	3954,18	4645,69	3494,44	4549,44	3005,79	4450,29	2530,00

The graphical evaluation and comparing of the limit loads  $N_{pl,EN}$ ,  $N_{ul,EN}$ ,  $N_{u,y,EN}$  and  $N_{u,z,EN}$ , of all members, in dependent on the steel strength, web slenderness  $\beta_w$  (ratio  $\gamma$ ) and length L, is clearly done on the following figures 2 and 3. Tables 3 and 4, as well as the figures 2 and 3, presents complete information about the effect of the all determining design parameters for each limit loads, respectively load-carrying capacity of the considered thin-walled steel members.

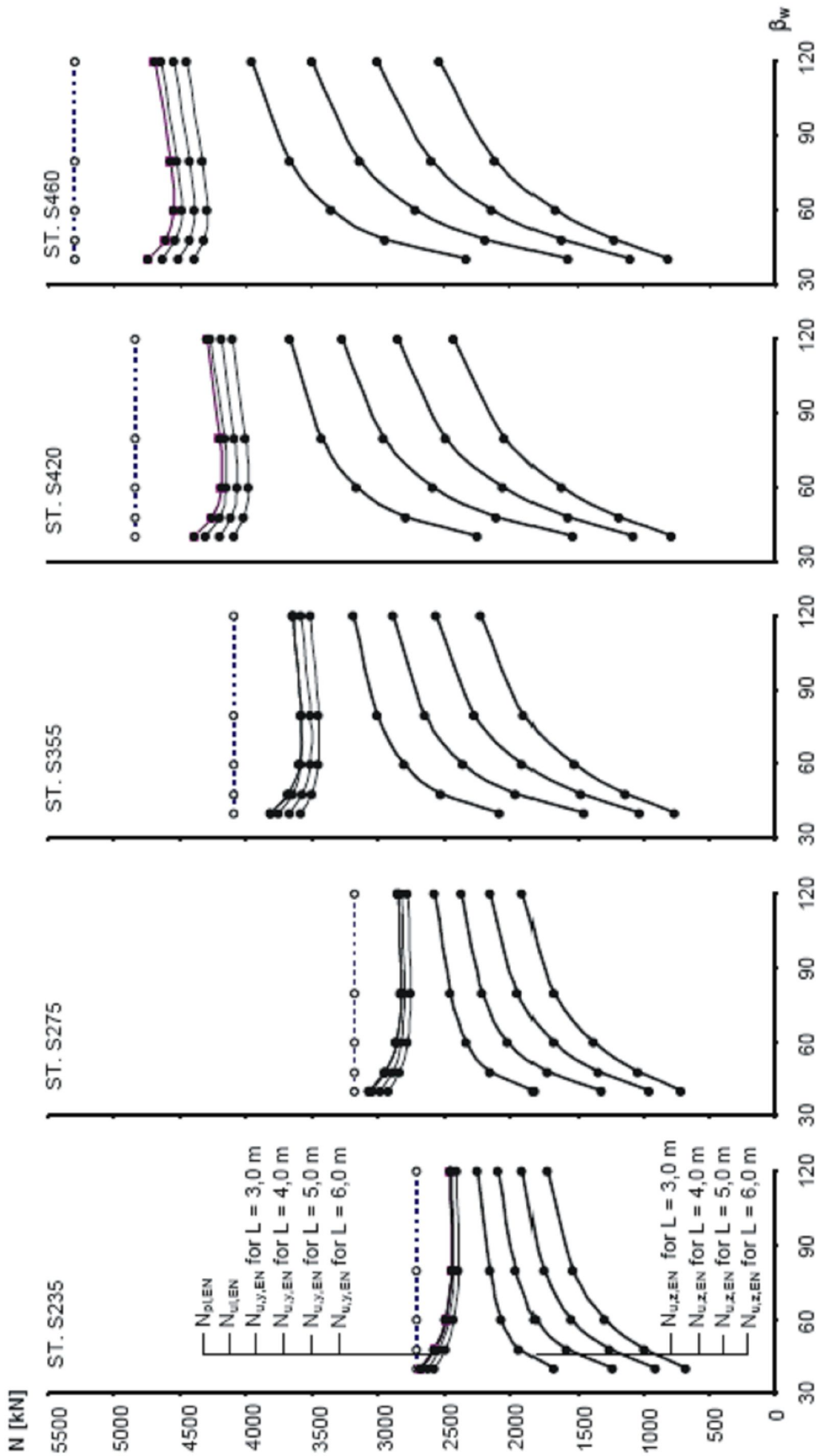


Figure 2. Dependencies of the theoretical loads  $N_{pl,EN}$ ,  $N_{ult,EN}$ ,  $N_{u,y,EN}$  and  $N_{u,z,EN}$  on the web slenderness  $\beta_w$  (ratios  $\gamma$ ) for each steel grade and the length  $L$  of the considered compressed members

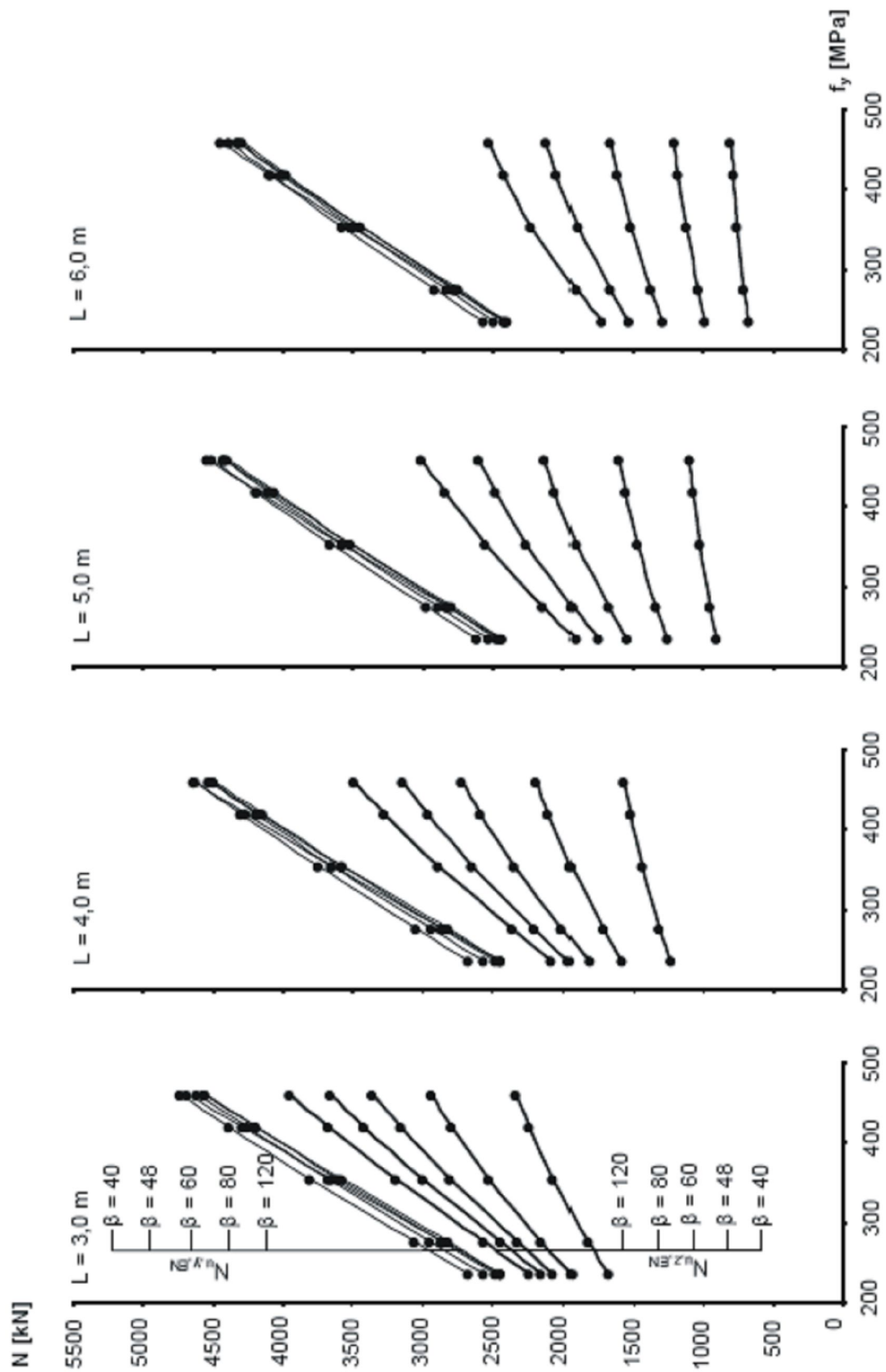


Figure 3. Dependencies of the theoretical loads  $N_{u,y,EN}$  and  $N_{u,z,EN}$  on the yield stress of the structural steels  $f_y$  for each length  $L$  and web slenderness  $\beta_w$  (ratios  $\gamma$ ) of the considered compressed members

### 3. CONCLUSION

Compressed members ultimate load  $N_{pl}$  depends only on the sectional area and the material strength. Logically, the ultimate loads  $N_{pl}$  are raised by increasing of the material strength. But this is just theoretical respectively comparative loads.

The effect of web slenderness  $\beta_w$  and sectional areas ratios  $\gamma$  on the local load-carrying capacity of the compressed members  $N_{ul}$  was proved. Generally, the effect of web slenderness  $\beta_w$ , could be effectively reduced by suitable distribution of the total cross-sectional area  $A$  to the web and flanges. From a certain ratio  $\gamma$ , the local load-carrying capacity of the compressed members is even increased with the increasing of the web slenderness  $\beta_w$ . Then, it is possible to state, that by suitable distribution of the total cross-sectional area  $A$ , it is advisable and favorable to design the cross-sections of the compressed members with a thin web.

The global buckling load-carrying capacity of the compressed members  $N_{u,y}$  and  $N_{u,z}$  are effected essentially by their slenderness  $\lambda_y$  and  $\lambda_z$ . The effects of the web slenderness  $\beta_w$  and the cross-section area ratio  $\gamma$  on the global buckling carrying capacity of the compressed members are decreased by the increasing of the slenderness  $\lambda_y$  and  $\lambda_z$ . However, by suitable distribution of the global cross-sectional area  $A$  to the web and flanges, the slenderness  $\lambda_y$  and primarily  $\lambda_z$  could be reduced. In the case of higher slenderness  $\lambda_y$  and  $\lambda_z$ , using of the higher strength steel is less effective till ineffective.

By application of the planned values' changes of the material reliability coefficients according to the European standard EN 1993-1-1:2005, all considered ultimate loads of the compressed members increased. In the case of higher strength steels, the consequential differences of the equivalent ultimate loads are very substantial.

### REFERENCES

- [1] Juhás,P.; Kriváček,J.: Investigation of Thin-Walled Compressed Combined Steel Elements, Building Research Journal, Vol. 41, No.4/2, 1993, p. 305-325.
- [2] Juhás, P., Juhásová, E.: Load-Carrying Capacity of Hybrid Compressed Steel Elements, In: Proc. of Annual Technical Session, SSRC, USA – Memphis, 22-24 July 2000.
- [3] Juhás,P.: Efektívnosť využívania ocelí vyšších pevností v tlačných prútoch. In: Zborník zo 43. celoštátnej konferencie výrobcov OK: HUSTOPEČE 2005, 8.12.2005, s. 3-6.
- [4] Juhás,P.: Buckling load-carrying capacity of steel hybrid thin-walled compressed members, Selected Scientific Papers, Journal of Civil Engineering, Vol.3, Issue1, Košice, 2006, p.9-28.
- [5] Juhás,P., Al Ali M., Kokoruďová, Z.:The elastic-plastic load carrying capacity of thin-walled steel with quasi-homogenous and combined cross-sections, Selected Scientific Papers, Journal of Civil Engineering, Vol.3, Issue1, Košice, 2008, p.7-18.
- [6] Juhás,P., Al Ali M., Kokoruďová, Z.: The experimental research of local elastic-plastic load carrying capacity of thin-walled steel members subjected to compression, Transactions of the Universities of Košice, Research reports from the Universities of Košice, 4, 2008, p. 56-65.
- [7] Juhás,P., Kokoruďová, Z.: Efektívne uplatňovanie ocelí vyšších pevností v tlačných prútoch nosných konštrukcií, Kvalita vo zvaraní, Tatranská Lomnica, 2009, s.65-75

The paper was elaborated within the framework of the research project VEGA 1/44220/07.

Ján KANÓCZ<sup>1</sup>

Viktória BAJZECEROVÁ<sup>2</sup>

## INVESTIGATION OF TIMBER - CONCRETE COMPOSITE BEAMS UNDER LONG TERM LOADING

### ABSTRACT

Experimental investigation of timber-concrete composite beams subjected to long term loading is presented. The first type of experimentally tested timber-concrete composite beams consisting from the vertically nailed timber planks with concrete deck on the top. Shear connection between the concrete layer and timber members by grooves in timber was realized, which guarantee the composite action of two layers. The second type of the composite beams consists from separated vertically oriented timber planks in certain distance covered by OSB sheet and from fiber reinforced concrete layer on the top. Shear transfer between the timber planks and upper layers by the pair of steel screws spaced along the timber beams was realized. Three by three from both types of beams to four point bending tests was exposed. Experimental results with existing theoretical models are compared.

**KEYWORDS:** timber – concrete, long – term behavior, experimental test

### 1. INTRODUCTION

Load carrying capacity of timber-concrete composite structural elements with numbers of different rheological factors is influenced. For the optimal design of timber-concrete members at full part of these factors has to be taken in to account.

In wood, at permanent environment effect of creep, and with changes of humidity content effect of mechano - sorptive creep is occurred. Deformation of concrete in time is fundamentally influenced by creep and shrinkage. Interaction of these materials in composite elements is also affected by stiffness and long - term behavior of shear connection. Wood and concrete are materials with different behavior in time and different reaction on thermal and humidity changes of environment. In composite elements it results in generation of inelastic strains and redistribution of stress in cross-section (Tab. 1). To determine load carrying capacity of composite wood-concrete element is possible for example by calculation of effective bending stiffness with considering of flexure of connection according to Additions B of EN 1995-1-1, Design of timber structures. But, this calculation technique do not considers with influence of rheological properties of composite materials as shrinkage, eventually bulking of materials, influence of composite on creep coefficient, influence of environmental changes.

<sup>1</sup>Associate Prof. PhD. Eng., Kanócz CONSULTING, a.s.i., Košice, SLOVAKIA,

<sup>2</sup> Eng., Technical University of Košice, SLOVAKIA.

To receive more information of timber concrete composite elements in years 2003 research project focused to their long term acting was opened [5].

Table 1. Rheology properties of composite materials

		TIMBER	CONCRETE
duration of load	$\varepsilon = f(t)$	visco-elastic strain in time	
	creep	slower creeping mechano-sorptive creep	faster creeping
influence of humidity changes	shrinkage/swelling	during entire lifetime	during concrete hardening
	moisture expansion coefficient	$3,0 \cdot 10^{-3}$	negligible
influence of thermal changes	thermal expansion coefficient	$3,5 \cdot 10^{-6}$	$10 \cdot 10^{-6}$

## 2. DESCRIPTION OF SPECIMENS

### 2.1 Beam system

First type of tested composite system is represented by 5,0 m long and 600 mm wide beam, created from three separated longitudinal vertically oriented timber planks (grade C22) with cross section 45 x 220 mm. Planks was covered by 15 mm thick OSB sheet. Thickness of the concrete layer is 50 mm. The problem of this composite system, mainly from the point of view of long term action, is the shrinkage of the wood and concrete respectively.

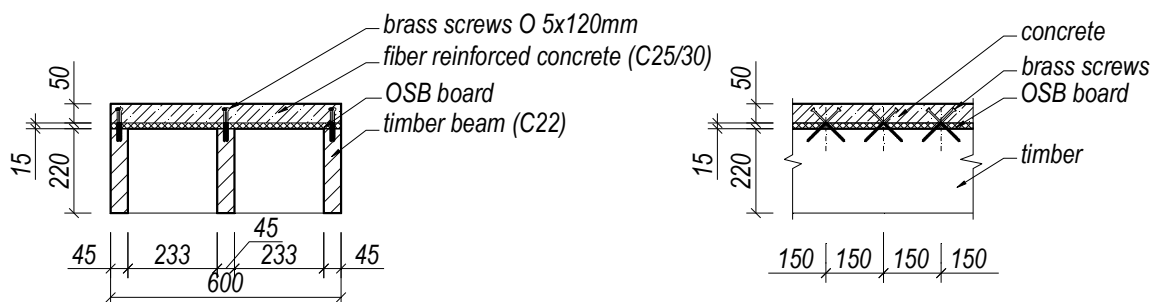


Fig. 1. Cross-section of specimen and shear connection

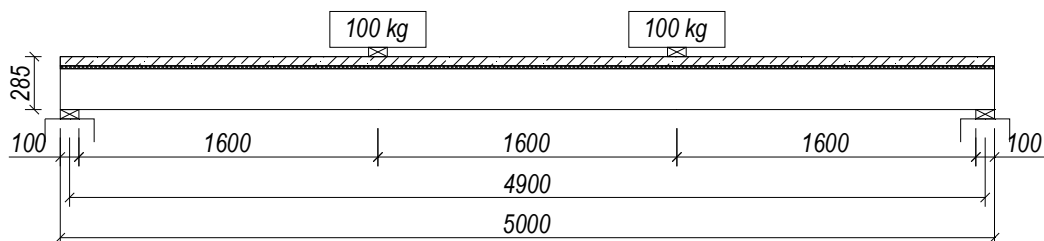


Fig. 2. Test set-up

To eliminate the influence of this phenomenon, steel fibre reinforced concrete was used for beam specimens. This type of reinforcement eliminates the cracks due to shrinkage of concrete and also improves the strength parameters of concrete layer, which leads to the high performance composite action of the beam. The shear connections between the concrete and planks by the common wood screws with diameter 5 mm and 120 mm length are



performed. Distance between the screws along the planks is 150 mm. In each position the pair of screws was drive in with slope of 45° to the planks top edge (Fig. 1).

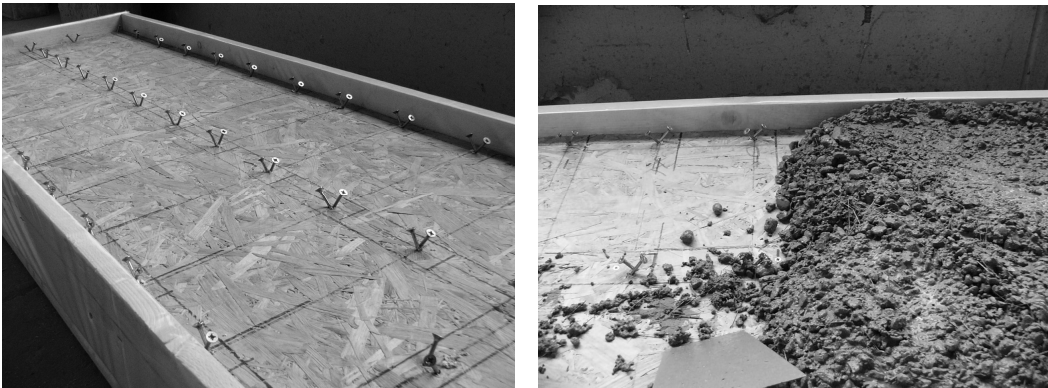


Fig. 3. Preparing of specimens

2.2 Slab system

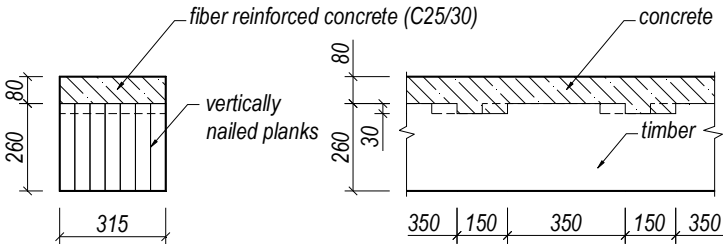


Fig. 4. Cross-section of specimen and groove connection

The second type of investigated composite timber – concrete system is beam with vertically nailed planks. The 5 m long beam with 340 mm depth and 315 mm width of cross section was built from 7 vertically nailed timber planks 45 x 260 mm cross section. Thickness of the fiber reinforced concrete layer is 80 mm and the grooves depth is 30 mm. The length and number of grooves was determined by preliminary calculation. Softwood – spruce with grade C22 and concrete with grade C25/30 was applied. To decrease the influence of wood shrinkage at the groove connection, in each second timber planks the grooves position was shifted by the half length of groove.

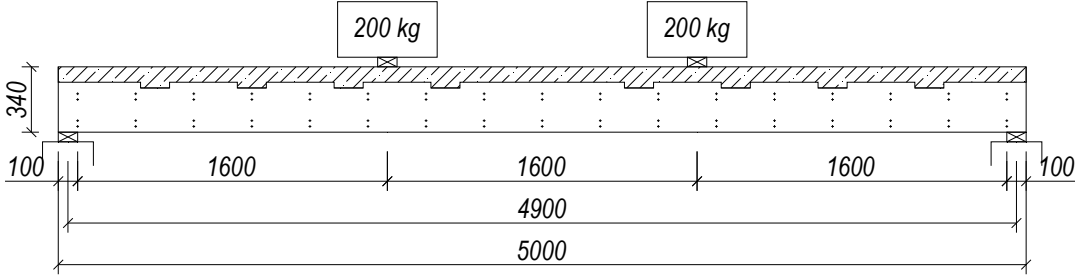


Fig. 5. Test set-up



Fig. 6. Preparing of specimens

### 2.3 Materials parameters

The mechanical parameter of used wood and concrete separately for the both materials by tests according to the relevant standards was determined. See overview in Tab.2 and Tab.3. Slip modulus  $K_{ser}$  of shear connections between timber and concrete by push out test was determined. This value for pair of screws with value 11 500 N/mm and for groove with value 24 000 N/mm was specified.

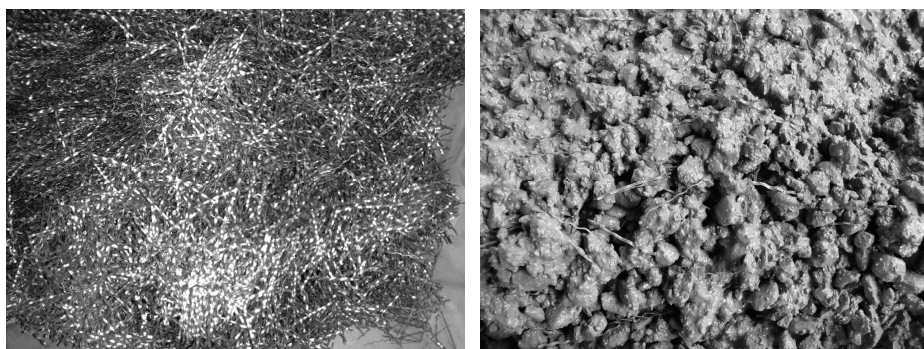


Fig. 7. Fiber reinforced concrete

Table 2. Parameters of timber layer

<i>Bending strength</i>	76,3 MPa
<i>Shear strength</i>	6,66 MPa
<i>E-Modulus</i>	8441 MPa
<i>Density</i>	435 kg/m <sup>3</sup>

Table 3. Parameters of concrete layer

<i>Compressive strength</i>	32,7 MPa
<i>Tensile strength in bending</i>	5,4 MPa
<i>E-Modulus</i>	30,4 GPa
<i>Density</i>	2342 kg/m <sup>3</sup>
<i>Volume fraction of hooked fibres</i>	0,5 %
<i>Fiber length</i>	35 (120) mm
<i>Fiber cross section</i>	1,0 x 0,2 mm

The long-term loading of three pieces of both types of timber-concrete specimens inside the laboratory is in progress till today (Fig.8). Humidity and temperature of internal environment is permanently recorded. Arrangement of long-term experimental test is showed on Fig. 2 and Fig. 5.



Fig. 8. Loaded specimens

### 3. COMPARISON WITH ANALYTICAL CALCULATION MODELS

Experimental results obtained during the last five years are compared with different analytical calculation model which was developed for timber-concrete composite beams under long term loading [1], [2], [3].

#### 3.1 Effect of shear connection flexibility and creep

The calculation model [1] takes to account the effect of flexibility of shear connection and different processes of creep in wood and concrete by modification of modulus of elasticity:

$$E_{0,d,ef} = \frac{1}{1 + \varphi_{d,com}} \cdot E_{0,t=0} \text{ for timber,} \quad E_{b,ef} = \frac{1}{1 + \varphi_{b,com}} \cdot E_{b,t=28d} \text{ for concrete,} \quad (1)$$

where  $\varphi_{i,com}$  is effective creep coefficient of materials in composite members, determined by multiply of final value of creep coefficient  $\varphi_{i,mat}$  and factor  $\psi_{i,s}$ . Effect of shrinkage is considered by factor  $C_{l,bnp}$ , which modify effective bending stiffness of composite beam and by alternate load. Effect of this load is accounted with effect of dead load.

Design is realized for three time step – begin and end of service life, but also between 3rd and 7th year. In this time is creep of concrete almost completed, whereas the timber reaches just 60% of final values of creep strains.

#### 3.2 Effect of load duration and creep

The calculation model [2] is based on summation of particular effect of dead and live load in time. Effects are counted by formulas according to EN 1995-1-1 Addition B for mechanically jointed beams. Creep is considered by effective creep coefficient of concrete (subscript  $c$ ), timber ( $t$ ) and connection ( $f$ ) according to:

$$E_{c,eff}(t) = \frac{E_c(t_i)}{1 + \varphi_c(t, t_i)}, \quad E_{t,eff}(t) = \frac{E_t}{1 + \varphi_t(t - t_i)}, \quad K_{eff} = \frac{K_{ser}}{1 + \varphi_f(t - t_i)}. \quad (2)$$

Value  $t_i$  is the loading time measured from the beginning of process of concreting. Trend of creep coefficient  $\varphi_c(t, t_i)$  and elastic modulus of concrete  $E_c(t_i)$  in time can be valuated according to Eurocode 2. Eurocode 5 defines only final value of creep coefficient of timber  $\varphi_f(t-t_i)$  specified like  $k_{def}$  in dependence on service class. Time behavior is evaluated by interpolation of values for different load-duration classes according to older version of Eurocode 5. For shear connection the value of creep coefficient  $\varphi_f(t-t_i)$  is recommended to be considered equal to double of value for timber  $\varphi_f(t-t_i)$ .

### 3.3 Effect of mechano-sorptive creep and environmental changes

This calculation method [3] improves the model described in chap. 3.2 by considering mechano-sorptive effect, shrinkage of concrete and influence of thermal and humidity changes of environment. Creep coefficient with considering of humidity changes is specified by:

$$\varphi_i(t-t_i) = \varphi_{ic}(t-t_i) + \varphi_{ims}(t-t_i) = \left( \frac{t-t_i}{t_d} \right)^m + \varphi^\infty \left[ 1 - e^{-\frac{c \cdot 2\Delta u}{100\Delta t}(t-t_i)} \right], \quad (3)$$

where  $\varphi_{ic}$  is creep coefficient,

$\varphi_{ims}$  is mechano-sorptive creep coefficient,

$t_d = 29\,500$  day,  $m = 0.21$ ,  $\varphi^\infty = 0.7$ ,  $c = 2.5$  are material parameters assumed by Toratti [4].

For simplification humidity content is considered constant in entire cross-section and trend of humidity in time is replaced piecewise by linear curve with annual period, hence change of humidity is estimated by difference between maximum and minimum average environment humidity value ( $u_{\varnothing, \max}$ ,  $u_{\varnothing, \min}$ ) by time period  $\Delta t = 365$  day.

Mechano-sorptive creep is considered by substitution of Eqn. 3 to Eqn. 2 for timber and shear connections. Calculation of influence of shrinkage  $\varepsilon_{cs}$ , yearly  $\Delta\varepsilon_y$  and daily  $\Delta\varepsilon_d$  changes of environment are mentioned in [3].

### 3.4 Comparison

Comparison of deflection in the mid span of test beam Type 1 (2.1) in time with analytical calculations is illustrated in the Fig. 9, estimated values of instant deflection and deflection after 5 years are compared with experiment in Tab. 4.

Table 4. Deflection of beam type 1 in time

deflection [mm]	age of construction [year]	
	0	5
experiment	3,06	6,78
Schänzlin	2,51	7,67
Ceccotti	2,51	4,27
Fragiacomo	2,52	4,86

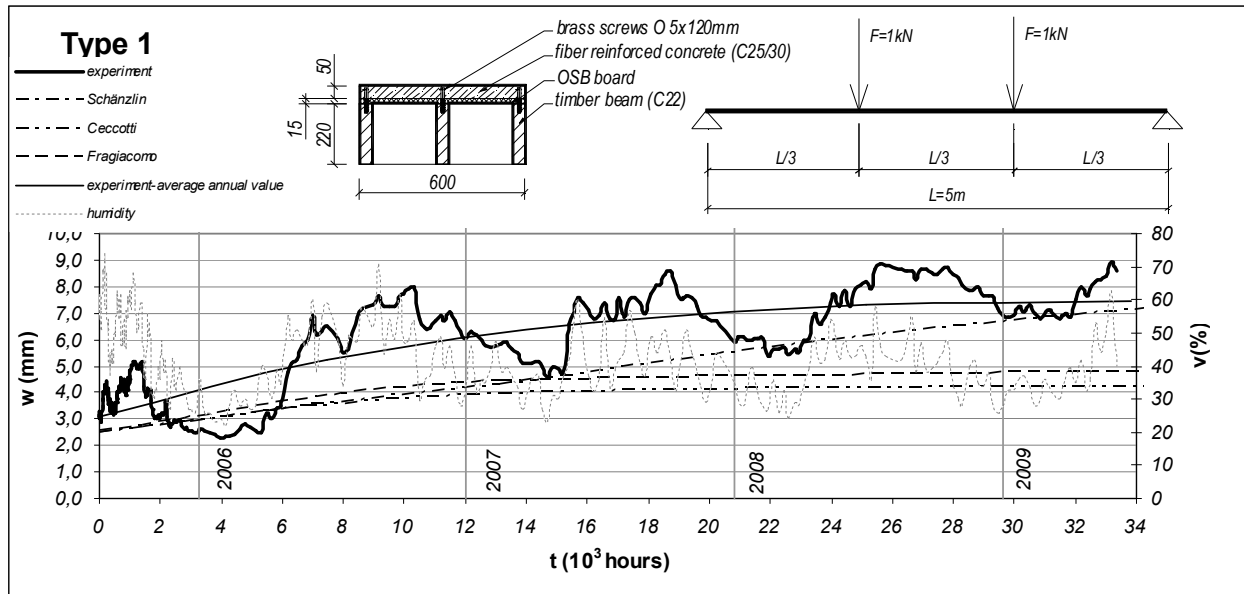


Fig. 9. Average mid span deflection of beams Type 1 in time

Comparison of deflection in the mid span of test beam Type 2 (2.2) in time with analytical calculations is illustrate in the Fig. 10, estimated values instant deflection and deflection after 5 years of are compared with experiment in Tab. 5.

Table 5. Deflection of beam type 2 in time

deflection [mm]	age of construction [year]	
	0	5
experiment	1,49	3,23
Schänzlin	1,22	4,25
Ceccotti	1,22	2,20
Fragiacomò	1,22	2,23

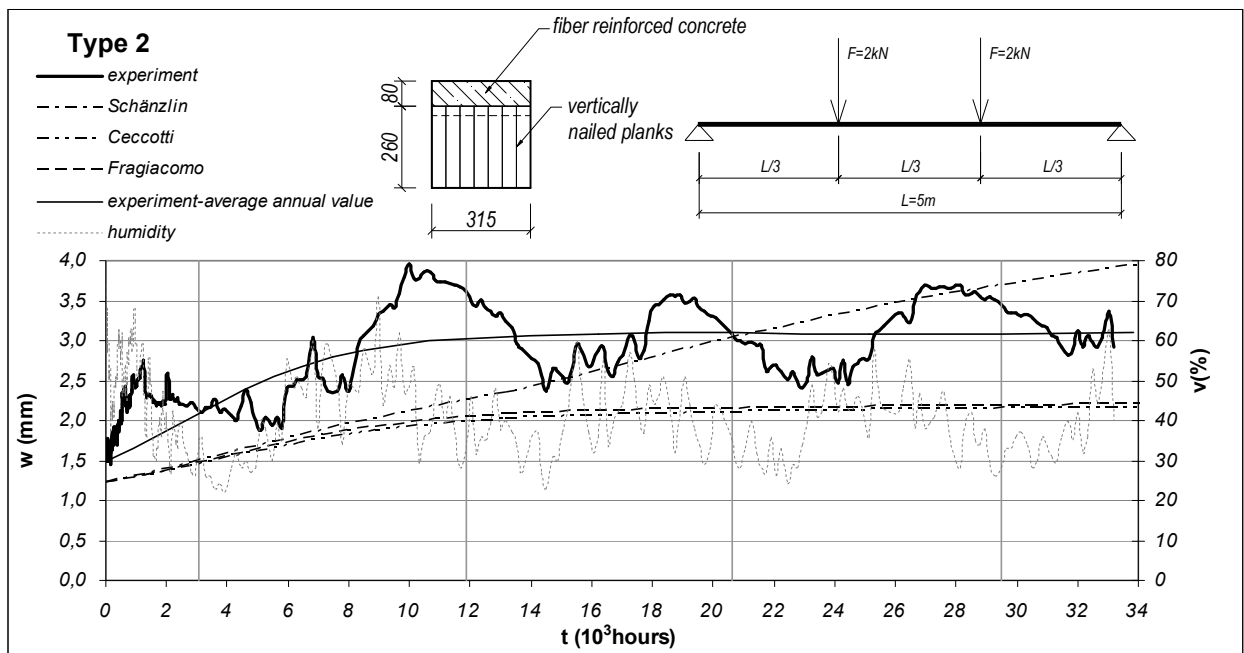


Fig. 10. Average mid span deflection of beams Type 2 in time

Differences in values of deflections can result from various theoretical approaches of analytical models to rheology properties of composite element. From comparison results, that deflection of beam Type 1 grows every year and reacts to environmental changes. Global creep coefficient reaches value of 1,6 at this time. The analytical models underestimate the values of deflection of experimental beams all the time. The reason can be in increased creeping of timber in part of screw connection.

Deflection of experimental beams Type 2 assign till now steady character reacts to environmental changes. Global creep coefficient reaches value of 0,6. Experimental values are for models [2], [3] above theoretical as well. Model according to [1] reaches in time after 2 year overestimate deflection.

#### 4. CONCLUSION

Reliable design of wood- concrete structural elements from aspect of long - time effect requires such calculation model, which can predict deformation of composite element with enough precision during their lifetime. From the above presented comparison resulting, that the selected calculation models are reasonable approaches to this problem. However, to improve calculation models further theoretical and experimental investigations are needed.

#### ACKNOWLEDGEMENTS

The author would like thank the support provided by VEGA Project No. 1/4157/07.

#### REFERENCES

- [1] Schänzlin, J.: Zum Langzeitverhalten von Brettstapel-Beton-Verbunddecken, Institut für Konstruktion und Entwurf, Universität Stuttgart, Dissertation, 2003.
- [2] Fragiaco, M., Ceccotti, A.: Long-term behavior of timber-concrete composite beams. I: Finite element modeling and validation. *Journal of Structural Engineering*, ASCE 2006, 132(1), pp. 13-22.
- [3] Fragiaco, M.: Long-term behavior of timber-concrete composite beams. II: Numerical analysis and simplified evaluation. *Journal of Structural Engineering*, ASCE 2006, 132(1), pp. 23-33.
- [4] Toratti T.: Creep of Timber beams in a variable environment. Helsinki University of Technology, Report 31. Dissertation, 1992
- [5] Záverečná správa - Projekt APVT 99-05402 – Štúdium mechanických vlastností vybraných kombinovaných konštrukčných prvkov, ŠDVÚ, Bratislava, 2005.

Dušan KATUNSKÝ<sup>1</sup>

## **STRUCTURAL PHYSICAL PROBLEMS RESEARCH OF INDUSTRIAL PRODUCTION HALL BUILDINGS**

### **ABSTRACT**

Research of the structural and physical problems of envelope structures and physical components of internal environment and their mutual interaction in industrial buildings mostly of a hall type is the subject of the investigation of this article. The research was solved in close touch with the grant projects VEGA 1/9023/02 “The Interaction of Physical Factors in the Creation of an Appropriate Working Environment” and 1/2562/05 “Evaluation of thermal, humidity and lighting conditions of the production industrial buildings“ joining with the research project **1/0695/08** with the title „Thermal flows in interaction of building construction and underground as well as external outdoor conditions for large space hall buildings“, supported by Slovak Fund for Scientific Research, task which is being presently elaborated.

**KEYWORDS:** industrial buildings, production halls, indoor microclimate, physical parameters, envelope structures, daylighting

### **1. INTRODUCTION**

Within the framework of those three research projects attention is focused on selected physical components of internal environment of hall industrial buildings, especially thermal, humidity and day lighting conditions in close touch with energy demand analysis. The aim of the whole research is to look for ways optimizing these conditions with regard to the design of a building envelope in close touch with environmental technique and energy intensity reduction during their operation. The solution of these questions in interaction with architecture and creation of structural detail of hall-type industrial buildings should lead to the change in approach to the envelope part design of an industrial building, so that the result would be a stately architecture, environmentally relevant, economically efficient and sustainable. The research project solvers/developers devoted in much attention to industrial buildings designed for

- textile,
- electrical,
- electronic,
- pharmaceutical
- and machinery production

---

<sup>1</sup> Prof. Ing. CSc., Technical University of Košice, Košice, SLOVAKIA

## 2. HEAT FLOWS IN ENVELOPE STRUCTURES

The specificity of the internal climate of industrial production buildings, mainly of a hall type, characterizes the non-homogeneity of the individual kinds of internal climate. This non-homogeneity is characterized by non-stationary energy flows in the building in space and time. Their qualitative and quantitative expression in a prediction level is not simple. One of the possibilities to make use of is the use of integrated simulation methods in marginal conditions of the exterior climate model in the form of a reference test year for the condition of the Slovak Republic.

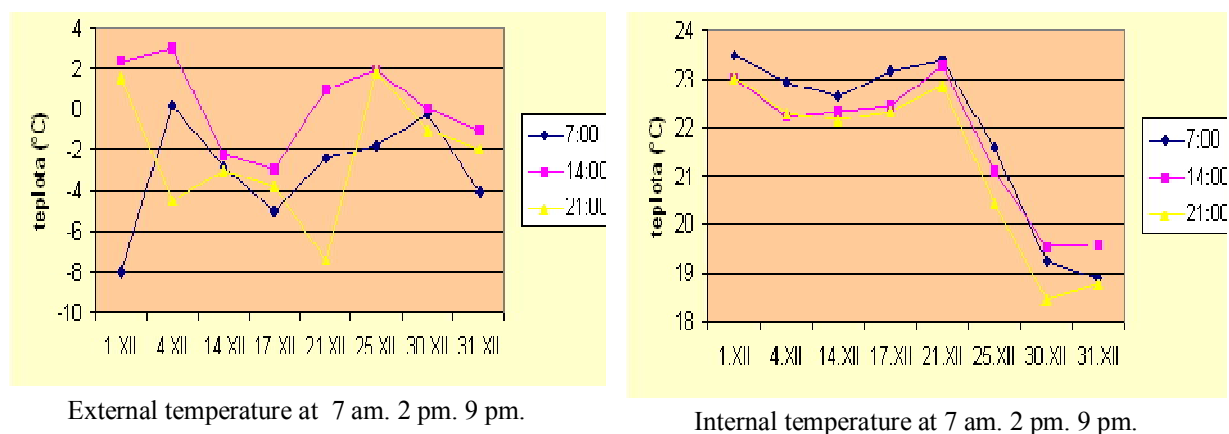


Fig. 1. Measured external and internal temperatures in production building (electro technical production) – in situ in winter period

The survey results have shown that a very serious problem is the temperature state of the internal air and relative humidity in industrial buildings. In industrial buildings, in majority of cases, there are more demanding conditions of heat-humidity state of the internal environment than in residential or non-residential buildings (administrative buildings).

## 3. HUMIDITY TRANSPORT IN ENVELOPE STRUCTURE IN HALL BUILDING

On the cellular concrete envelope of a hall-type industrial building the diffusion of water vapor was observed simultaneously with the effect of liquid transport of humidity. For a non-linear mathematical model of heat and humidity transfer in porous materials a numerical algorithm of solution was created. It concerns the determination of non-stationary heat and humidity transfer not only in X-direction, e.g. through the mass of the external envelope (the thickness of the wall), but also depending on time  $t$  (s).

The calculation results have proved that the proposed method of solution supplies satisfactory numerical problem solutions in corresponding marginal conditions of solutions. On the specific hall-type building measurements of heat and humidity on the external envelope in situ were performed. At the same time a verification of proposed calculation models was carried out. The results obtained from measurements are comparable with the numerical solution of proposed models of heat and humidity transfer. Pavlušová [7].

## 4. ENERGY CONSUMPTION FOR HEATING IN INDUSTRIAL BUILDING

Experimental measurements in situ were carried out in hall-type industrial buildings that have identical shape but the orientation of which is in contrary compass points. In winter period the measurements of surface temperatures of envelope structures, heat-humidity



conditions of internal environment and heat flows were conducted. At the same time the readings of heat consumption for heating were carried out. The measurements results have shown that the methods of evaluation of heat-moisture conditions of internal environment of flat and non production buildings cannot be exactly applied for assessment of industrial hall type buildings. Katunska [2]

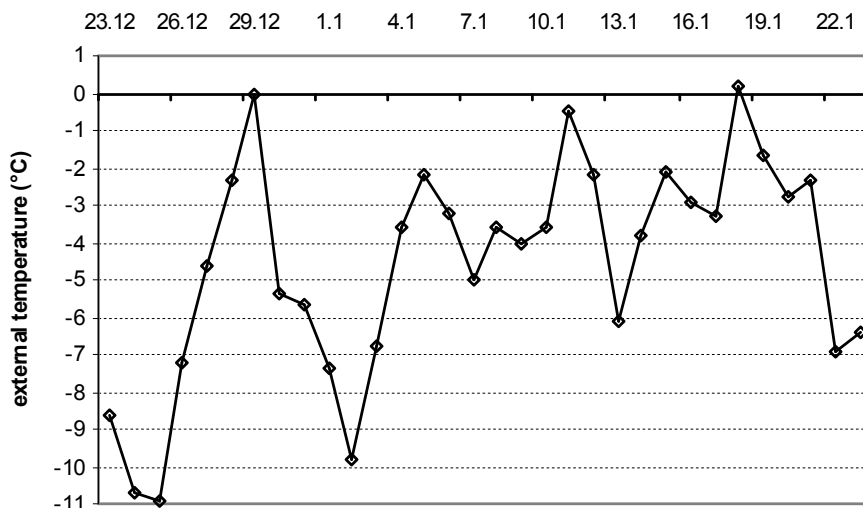


Fig. 2 External temperature changes in measured days from 23. December to 22. January

Normative regulations valid for the assessment of energy needs for heating of flat building in situ cannot be applied to industrial buildings. From the solution of this subtask many regressive dependences of energy intensity were stated. Figures 7,8 show two of them. The results of the whole experimental research were evaluated in [2] and further published in [6]. In case of evaluation of industrial hall-type buildings it is inevitable to consider and differentiate the specifics of a production operation. Similar conclusions also apply to the assessment of energy needs for heating.

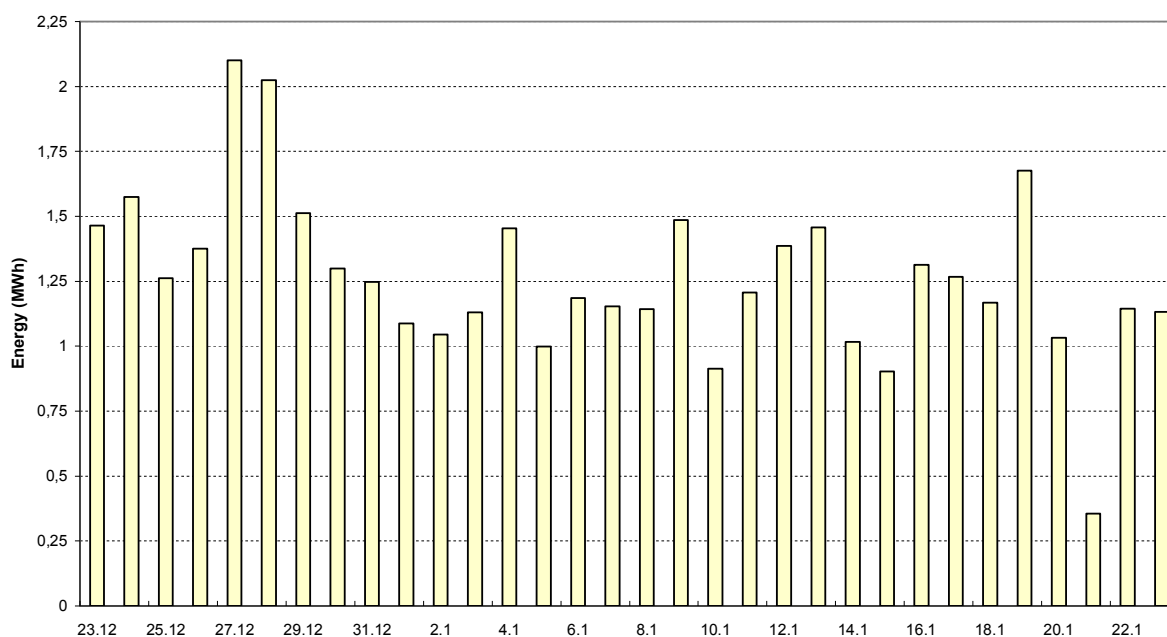


Fig. 3 Measured values of energy consumptions in measured days in production hall

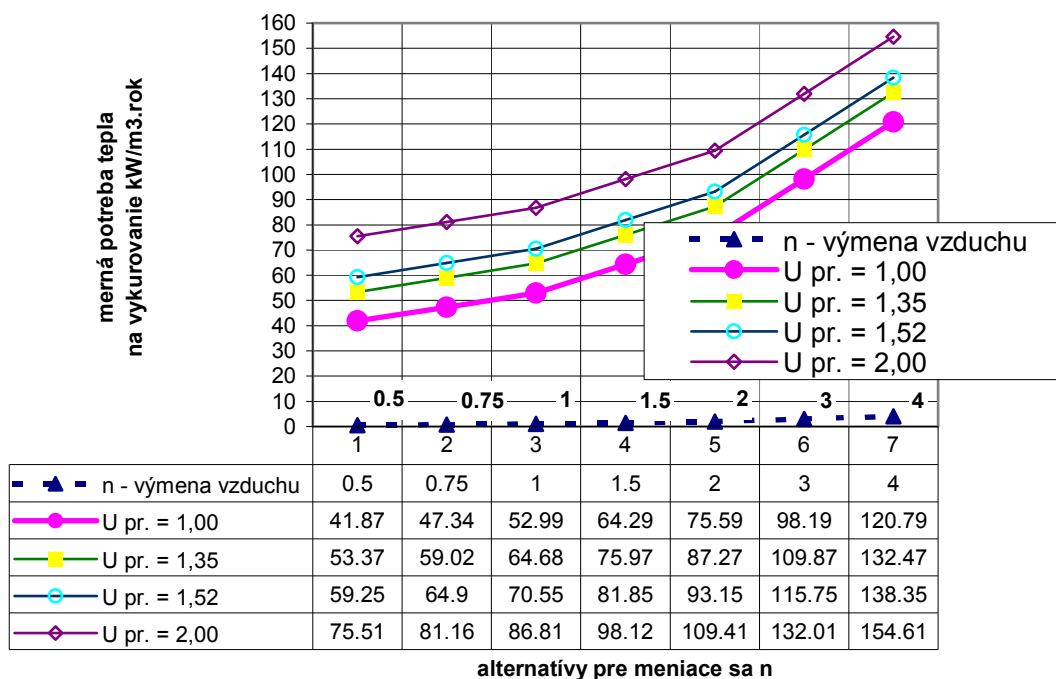


Fig. 4. Heat consumption for heating changes depending on changes of U values (heat transfer coefficient  $W/m^2K$ ) and also exchange of n - air interchange

## 5. OVERHEATING IN INDUSTRIAL BUILDING IN SOMMER PERIOD

Heat protection of industrial buildings in summer period at present significantly falls behind the level achieved in flat but also non-flat building structures. As the survey results have shown the most significant problem of industrial buildings is their heat instability in summer period which manifests itself most distinctively in hall – type buildings. The present state in the field of calculation and evaluation of heat stability is oriented more towards residential and non-residential (administrative buildings).

What is the real state in the field of heat stability of hall-type buildings in summer period was the subject of solution thesis of Lopusniak and published in [3], [5]. The objectives of the subtask can be summarized in the following points:

- obtaining factual, real heat values of the internal air by taking measurement in situ in selected hall-type buildings in summer period,
- verification of usability and accuracy of the chosen calculation methods (The method according to Slovak National Standard - STN, EN ISO and the calculation simulation by applying ESP-r) for evaluation of heat stability of hall-type buildings in summer period ,
- determination of the effect of the basic and supplementary entry factors and their parameters on the course of heat of internal air by calculation testing ,
- Proposal of requirements for the evaluation of heat stability of hall-type buildings in summer period and the creation of a simplified methodology for evaluation of heat stability of hall-type buildings in summer period, reflecting the proposed requirements.

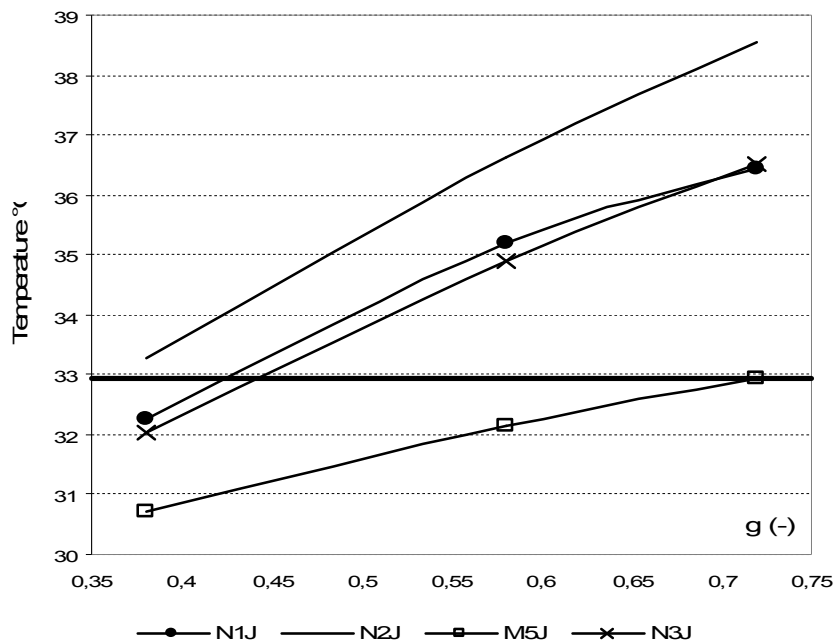


Fig. 5. The dependence  $\theta_{ai,max}$  ( $^{\circ}\text{C}$ ) on g - value of glazing of selected calculation combination for the intensity of air exchange  $n = 1$  (1/h) of the south orientation of a building model; the horizontal line represents the maximum temperature of the reference combination

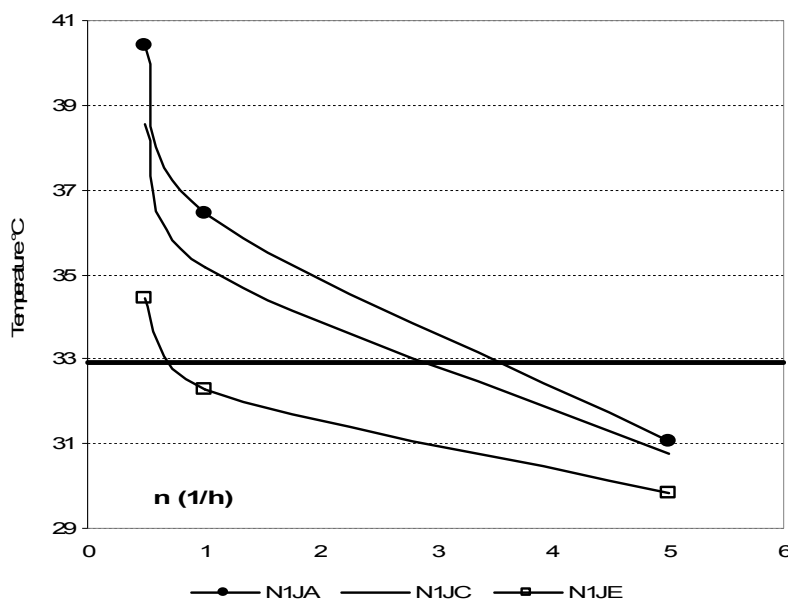


Fig. 6. The dependence  $\theta_{ai,max}$  ( $^{\circ}\text{C}$ ) on the air exchange intensity for the chosen calculation combination; the horizontal line represents the max. temperature of the reference combination

## 6. THERMAL FLOWS INTO UNDERGROUND OF INDUSTRIAL BUILDING

Physical technical requirements, maintenance qualities details and framework basic structure are important in industry production building and underground. All criteria of thermal protection of buildings ought to meet floor structure in joining with another bear and ground structures. Precise and correct design of floor structures in joining with another structure can significantly influence industry production building energy requirements. Experimental measurement of temperatures in underground is realized in production building

(72 x 36 m, height 10 m) in five search units in soil in deepness 1, 2 and 3 meters under floor and in distance 0,5 m; 1,0 m; 1,5 m; 2 m; from external wall. One search unit is located in soil in the middle of the hall object underground. Measurements are performed continually during the year. The results were evaluated and published in [8], [10].

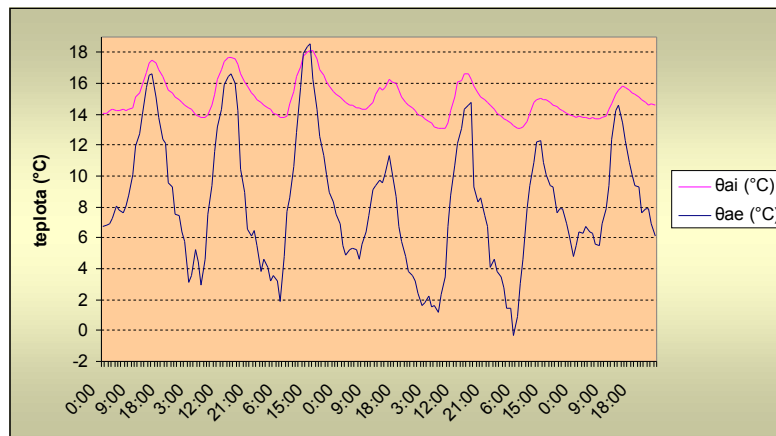


Fig. 7. Dependence of internal and external temperatures in chosen days in March 2007

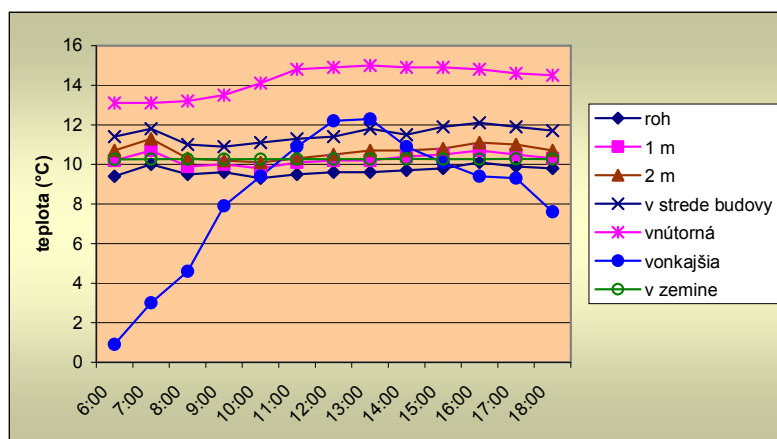


Fig.8. The dependence of temperatures changes in soil in deepness 1,2,3 m underground in chosen day in March 2007

## 7. EVALUATION OF DAYLIGHTING IN INDUSTRIAL BUILDING

Another subtask of the research project was the analysis of the qualitative and quantitative state of daylighting in the hall-type industrial buildings. The primary objective was the comparison of the results of computer simulation of daylighting with the values measured in situ in real conditions of a selected industrial building. From the measurements results there ensued that the side illumination, e.g. illumination from sides only and not from above produces significant deficit of illumination in the zones (areas) which are remote from transparent fillings. In evaluating the level of daylighting based on normative calculation procedures in the SR, simplified and in principle extreme external conditions are used. Present development of calculation software makes it possible to solve time demanding extensive problems in order to achieve a more accurate result in a relatively shorter period of time. Despite of the fact that at present time in the conditions of the Slovak Republic it is not common to utilize sophisticated simulation programs in design practice, for the effectiveness

in the process of architectonic and design creation of buildings especially for large hall type buildings – industrial, multipurpose sport, cultural and civic buildings, it will be inevitable to determine marginal conditions of the calculation itself, e.g. to extend the TRY-structure.

Only on the base of the marginal conditions reflecting the specifics of the conditions of the SR it will be possible to effectively designate the conditions and the level of daily illumination of indoor environment in a real interior. The results of the task are defined in [1].

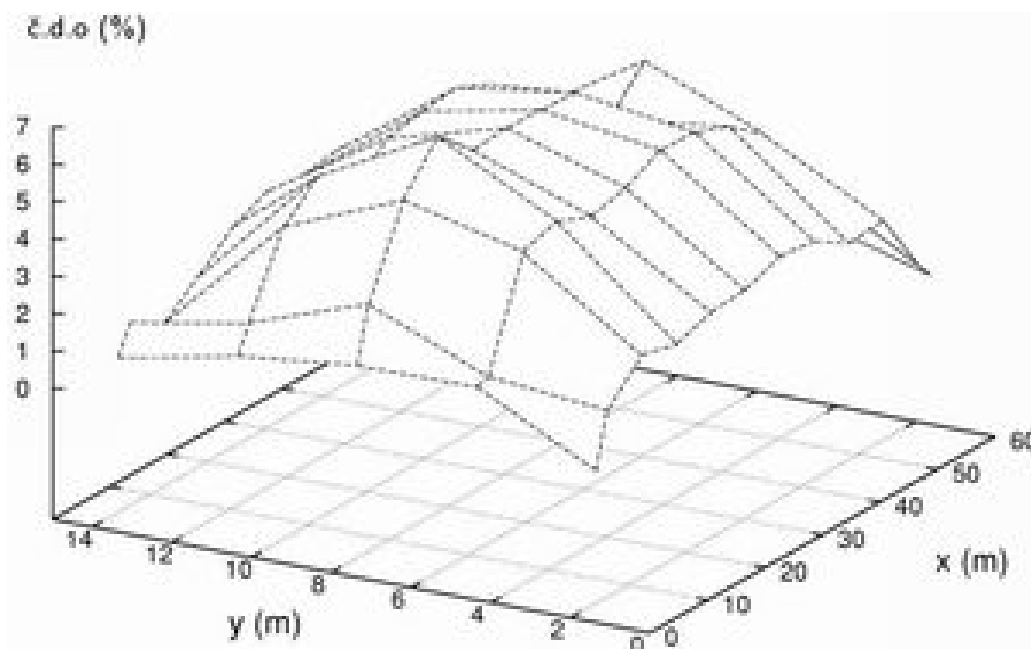


Fig. 9. Calculated daylighting coefficient  $D$  (%) in large production hall illuminated by skylights located in roof construction

## CONCLUSIONS

The focusing of the solution of experimental tasks ensuing from the stated objectives for the research will be concentrated into the analysis of the condition of the internal (indoor) work environment of selected hall-type buildings. In view of the persisting expansion of building production in the field of industrial building in the Slovak republic, the focusing of the research presents a current area of the development of science and technology. At the same time the possibility of active utilization of the knowledge from the solution of the research are arising in real conditions of design of new industrial buildings. It is inevitable to assess and analyze the building as a whole in interactions of the components of internal environments-outer climate and energy consumption. That is why the attention will be focused especially on the interaction, e.g. of the internal air temperature - relative humidity - energy consumption; the level of daylight - overheating in summer period - demand for HVAC. Simultaneously, the solution of individual subtasks is supposed in the area of the transfer of heat to the subsoil and in the field of inclusion of former and no-used industrial buildings in the active building stock, using all the knowledge for securing their further active utilization. Again two kinds of experimental research will be applied in mutual combination and checking, e.g. the methods of experimental measurements in situ and the methods of experimental calculation by simulation programs. [11], [12].

## REFERENCES

- [1] Dolníková, E., Katunský, D. Assessment of the Daylighting in One Storey Industrial Building. In: Design and Construction., ISSN 1335-5007, Bratislava 2002, vol. 4, no. 6, p. 9-11.
- [2] Katunská, J. The Influence of Selected Factors on Energy Balance of Hall-Type Objects: Dissertation thesis. TU in Košice – Faculty of Civil Engineering, 2001
- [3] Lopušniak, M. Thermal Stability of Hall-Type Objects and the Possibility of its Evaluation with the Aid of prEN ISO 13791 and prEN ISO 13792. In Tepelná ochrana budov, Praha, Czech republic., ISSN 1213-0907, 2004, vol.7, no. 4, p. 3-8
- [4] Katunský, D. Industrial Hall Objects: Development of Design and Functional Requirements. TULIP and TU in Košice 2003. ISBN 80-8073-001-6
- [5] Katunský, D., Lopušniak, M. Interaction of Selected Parameters within Design of Suitable Working Environment, in: Healthy Buildings 2006, Design and Operation of Healthy Buildings, Proceedings: Vol.3 ISIAQ Lisboa Portugal 2006, pg. 147-152, ISBN 978-989-95067-1-8
- [6] Katunská, J., Katunský, D. Evaluation of Internal Microclimate Quality in the Large Space Industrial Hall. In Internationale Zeitschrift für Bauinstandsetzen und Baudenkmalpflege. D-Freiburg: Aedificatio Publishers. ISSN 0947-4498, 2002, Jahrgang Heft 4, vol. 8, p. 371-378
- [7] Pavlušová, E. Pavlušová, E. Analysis of the Effects of Transfer of Heat and Humidity through Porous Envelope of Hall-Type Buildings : Dissertation thesis. TU in Košice – Faculty of Civil Engineering, 2000.
- [8] Rusnák, A.: Vysokoestetické riešenia podlahových konštrukcií v priemyselných budovách halového typu – 1.časť, In: www.abcinterier.sk, v podtitule PROFI
- [9] Rusnák, A.: Analýza priebehu teplôt v podzákladi ako súčasť vstupných čiastkových okrajových podmienok pre tepelno-technické výpočty spodnej stavby, In: Juniorstav 2007, Január 2007, Brno, zborník abstraktov str. 38, ISBN 978-80-214-3337-3, zborník príspevkov (CD)
- [10] Rusnák, A., Sedláková, A.: Podlahové konštrukcie v priemyselných budovách, In: Materiály pro stavbu 5/2007, Jún 2007, str.42-46, ISSN 1213-0311
- [11] Katunský, D. et al. Evaluation of Physical Conditions of the Large Production Industrial Buildings, in Czasopismo techniczne B z. 5-B/2006 International Seminar Energodom 2006 Part I. P 259-267
- [12] Katunský, D. Thermal flows in interaction of building constructions as underground and envelope structures, in IX. International Seminar Energodom 2008, Budownictwo niskoenergetyczne, Poland on CD pgs 203-210, ISBN 83-86161-05-1

Yevhen KHARCHENKO<sup>1</sup>  
Taras PIDHAYNYY<sup>2</sup>

## MATHEMATICAL MODELLING OF TRANSVERSE AND TORSION VIBRATIONS OF COMPOUND METALWARES

### ABSTRACT

Mathematical models and algorithms of calculation of free transverse and torsion vibrations of long-length metalware on example of vehicle's body are developed. Load-carrying system is considered as a continuous beam with step change of the cross-section. Characteristics of beam's rigidity are defined experimentally. Modal analysis is carried out using a matrix method of initial parameters. Results of calculation of the lowest eigenfrequencies of vehicle's body with experimental results are compared.

**KEYWORDS:** mechanical vibratory system, modal analysis, compound metalware, continuing.

### 1. INTRODUCTION

In engineering industry and construction industry compound metalwares are widely applied, for example, vehicle's and bus's bodies, derricks, columns and frames of road bridges, lift cranes, etc. During of use significant dynamic loads influence them, and that can be the cause of resonance phenomena and, as consequence, excessive strains and even breaking. Therefore execution of modal analysis of such metalwares has essential practical value. Dynamic calculation of compound metalwares quite often is considerably problematical. Because elements forming mechanical system are numerous, various, have difficult geometry and properties of links. Therefore improvement of methods of calculation of compound systems on a basis of application of tools of continuing is actual problem [1], [2].

For the purpose of selection of rational variant of design of vehicle's body practical value has approximate (with inaccuracy 15-20% max) definition of eigenfrequencies of free vibrations of research models. Using of difficult software complexes and accordingly space shell or shell-rod calculating models for this is unpractical through superfluous expenses of time for decision of a problem [3], [4]. Experimental research of free vibrations of mechanical system is also too labour- and time-consuming. Therefore we should use simplified methods of calculation which give the possibility to estimate dynamic characteristics of metalware using limited number of generalized elastic-inertial parameters which are defined theoretically or experimentally [5], [6], [7].

<sup>1</sup> Prof., Dr.Sci.Tech., Lviv Polytechnical National University, Lviv, UKRAINE

<sup>2</sup> Post-graduate, Lviv Polytechnical National University, Lviv, UKRAINE

In article mathematical models and algorithms of calculation of free transverse and torsion vibration of long-length metalware on example of vehicle's body are offered. Load-carrying system is considered as a continuous beam with step change of the cross-section. Characteristics of beam's rigidity are defined experimentally. Modal analysis is carried out using a matrix method of initial parameters. Results of calculation of the lowest eigenfrequencies of vehicle's body with experimental results are compared.

## 2. TRANSVERSE VIBRATIONS OF VEHICLE'S BODY

Vehicle's body is schematically represented on fig. 1, where  $l_i$  and  $d_i$  ( $i=1, 2, \dots, 5$ ) are lengths of sections of metalware;  $l_0$  is distance between the supporting knots of suspension;  $m_i$  ( $i=1, 3, 4, 6$ ) are the masses of loads which imitate the equipment of vehicle and passengers.

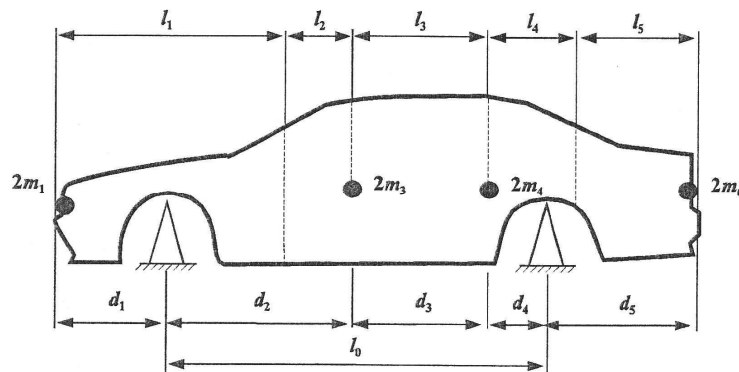


Fig. 1. Scheme of vehicle's body.

Consider free transverse vibrations of vehicle's body in a longitudinal vertical plane. Calculation scheme of bearing metalware is presented in form of a beam which consists of five sections with length  $l_i$  ( $i=1, 2, \dots, 5$ ) (fig. 2). Loads with weights  $2m_1, 2m_3, 2m_4, 2m_6$  are rigidly connected with beam on borders of sections.

Cross-sections of the beam are identified by coordinate axis  $x_i$  ( $i=1, 2, \dots, 5$ ) with origins on the left borders of the proper sections. Area  $A$  of construction's cross-section is supposed as a constant and determined by formula

$$A = \frac{m}{\rho l}, \quad (1)$$

where  $m$  is mass of vehicle's body;  $l$  is total length of vehicle's body;  $\rho$  is density of the material. Axial moment of inertia of cross-section for each beam's sections is calculated as

$$I_{zi} = r_{zi}^2 \cdot A, \quad (2)$$

where  $r_{zi}$  is axial radius of inertia of cross-section.

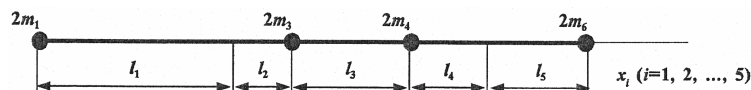


Fig. 2. Calculation scheme for research of transverse vibrations of vehicle's body.

Suppose cross-section of vehicle's body is rectangle with height  $h_i$  and width  $b_i$ , and area of bearing elements is evenly distributed on the contour of this rectangle. Then



$$r_{zi} = \frac{h_i^2 (h_i + 3b_i)}{12(h_i + b_i)}. \quad (3)$$

Test sample of vehicle's body is loaded by static loadings  $F_i$  ( $i=1, 3, 4, 6$ ) according to scheme represented on fig. 3. Maximal movement  $\Delta$  in point of application of force  $F_4$  is determined experimentally. Then we find constant bending stiffness of bearing construction.

$$EI_z = \frac{1}{\Delta} \left( -\frac{F_1 d_{23} d_1 d_4 (2l_0 - d_{23})}{6l_0} + \frac{F_3 d_2 d_4 (l_0^2 - d_2^2 - d_4^2)}{6l_0} + \frac{F_4 d_{23} d_4 (l_0^2 - d_{23}^2 - d_4^2)}{6l_0} - \frac{F_6 d_{23} d_5 d_4 (l_0 + d_{23})}{6l_0} \right), \quad (4)$$

where  $E$  is averaged value of coefficient of elasticity;  $I_z$  is averaged value of moment of inertia of cross-section;  $d_{23}=d_2+d_3$ .

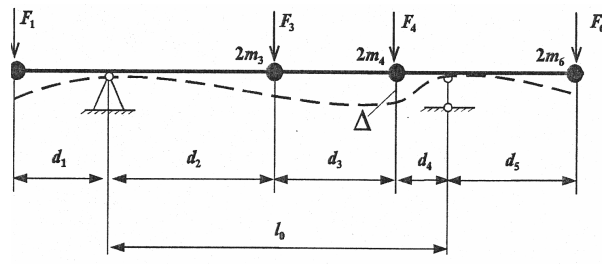


Fig. 3. Scheme of static loading of vehicle's body.

Suppose bending stiffness of each section equals averaged value of bending stiffness that is determined by expression (4). Then we calculate reduced coefficient of elasticity.

$$E_i = \frac{EI_z}{I_{zi}} \quad (i=1, 2, \dots, 5). \quad (5)$$

Thus calculation model of vehicle's body is beam with constant bending stiffness and with variables moment of inertia of cross-section and coefficient of elasticity. Vibrations processes are analyzed taking into account shear deformations and inertia of rotating movement of cross-section of construction according to Timoshenko's beam theory.

Equations of transverse vibrations of section of vehicle's body are written, using calculation scheme represented on fig.2

$$\begin{aligned} \frac{E_i I_i}{l_i^2} \frac{\partial^2 \varphi_i}{\partial \xi_i^2} + kGA \left( \frac{1}{l_i} \frac{\partial w_i}{\partial \xi_i} - \varphi_i \right) - \rho I_i \frac{\partial^2 \varphi_i}{\partial t^2} = 0, \\ kGA \left( \frac{1}{l_i^2} \frac{\partial^2 w_i}{\partial \xi_i^2} - \frac{1}{l_i} \frac{\partial \varphi_i}{\partial \xi_i} \right) - \rho A \frac{\partial^2 w_i}{\partial t^2} = 0 \quad (i=1, 2, \dots, 5), \end{aligned} \quad (6)$$

where  $w_i$  is sag;  $\varphi_i$  is angle of inclination of line which tangent to beam's axis which is bent by moment of flection;  $\xi_i = x_i/l_i$  is relative longitudinal coordinate ( $x_i$  – absolute coordinate of cross-section);  $t$  is time;  $G$  is shear modulus;  $k$  is coefficient which characterizes influence of shear deformation.

Eliminating unknown  $\varphi_i$  from equations (6), we obtain equation of transverse vibrations in form

$$\frac{E_i I_i}{l_i^4} \frac{\partial^4 w_i}{\partial \xi_i^4} - \frac{\rho I_i}{l_i^2} \left( 1 - \frac{E_i}{kG} \right) \frac{\partial^4 w_i}{\partial \xi_i^2 \partial t^2} + \rho A \frac{\partial^2 w_i}{\partial t^2} = 0 \quad (i=1, 2, \dots, 5). \quad (7)$$

Solution of equation (7) must satisfy such boundary conditions

$$M_1 = 0, 2m_1 \frac{\partial^2 w_1}{\partial t^2} - Q_1 = 0, \text{ as } \xi_1 = 0; \quad (8)$$

$$w_{i-1} - w_i = 0, \varphi_{i-1} - \varphi_i = 0, M_{i-1} - M_i = 0,$$

$$2m_i \frac{\partial^2 w_i}{\partial t^2} + Q_{i-1} - Q_i = 0 \quad (i=2, 3, 4, 5), \text{ as } \xi_{i-1} = 1, \xi_i = 0; \quad (9)$$

$$M_5 = 0, 2m_6 \frac{\partial^2 w_5}{\partial t^2} + Q_5 = 0, \text{ as } \xi_5 = 1. \quad (10)$$

Here  $m_1 = m_5 = 0$ ;  $M_i$  is moment of flexion ( $i=1, 2, \dots, 5$ );  $Q_i$  ( $i=1, 2, \dots, 5$ ) is transverse force:

$$M_i = -\frac{E_i I_i}{l_i} \frac{\partial \varphi_i}{\partial \xi_i}, \quad Q_i = \frac{kGA}{l_i} \frac{\partial w_i}{\partial \xi_i} - kGA \varphi_i. \quad (11)$$

Equations (7)–(10) form a mathematical model of transverse vibrations of vehicle's body. These equations must be solved taking into account expressions (6), (11).

### 3. TORSION VIBRATIONS OF VEHICLE'S BODY

Vehicle's body is schematically represented on fig. 4, where  $l_i$  and  $d_i$  ( $i=1, 2, \dots, 5$ ) are lengths of sections of metalware;  $l_0$  is distance between the supporting knots of suspension;  $m_i$  ( $i=1, 3, 4, 6$ ) are the masses of loads which imitate the equipment of vehicle and passengers;  $a_i$  ( $i=1, 3, 4, 6$ ) are distances between centers of loads' masses.

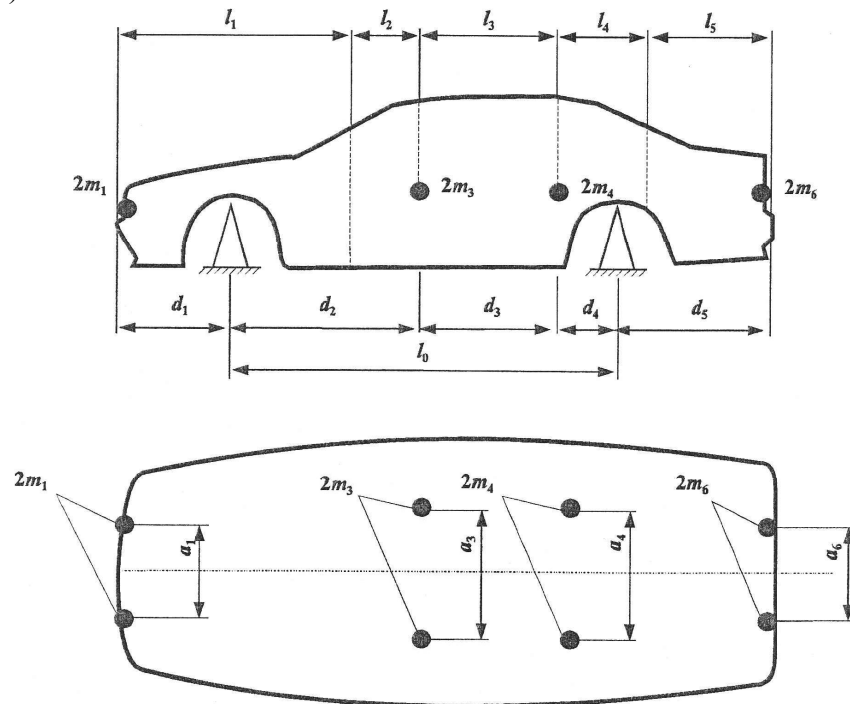


Fig. 4. Scheme of vehicle's body.

Consider free torsion vibrations of vehicle's body. Suppose calculation scheme of bearing metalware in form of a beam (fig. 5) with constants elastic-inertial parameters on sections with length parameters  $l_i$  ( $i=1, 2, \dots, 5$ ). Consider each pair of loads in form of solid body with moment of inertia  $J_i = m_i a_i^2 / 2$  ( $i=1, 3, 4, 6$ ).

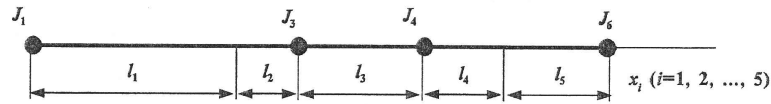


Fig. 5. Calculation scheme for research of torsion vibrations of vehicle's body.

Cross-sections of the beam are identified by coordinate axis  $x_i$  ( $i=1, 2, \dots, 5$ ) with origins on the left borders of the proper sections. Area  $A$  of construction's cross-section is supposed as a constant and determined by formula (1). Polar moment of inertia of cross-section for each beam's section is calculated as

$$I_{pi} = r_i^2 \cdot A \quad (i=1, 2, \dots, 5), \quad (12)$$

where  $r_{zi}$  is polar radius of inertia of cross-section and it is determined by formula (3).

Rigidity properties of metalware are determined by values of reduced shear modulus. For each section these values are determined by formula

$$G_i = \frac{c}{I_{pi}} \quad (i=1, 2, \dots, 5). \quad (13)$$

Values  $c$  is determined experimentally, spinning vehicle's body on section  $l_0$

$$c = c_0 \cdot l_0, \quad (14)$$

where  $c_0$  is torsion rigidity of section  $l_0$ .

Thus calculation model of vehicle's body is beam with constant bending stiffness and with variables polar moment of inertia of cross-section and shear modulus.

Equations of torsion vibrations of section of vehicle's body are written, using calculation scheme represented on fig.5

$$\frac{q_i^2}{l_i^2} \frac{\partial^2 \varphi_i}{\partial \xi_i^2} - \frac{\partial^2 \varphi_i}{\partial t^2} = 0 \quad (i=1, 2, \dots, 5), \quad (15)$$

where  $\varphi_i$  is angle movement;  $q_i$  is velocity of wave propagation of elastic deformation

$$q_i = \sqrt{G_i / \rho}. \quad (16)$$

Solution of equation (15) must satisfy such boundary conditions

$$J_1 \frac{\partial^2 \varphi_1}{\partial t^2} - \frac{G_1 I_{p1}}{l_1} \frac{\partial \varphi_1}{\partial \xi_1} = 0, \text{ as } \xi_1=0; \quad (17)$$

$$J_i \frac{\partial^2 \varphi_i}{\partial t^2} + \frac{G_{i-1} I_{p,i-1}}{l_{i-1}} \frac{\partial \varphi_{i-1}}{\partial \xi_{i-1}} - \frac{G_i I_{pi}}{l_i} \frac{\partial \varphi_i}{\partial \xi_i} = 0, \varphi_i = \varphi_{i-1} \quad (i=2, 3, 4, 5), \text{ as } \xi_{i-1}=1, \xi_i=0; \quad (18)$$

$$J_6 \frac{\partial^2 \varphi_6}{\partial t^2} - \frac{G_5 I_{p5}}{l_5} \frac{\partial \varphi_5}{\partial \xi_5} = 0, \text{ as } \xi_5=1, \quad (19)$$

moreover  $J_2=J_5=0$ .

Equations (15), (17)–(19) form a mathematical model of torsion vibrations of vehicle's body.

#### 4. RESULTS AND CONCLUSIONS

Offered mathematical models are executed with application of matrix method of initial parameters in the form of computer programs for definition of eigenfrequencies and eigenforms transverse and torsion vibrations of vehicle's bodies. Results of calculations of lowest eigenfrequencies of typical design of vehicle's body, and also experimental values of corresponding frequencies are adduced in table 1 and 2.

Comparison of theoretical and experimental results shows, that inaccuracy of definition of lowest eigenfrequencies of mechanical system by means of offered technique doesn't exceed 15 %. Offered mathematical models give the possibility to find lowest eigenfrequencies and eigenforms of compound metalware on the basis of simple algorithm which is reduced to solving of transcendental equations with application of simple operations with matrixes. It provides appropriate efficiency of calculations of difficult mechanical systems on vibrations.

Table 1. Values of lowest eigenfrequencies of transverse vibrations of vehicle's body (Hz)

Without loads		With loads	
Without windows	With windows	Without windows	With windows
a) calculated values			
36,60	43,49	25,08	29,76
b) experimental values			
–	40,87	–	28,20

Table 2. Values of lowest eigenfrequencies of torsion vibrations of vehicle's body (Hz)

Without loads		With loads	
Without windows	With windows	Without windows	With windows
a) calculated values			
28,500	34,252	23,189	27,870
b) experimental values			
–	40,000	–	24,600

Thus, using of continuous calculating models gives the possibility with sufficient accuracy to estimate lowest eigenfrequencies of free vibrations of vehicle's bodies. Offered approach can be used in engineering practice for the purpose of reduction of levels of noise and vibrations of vehicles at the expense of elimination of resonant operating regimes of bearing metalwares. It will facilitate reduction of materials consumption, increase of functional reliability and improve of comfortableness of vehicles.

## REFERENCES

- [1] Филиппов А. П. *Колебания деформируемых систем*. М.: Машиностроение, 1970. – 732 с.
- [2] Бидерман В. Л. *Теория механических колебаний*. – М.: Высшая школа, 1980. – 408 с.
- [3] Еременко С. Ю. *Методы конечных элементов в механике деформируемых тел*. Харків: Основа, 1991. – 272 с.
- [4] Rusiński E. *Metoda elementów skończonych. System COSMOS/M*. – Warszawa: Wydawnictwa Komunikacji i Łączności, 1994. – 392 s.
- [5] Харченко Є. В. *Динамические процессы буровых установок*. – Львів: Світ, 1991. – 176 с.
- [6] Харченко Є. В. *Континуально-дискретна математична модель крутильних коливань баштових бурових вишок* // *Машинознавство*. – 1997. – №1. – С. 41–46.
- [7] Підгайний Т. Ю. *Математичне моделювання крутильних коливань каркасної металоконструкції* // *Оптимізація виробничих процесів і технічний контроль в машинобудуванні та приладобудуванні* / *Вісник НУ «Львівська політехніка»*. – 2007. – №583. – С. 52–57.

Rafał KLICH<sup>1</sup>

Andrzej WOJNAR<sup>2</sup>

Aleksander KOZŁOWSKI<sup>3</sup>

## INITIAL STIFFNESS OF BOLTED JOINTS USED IN STEEL THIN WALLED STRUCTURES

### ABSTRACT

Bolted lap joints are often used in steel thin walled structures. In the global analysis, this kind of joints is conventionally considered as a hinge. Such simplification has an influence on increasing the value of bending moment in a beam, and the size of its cross section. In fact, such connections are semi-rigid. Their moment-rotation ( $M-\phi$ ) characteristic can be effectively predicted by experimental testing, but such tests in a majority of cases are costly and labour-absorbing. The numerical simulations are alternative method to obtain the flexibility parameters of such joints. This simulations can be carried out using the computer software based on FEM, ie. ADINA software. A next possibility to obtain joint flexibility characteristics is mechanical modeling of the joint.

This paper presents the mechanical model of bolted lap joint permitting to calculate the initial stiffness of connection. To create this model a component method was used.

**KEYWORDS:** thin walled steel structures, bolted lap joints, initial stiffness of joints.

### 1. INTRODUCTION

Light gauges steel frames are very often used because of their small self weight. This kind of frames is made from thin-walled steel profiles connected by means of the bolted joints with gusset plate. In practice, non-preloaded bolts of small-diameters (10, 12mm) are used. In the global analysis, this kind of joints is conventionally considered as a hinge. In fact, such connections are semi-rigid. To take into account in the global analysis real joint behavior, joint characteristics are needed. Such characteristics are moment-rotation relation and their parameters as: initial stiffness, moment resistance and rotation capacity. The best way to get these data is to conduct experimental tests, but it is very expensive and time consuming [1], [2], [3]. Alternative to experimental test is mechanical modeling [4], [5] or numerical simulation [6]. In the paper preliminary, mechanical model of chosen bolted lap joint is presented. In this model component method as well as numerical simulation is used.

<sup>1</sup> MSc. Eng., Rzeszow University of Technology, Rzeszow, POLAND,

<sup>2</sup> PhD. Eng., Rzeszow University of Technology, Rzeszow, POLAND,

<sup>3</sup> Associate Prof. PhD, DSc. Eng., Rzeszow University of Technology, Rzeszow, POLAND.

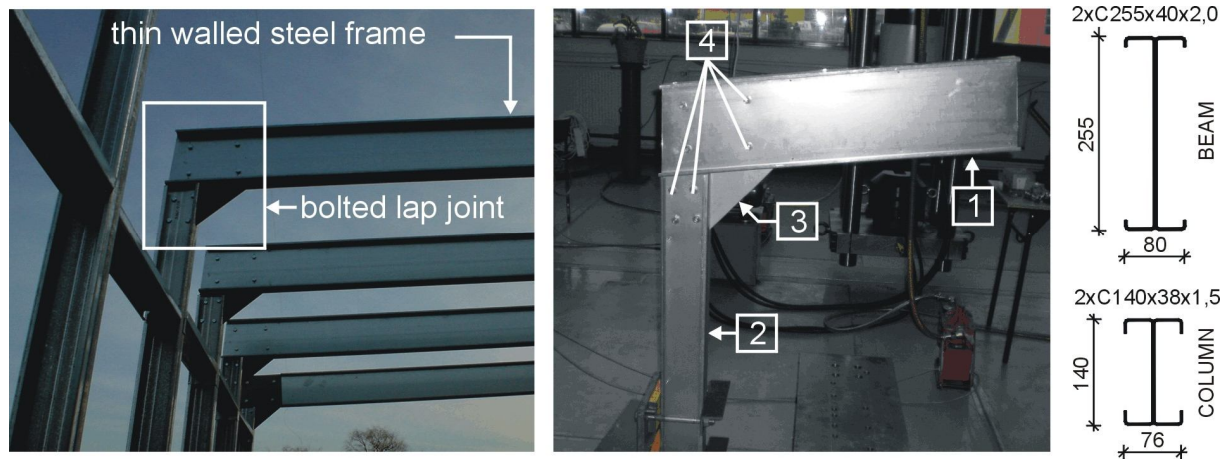


Fig. 1. The view of analyzed connection.

Investigated joint (Fig. 1) consists of: (1) - the beam, (2) - the column, (3) - gusset plate and bolts (4). Beams and columns are made of cold formed, thin walled steel profiles. The thickness of member's flanges and web is 2,0 mm for beam and 1,5 mm for column. The beam and column are connected to each other using the gusset plate and bolts. The thickness of gusset plate is 4,0 mm. The diameter  $d$  of bolts is 12 mm. The connection is non-preloaded. All members are made from steel grade S235, bolts grade is 5.8.

## 2. MECHANICAL MODEL OF BOLTED LAP JOINT

Mechanical model of bolted lap joint was created taking into consideration the following assumptions:

1. All parts of the connection work in elastic range.
2. All deformations and displacements are small, so the geometrical relations have a linear character.
3. The principle of flat cross-section is valid.
4. The connection is loaded by bending moment.

Proposed mechanical model are presented in Figure 2. This model was built from three component groups:

- P1 – the component group representing the connection between the beam and gusset plate, characterized by stiffness  $S_{j,b}$ .
- P2 – the component group representing the gusset plate in compression, characterized by stiffness  $S_{j,g}$ .
- P3 – the component group representing the connection between column and gusset plate, characterized by stiffness  $S_{j,c}$ .

The initial stiffness of bolted lap joint  $S_{j,ini}$  can be calculated according to formula:

$$S_{j,ini} = \frac{1}{\frac{1}{S_{j,b}} + \frac{1}{S_{j,c}} + \frac{1}{S_{j,g}}} \quad (1)$$

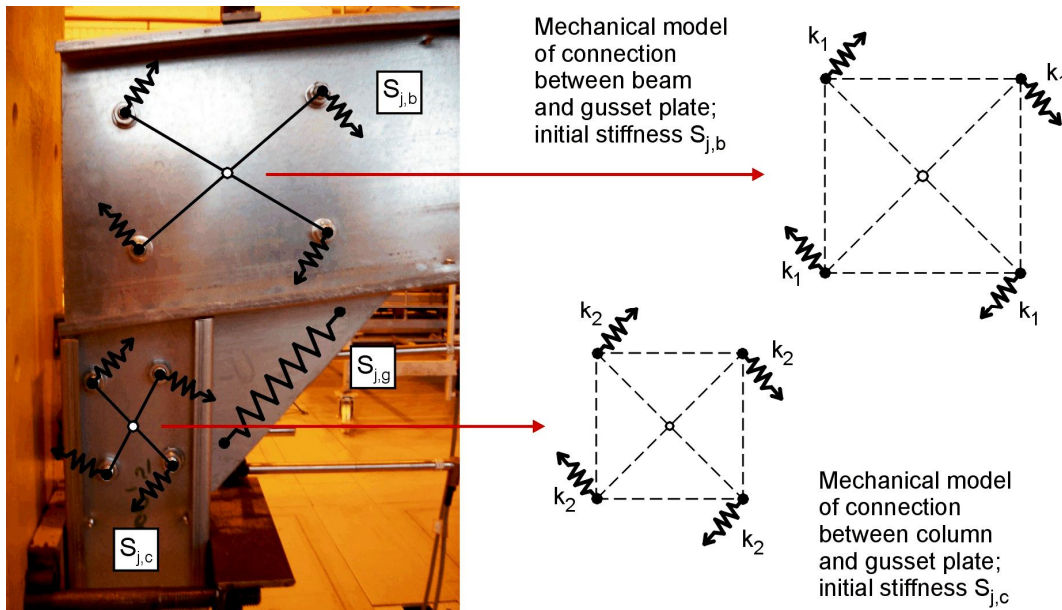


Fig. 2. Mechanical model of investigated joint

In the preliminary model presented here, the stiffness of connection part P2 of joint is assumed to be equal to infinity ( $S_{j,g} = \infty$ ) and was neglected in the analysis. For that reason, equation (1) was transformed to:

$$S_{j,ini} = \frac{1}{\frac{1}{S_{j,b}} + \frac{1}{S_{j,c}}} \quad (2)$$

To obtain the initial stiffness  $S_{j,b}$  and  $S_{j,c}$  of component parts P1 and P3, the mechanical model of this part was created (Fig.3). This model was loaded by displacement - the rotation on angle  $\phi$ . Forces in springs were calculated according to formula:

$$F_{1/2} = k_{1/2} \cdot \Delta L_{1/2} \quad (3)$$

where:

- $F_{1/2}$  - the force in springs,
- $k_{1/2}$  - stiffness of spring,
- $\Delta L_{1/2}$  - displacement of spring,
- 1/2 - connection gusset plate with beam/column.

The displacement of springs representing the components of joint, was calculated using formula (4). Taking into consideration equations (3) and (4), forces in springs can be calculated by formula (5).

$$\Delta L_{1/2} = r_{1/2} \cdot \text{tg}\phi = \sqrt{x_{1/2}^2 + y_{1/2}^2} \cdot \text{tg}\phi \quad (4)$$

$$F_{1/2} = k_{1/2} \cdot r_{1/2} \cdot \text{tg}\phi = k_{1/2} \cdot \sqrt{x_{1/2}^2 + y_{1/2}^2} \cdot \text{tg}\phi \quad (5)$$

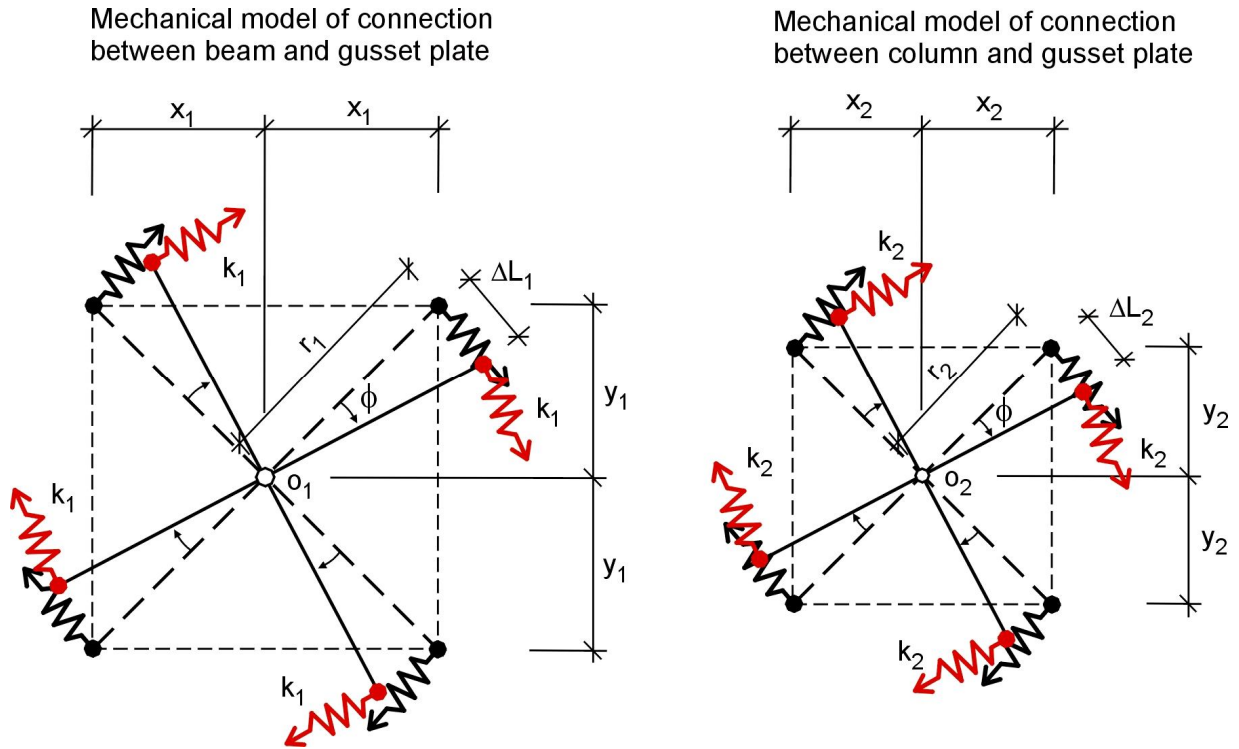


Fig. 3. Mechanical model of component parts P1 and P3

Bending moment, as a reaction of the joint to the rotation of joint on angle  $\phi$ , was calculated according to formula:

$$M = \sum_1^4 F_{1/2} \cdot r_{1/2} = \sum_1^4 k_{1/2} \cdot r_{1/2} \cdot \text{tg}\phi \cdot r_{1/2} = \sum_1^4 k_{1/2} \cdot r_{1/2}^2 \cdot \text{tg}\phi = \sum_1^4 k_{1/2} \cdot [x_{1/2}^2 + y_{1/2}^2] \cdot \text{tg}\phi \quad (6)$$

$$M = 4 \cdot k_{1/2} \cdot [x_{1/2}^2 + y_{1/2}^2] \cdot \text{tg}\phi \quad (7)$$

due to assumption 2:  $\text{tg}\phi \approx \phi$ ;  $\Rightarrow M = 4 \cdot k_{1/2} \cdot [x_{1/2}^2 + y_{1/2}^2] \cdot \phi \quad (8)$

The initial stiffness of lap bolted joint was calculated as:

$$S_{j,\text{ini}} = \frac{M}{\phi} = \frac{4 \cdot k_{1/2} \cdot [x_{1/2}^2 + y_{1/2}^2] \cdot \phi}{\phi} = 4 \cdot k_{1/2} \cdot [x_{1/2}^2 + y_{1/2}^2] \quad (9)$$

### 3. STIFFNESS OF COMPONENTS

The following components should be included in mechanical model:

- spring of stiffness  $k_b$  representing the web panel of beam in bearing,
- spring of stiffness  $k_g$  representing the gusset plate in bearing,
- spring of stiffness  $k_c$  representing the web panel of column in bearing,
- spring of stiffness  $k_s$  representing the shank of bolt in shear.



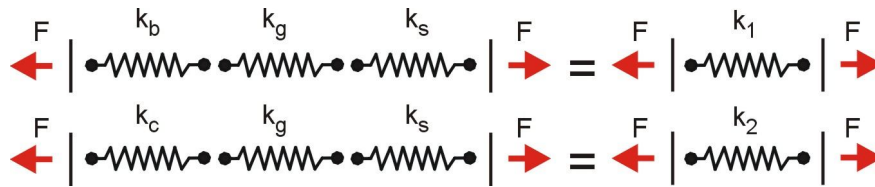


Fig. 4. The method of calculation of stiffness  $k_1$  and  $k_2$ .

Stiffness  $k_{1/2}$  of springs can be calculated using formulas (10), see Fig. 4.

$$\frac{1}{k_1} = \frac{1}{k_b} + \frac{1}{k_g} + \frac{1}{k_s}; \quad \frac{1}{k_2} = \frac{1}{k_c} + \frac{1}{k_g} + \frac{1}{k_s} \tag{10}$$

To obtain the initial stiffness of joint components, numerical simulations using ADINA software was preformed [7]. The numerical model of components: the web panel of beam and column in bearing, the gusset plate in bearing, the shank of bolt in shear, is presented in Fig. 5.

3D, 20-nodes solid elements were used to build the model. Between the surfaces modeling the shank of the bolt and the hole, the contact surfaces enabling to transfer only compressing forces were used. All models were loaded by displacement  $\Delta$ . The force  $P$  was calculated as a reaction resulted form applied load. The material characteristics of webs and gusset plate were obtained from tensile coupon tests (Fig. 6). The yield and ultimate stress of bolt steel were admitted according to obligatory codes depending on steel grade of bolt.

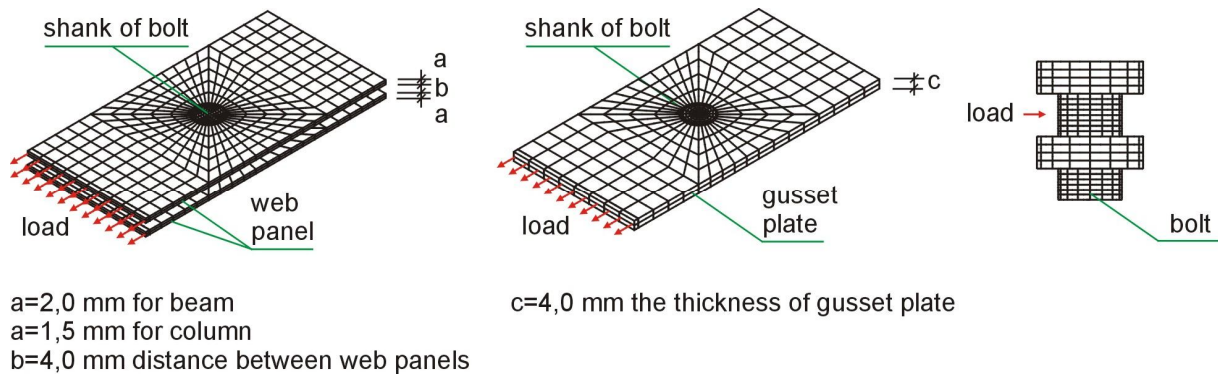


Fig. 5. Numerical models of components.

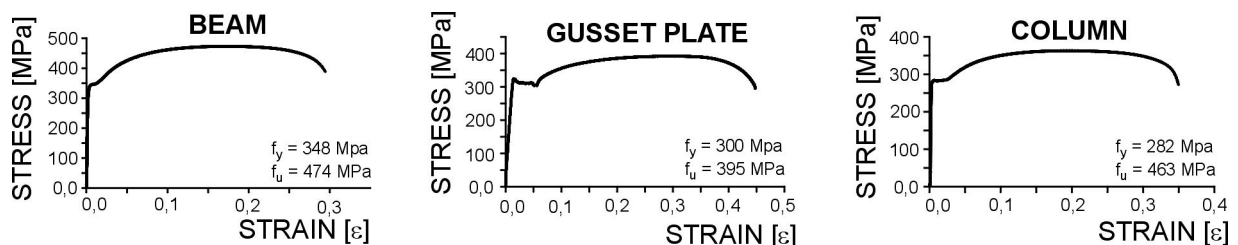


Fig. 6. Material characteristics of elements used in numerical simulation.

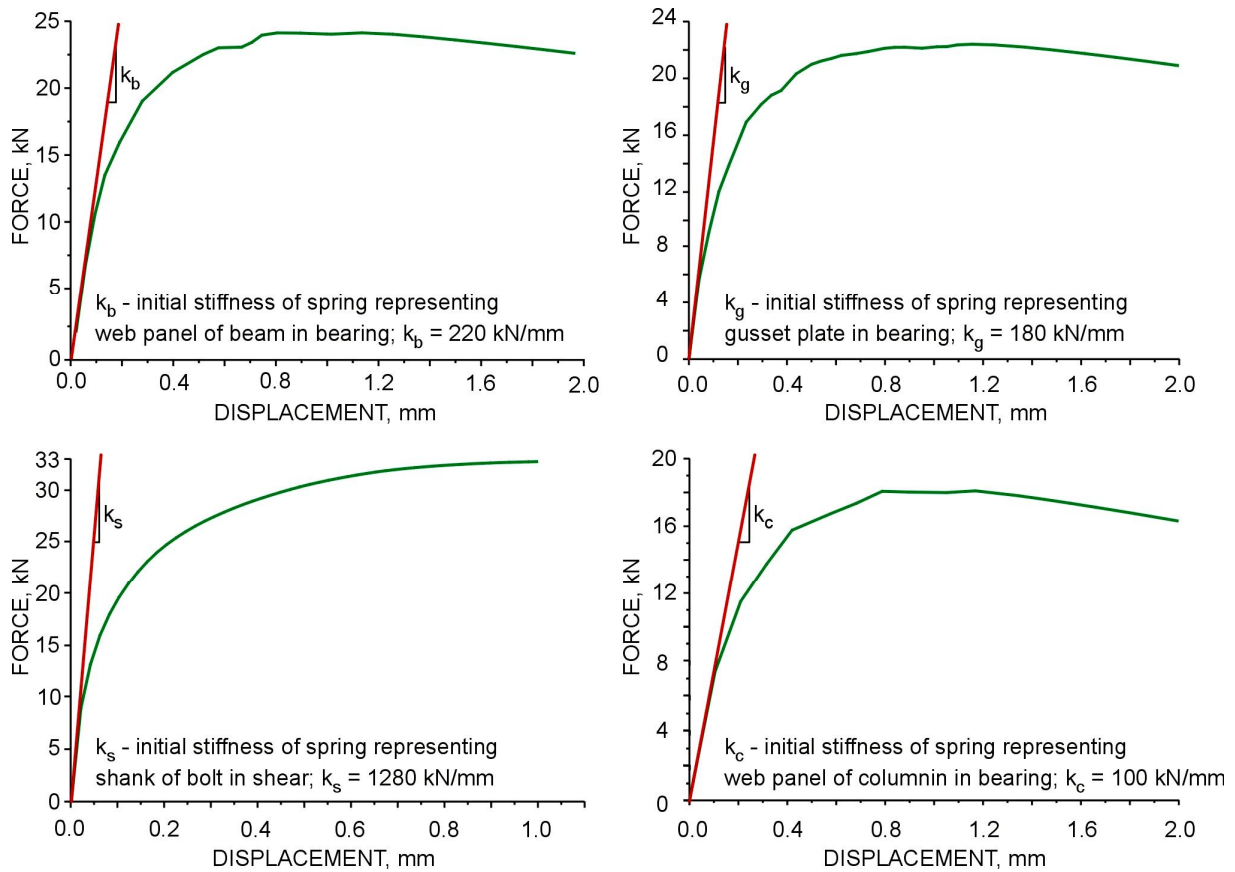


Fig. 7. The initial stiffness of spring representing the component of joint.

Results of numerical calculations, as a P- $\Delta$  diagrams were presented in Fig. 7. The initial stiffness of components was obtained based on the P- $\Delta$  (force-displacement) diagram, as a tangent to a curve in the initial point of force-displacement graph.

Obtained values are:

$$k_b = 220 \text{ kN/mm},$$

$$k_g = 180 \text{ kN/mm},$$

$$k_s = 1280 \text{ kN/mm},$$

$$k_c = 100 \text{ kN/mm}.$$

#### 4. COMPARISON OF THE RESULTS OBTAINED FROM MECHANICAL MODEL WITH EXPERIMENTAL TEST

Based on the component stiffness values obtained from numerical simulations, stiffness  $k_1$  and  $k_2$  was calculated according to formula (10):

$$\frac{1}{k_1} = \frac{1}{k_b} + \frac{1}{k_g} + \frac{1}{k_s}; \quad \frac{1}{k_1} = \frac{1}{220 \frac{\text{kN}}{\text{mm}}} + \frac{1}{180 \frac{\text{kN}}{\text{mm}}} + \frac{1}{1280 \frac{\text{kN}}{\text{mm}}}; \quad k_1 = 92 \frac{\text{kN}}{\text{mm}}$$

$$\frac{1}{k_2} = \frac{1}{k_c} + \frac{1}{k_g} + \frac{1}{k_s}; \quad \frac{1}{k_2} = \frac{1}{100 \frac{\text{kN}}{\text{mm}}} + \frac{1}{180 \frac{\text{kN}}{\text{mm}}} + \frac{1}{1280 \frac{\text{kN}}{\text{mm}}}; \quad k_2 = 61 \frac{\text{kN}}{\text{mm}}$$

The initial stiffness of component groups was calculated according to formula (9). The geometrical dimensions of joint were measured and their values are:

- for component group P1 representing beam and gusset plate:  $x_1=90\text{mm}$ ,  $y_1=60\text{mm}$  (Fig.3):

$$S_{j,b} = 4 \cdot k_1 \cdot [x_1^2 + y_1^2] = 4 \cdot 92 \cdot [90^2 + 60^2] = 4300 \frac{\text{kNm}}{\text{rad}}$$

- for component group P3 representing column and gusset plate:  $x_2=40\text{mm}$ ,  $y_2=30\text{mm}$  (Fig.3).

$$S_{j,c} = 4 \cdot k_2 \cdot [x_2^2 + y_2^2] = 4 \cdot 61 \cdot [40^2 + 30^2] = 610 \frac{\text{kNm}}{\text{rad}}$$

The initial stiffness of joint was calculated according to formula (2):

$$S_{j,ini} = \frac{1}{\frac{1}{S_{j,b}} + \frac{1}{S_{j,c}}} = \frac{1}{\frac{1}{4300} + \frac{1}{610}} = 540 \frac{\text{kNm}}{\text{rad}}$$

The value of initial stiffness calculated based on presented mechanical model of joint, was compared with the value of stiffness of the same joint obtained during an experimental test [3]. In the experiment value of  $S_{j,ini} = 800 \text{ kNm/rad}$  was obtained.

Differences between experimental test result and result obtained using mechanical model can be explained in the following way. During experiment, according to test set-up, not only bending moment but also axial force was applied to the joint, what influence the stiffness of the joint. It is well known, that compressive force acting together with bending moment increase stiffness of the joint.

## 5. CONCLUSIONS

The following conclusions can be drawn:

- mechanical modeling of bolted thin walled steel structures joints is a valuable alternative to experimental testing of joints,
- preliminary model presented in the paper, which not include all components and their interactions, gives results which can be accepted from the engineering point of view. This model will be further improved in the future,
- stiffness of the particular components of the joint: web panel of beam in bearing, gusset plate in bearing, web panel of column in bearing and shank of bolt in shear was obtained by the numerical simulation. There is a need to conduct both experimental tests as well as analytical modeling of these components, to obtain close, simple formulas, similar to that like for components included in [4].

## REFERENCES

- [1] Dunai L., Foti P.: Experimental behaviour modes of cold-formed frame-corners. Connections in Steel Structures V, Amsterdam, 2004.
- [2] Wuwer W.: Podatne połączenia na sworznie jednostronne w prętowych konstrukcjach cienkościennych. Gliwice, Zeszyty Naukowe Politechniki Śląskiej, 2006.
- [3] Klich R., Wojnar A., Kozłowski A.: Badania doświadczalne węzłów narożnych ram wykonanych z profili cienkościennych, Oficyna Wydawnicza Politechniki Rzeszowskiej,

Zeszyty Naukowe Politechniki Rzeszowskiej, Seria: Budownictwo i Inżynieria Środowiska, Rzeszów, 2008.

- [4] EN 1993-1-8. 2005. Eurocode 3 - Design of steel structures – Part 1-8: Design of joints. CEN.
- [5] Pietrapertosa C., Piraprez E., Jaspart J.P.: Ductility requirements in shear bolted connections. Connections in Steel Structures V. Amsterdam 2004.
- [6] Raus R., Ziemiański L.: Modelowanie zakładkowego połączenia śrubowego ze szczególnym uwzględnieniem początkowej fazy pracy. Konferencja naukowa: Węzły podatne w konstrukcjach stalowych. Rzeszów 1998.
- [7] ADINA R&D, Theory and Modeling Guide, 2003.

Stanisław KUŚ<sup>1</sup>

## DEVELOPMENT OF FUNICULAR STRUCTURES FROM PLANE TO SPACE

### ABSTRACT

The paper presents the origin of the idea of funicular structures from the mathematical equation:  $y = ax^2 + bx + c$  till the three dimensional folded structures of single, double and triple curvature chords. About 1860 they were used as effective bridge beams in Great Britain and Germany – and after the Second World War in Poland for industrial and sport halls as elegant shape structures space.

**KEYWORDS:** equation of second order, funicular structures bridge beams and roof curved structures.

### 1. GENESIS OF IDEA.

The origin of funicular structures, as well formerly planes on their beginning and space structures as actually, lies in precise adoption of mathematics to the mechanical application. Application of the theory to the shaping of structures. Let us begin with the mathematics which indeed was at the beginning with all known symbols and significations:

$$y = ax^2 + bx + c$$

equation of parabola

$$\frac{dy}{dx} = 2ax + b$$

first derivative

$$\frac{d^2y}{dx^2} = 2a = \frac{M}{EJ} = K = \frac{1}{R}$$

curvature

$$\frac{d^3y}{dx^3} = \frac{dM}{dx} = V = 0$$

transverse force, first derivative of the moment

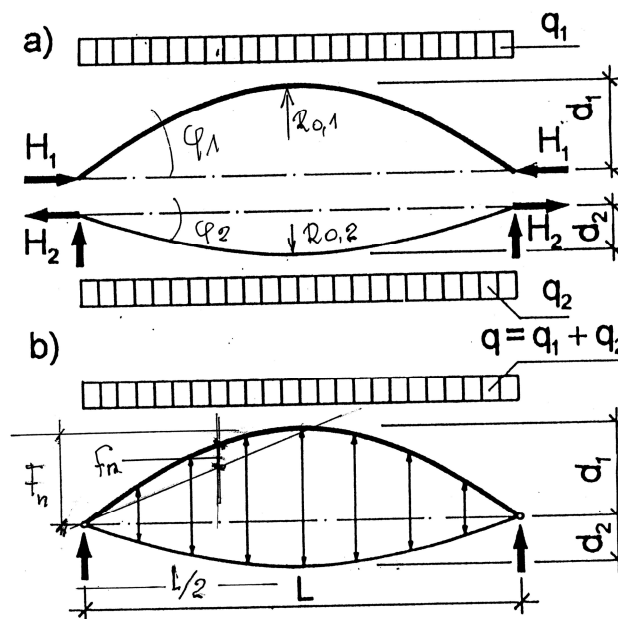
<sup>1</sup> Prof. D.Sc. PhD. Eng., Rzeszów University of Technology, Rzeszow, POLAND

The diagram of moment  $M_{(x)}$  for the continuous load of the simple beam is also presented by the same equation of second order. The curvature of this beam is linearly proportional to this moment for constant values of Young's modulus and second moment of area  $J$ . But the curvature of parabola in the apex is equal  $K = \frac{1}{R} = \frac{8d}{L^2}$  and  $R = \frac{L^2}{8d}$ ;

$$a = \frac{L^2}{4d}$$

where  $d$  – rise of arch, depth

So if we can create a structure with upper and bottom chords, belts or flanges parabola-like we will receive the two belts girder with constant horizontal component force in both chords. Due to their inclination they are axially stressed with zero transversal force. (Fig.1)



a) Fig. 1 Diagram of internal forces in the two chords (belts) funicular structure under the constant load: a) scheme of separated chords, b) scheme of connected chords.

$$H_1 = q_1 R_{0,1} \quad R_{0,1} = \frac{L^2}{8d_1} \quad K_{0,1} = \frac{1}{R_{0,1}}$$

$$H_2 = q_2 R_{0,2} \quad R_{0,2} = \frac{L^2}{8d_2} \quad K_{0,2} = \frac{1}{R_{0,2}}$$

$$H_1 + H_2 = 0 \quad q_1 R_{0,1} = q_2 R_{0,2}$$

When

$$q_1 + q_2 = q \quad \frac{q_1}{q_2} = \frac{K_{0,1}}{K_{0,2}} = \frac{d_1}{d_2}$$

$$q_1 = q \frac{d_1}{d_1 + d_2} \quad q_2 = q \frac{d_2}{d_1 + d_2}$$

$$N = \frac{H}{\cos \varphi} = q \frac{1}{K_{0,1} + K_{0,2}} = q \frac{R_{0,1} R_{0,2}}{R_{0,1} + R_{0,2}} = q \frac{L^2}{8(d_1 + d_2)}$$

where:

$R_{01}$   $R_{02}$  radius of curvature of parabola in the apex-in axis of symmetry,

$H$  – horizontal component of tension  $T$  and compression  $C$  in bottom and upper belt,  $d$  or

$f$  – depth, or height, rise of arch

$N$  – longitudinal force,

Equations of equilibrium

The statements presented on Fig. 1 permit to obtain the following conclusions:

- The total constant load  $g$  is distributed to the compressed convex upper chord  $C$  and to the tensioned bottom concave one  $T$ , proportionally to their depth  $d_1$ ,  $d_2$  divided by the total lever of interior forces  $(d_1 + d_2)$ ,
- The longitudinal horizontal force in belts  $H$  being equal in both belts in the middle, in apex of structure and increases to  $N$  in the direction to the supports according to the cosine angle of inclination of belts  $\varphi_1$  and  $\varphi_2$ ,
- The vertical ties joining both parabolas upper and bottom are compressed when the load lies on the upper chord, and tensioned when it is suspended to the bottom one,
- The connection between both chords protects the compressed chord from buckling in vertical plane.

## 2. FIRST APPLICATIONS

These statically properties of funicular parabolic shape of the chords in comparison to the parallel rectangular beams or truss demanded also less steel for the bridges and less human work.

Therefore these funicular shapes have been invented already in 1859 in England by Isambard Kingdom Brunel and applied in the Saltash bridge over the river Tamar ( $l=136,5m$ ) (Fig. 2) near Plymouth.



Fig. 2 The Saltash Bridge (England) designed by Isambard Kingdom Brunel as funicular truss, (1859) with 2 chords.

The span of the truss  $L = 139\text{m}$  and the depth in the middle  $d = 19\text{m}$   $\left(\frac{f}{L} = \frac{1}{7,3}\right)$ . The top chord is made of elliptical steel tube, the bottom is of wrought iron links.

Similar structure has been designed by ing. Franz Pauli from Bavaria and built in bridge over Rein in Mayance. Both engineers have been distinguished for the creative invention with the noble title “sir” Brunel by queen Victoria and the title “von Pauli” by Kanzler Bismarck. Lot of similar bridges has been built in the USA.

Even professor W. Ritter from the famous Polytechnic School in Riga supposed that lot of crash of steel railway bridges in the early period of railway transport have been caused by the oscillations of the structure due to the vibrations of the passing trains. Support in the neutral axis of the structure maybe will avoid them.



Fig. 3 The Bridge in Hamburg (1887 – Germany) created by three funicular spans of  $L = 100\text{m}$  called as “fish shape”. The stiff short column acts as the hoisted support in axis for simple spans. The axial horizontal railway is partly supported by studs and partly suspended on the hangers.

The proof that even today the funicular shape is esthetically attractive gives the new Kotlarski Bridge in Cracow (Poland). It has been chosen by the city after an open competition, and built nevertheless his higher cost.





Fig. 4 The Kotlarski Bridge in Cracow ( Poland ), span  $L = 166\text{m}$ , build 2004.

Four funicular parallel bridge arch's are of different heights. Perpendicular curved stiffening beams keep the top chords in balance. The bottom belt is of smaller depth due to the danger of flood of Vistula River. Vertical connecting rods work partly as struts and partly as ties. The idea of aesthetics dominates in this urban bridge.

### 3. TRANSFORMATION FROM TWO TO THREE DIMENSIONAL STRUCTURE OR FOLDED SECTION.

The funicular idea may be presented even more general: If the curvature of the bottom chord  $K_{02} = 0$  we have to do with an arch with horizontal tie; when the curvature  $K_{01} = 0$  we have the simple straight beam with suspended tie. The first convex model has been applied in Poland in some thousand units for the roofs of industrial buildings with funicular  $18,00 - 60,00\text{m}$  span. The plane precast prestressed arch-like beams are working as the diaphragms of the short cylindrical shells when they are monolitized with the precast concrete ribbed slabs. They proved to be very efficient and durable structure after half hundred years of exploitation

(Fig. 5). Transformation of two dimensional structure to three dimensional is received by concreting the gap as shown on Fig. 5

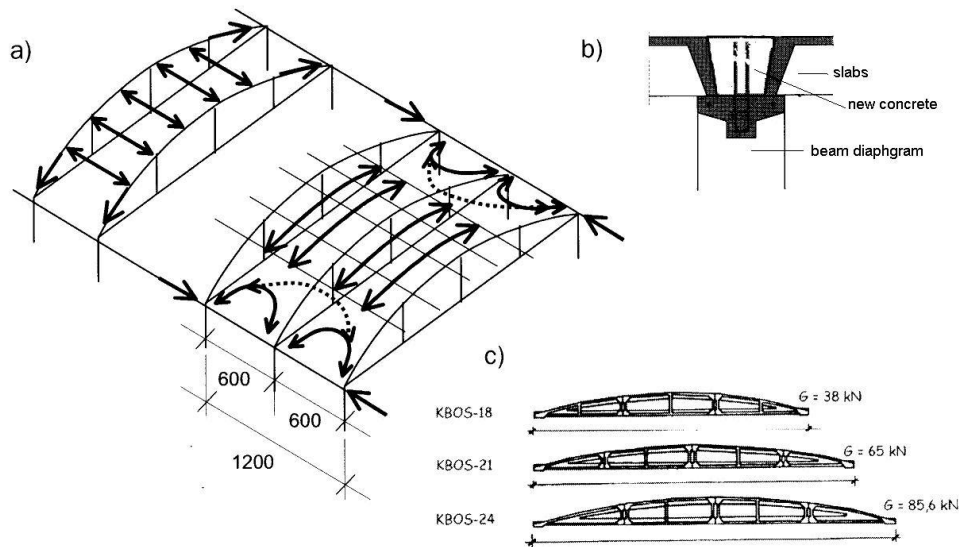


Fig. 5 Funicular concrete prestressed beams arc-like with straight tie

$\left(\frac{f}{L} = \frac{1}{15}\right)$  work as diaphragms of short cylindrical shells created by precast and prestressed units.

- transformation of plane funicular arc-like structure into the space short shell by gluing with fresh concrete the gap between slab and the upper belt of beam
- fill of gap between two units with concrete – monolitization
- examples of the funicular shape of beams precast and prestressed, working as diaphragms.

The arrows show the direction of forces before, and after monolitization.

Fig. 6 is presenting the other transformation of the robust rectangular section of a beam into the folded structure with much bigger stiffness but with the same area. The section may be as well concrete or steel. If steel one is accepted the elastic springs represent vertical and horizontal stiffeners as advantage of folding.

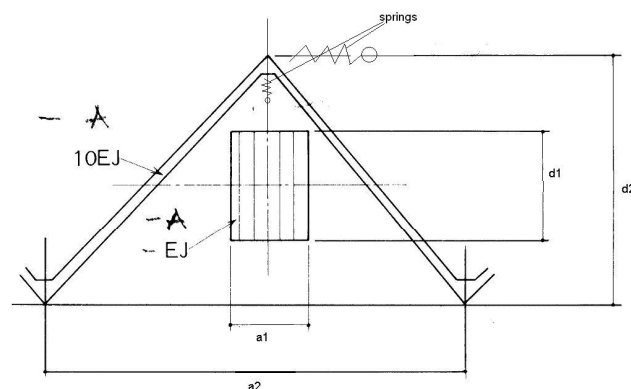


Fig. 6 The idea of three dimensional folded structure in comparison with the plane of the same mass. The inclined form work creates elastic stiffeners of compressed chord in both directions.

All these structures may be or with parallel folding along the span, or curved along in vertical and in horizontal plane.

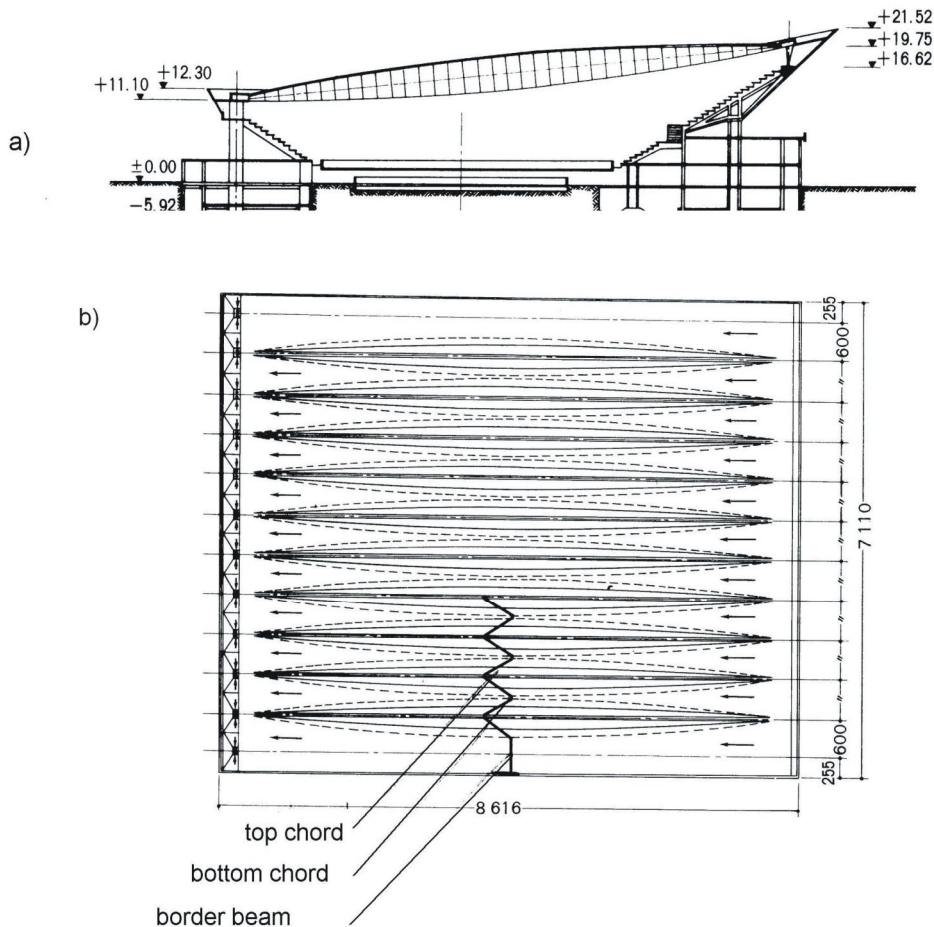


Fig. 7 Section and plan of the Olivia Hall in Gdansk (Poland). The steel structure is parabolic curved as well in vertical as in horizontal plane.

The span is  $L = 83\text{m}$  and the lever of internal forces  $f = 4,0\text{m}$  ( $\frac{f}{L} \approx \frac{1}{20}$ ). The lower

chord is prestressed to diminish the deflection of very flat structure.

a) section of the total structure

b) plan of the roof

The structure of the roof of the known from “Solidarity” meeting Olivia Hall in Gdansk is an example of folded shape with double curvature. The double funicular shape in vertical and horizontal plane permits to take the gravity loads and the wind forces. Connecting tensioned and compressed chords on their end in one point permits to support the folded roof by the column in one point. In vertical plane the chords are connected by compressed struts. Their compression is caused by shortening of the bottom concave chord by the prestressing force. The horizontal struts connect the neighboring bottom chords, which transfer the wind forces up to the border edge, a kind of attics. The funicular shape is applied also in the main tribune beam and in the foundations. Their depth is proportional to their bending moments.

The view of the structure is presented on Fig. 8. During assembling the structure has been divided into  $6,00 \times 80,00\text{m}$  sections as analyzed in statical calculation. Divided along half of the straight top chord composed of two double T steel sections of  $500\text{mm}$  depts.

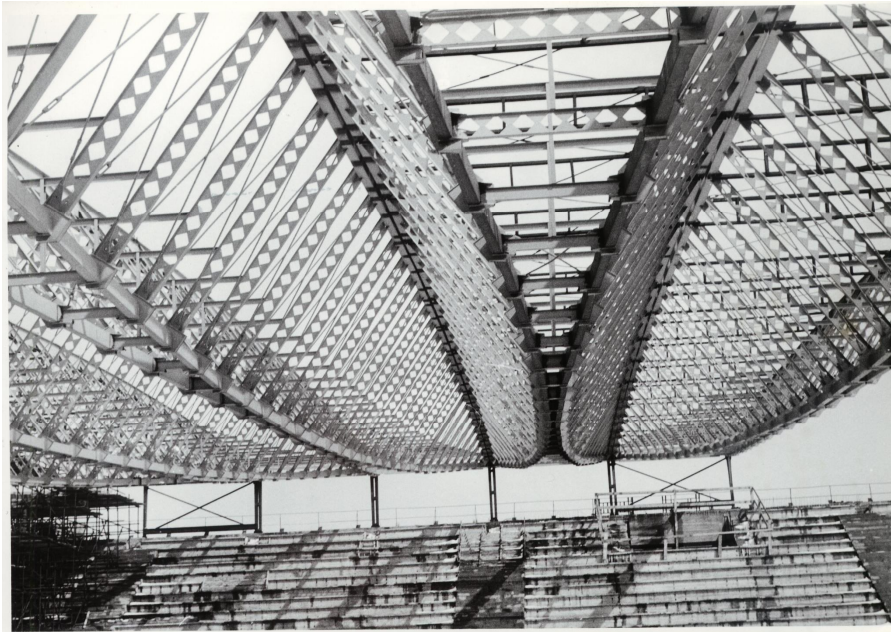


Fig.8 View of the Olivia structure during assembling. The curved is the bottom - concave chord, straight in photo is the top convex chord.

The idea of different solutions of the parallel and inclined funicular structures is presented on the drawing Fig. 9 for fixed and pin supported folded beam.

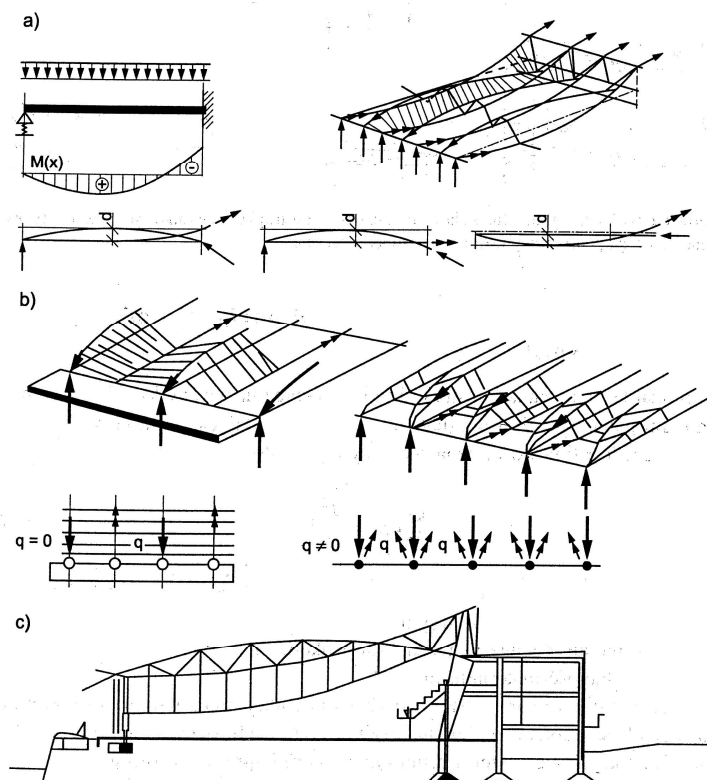


Fig. 9 Different solutions of double chords statically indeterminate systems  
 a) fixed and freely supported diagram of static scheme  
 b) edge horizontal beam and double curved chords  
 c) section of real structure realized in Konin and Pulawy in Poland.

Main idea of this drawing lies in presenting, that the vertical reaction of the two chord folded beam of funicular shape depends from the curvature of the chord. If the two curvature of the chord convex or concave at support have only horizontal component there is no need for supporting vertical column but there is need of edge beam to take the horizontal component of the force in neighboring parabolic chord. Such original structures as shown on Fig. 9 have been built in Poland for the swimming pools.

#### 4. MULTI SPAN FUNICULAR STRUCTURE

The most ingenious spatial funicular structure for 3 span has been realized at the big first in Poland warehouse Supersam at Warsaw (Fig. 10)

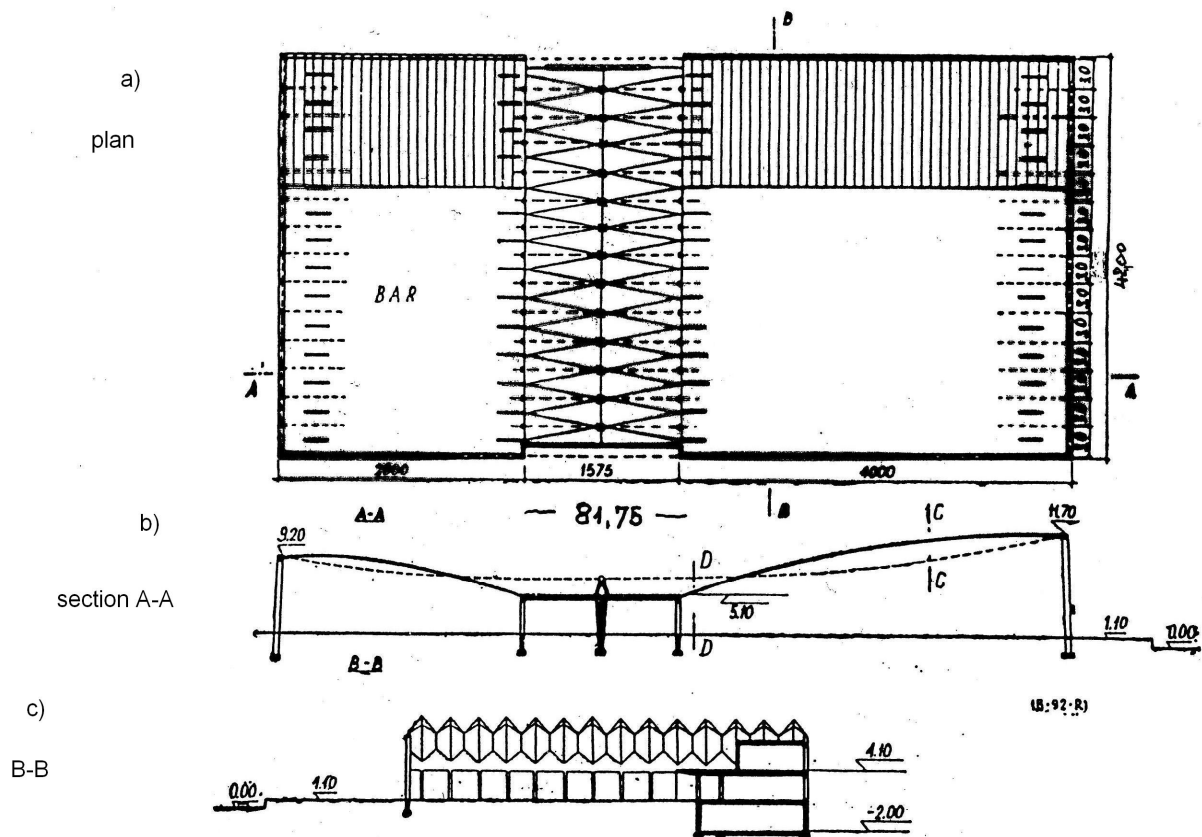


Fig. 10 Three span funicular system Supersam Warsaw

- a) plan
- b) longitudinal section
- c) transversal section

Main structural conception of this famous structure is based on the geometrical properties of parabola presented on drawing (Fig. 11).

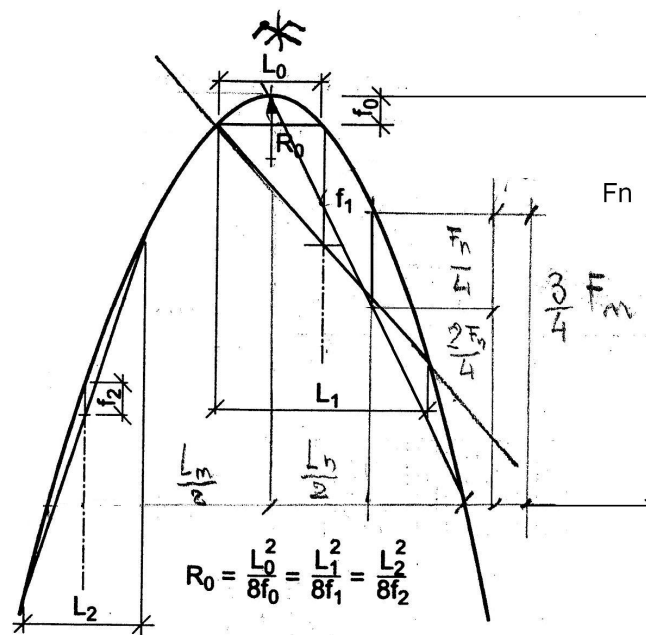


Fig. 11 Structurally important properties of parabola. Radius of curvature in apex  $R_0$  can be defined in axis as on Fig. 1. But it can be also calculated independently by facultative secant, its horizontal plan  $L$  and corresponding vertical depth  $f_n$  between the secant and parabola.

When the apex is connected by the secant with the optional end of parabola (support of structure) the value of  $f_n$  is equal:  $f_n = (0,75 - 0,5)F_n = 0,25F_n$  where  $F_n$  means the total depth. So if we have concave and convex half parabolas with their depth in the axis we know the radius of curvature in their axis. Then according to Fig. 1 we know the forces in the parabolic chords of structure.

As it was stated on the beginning of this report, the values of forces in chords depend of the curvature of parabola at apex. But for the roof with 3 different span we will keep the same constant horizontal force in convex and concave chords, but not only in one span, but in all three. The total folded roof should also be flat and horizontal on both top sides of the building. At edges therefore we have shaped two half of the parabolas with opposite apexes, and different depth and curvature. This concept is presented in the drawing Fig. 12. There are three different spans. The bigger (40m) is chosen as the ruling and principal. The middle (14m) is 2,0m lower, and its concrete roof should carry the horizontal longitudinal compressive force. The third, little smaller (26m) must be adapted with its height to keep the same forces in tension and compression as in the biggest principal span.

This principle has been also simply presented on the diagram of bending moments when the load is located on both funicular roofs and the weight of the middle roof is carried separately.

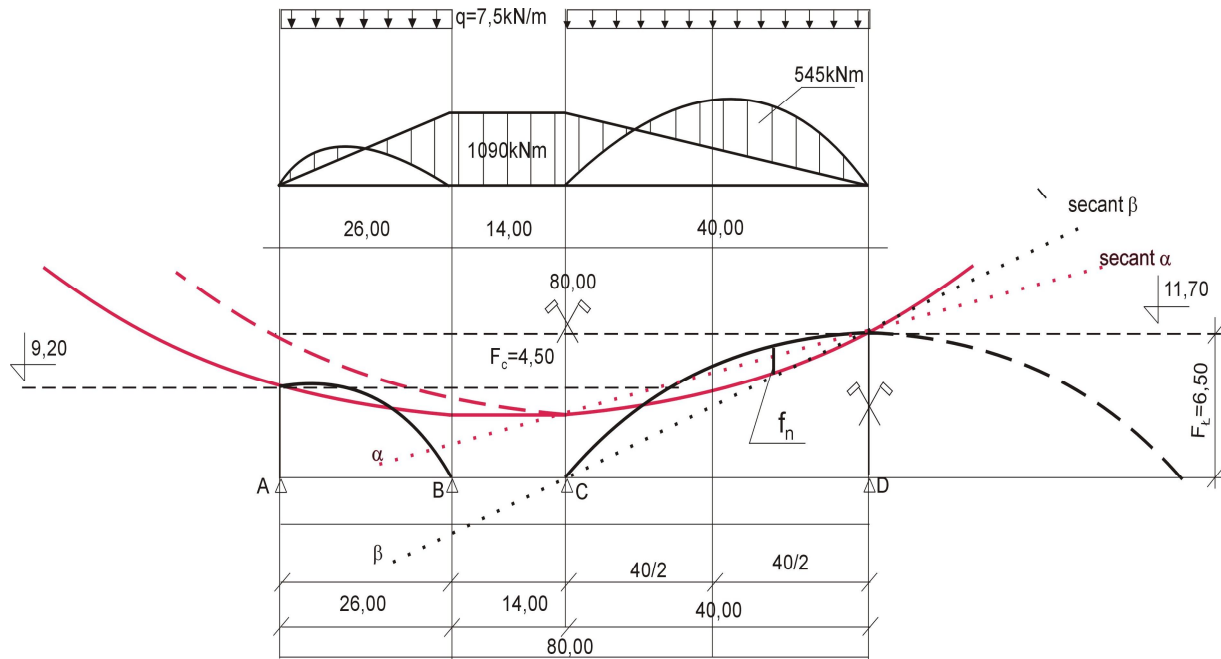


Fig. 12 Shaping of section of Supersam by 2 half chords of parabola with positive – convex  $F_L$  and negative  $F_c$  – concave.

a) diagram of bending moments for 3 span

b) system of parabolic chords: convex with apex in support C concave with apex D, horizontal part B-C. Part A-B proportionally adapted height.

The sequence of creation of the shape is therefore as follows:

- half of 80m span of the convex – compressed parabola arch with apex at the border D, bottom in C and height  $F_L = 6,50\text{m}$  is chosen as basic.
- Half of 80m span of the concave – tensioned parabola has the low apex at point C. the horizontal tangent at this apex permits to prolong the tangent of the apex to B, - 14m over the middle of concrete roof without changing of force in this tie. It will hang over the concrete roof.
- The height of the building at point A – 26m must have the same ordinate as at the tie on longer span at the same abscissa.
- Therefore the convex, shorter parabola at point 3 must be turned in point B to obtain on the end the same height as the concave chord.

These, rather complex transformations of the funicular parabolic chords permit to obtain constant horizontal force in concave and convex parabolic chords. the different only by the value of cosine  $\varphi$ . For the defined values of dimensions and load  $q=7,5\text{kN/m}$  we received the results of calculation as follows:

$$R_{01} = \frac{L^2}{8d_1} = \frac{80^2}{8 \cdot 6,50} = 123\text{m} = \frac{L}{2 \cdot 8f_1} = 123\text{m}$$

$$f_1 = 0,25 \cdot 6,50 = 1,625\text{m}$$

$$R_{02} = \frac{L^2}{8d_2} = \frac{80^2}{8 \cdot 4,50} = 178\text{m} = \frac{L}{2 \cdot 8f_2} = 178\text{m}$$

$$f_2 = 0,25 \cdot 4,50 = 1,125\text{m}$$

Horizontal force in compressed C and tensioned T chord:

$$T = C = q \frac{R_{01} \cdot R_{02}}{(R_{01} + R_{02})} = \frac{178 \cdot 123}{(178 + 123)} \cdot 7,5 = 545 \text{ kN}$$

$$\cos \varphi \approx 0 \quad \sigma_{01} = \frac{C}{A_C} \quad ; \quad \sigma_{02} = \frac{T}{A_T}$$

This example shows that with very impressive conception by pure parabolic geometry and short analytical calculation can be received very logical and elegant structure.

The drawing on Fig. 13 illustrates that by simple hoisting of concave chord up and down the statical system may be changed from simple support beam with two symmetrical spans to symmetrical cantilevers. The compressed convex parabola remains constantly stable.

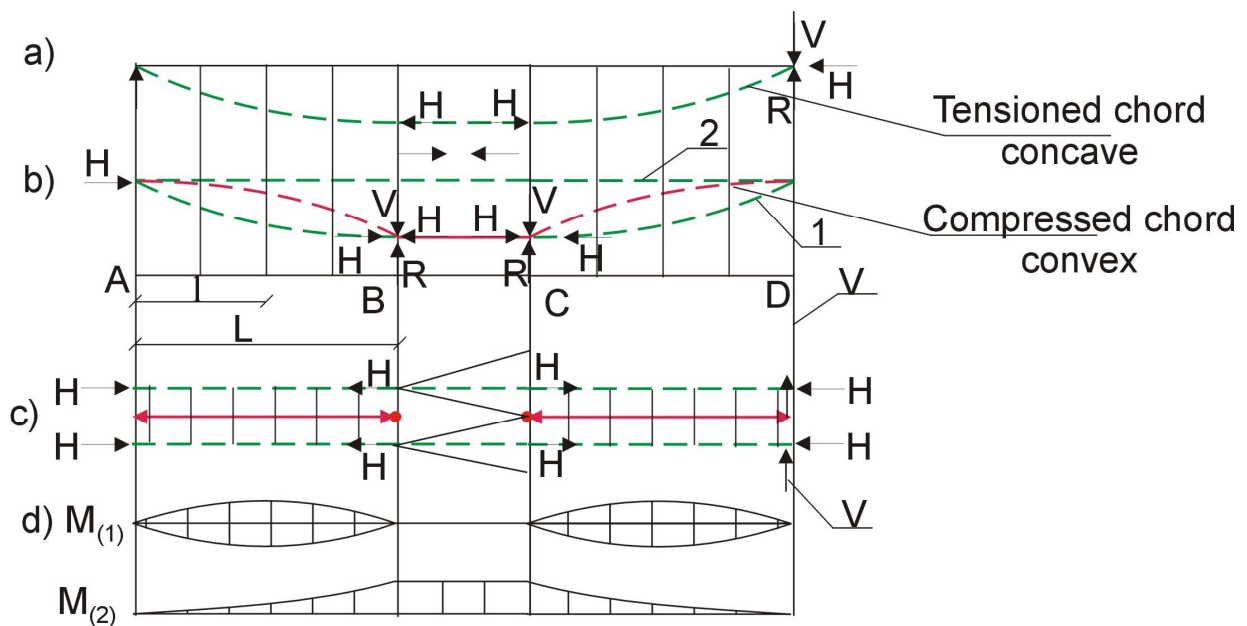


Fig. 13 Possible others shapes. Hoisting of concave parabola chord change the values of concordant bending moments and also the height of other span. If the spans are identical, the height of building is symmetrical the same on both sides.

- a) ruling parabola
- b) hoisted to straight or pushed down parabola
- c) plan of compressed and tensioned chords
- d) corresponding bending moments to 1 and 2



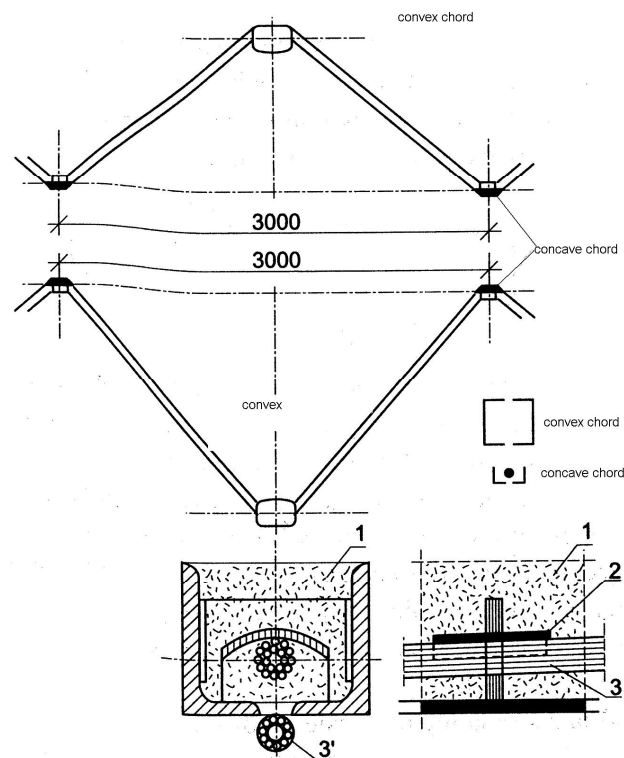


Fig. 14 Sections of the roof in different points show that convex and concave chords are once up and then down.

Fig. 14 illustrates the real sections of the realized steel construction. Depending of the distance from the apex the convex parabola is or higher or lower than the concave chord. The tensioned chord section is prestressed along the total length of 81,75m. The aim of prestressing lies in diminishes of the deflections of very flat structure and to increase the safety of steel welded profiles. The nether presenting strand is foreseen only in brain for future durability.

The total 3 span structure may be loaded by snow only on one span. Therefore in the middle of the central span, a steel column is foreseen to fix the tensioned concave, but horizontal in this abscissa point prestressed steel section of the tie (Fig. 10). View of tie total structure is presented on Fig. 15

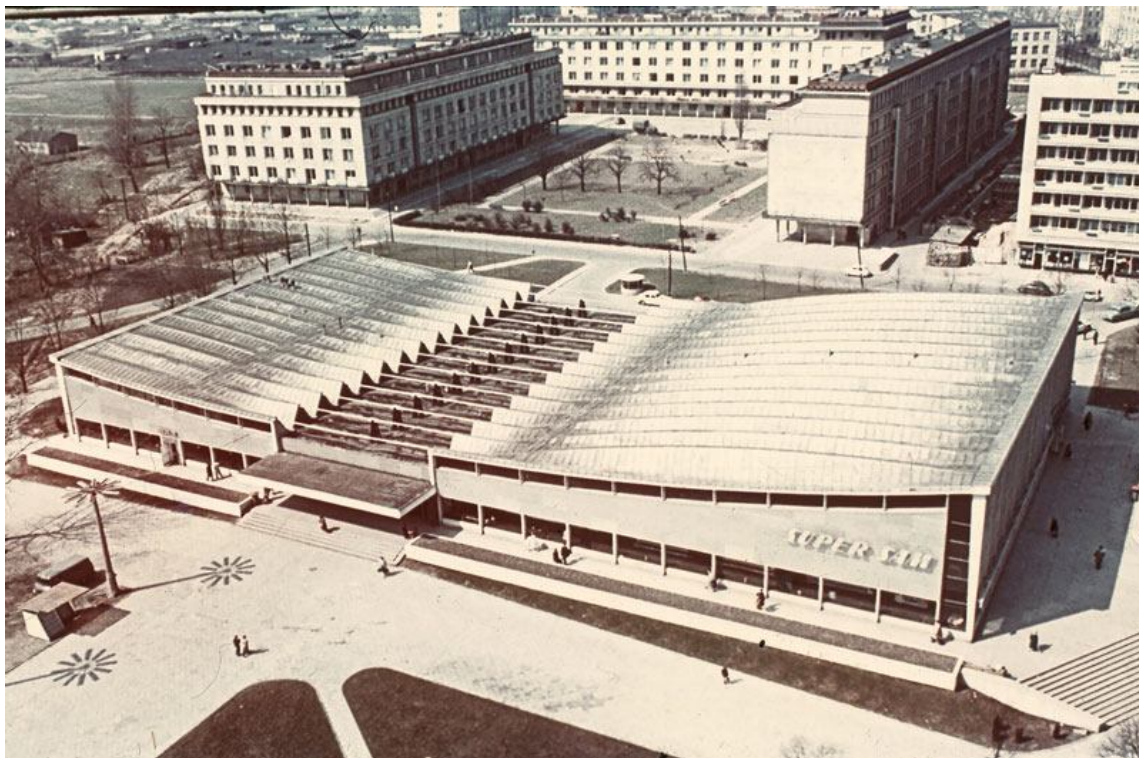


Fig. 15 View of the realized structure of Supersam – three span folded funicular structure of the roof.

## 5. CONCLUSION

The final conclusion of this report states that geometrical imagination and logical flow of internal forces can create efficient, economic and elegant structures.

Drawing pictures by Grzegorz Rybicki, Rzeszow University of Technology

Andrzej J. MACHOWSKI<sup>1</sup>  
Izabela A. TYLEK<sup>2</sup>

## JOINT EFFECT OF STEEL FRAME EQUIVALENT GEOMETRICAL IMPERFECTIONS

### ABSTRACT

In the paper, in first order critique of hitherto existing conceptions of taking into consideration equivalent imperfections of initial tilt and initial bow joint effect on carrying capacity of steel frames is presented.

Statistically based models of random equivalent imperfections assumed in the paper were obtained utilizing authors' research. Combination of column initial tilts random sequence and column random initial bows multiplied by random binary sequence is considered.

Conception mentioned above is applied to analyse carrying capacity of 2-bay 5-story example steel frame. Numerical simulations of considered frame carrying capacity are conducted. It enables to evaluate influence of taking into consideration column random initial bows aside from column random initial tilts on steel frame carrying capacity.

Results obtained out of conducted analyses shows that influence of column random initial bows on frame limit strength value associated with limit point on frame equilibrium path is slight. This influence turns out significant in case of frame ultimate load carrying capacity analysis according to the most efforted cross-sections criterion.

**KEYWORDS:** Multistorey steel frames, random equivalent initial tilt, random equivalent initial bow, joint effect.

### 1. INTRODUCTION

According to contemporary Standard Recommendations and literature effect of imperfections should be taken into consideration in calculations of multistorey steel frames. This conception is fulfilled in simplified way by introducing equivalent geometrical imperfections: initial tilts  $\phi_{0z}$  (column initial out-of-plumbs, eccentricity in column field joints, assembly stresses, random changeability of beam-column joint rigidity) and initial bow  $e_{0z}$  (column misalignment and column residual stresses).

This approach approximately takes into consideration steel skeleton fabrication conditions, in particular: columns division on assembly parts and its assembly with random

<sup>1</sup> Assoc. Prof. DSc. PhD., Cracow University of Technology, Cracow, POLAND,

<sup>2</sup> PhD., Cracow University of Technology, Cracow, POLAND.

out-of-plumbs – causing significant changes of moment values in equilibrium equations – because of vertical forces large values occurrence.

In advanced analysis, connected with determination of structure equilibrium path, both geometrical imperfections ( $\phi_{0z}$  and  $e_{0z}$ ) are taken into consideration in stage of static calculations. Basic values of this imperfections may be assumed as deterministic (standard) e.g. according to [15] i.e.  $\phi_0 = 1/200$ ,  $e_0$  according to tab. 5.1.

In traditional (simplified) approach only column equivalent initial tilts are introduced in static calculations, whereas column equivalent initial bows are taken into account during designing in beam-column formula.

The subject of this paper is evaluation of column equivalent initial tilts and column equivalent initial bows joint effect. Analysis of imperfections mentioned above joint effect should take into consideration their random character. In this end statistically based models of: random equivalent initial column bow and random equivalent initial tilt [7, 17], were taken into account.

Additional effect of column equivalent initial bow on frame carrying capacity, in elastic and elastic-plastic behaviour of structure, was analyzed on example of vertical planar frame bracing system of 5-story steel skeleton.

## 2. RANDOM EQUIVALENT INITIAL BOW

Random buckling coefficient was determined in papers [5, 7] utilizing Fukumoto and Itoh statistical data [4] and applying randomization of compressed steel bar flexural buckling resistance standard formula.

Random flexural buckling resistance of compressed steel bar  $\underline{N}_b$  (random values are underlined) was expressed by means of bar cross-section random plastic resistance  $\underline{N}_{pl} = A \cdot \underline{R}_{pl} = A \cdot \underline{f}$  (where  $A$  – nominal area of bar cross-section,  $\underline{R}_{pl} \equiv \underline{f}$  – random plastic resistance of structural steel corrected for random deviation of cross-section area) and random buckling coefficient  $\underline{\varphi}$ , in form

$$\underline{N}_b = \underline{\varphi} \cdot \underline{N}_{pl} \quad (1)$$

For random flexural buckling resistance  $\underline{N}_b$  and bar cross-section random plastic resistance  $\underline{N}_{pl}$  logarithmic-normal distributions were assumed [5, 7]. It follows that buckling coefficient  $\underline{\varphi}$  stochastically independent of  $\underline{N}_{pl}$  has also logarithmic-normal distribution.

Appropriate sets of data have been statistically processed [5, 7], with a mean-square approximation of experimental random buckling coefficient  $\underline{\varphi}$  distribution parameters by means of function

$$\check{\varphi}(\Lambda) = (1 + \Lambda^{2n_1})^{-1/n_1}, \quad v_\varphi(\Lambda) = v_m \cdot \left( \frac{21 \cdot \Lambda}{1 + (\Lambda)^2} \right)^\alpha, \quad (2)$$

where:

$$\Lambda = \overset{df}{\bar{\lambda}} = \sqrt{\check{N}_{pl} / \check{N}_E} = \sqrt{(A \cdot \check{f}) / (\pi^2 \cdot \check{E} / \lambda^2)}. \quad (3)$$

$\Lambda$  – non-random relative slenderness defined, as in [14], for central values (medians)  $\check{N}_{pl} = A \cdot \check{f}$ ,  $\check{N}_E = \pi^2 \cdot \check{E} / \lambda^2$ ,  $\lambda$  – bar slenderness.

Empirical parameters [7]:  $n_l$ ,  $v_m$ ,  $\alpha$  and  $l$  for Standards [14, 15] buckling curves: „a”, „b” and „c” [14] are presented in tab. 1.

Table 1. Empirical parameters for formula (2)

buckling curve	$n_l$	$v_m$	$\alpha$	$l$
„a”	3,0	0,10	2	0,8
„b”	2,6	0,11	2	0,9
„c”	2,2	0,13	2	1,0

For logarithmic-normal distributions parameters:  $\check{\varphi}$ ,  $v_\varphi$  and design value of standard buckling coefficient  $\varphi_N$  is related as follows (see e.g. [12])

$$\varphi_N \stackrel{df}{=} N_{b,d}/N_{pl,d} = \check{\varphi}(\Lambda) \cdot \exp\left(\beta_R \left(v_R - \sqrt{v_R^2 + v_\varphi^2}\right)\right), \quad (4)$$

where:  $v_R \approx 0,10$ - logarithmic coefficient of variation for corrected plastic resistance,

$\beta_R$  – partial reliability index for resistance.

Values obtained form (4) for  $\beta_R = 3,0$  and parameters according to Tab. 1 are very close to standard values [14, 15]. For buckling curve “b” discrepancy is about 2% [10].

To determinate column random equivalent initial bow we use well-known formula of dimensionless equivalent initial deflection  $\varepsilon_0$  [3, 16] of hinged bar with and sinusoidal initial bow (the formula is based on bar resistance conservation criterion)

$$\varepsilon_{0z} = e_{0z}/r = (\varphi^{-1} - 1) \cdot (1 - \varphi \cdot \Lambda^2) = \varphi^{-1} + \varphi \cdot \Lambda^2 - (1 + \Lambda^2), \quad (5)$$

where:  $e_{0z}$  - bar equivalent initial bow,

$r = W/A$  - radius of cross-section core.

Random imperfection  $\underline{\varepsilon}_{0z} = \underline{e}_{0z}/r$  was obtained, according to our new proposition, utilizing randomization (5) by introducing random logarithmic-normal bucking coefficient  $\underline{\varphi}$  with parameters according to (2) and Tab. 1

$$\underline{\varepsilon}_{0z} = \underline{e}_{0z}/r = (1 - \underline{\varphi} \cdot \Lambda^2) \cdot (\underline{\varphi}^{-1} - 1), \quad (6)$$

According to mechanical interpretation and property of logarithmic-normal distribution quantity  $\varepsilon_{0z} = e_{0z}/r$ , similarly as other quantities in (5), are treated as non-negative (or positive) what fallows that function  $\varepsilon_{0z}(\varphi)$  is determined for  $\varphi \in (0, \min(1, 1/\Lambda^2))$ . In this range of  $\varphi$  values of function  $\varepsilon_{0z}(\varphi)$  is monotonically decreasing (Fig. 1a).

Probability density function (truncated distribution) of random variable  $\underline{\varepsilon}_{0z}$  (6) is obtained from transformation of random variable  $\underline{\varphi}^{-1}$  probability density function (see i.e. [13])

$$f(\varepsilon_{0z}; \Lambda) = \frac{c}{\sqrt{2\pi} \cdot v_\varphi \cdot \varphi(\varepsilon_{0z})} \cdot \exp\left\{-\frac{\ln^2[(\varphi(\varepsilon_{0z})/\check{\varphi} + 1)]}{2 \cdot v_\varphi^2}\right\} \cdot \left|\frac{d\varphi(\varepsilon_{0z})}{d\varepsilon_{0z}}\right|, \quad (7)$$

where:  $\varphi(\varepsilon_{0z}) = (a - b)/(2 \cdot \Lambda^2)$ ,  $d\varphi/d\varepsilon_{0z} = (1 - a/b)/(2 \cdot \Lambda^2)$ ,  $a = a(\varepsilon_{0z}; \Lambda) = \varepsilon_{0z} + \Lambda^2 + 1$ ,

$$b = b(\varepsilon_{0z}; \Lambda) = \varepsilon_{0z}^2 + 2 \cdot \varepsilon_{0z} \cdot (1 + \Lambda^2) + (1 - \Lambda^2)^2, \quad c = 1/F(1), \quad F(1) = \int_0^1 f(\varepsilon_{0z}; \Lambda) d\varepsilon_{0z}.$$

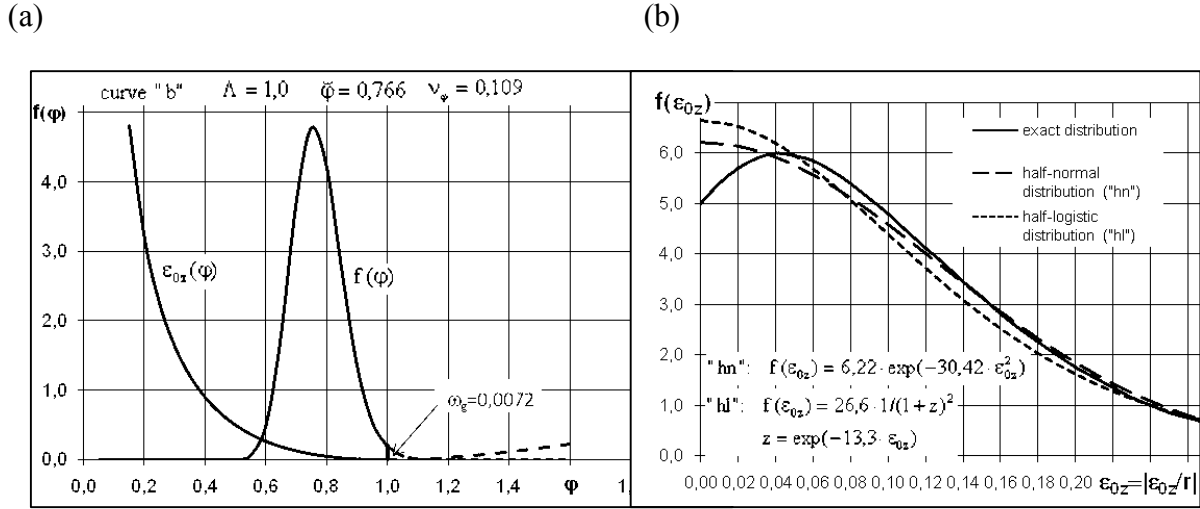


Fig. 1. (a) Relation  $\varepsilon_{0z}(\varphi)$ , (b) probability density function  $f(\varepsilon_{0z}; \Lambda)$  for buckling curve “b”

Probability density of “exact” distribution according to (7) shows (beside of close vicinity of point  $\varepsilon_{0z} = 0$ ) very good compatibility with density of half-normal distribution (“hn”) and good compatibility with density of half-logistic distribution (“hl”) – Fig. 1b. One-parameter half distributions mentioned above were matched according to mean values conformity criterion.

From numerical integration of function (7) almost linear dependence of mean values  $\bar{\varepsilon}_{0z}$  and standard deviations  $\sigma_{\varepsilon_{0z}}$  on  $\Lambda$ , for appropriate half-normal distributions, are obtained (Fig. 2a):

$$\bar{\varepsilon}_{0z} = C_{\bar{\varepsilon}} \cdot \Lambda, \quad \sigma_{\varepsilon_{0z}} = C_{\sigma_{\varepsilon}} \cdot \Lambda, \tag{8}$$

Direction coefficients  $C_{\bar{\varepsilon}}$  and  $C_{\sigma_{\varepsilon}}$  are given in Tab. 2.

Values of coefficient  $C_{\sigma_{\varepsilon}}^*$  (for relationship  $\sigma_{\varepsilon_{0z}}^* = C_{\sigma_{\varepsilon}}^* \cdot \Lambda$ ), corresponding to normal distribution  $\underline{\varepsilon}_{0z}^*$  with changeable signs and zero mean value is obtained (Tab. 2) from relationship  $C_{\sigma_{\varepsilon}}^* = C_{\sigma_{\varepsilon}} / \sqrt{1 - 2/\pi}$ .

Table 2. Coefficient values for formula (8)

buckling curve	$C_{\bar{\varepsilon}}$	$C_{\sigma_{\varepsilon}}$	$C_{\sigma_{\varepsilon}}^*$
“a”	0,065	0,045	0,075
“b”	0,085	0,065	0,110
“c”	0,120	0,085	0,140

In Fig. 2b values of  $\varepsilon_{0z}(\Lambda)$ , obtained from half-normal distribution  $\varepsilon_{0z}$  with parameters according to Tab. 2, were compared (for bucking curve “b”) with values from Standard Recommendations and values from formula (5). Straight lines “1” and “2” are

obtained for assumed probability  $\omega$  of exceeding  $\varepsilon_{0z}$  value in half-normal distribution. Straight line “2” corresponding to value turns out very close to straight line “3” characterized with equation  $\varepsilon_{0z} = 0,3 \cdot \lambda / 100 = 0,3 \cdot \Lambda \cdot \lambda_1 / 100$  (for  $\lambda_1 = 0,84$ ) – representing traditional British Recommendations (BS 449). Broken line “4”, according to Eurocode 3 – with equation:  $\varepsilon_{0z} = 0,34 \cdot (\bar{\lambda} - 0,2)$  - for  $\bar{\lambda} > 0,2$  and  $\varepsilon_{0z} = 0$  - for  $\bar{\lambda} \leq 0,2$ , (taking relationship  $\Lambda = 1,12 \cdot \bar{\lambda}$  into consideration) shows very good compatibility with curve “5” obtained from (5) substituting  $\chi(\bar{\lambda})$  in place of  $\varphi(\lambda)$  and  $\bar{\lambda}$  in place of  $\Lambda$ . Occurrence of  $\varphi$  and  $\Lambda$  quantities in non-linear form in (6) cause significant mutual discrepancy between curves “5” and “6” (Fig. 2b) despite of affirmed earlier good compatibility of buckling curves [10].

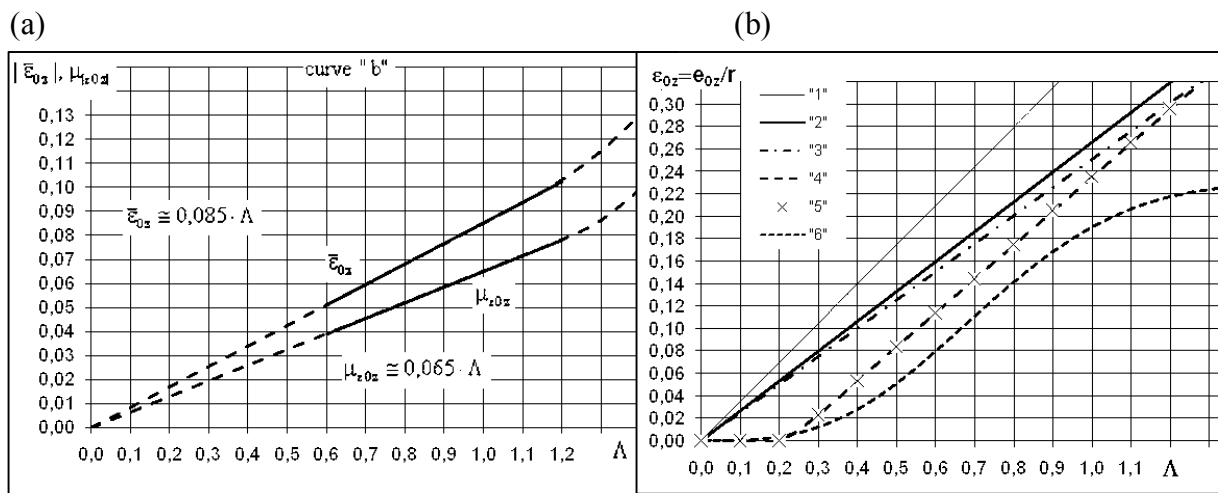


Fig. 2. (a) Relation  $\bar{\varepsilon}_{0z}(\Lambda)$  and  $\sigma_{\varepsilon_{0z}}(\Lambda)$  for curve “b”, (b) comparison of relation  $\varepsilon_{0z}(\Lambda)$  according to different formulas

### 3. RANDOM EQUIVALENT INITIAL TILT

Random equivalent initial tilt of column single story is interpreted as sum of: column initial tilt  $\phi_0^{(1)}$ , eccentricity in column field joints  $e_{s0}$  and assembly stresses  $S_0$  (Fig. 3a÷c) and be written as follows [7, 9]:

$$\phi_{0z} = \phi_0 + \phi_{0e} + \phi_{0S}, \tag{9}$$

Effects of imperfections mentioned above were brought to equivalent couples of forces, assuming that these forces are proportional to column vertical load  $P$  accumulated at building height.

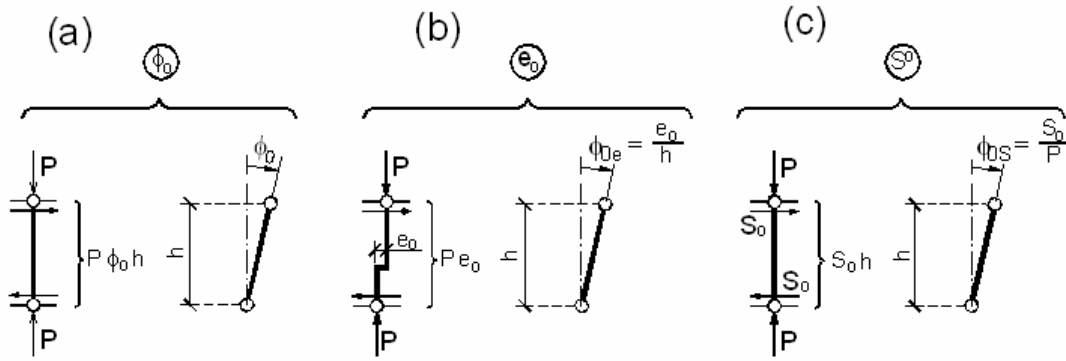


Fig. 3. A conception of column equivalent initial tilt, (a), (b), (c) equivalent couples of forces and P- $\Delta$  moments

For mutually stochastically independent:  $\underline{\phi}_0$ ,  $\underline{\phi}_{0e}$  and  $\underline{\phi}_{0s}$  variance of equivalent sway ratio is has form

$$\sigma_{\phi z}^2 = \sigma_{\phi_0}^2 + \sigma_{\phi_e}^2 + \sigma_{\phi_s}^2, \quad (10)$$

Assuming for all components of (9) relationship between limit of tolerance  $\phi^{(t)}$  (for permissible defectiveness  $w = 5\%$ ) and standard deviation as in normal distribution  $\phi^t \cong 2 \cdot \sigma_{\phi}$  [7, 8] we obtain:  $\sigma_{\phi z}^2 \cong 6(\%)^2$  – for standard [14, 15] value of equivalent initial sway ratio  $\phi_{0z}^{(t)} = 1/200$ ,  $\sigma_{\phi_0}^2 \cong 3(\%)^2$  – for post-erection tolerance  $\phi_0^t = 1/300$  of column non-verticality,  $\sigma_{\phi_e}^2 \cong 1(\%)^2$  – for tolerance value  $\phi_{0e}^t = 1/500$ , results from dividing of standard [14, 15] column field joints eccentricity tolerance  $e_0 = 5$  mm by minimum story  $h = 2500$  mm. For tilt  $\phi_{0s}$ , substituting for unknown assembly stresses, we obtain then  $\sigma_{\phi_s}^2 = 2(\%)^2$ .

Mathematical model of column single story initial tilt was determined on the basis of column out-of-plumbs post-fabrication measurements, carried out after all frames erection and after construction of all floors.

Most extensive statistical analysis of measurements mentioned above was conducted in [7, 8] which also includes results obtained earlier by Beaulieu [1] and Lindner [6].

Conducted analysis showed that that mathematical model of stationary gaussian random noise  $\phi_{ijk}^x$  and  $\phi_{ijk}^y$  (stationary random series with mean value  $\bar{\phi} = 0$  and constant variance  $D_{\phi} = \sigma_{\phi}^2 = \text{const.}$ ) is justified if empirical variance fulfils a constraint

$$\sigma_{\phi}^2 \leq 3(\%)^2, \quad (11)$$

what agrees with keeping initial tilt standard tolerance.

The second conclusion was that only exist weak autocorrelation dependence between tilts of columns in the same vertical planar frames and lack of correlation between any other initial tilts.

For design purposes it is very convenient to assume one value of equivalent initial tilt for frame as a whole  $\underline{\phi}^{\text{EFF}}$  instead of column initial tilts random sequences  $\underline{\phi}_{ip}$ .



Post-fabrication column out-of-plumbs cause additional bending moments from vertical load for frame as vertical cantilever [7, 8].

For bar-disk analytical scheme of multi-storey skeletal structure with rigid floor-disks effective initial random tilt for i-th story of building  $\underline{\phi}_i^{\text{eff}}$  may follow from conservation of global moment increment condition (if torsional effect for building as vertical cantilever is neglected)

$$\Delta \underline{M}_i^\phi = \sum_{p=1}^s P_{ip} \cdot h_i \cdot \underline{\phi}_{ip} = P_i \cdot h_i \cdot \underline{\phi}_i^{\text{eff}}, \quad (12)$$

where:  $P_i = \sum P_{ip}$ , ( $p = 1 \dots s$ ) - sum of all vertical loads acting on building above i-th story,  
 $P_{ip}$  (for s columns  $i = 1, 2, \dots, s$ . on i-th story of building) – sum of vertical loads above i-th story in p-th column.

hence i-th story equivalent initial tilt

$$\underline{\phi}_i^{\text{eff}} = \sum_{p=1}^s w_{ip} \cdot \underline{\phi}_{ip} = \mathbf{w}_i \underline{\phi}_i^T, \quad (13)$$

Story random initial tilt  $\underline{\phi}_i^{\text{eff}}$  is normal random variable with parameters [7, 8]:

$$E\{\underline{\phi}_i^{\text{eff}}\} = 0, \quad \sigma_{\phi_i}^2 = k_{c,i}^2 \cdot \sigma_\phi^2, \quad (14)$$

where

$$k_{c,i}^2 = \mathbf{w}_i \boldsymbol{\rho}_s \mathbf{w}_i^T = \sum_{p=1}^s w_{ip} \cdot \sum_{q=1}^s w_{iq} \cdot \rho_{pq} \quad (15)$$

is positively defined quadratic form of s-variable:  $w_{i1}, \dots, w_{ip}, \dots, w_{is}$ . with symmetric matrix of coefficients  $\boldsymbol{\rho}_s$  equal to normalized correlation matrix  $\boldsymbol{\rho}_s$  of random vector  $\underline{\phi}_i$ .

Values of reduction coefficient  $k_{c,i}$  according to (15) have been analysed in detail in [7, 8]. Conducted analysis showed that among standard formulas closest to obtained result is that in Polish Standard [4], on condition that only columns with vertical load (above i-th story) arrangement parameter  $c \geq 0,5$  are taken into account.

Safe approximation of effective random initial tilt for frame as a whole may be defined as follows

$$\underline{\phi}_i^{\text{EFF}} = \max_{i=1}^n |\underline{\phi}_i^{\text{EFF}}| = \max_{i=1}^n \left| \sum_{t=i}^n V_t \cdot \sum_{q=i}^t h_q \cdot \underline{\phi}_q^{\text{eff}} \cdot \left( \sum_{t=i}^n V_t \cdot \sum_{q=i}^t h_q \right)^{-1} \right|, \quad (16)$$

$\underline{\phi}_i^{\text{EFF}}$  – effective random initial tilt for frame as a whole, which guarantee safe estimation of additional bending moment for i-th story of frame as vertical cantilever,

$\underline{\phi}_i^{\text{eff}}$  – according to (13),

$V_t$  – sum of vertical loads imposed immediately to t-th story.

Analyses conducted in [7, 8] showed that within confines of discussed conception reduction of initial tilt standard deviation and characteristic value depending on story number is unfounded. This reduction is justified only in special cases [11, 17], e.g. with reference to frames fulfilled “strong columns” condition (columns remain elastic up to plastic mechanism formation).

#### 4. JOINT EFFECT OF EQUIVALENT INITIAL TILT AND INITIAL BOW

Random equivalent bar initial bow  $\underline{e}_{0z}$  with column random initial tilt  $\underline{\phi}_{0z}$  makes up set equivalent random geometrical imperfections necessary for random carrying capacity calculation on the level of so called “advanced analysis” and reliability analysis of steel skeletons.

Effect of mentioned above equivalent imperfections interaction was analyzed (in elastic and elastic-plastic behaviour of structure) on the example of vertical planar frame bracing system of 5-story steel skeleton (Fig. 4).

Keeping ideal initial structure geometry, random geometric imperfections were introduced as equivalent imperfectional loads – Fig. 4.

Random sequences of story initial tilts were computer generated in the form of vector  $\underline{\phi}^{\text{eff}} = \{\underline{\phi}_i^{\text{eff}}\}$  which elements were normal variable with parameters according to (6). Weak correlation between initial tilts in vertical series.

Assumed in calculations mathematical model of column random equivalent initial bow was product of random initial bow and random binary sequence. Value of column random initial bow was determined on the basis of knowledge of probability density function and characteristics of random dimensionless column bow distribution. Normal distribution with parameters  $\{\bar{\varepsilon}_{0z}^* = 0, \sigma_{\varepsilon 0z}^* = C_{\sigma\varepsilon}^* \cdot \Lambda\}$  ( $C_{\sigma\varepsilon}^*$  according to Tab. 2) was assumed. It was assumed that column splices are located on every story so there is no correlation between initial bows of individual columns.

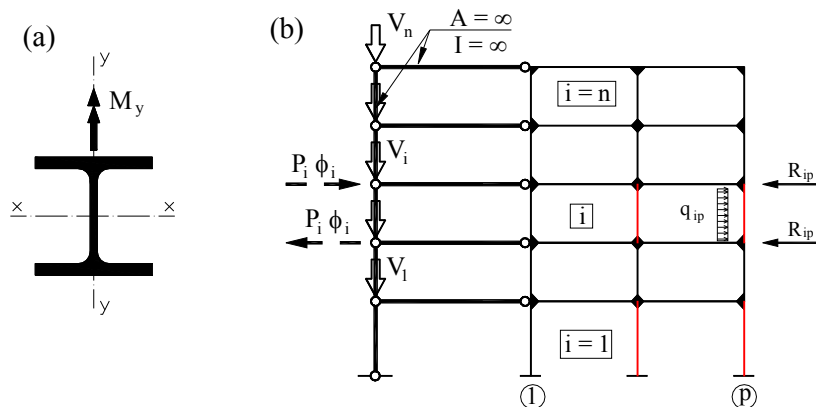


Fig. 4. Analyzed planar bracing system of 5-story skeletal steel structure [17]

In advanced analysis additional effect of column equivalent initial bows on frame carrying capacity (associated with limit point on frame equilibrium path) was determined by comparison of frame initial tilt  $\underline{\phi}^{\text{EFF}}(\underline{\phi}_{0z})$  (substitutes for story random initial tilts) standard deviation with frame initial tilt  $\underline{\phi}^{\text{EFF}}(\underline{\phi}_{0z}, \underline{e}_{0z})$  (substitutes for story random initial tilts and column random initial bows) deviation values. In both case the same sequences of story random initial tilts were considered.

Equivalent random initial tilt of frame as a whole  $\underline{\phi}^{\text{EFF}}$  was determined on the basis of conservation of carrying capacity associated with limit point on frame equilibrium path criterion. According to applied simulation procedure, for every realization of equivalent imperfectional loads set respective frame equilibrium path and frame carrying capacity were determined. Next the effective initial tilt of frame as a whole  $\underline{\phi}^{\text{EFF}}$  was chosen in agreement

with condition of frame limit carrying capacity conservation.

Computer program ANSYS 8.0, based Finite Element Method, were utilized in order to obtain frame equilibrium path and frame limit carrying capacities. Two-dimensional bar structure model with regular mesh and elastic-plastic (bilinear) model of material was assumed. Description of the material model was based on Huber-Mises-Hencky plasticity criterion, associative flow rule and rule of kinematics hardening. Development of plastic zones (in cross section and along length of element) and large displacements (translations and rotations) with small deflections were taking into consideration.

Calculations were conducted for 300 elements population.

According to obtained results additional influence of column random equivalent initial bows on frame carrying capacity is in advanced analysis may be neglected.

Results of earlier works [2] indicated that interaction of global (tilts) and local (bows) geometric imperfections causes reduction of frame carrying capacity by 10%, but authors assumed deterministic (instead of random) values of equivalent imperfections and selected some combinations of global and local equivalent geometric imperfections, compatible with first buckling eigenvector of ideal elastic frame and combinations of initial bows acceptable for the sake of columns splices.

In elastic analysis frame equivalent initial tilt  $\underline{\phi}^{\text{EFF}}$  was determined according to criterion of imperfection loads local effect conservation in beam-column element for random sequence of story equivalent initial tilts  $\underline{\phi}_i^{\text{ef}}$  and set of random equivalent initial bows  $\underline{e}_{\text{ip}}$  and for equivalent initial tilt for frame as a whole  $\underline{\phi}^{\text{EFF}}$  [9, 17]. Similarly as in advanced analysis values of standard deviations for  $\underline{\phi}^{\text{EF}}(\underline{\phi}_{0z})$  and  $\underline{\phi}^{\text{EF}}(\underline{\phi}_{0z}, \underline{e}_{0z})$  were compared.

In this case effect of column random initial bows on value of frame initial tilt  $\underline{\phi}^{\text{EFF}}$  should be taken into account.

## 5. CONCLUSIONS

In the paper effects of column initial tilts and initial bows interaction were investigated using probabilistic approach, introducing into calculations, in elastic and elastic-plastic structure behaviour, statistically based models of equivalent imperfections.

Analyses of 2-bay 5-story frame planar bracing system with random sequences of story initial tilts and random sets of column initial bows showed slight influence of column random initial bows on frame carrying capacity and equivalent initial tilt of frame as a whole  $\underline{\phi}^{\text{EFF}}$ . It is favourable statistic effect which justifies passing over of local geometric imperfections influence in planar frames advanced analysis. Taking into consideration column random initial bows, besides of column random initial tilts, turns out necessary in traditional calculations of elastic frames.

## REFERENCES

- [1] Beaulieu D., Adams P.F., *Significance of structural out-of-plumb forces and recommendations for design*. Canadian Journal of Civil Engineering. Vol.7/1980.
- [2] De Luca A. & Mele E., *Analysis of steel frames in the light of Eurocode 3 and new research results*. In: Plastic hinge based methods for advanced analysis and design of steel frames. SSRC, Lehigh Univ. Bethlehem. PA USA, 1993.
- [3] ECCS. European specifications for steel structures. 1-st ed. 1974.

- [4] Fukumoto Y., Itoh Y., *Multiple buckling curves based on experimental data*. Construction Métallique, No.3/1984 (in French).
- [5] Gwóźdź M., *The problems of random resistance of metal bars*. Cracow University of Technology, Publ. No.4, Cracow, 1997 (in Polish).
- [6] Lindner J., Gietzelt R., *Imperfektionsannahmen für Stützenschiefstellungen*. Stahlbau, No.4/1984.
- [7] Machowski A., *Problems of limit states and reliability of steel multistory building frames*. Cracow University of Technology, Monograph No.262, Cracow, 1999 (in Polish).
- [8] Machowski A., *Initial random out-of-plumbs of steel frame columns*. Archives of Civil Engineering, XLVIII, 2.
- [9] Machowski A., Tylek I., *The equivalent imperfection concepts of steel frame*. L Konferencja KILiW PAN i KN PZiTB Krynica 2004. Tom II (in Polish).
- [10] Machowski A., Tylek I., *Random equivalent initial bow imperfection of compressed steel bar*. Quality and reliability in building industry. IV International Scientific Conference. Levoča, 2006.
- [11] Machowski A., Tylek I., *Conceptions of equivalent imperfections in analysis of steel frames*. The International Journal of Advanced Steel Construction, Vol.4, No.1 (2008).
- [12] Murzewski J., *Reliability of engineering structures*. Arkady, Warsaw, 1989 (in Polish).
- [13] Papoulis A., *Probability, random variables and stochastic processes*. McGraw-Hill Book Company, New York, 1965.
- [14] PN-B-03200: 1990: Steel structures. Analysis and design (in Polish).
- [15] PN-EN 1993-1-1: 2006. Eurokod 3: Design of steel structures. Part 1.1. General rules and rules for buildings (in Polish).
- [16] Rondal j., Maquoi R., *The Ayrton-Perry formulation for buckling of metallic bars*. Construction Métallique, No.4/1979 (in French).
- [17] Tylek I., *Equivalent geometrical imperfections of multistory steel building frames*. Doctoral Thesis. Cracow University of Technology, Cracow, 2007 (in Polish).

Mariusz MAŚLAK<sup>1</sup>

## MOMENT REDISTRIBUTION IN STEEL CONTINUOUS BEAM ACCORDING TO LIMITED PLASTICITY CONCEPT

### ABSTRACT

Conventional approach to elastic – plastic analysis of steel continuous beam, according to which it is assumed that two plastic hinges occur in an edge span at the ultimate limit state, not always gives safe evaluations of real member resistance. The reason is mainly the possibility of unlimited accumulation of permanent strains. Therefore some limitations of moment redistribution should be defined. Two of them are proposed and discussed by the author in the present paper. It is accepted that the first plastic hinge arises in the cross-section in which maximum elastic bending moment is induced; however, in the second critical cross-section its appearance is not admissible. Only elastic in the first case, or limited elastic – plastic ultimate moment in the second example is there considered. The design methodology presented in the article is connected with the reduction of member redundancy and transformation of the whole beam into unstable mechanism is not allowable.

**KEYWORDS:** redundant system, plastic reserve, ultimate limit state, moment redistribution

### 1. INTRODUCTION

The European recommendations for design of steel structures allow to take advantage of complete plastic redistribution of moments for redundant systems, provided that the cross-sections of all members are not too slender (belong to class 1). As a result of such methodology it is accepted that the structure can be transformed into an unstable mechanism at the ultimate limit state. To prevent the collapse imminence and to secure required safety level some limitations in global plastic analysis of the structure should be imposed. In the present paper the limited plasticity concept concerning continuous steel beams with equal span length and steady cross-section is presented and discussed. Two separate cases are studied in details, the first one with uniformly distributed both dead loads and imposed loads, and the other in which all applied forces are concentrated, therefore the localization of maximum mid-span moment after redistribution is known in advance.

The cross-sections of class 1 have sufficient rotation capacity. It means that in considered members plastic hinges can be formed without web crippling. Full plasticization of the critical cross-section is then the result of stress redistribution; however, the bending moment equal:

<sup>1</sup> Assistant Prof. PhD. Eng., Cracow University of Technology, Cracow, POLAND

$$M_{pl} = W_{pl} f_y / \gamma_{M0} = \alpha_{pl} W f_y / \gamma_{M0} = \alpha_{pl} M_{el} \quad (1)$$

can be adopted as the measure of its resistance  $M_R$ . In the above equation symbol  $f_y$  denotes the nominal value of steel yield point,  $\gamma_{M0}$  - partial safety factor,  $W_{pl}$  and  $W$  - suitable bending moduli; plastic and elastic, respectively. Let us underline that the coefficient  $\alpha_{pl} = W_{pl}/W$  determines the ratio of plastic reserve attainable for the section in relation to the conventional elastic resistance. The simplified constant value  $\alpha_{pl} = 1,14$  is in general accepted in Polish standards for beams made of hot-rolled I-section profiles.

The standard PN-EN 1993-1-1 [1] admits full plastic redistribution of stresses in critical cross-sections subject to bending. This assumption leads to quite simple methodology of elastic-plastic analysis of beams; however, it is not strictly correct and therefore arouses controversy. In fact some additional limitations have to be satisfied to secure that proposed design approach will be accurate. They were formulated by *J. Dutheil* [2] in his theory of limited plasticity (*adaptation contrôlée*). The following three conditions restricting a real beam resistance are particularly important:

- limitation of permanent strains of edge fibres at the support sections (*condition d'allongement*),
- limitation of deflection at the point of maximum mid-span moment (*condition de deformation*),
- requirement of elastic unloading to prevent the accumulation of permanent strains in plastic hinges (*condition de détente élastique*).

The *Dutheil's* theory has been promoted in Poland by *J. Mutermilch* [3], *M. Łubiński* and *M. Gizejowski* [4] as well as *S. Piechnik* [5]. The design plasticity ratio for sections  $\alpha_p$ , lower than analogous full plasticity ratio for sections  $\alpha_{pl}$ , has been introduced to the Polish standard PN-90/B-03200 [6] as a consequence of such analysis. Its value can be calculated from the following equation:

$$\alpha_p = 0,5(1 + \alpha_{pl}) = 0,5(1 + W_{pl}/W) \quad (2)$$

Let us notice that if  $\alpha_{pl} = 1,14$  then  $\alpha_p = 1,07$ . The coefficient  $\alpha_p$  given in Eq. 2 is frequently connected with the state when one of the sectional elements, the flanges or the web, is subject to plastic deformation, and the other one works in elastic range. The web is usually the supporting element whereas the flanges are supported. Such an approach is similar to the rules of post-critical design of members made of thin-walled sections. In reality it is only not quite accurate approximation. More precise formulation, resulting from the mechanical model presented above, has been given by the author [7] for hot-rolled sections:

$$\alpha_p = \alpha_{pl} - t_w h_w^2 / (12W) \quad (3)$$

as well as for welded beams:

$$\alpha_p = 1 + \frac{t_f (\xi + 2)}{2\xi (h_w + t_f) + h_w}, \quad \text{where} \quad \xi = \frac{A_f h}{A h_w} \quad (4)$$

In Eqs. 3 and 4 symbols  $A$  and  $A_f$  mean the area of the whole cross-section and the area of two flanges, respectively. Furthermore,  $h$  is the height of the whole cross-section,  $h_w$  - height of the web only,  $t_f$  - thickness of the flange,  $t_w$  - thickness of the web.

## 2. LIMITED PLASTICITY OF REDUNDANT SYSTEMS

The technique of balancing of ultimate moments in critical cross-sections is commonly used in plastic analysis of structures which are statically indeterminate. In the case of continuous beams considered in the present paper examination of only a span localized on the edge of the beam is sufficient. It is the consequence of the fact that the bending moments generated in such span are maximal. Furthermore, let us notice that the local collapse which takes place in single span has to be recognized as a global failure of the whole member. According to this approach it is accepted that both bending moment  $M_B$  at the support  $B$  and bending moment  $M_1$  in the mid-span  $AB$  can reach the limit value  $M_{pl} = \alpha_{pl} M_{el}$ . In other words the ultimate limit state of the beam is determined by two plastic hinges which are induced in considered span.

A new concept of moment redistribution along the beam, connected with limited plasticity theory, is proposed by the author in the present paper. Only one plastic hinge is generated in the section identified with the greatest value of elastic bending moment. In the second critical cross-section reaching the lower limit value  $\eta M_{el} < M_{pl}$  is permitted. If such assumptions are satisfied the redundant system in a general case may reduce its redundancy, or even become statically determined, but it never will be transformed into unstable mechanism at the ultimate limit state. Presented approach to elastic - plastic analysis of a structure is the generalization of conventional design methodology. Let us notice that if the value  $\eta = 1,14$  is taken into consideration then  $\eta = \alpha_{pl}$  and full moment redistribution is admitted. On the other hand, the particular case when  $\eta = 1,0$  is noteworthy. This limitation means that only elastic bending moment  $M_{el}$  is acceptable in the second critical cross-section. Such suggestion has been proposed by *J. Murzewski* [8].

## 3. THE CASE OF UNIFORMLY DISTRIBUTED LOADS

Let us start the examination of the procedure of limited moment redistribution from the continuous beam with load arrangement and envelope of bending moments shown in Fig. 1. Both dead load  $g$  and imposed load  $q$  are uniformly distributed. Two load cases are taken into consideration. The first one, denoted as  $I$ , gives the maximum elastic bending moment  $M_B$  at the support  $B$ ; whereas, the second, marked as  $II$  – maximum elastic bending moment  $M_1$  in the mid-span  $AB$ . It is essential that in this case  $|M_B^I| > M_1^{II}$ , independently on the number of spans, therefore the first plastic hinge always will be induced at the support  $B$ .

The elastic bending moments can be formally written as:

$$M_B^I = -(a_g^{el} g + a_q^I q) L^2 \quad \text{and} \quad M_B^{II} = -(a_g^{el} g + a_q^{II} q) L^2 \quad (5)$$

where  $a_g^{el}$ ,  $a_q^I$ ,  $a_q^{II}$  are the load effect coefficients defined for a perfectly elastic beam and particular load cases;  $I$  and  $II$  (let us notice that  $a_g^{el} = a_g^I = a_g^{II}$ ),  $L$  is the span length. Similarly, by means of the same convention, we can write the residual moment  $M_B^0$ :

$$M_B^0 = (a_g^0 g + a_q^0 q) L^2 \quad (6)$$

From the equilibrium equation we have:

$$M''(x_1) = M_1'' = 0,5px_1(L - x_1) - |M_B''| x_1/L \quad (7)$$

where  $p = g + q$ ,  $x_1$  is a position of critical cross-section in the mid-span  $AB$  after redistribution, unknown in advance. Static approach to plasticity theory leads to the equations:

$$|M_B^I| = \alpha_{pl} M_{el} + M_B^0 \quad \text{and} \quad M''(x_1) = M_1'' = \eta M_{el} - M_B^0 x_1/L \quad (8)$$

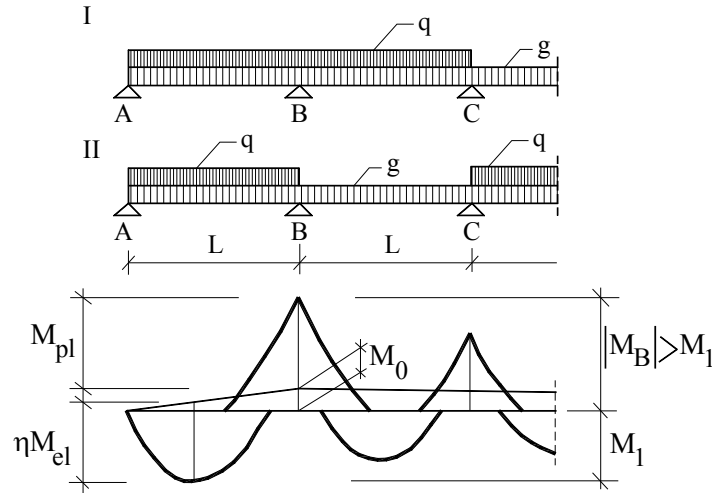


Fig. 1. Load arrangements and limited moment redistribution for a beam loaded with uniformly distributed loads

Substituting Eq. 7 to Eq. 8 and eliminating  $M_{el}$  gives:

$$M_B^0 = \frac{\frac{\eta}{\alpha_{pl}} |M_B^I| + \frac{x_1}{L} |M_B''| - \frac{px_1}{2} (L - x_1)}{\frac{\eta}{\alpha_{pl}} + \frac{x_1}{L}} \quad (9)$$

hence:

$$a_g^0 = a_g^{el} - \frac{x_1}{2L} \frac{1 - \frac{x_1}{L}}{\frac{\eta}{\alpha_{pl}} + \frac{x_1}{L}} \quad \text{and} \quad a_q^0 = \frac{\frac{\eta}{\alpha_{pl}} a_q^I + \frac{x_1}{L} a_q^{II} - \left(1 - \frac{x_1}{L}\right) \frac{x_1}{2L}}{\frac{\eta}{\alpha_{pl}} + \frac{x_1}{L}} \quad (10)$$

Consequently, after redistribution:

$$a_g = a_g^{el} - a_g^0 \quad \text{and} \quad a_q = a_q^I - a_q^0 \quad (11)$$

In Eq. 11 parameters  $a_g$  and  $a_q$  are the influence coefficients defined for an elastic – plastic beam which transform  $g$  and  $q$  into statically admissible moments at the support  $B$  and in the mid-span  $AB$  in proportion  $M_B/M_1 = \alpha_{pl}/\eta$ .

Having calculated the value of  $M_B^0$ , the maximum moment in the mid-span  $M(x_1) = M_1$  after redistribution can be determined by the formula:



$$M(x_1) = M_1 = M''(x_1) + M_B^0 \frac{x_1}{L} = \frac{\left( |M_B^I| - |M_B^{II}| \right) \frac{x_1}{L} + \frac{px_1}{2} (L - x_1)}{\frac{\eta}{\alpha_{pl}} + \frac{x_1}{L}} \frac{\eta}{\alpha_{pl}} \quad (12)$$

and finally the position of the critical cross-section in which this moment is localized may be found as follows:

$$\frac{dM(x_1)}{dx_1} = 0 \rightarrow x_1 = \frac{\eta L}{\alpha_{pl}} \left[ \sqrt{1 + \frac{\alpha_{pl}}{\eta} + 2(a_q^I - a_q^{II}) \frac{\alpha_{pl}}{\eta} \frac{q}{p}} - 1 \right] \quad (13)$$

Values of the coefficients  $a_g$  and  $a_q$  depend not only on the way of the limitation of moment redistribution and on the number of spans determining the considering beam but also on the ratio  $\xi = q/p$ . Suitable functions  $a_g = a_g(\xi)$  as well as  $a_q = a_q(\xi)$ , assessed for particular values of  $\eta$  parameter, are shown in Fig. 2 (in Fig. 2a for  $\eta = 1,0$ , in Fig. 2b for  $\eta = \alpha_p = 1,07$  and in Fig. 2c for  $\eta = \alpha_{pl} = 1,14$ ). The number of spans in an examined beam is marked in a circle for each dependence. Calculated values  $a_g$  and  $a_q$  are also presented in Tab. 1 for comparative purposes.

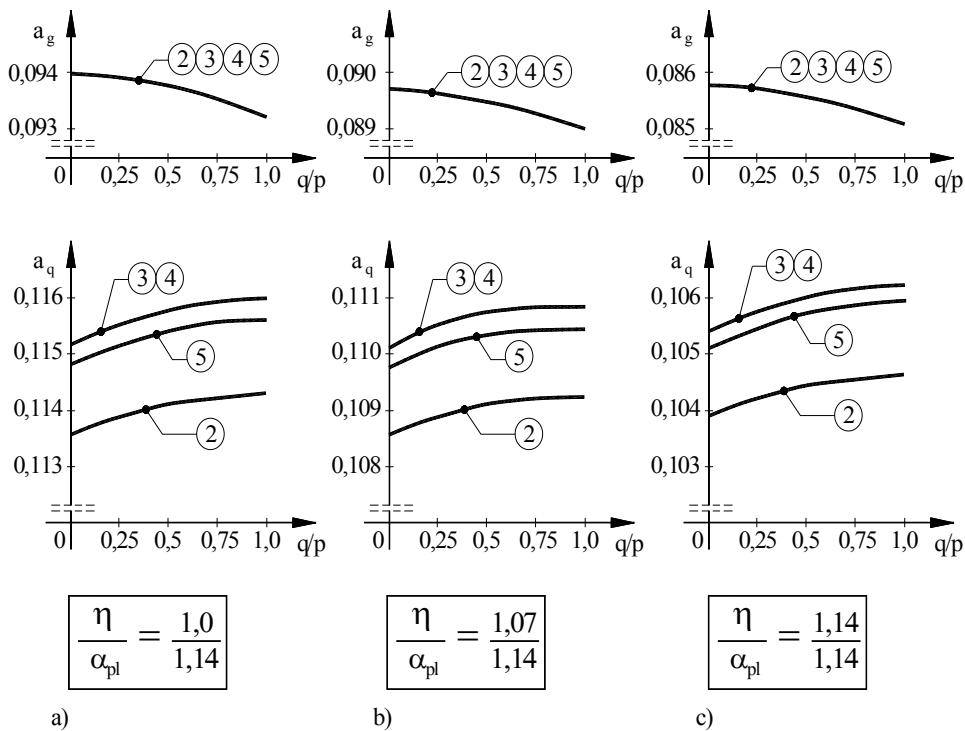


Fig. 2. Coefficients  $a_g$  and  $a_q$  determined for different techniques of moment redistribution, in the case of a beam with uniformly distributed loads

Table 1. Comparison of the results obtained for particular approaches to moment redistribution, in the case of a beam loaded with uniformly distributed loads

Number of span		2			3			4			5		
$\xi = q/p$		0	0,5	1	0	0,5	1	0	0,5	1	0	0,5	1
$a_q$	1,0/1,14	0,0940	0,0938	0,0933	0,0940	0,0938	0,0932	0,0940	0,0938	0,0932	0,0940	0,0938	0,0932
	1,07/1,14	0,0897	0,0895	0,0890	0,0897	0,0895	0,0889	0,0897	0,0895	0,0889	0,0897	0,0895	0,0890
	1,14/1,14	0,0858	0,0856	0,0851	0,0858	0,0856	0,0850	0,0858	0,0856	0,0850	0,0858	0,0856	0,0851
$a_q$	1,0/1,14	0,1136	0,1141	0,1143	0,1152	0,1158	0,1160	0,1152	0,1158	0,1160	0,1149	0,1154	0,1156
	1,07/1,14	0,1085	0,1091	0,1092	0,1101	0,1107	0,1108	0,1101	0,1107	0,1108	0,1098	0,1103	0,1105
	1,14/1,14	0,1039	0,1044	0,1046	0,1054	0,1060	0,1062	0,1054	0,1060	0,1062	0,1051	0,1057	0,1059
$\alpha_u$	1,0/1,14	1,3302	1,2025	1,0939	1,0642	1,0356	1,0090	1,1387	1,0881	1,0435	1,1174	1,0707	1,0292
	1,07/1,14	1,3938	1,2590	1,1445	1,1150	1,0842	1,0555	1,1931	1,1392	1,0916	1,1708	1,1209	1,0767
	1,14/1,14	1,4571	1,3153	1,1950	1,1657	1,1326	1,1019	1,2473	1,1901	1,1396	1,2240	1,1710	1,1241

Dependence  $x_1 = x_1(\xi)$ , which is approximately linear, is demonstrated in Fig. 3. also for selected values of  $\eta$ .

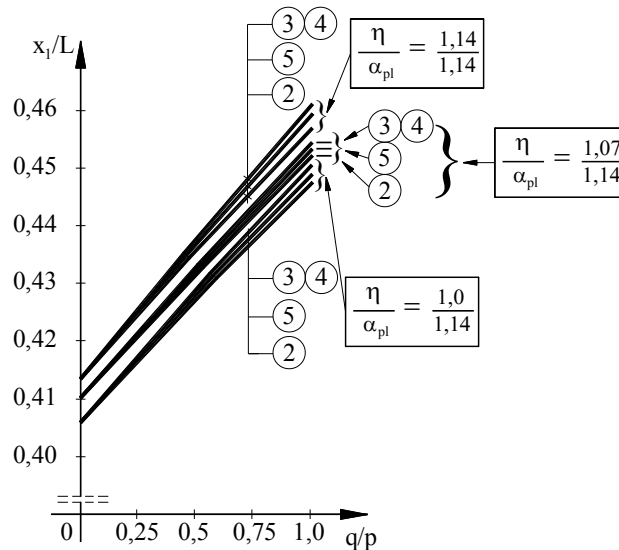


Fig. 3. Position of the critical cross-section in the mid-span  $AB$  after redistribution in the case of a beam with uniformly distributed loads

The objective measure of plastic reserve of member resistance, attainable for different limitations of moment resistance, is the limited plasticity ratio for system  $\alpha_u$ . In general its value gives the information how many times the member resistance can be increased due to the limited moment redistribution in relation to the analogous resistance adequate for the moment when the first plastic hinge occurs. In the case of the considered beam we have:

$$\alpha_u = \frac{a_g^{el} g + a_q^l q}{a_g g + a_q q} = \frac{a_g^{el}(1-\xi) + a_q^l \xi}{a_g(1-\xi) + a_q \xi} \geq 1,0 \quad (14)$$

Values of  $\alpha_u$  parameter, calculated for each examined beam and for particular kinds of the limitation of moment redistribution, are presented in Fig. 4 (in Fig. 4a for  $\eta=1,0$ , in

Fig. 4b for  $\eta = \alpha_p = 1,07$  and in Fig. 4c for  $\eta = \alpha_{pl} = 1,14$ ) as functions  $\alpha_u = \alpha_u(\xi)$ . In conclusion the fact that in each cases the greatest plastic reserve of a system is attainable for two-span beam should be underlined.

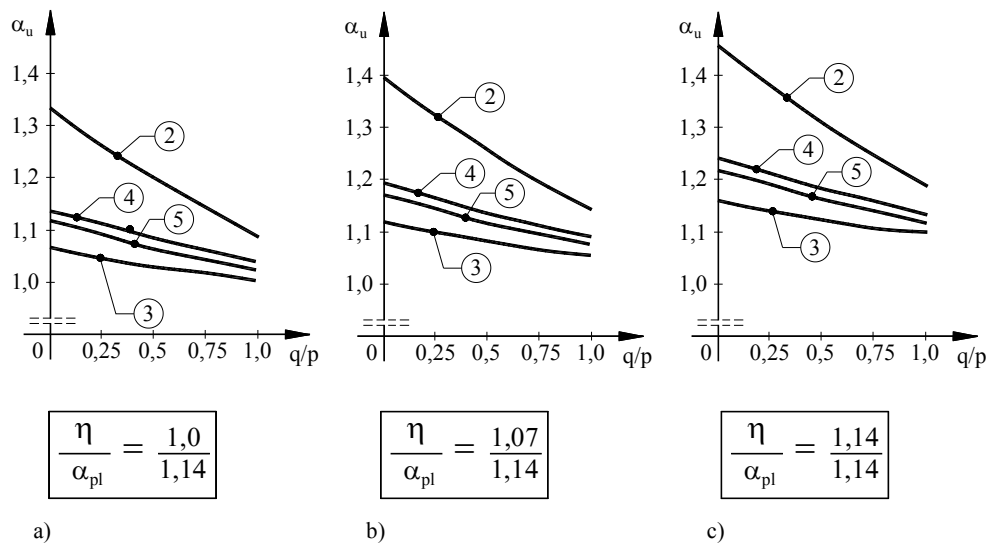


Fig. 4. Limited plasticity ratios for system  $\alpha_u$  calculated for different ways of moment redistribution, in the case of a beam loaded with uniformly distributed loads

#### 4. BEAM WITH CONCENTRATED LOADS

In the case of beams for which all applied loads (both dead loads  $G$  and imposed loads  $Q$ ) are concentrated the maximum elastic bending moment not always occurs at the support  $B$ . It is also possible that the first plastic hinge will be induced in the mid-span  $AB$ , the most frequently exactly under the applied load  $P = G + Q$ . In fact the way of moment redistribution depends on the number of forces in a single span. Generally, if there are more than one concentrated force in span  $AB$  then always  $|M_B^I| > M_1^{II}$ . On the other hand, if the beam presented in Fig. 5 is considered (only one force  $P$  in span  $AB$ ) the opposite inequality  $|M_B^I| < M_1^{II}$  is true. The important exception has to be analyzed for a two-span beam. In such case  $|M_B^I| = 0,188GL + 0,188QL = 0,188PL$  and  $M_1^{II} = 0,156GL + 0,203QL$ , hence from the condition  $|M_B^I| < M_1^{II}$  we have the limitation  $\xi = Q/P > 0,68$ .

The position of maximum mid-span moment after redistribution in the beam presented in Fig. 5 is known in advance. Value of  $x_1$  does not depend on the ratio  $\xi = Q/P$ , because always  $x_1 = 0,5L$ . Because of the fact that the first plastic hinge occurs in the mid-span  $AB$  the technique of limited moment redistribution is slightly more complicated. Two essential equations result from the static approach to plasticity theory:

$$|M_B^I| = \eta M_{el} - M_B^0 \quad \text{and} \quad M^{II}(0,5L) = \alpha_{pl} M_{el} + M_B^0 / 2 \quad (15)$$

In addition:

$$M_B^I = -(a_g^{el} G + a_q^I Q)L, \quad M_B^{II} = -(a_g^{el} G + a_q^{II} Q)L \quad \text{and} \quad M_B^0 = (a_g^0 G + a_q^0 Q)L \quad (16)$$

Furthermore, from the equilibrium equation we have:

$$M''(0,5L) = PL/4 - |M_B''|/2 \quad (17)$$

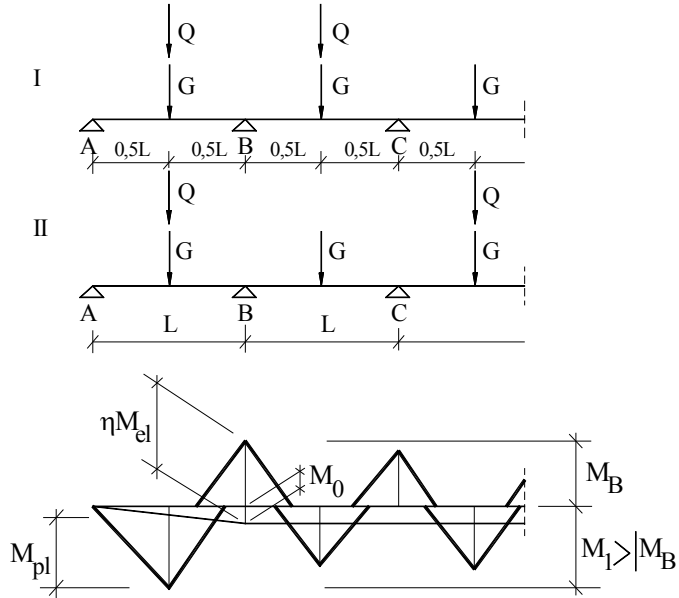


Fig. 5. Load arrangements and limited moment redistribution for a beam loaded with concentrated loads when only one force is applied in the mid-span

Additional inequality is extremely important. After redistribution bending moment in the mid-span  $AB$  still has to be greater than analogous moment at the support  $B$ , hence:

$$\eta[M''(0,5L) - M_B^0/2] \geq \alpha_{pl} [ |M_B^I| + M_B^0 ] \quad (18)$$

Finally, we obtain the maximum possible value of residual moment  $M_B^0$ :

$$M_B^0 = \frac{\eta PL - 4\alpha_{pl} |M_B^I| - 2\eta |M_B^{II}|}{4\alpha_{pl} + 2\eta} \quad (19)$$

which means that:

$$a_g^0 = \frac{\eta}{4\alpha_{pl} + 2\eta} - a_g^{el} \quad \text{and} \quad a_q^0 = \frac{\eta - 4\alpha_{pl} a_q^I - 2\eta a_q^{II}}{4\alpha_{pl} + 2\eta} \quad (20)$$

Consequently:

$$a_g = a_{1,g}^{el} + a_g^0/2 \quad \text{and} \quad a_q = a_{1,q}^{II} + a_q^0/2 \quad (21)$$

Parameters  $a_{1,g}^{el}$  and  $a_{1,q}^{II}$  are also the load effect coefficients (see Eq. 5); however, now they are determined for the mid-span  $AB$  critical cross-section.

Values of  $a_g$  and  $a_q$  in this case do not depend on the ratio  $\xi$ . They are collected in Tab. 2 for particular ways of the limitation of moment redistribution. The limited plasticity ratio for system  $\alpha_u$  is in this example calculated in a slightly different way:

$$\alpha_u = \frac{a_{1,g}^{el}g + a_{1,q}^{II}q}{a_gg + a_qq} = \frac{a_{1,g}^{el}(1-\xi) + a_{1,q}^{II}\xi}{a_g(1-\xi) + a_q\xi} \geq 1,0 \tag{22}$$

Table 2. Comparison of the results obtained for particular approaches to moment redistribution, in the case of a beam loaded with concentrated loads when only one force is applied in the mid-span

Number of span		2			3			4			5		
$\xi = Q/P$		0	0,5	1	0	0,5	1	0	0,5	1	0	0,5	1
$a_g$	1,0/1,14	0,174			0,174			0,173			0,174		
	1,07/1,14	0,170			0,170			0,170			0,170		
	1,14/1,14	0,167			0,167			0,166			0,167		
$a_q$	1,0/1,14	0,206			0,209			0,209			0,209		
	1,07/1,14	0,202			0,205			0,205			0,205		
	1,14/1,14	0,198			0,200			0,200			0,200		
$\alpha_u$	1,0/1,14	1,0	1,0	1,0	1,007	1,014	1,019	1,0	1,0	1,005	1,0	1,0	1,009
	1,07/1,14	1,0	1,0	1,004	1,029	1,035	1,041	1,0	1,013	1,027	1,005	1,019	1,031
	1,14/1,14	1,0	1,0	1,025	1,050	1,057	1,062	1,017	1,034	1,048	1,026	1,040	1,052

The plastic reserve obtained in this case as a result of limited moment redistribution is much lower than analogous one, calculated for the beam with uniformly distributed loads. Suitable functions  $\alpha_u = \alpha_u(\xi)$  are presented in Fig. 6 (in Fig. 6a for  $\eta=1,0$ , in Fig. 6b for  $\eta=\alpha_p=1,07$  and in Fig. 6c for  $\eta=\alpha_{pl}=1,14$ ). The value  $\alpha_u$  is greater for greater  $\xi$  parameter, contrawise to the solution obtained by means of Eq. 14. Moreover, the greatest plastic reserve is attainable for three-span beam, not for two-span beam as it has been shown in the previous example (see Fig. 4).

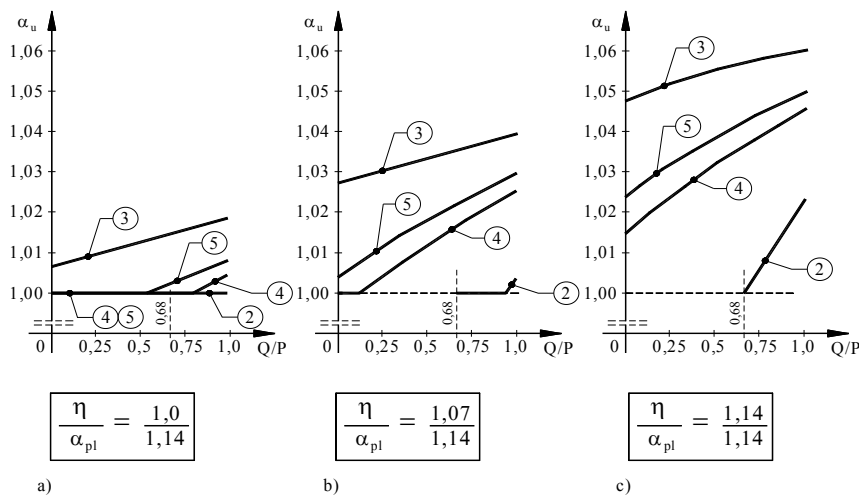


Fig. 6. Limited plasticity ratios for system  $\alpha_u$  calculated for different ways of moment redistribution, in the case of a beam loaded with concentrated loads when only one force is applied in the mid-span

## 5. CONCLUSIONS

The basic aim of the limitation of plastic reserve attainable for beams as a result of moment redistribution is to protect considered member against the possibility of accumulation of permanent strains. Analysis presented in the present article allows to determine the ratio of such reduction in relation to the analogous plastic reserve, calculated according to methodology which deals with the balancing of ultimate bending moments in critical cross-sections. In the case of the continuous beam loaded with uniformly distributed loads examined reserve decreases from 17 ÷ 46% (Fig. 4c) to 12 ÷ 39% (Fig. 4b) if we accept the ultimate moment  $\alpha_p M_{el}$  in mid-span  $AB$ , or even to 6 ÷ 33% (Fig. 4a) if the moment  $M_{el}$  is there adopted. Similarly, considering the example with concentrated loads, we conclude that analyzed plastic reserve is reduced from maximum 6,2% (Fig. 6c) to 4,1% (Fig. 6b) or to 1,9% (Fig. 6a), respectively. Let us notice that in this case such reserve cannot be taken into consideration ( $\alpha_u = 1,0$ ) if the ratio  $\xi = Q/P$  is not large enough.

The influence of an interaction between bending moment and shear force is neglected in this study. Some suggestions in this field were given by the author in [7]. Presented solutions can be applied to the engineering practice only if the beam is protected against all forms of the instability modes.

## REFERENCES

- [1] PN-EN 1993-1-1, Eurokod 3: Projektowanie konstrukcji stalowych, Część 1-1: Reguły ogólne i reguły dla budynków.
- [2] Dutheil J., La conception des ossatures metalliques basee sur la deformation plastique, *Ossatures Metalliques*, 3, 1949, 143-162.
- [3] Mutermilch J., O wymiarowaniu konstrukcji stalowych metodą plastyczności ograniczonej, *Inżynieria i Budownictwo*, 9, 1949, 359-366.
- [4] Łubiński M., Giżejowski M., Problemy projektowania plastycznego pełnościennych belek ciągłych, *Inżynieria i Budownictwo*, 8, 1983, 338-344.
- [5] Piechnik S., Współczynnik adaptacji plastycznej Dutheila, *Inżynieria i Budownictwo*, 11, 1993, 482-483.
- [6] PN-90/B-03200, Konstrukcje stalowe. Obliczenia statyczne i projektowanie.
- [7] Maślak M., Projektowanie belek ciągłych metodami plastyczności ograniczonej, Praca doktorska, Politechnika Krakowska, 1997.
- [8] Murzewski J., Reliability requirements and design situations of steel structures, *Celostatna Konferencja Medzna Unosnost Kovovych Konstrukcii*, Bratislava, 1986, t. 2, 42-51.

Karel MIKES<sup>1</sup>  
Ondrej JIRKA<sup>2</sup>

## SEMI – RIGID JOINTS OF TIMBER STRUCTURES

### ABSTRACT

Traditional timber joints behaviour remains badly known. Recent studies have shown that some kind of carpentry joints can be considered as semi-rigid connections. Their rigidity (bending stiffness) in general sense plays an important role in computation of the global deformations and force distribution of timber roofing frames. Developments in computer-controlled manufacture of timber members enable a revival of traditional timber connections without steel fasteners. This study will focus on deformation, failure processes and bending stiffness of rafter-tie beam connection and modern tenon (dovetail) joint as secondary beam-main beam connection (both joints are made by CNC wood-working machine).

**KEYWORDS:** carpentry joints, semi-rigid, bending stiffness, tenon (dovetail) joint

### 1. INTRODUCTION

Wood is a unique structural material. It stands alone in many characteristics when compared with man-made materials such as steel, concrete, stone, brick, and most synthetics. It is multicomponent, hygroscopic, inhomogeneous, inelastic, fibrous, porous, biodegradable and renewable. Wood is also cellular organic material from which timber is cut for construction purposes. The tubular cells of timber have an orientation that gives different properties, depending on the direction of the grain, and produce a highly anisotropic material (i.e. having different properties in different directions). This explains why timber is subject to different permissible stresses depending upon whether the direction of loading is parallel or perpendicular to the grain [3]. Timber is one of the oldest structural material but its deformation and failure processes are poorly understood compared to information about other materials like steel or concrete.

Timber frameworks and roofs are one of the most important and widespread patrimonial structures and they represent one of the most important ancient engineering works spanning over considerable distances. They involve not only an evidence of structural knowledge and creativity of their makers but also a good deal of structural beauty. The roofing frameworks have passed a long way of development of their structural schemes and improvements of their layout [2]. The development of roofing frameworks and also building frames was accompanied by changes in joints and their structural behaviour. Unfortunately,

---

<sup>1</sup> PhD., Ing., Czech Technical University in Prague, Prague, CZECH REPUBLIC,

<sup>2</sup> Ing., Czech Technical University in Prague, Prague, CZECH REPUBLIC.

these structures are vulnerable, and damaged joints can lead to some modifications of the global behaviour of the structure.

Timber joints are often less effective than corresponding joints in steel, for instance, because of the relatively low embedding strength and low strength in shear, and particularly in tension, perpendicular to grain. Relatively large spacing and distances to end and edge are therefore needed to avoid splitting. This means that the necessary load transfer areas are quite large, and may often determinate the size of timber framework members [4]. This shows that great attention must be paid to the design of joints. In some cases, the joints are quite complicated, especially where there are tension forces. These designs have remained out of use for a period, but due to the introduction of CNC wood-working machines, some carpentry joints may again be of interest because of their fire resistance, or for use in structures with many similar compression members. Some examples of joints made up by these technique shows fig. 1.



Fig.1. Various types of carpentry joints made by CNC wood-working machines – main advantage is an excellent accuracy of these connections

This study will focus on deformation, failure processes and bending stiffness of rafter-tie beam connection and modern tenon (dovetail) joint as secondary beam-main beam connection (both joints are made by CNC wood-working machine), see figure 2. To characterize the behavior of the frameworks, different types of joints and geometries will be studied. In order to validate the results, it will be made comparison of analytical, numerical and of course experimental approaches. Comparison should bring out some new knowledge of understanding carpentry joints behaviour which is most important in the field of structural design and timber repair and their retention for next generation.



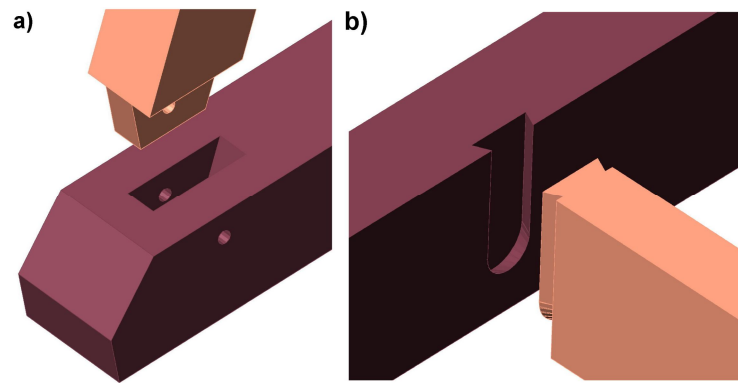


Fig.2. a) Traditional rafter-tie beam connection, b) modern dovetail (tenon) joint as secondary beam – main beam connection

The analytical method is based on the component method, frequently used in steel construction. This method consists in associating stiffness to each couple of surfaces in contact. The joint is decomposed into components, which are represented by force – deformation diagram. It provides quick results according to geometrical parameters and elastic properties.

3D finite models (by ANSYS) will be used for numerical solution of these connections. These models will take into account contact and orthotropic elasticity. Contact will be introduced by non linear springs or contact “surface to surface”

All these results will be compared to the laboratory tests. Pilot experiments of rafter-tie beam connection (hand-made) were performed by Institute of Theoretical and Applied Mechanics in Prague (ITAM) [1]. We will use these data for calibration of our own experiments. Our own experimental research is currently being conducted. These experiments will observe deformation, failure processes and bending stiffness of rafter-tie beam connection and modern tenon joint as secondary beam-main beam connection, both connections are made by CNC wood-working machine.

## 2. THE MAIN POINTS OF OUR STUDY

1. Analysis of current approach in field of design carpentry connections
2. Experimental part
  - 2.1. Evaluation of experiments performed by ITAM
  - 2.2. Performance our own experiments
3. Numerical simulation (finite-element method)
4. Analysis by component method
5. Conclusions

## 3. CURRENT APPROACH

In many cases the internal forces are passed on by contact and friction in the joint areas, without any fasteners. Because of important sections used in old timber structures, in many cases only the serviceability limit states are restrictive. In this case, taking into account the rotational stiffness of the joint can be useful but the modelisation of timber framework is not so easy through lake of information about carpentry joints. Following figures show some kinds of connections and nowadays analytical approaches of their design.

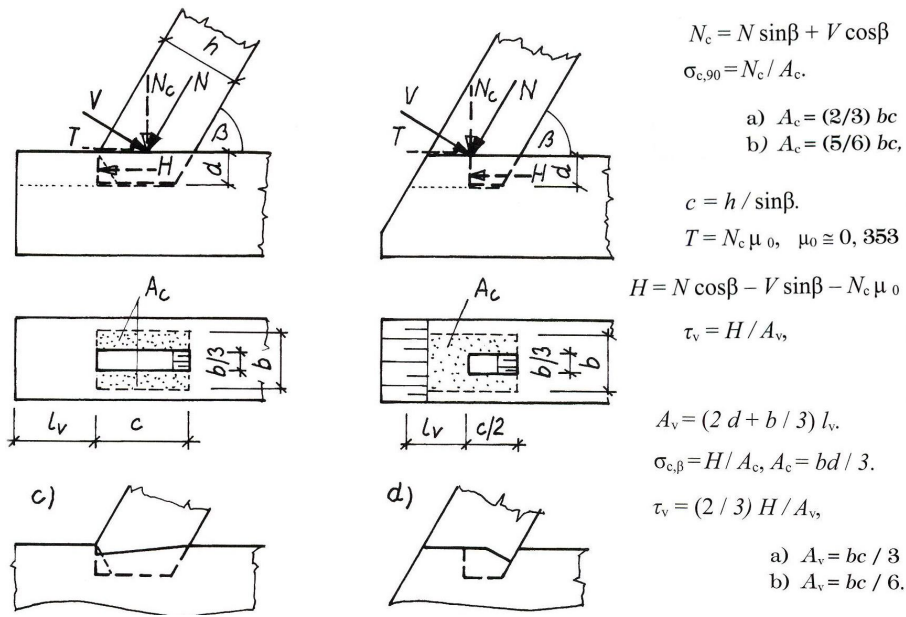


Fig.3. Sloping tenon joint – determination of design stresses

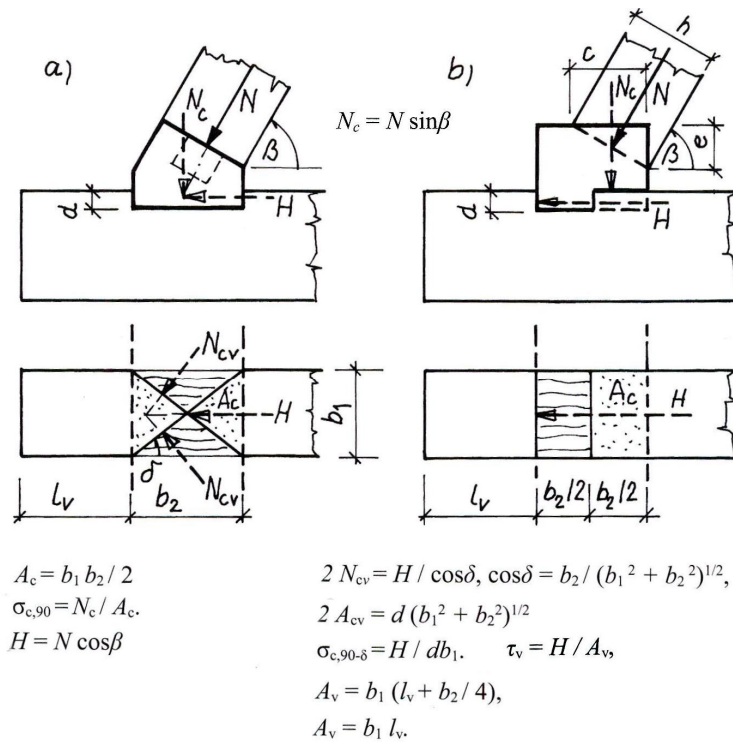


Fig.4. Cogging joint – determination of design stresses

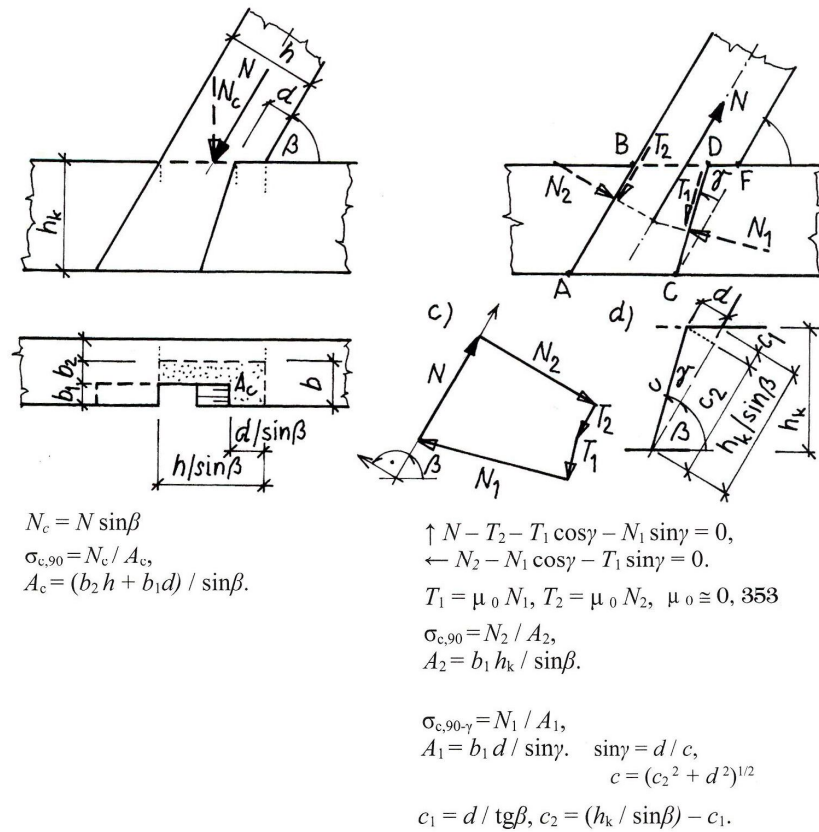


Fig.5. Dovetail connection – determination of design stresses

**4. EXPERIMENTAL PART**

For calibration our experiments we use data from experiments of rafter-tie beam connection (hand-made) which were performed by Institute of Theoretical and Applied Mechanics in Prague (ITAM) [1]. There were two sets of rafter tie beam connection (one was made from pine wood and second one from oak). These joints were submitted monotonic and cyclical loading with different levels of eccentricity. Test set up shows fig.5.

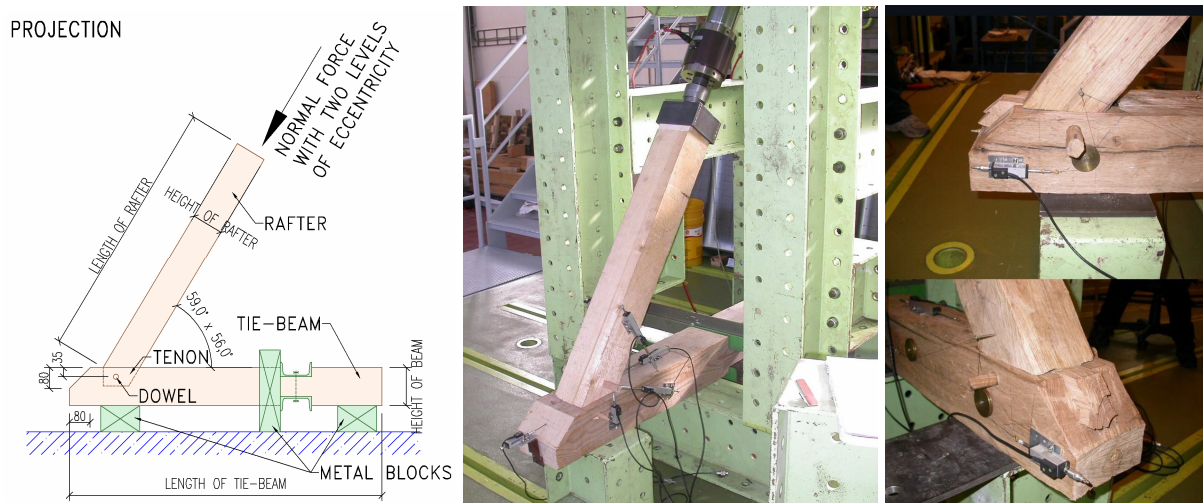


Fig.6. Test arrangement, geometry and fixing of the joint during experiment, one type of failure of the after test

Table.1. different types of failure during experiments (ITAM)

		P1	P2	P3	P4	P5	P6	O1	O2	O3	O4	O5	O6
Failure of wood dowel				•	•	•	•	•	•	•	•	•	•
Embedding rafter to the tie beam	0-2mm	•						•		•	•	•	
	2-5mm		•		•				•				
	> 5mm			•		•	•						
Failure of tenon of the rafter						•		•	•		•		•
Failure of the heel of the tie beam	Shear failure			•	•	•	•		•	•			
	Tensile failure			•			•						
	Rise of cracks		•								•		

## 5. PREPARED EXPERIMENTAL RESEARCH

The experimental research is currently being prepared. We have prepared two kinds of carpentry joints. First is similar rafter-tie beam like joint which was tested by ITAM but this joint is made by CNC wood-working machine. Second connection is modern dovetail joint as secondary beam – main beam connection. All of these connections have been built with spruce wood and with moisture content of 20%.

Geometry of rafter – rafter tie beam carpentry joint is the same like ITAM performed. This connection will be submitted normal monotonic load with eccentricity to simulate bending moment. During the experiment will be measured following values: embedding of rafter to the tie beam, failure of the heel of tie beam and the most important thing is sloping of the rafter to determinate  $M-\Phi$  diagram.  $M-\Phi$  diagram is very important to describe semi – rigid behaviour of the joint. It is also necessary to know, in each instant, the position of instantaneous centre of rotation.

Second described timber joint is modern dovetail joint, we have prepared 8 dovetail joints and during our experimental research we want determinate bending stiffness and shear capacity of this kind of connection. Principles of these tests are shown in the figure below. Geometry of each joint is shown in fig. 9-10.

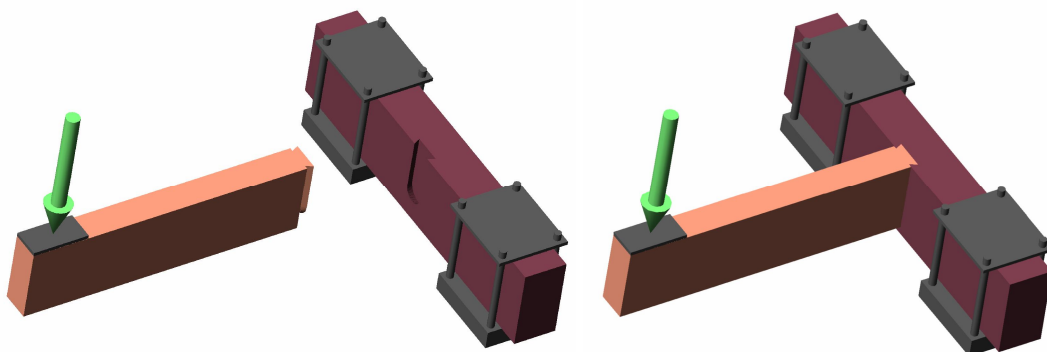


Fig.7. Principle of the experiment to determinate the bending stiffness of the dovetail joint

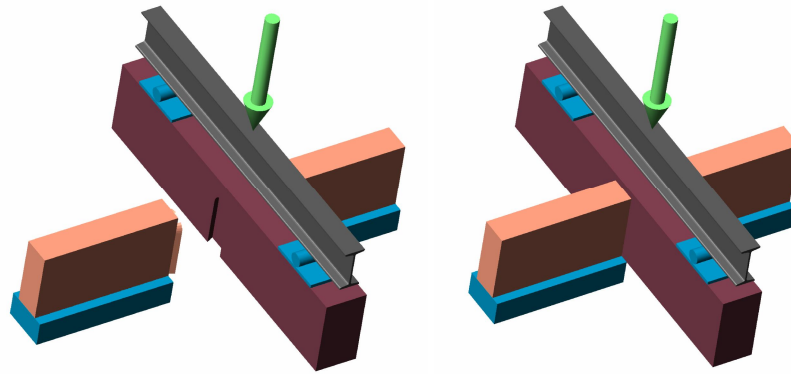


Fig.8. Principle of the experiment to determinate the shear capacity of the dovetail joint

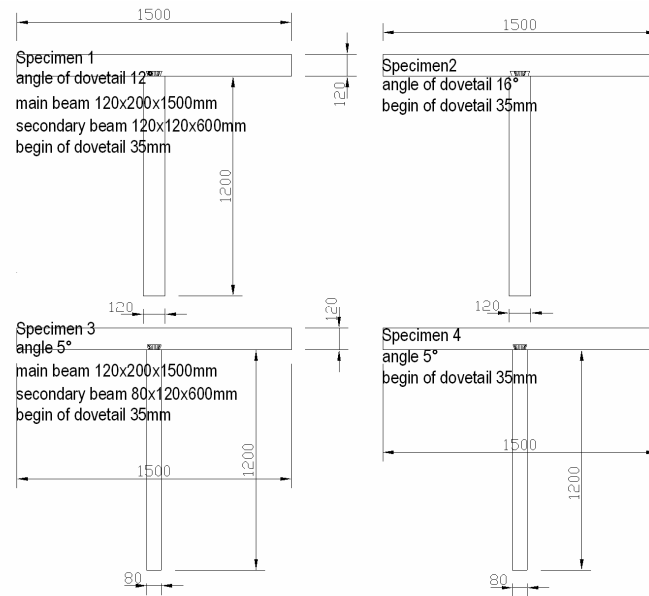


Fig.9. Geometry of the experiment to determinate the bending stiffness

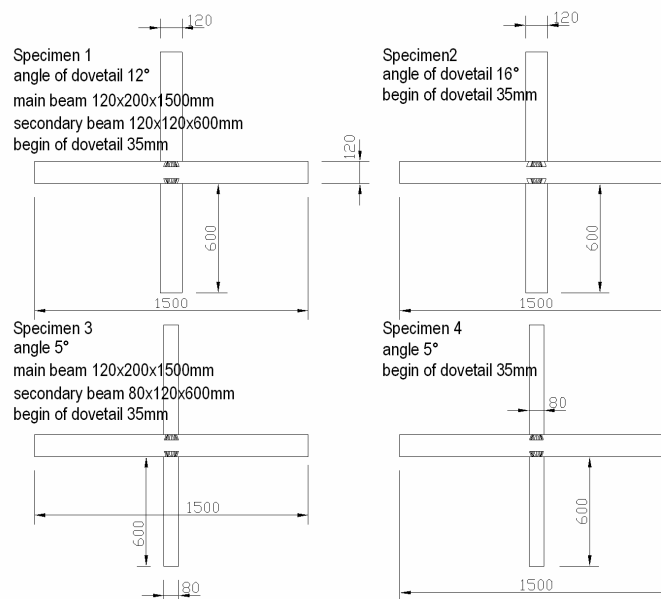


Fig.10. Geometry of the experiment to determinate the shear capacity

## 5. NUMERICAL SIMULATION (FINITE ELEMENT METHOD)

3D finite models (by ANSYS) will be used for numerical solution of these connections. These models will take into account contact and orthotropic elasticity. Contact will be introduced by non linear springs or contact “surface to surface”

## 6. COMPONENT METHOD

The component method will be applied to the joint to derive simple model of joint behaviour subjected to static load. The joint will be decomposed into components, which are represented by force – deformation diagram. It is supposed the dowel resists to shear and clearly fixes the position of the centre of rotation of the connection. The principle of component method is shown below.

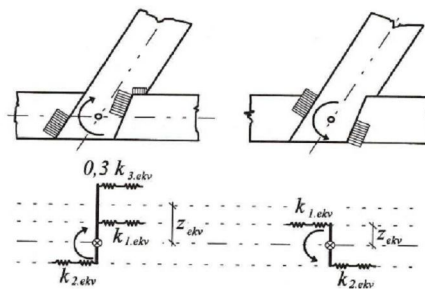


Fig.11. The contact surfaces and the component model for loading in clockwise and counter-clockwise directions

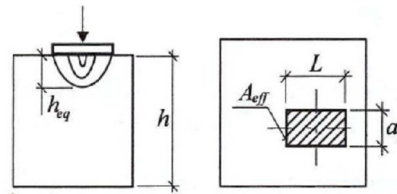
The presented connection is composed from one type of component only – timber in compression. The resistance of the material in compression with respect to the direction of  $\beta$  fibers of the wood is:

$$f_{c,\beta,d} = \frac{f_{c,0,d}}{\frac{f_{c,0,d}}{f_{c,90,d}} \sin^2 \beta + \cos^2 \beta}$$

The resistance of the component  $F_{u,i}$  can be derived from area in compression  $A_i$

$$F_{u,i} = A_i f_{c,\beta,d}$$

Stiffness of this component is calculated on basis of theory of deformation of elastic half space



The deformed zone in the joint can be predicted using concept of effective height. The deformation of the block under a rectangular rigid plate was solved by several authors. Solution by Lambert and Whitman gives deformation:

$$\delta_c = \frac{F_c \alpha a_r}{E_a A_r}$$

Where  $F_c$  is applied compressed force,  $a_r$  is width of rigid plate,  $E_a$  is Young's modulus of wood,  $A_r$  is area of the plate,  $L$  is length of the plate. The factor  $\alpha$  depends on ratio between  $L$  and  $a_r$  and on Poisson's ratio of the material

The stiffness of the component expressed in form suitable for component method gives:

$$k_c = \frac{F_c}{E_{90} \delta_c} = \frac{E_a \sqrt{L \alpha_r}}{0,8 E_{90}}$$

The bending moment resistance is given by

$$M_u = \sum_i F_{u,i} z_i$$

The initial bending stiffness can be calculated from stiffness of the components

$$s_j = \frac{M}{\varphi} = \frac{E z_{ekv}^2}{\sum_i \frac{1}{k_{i,ekv}}}$$

Where the components in series should be replaced by single spring whit stiffness  $k_i$ :

$$\frac{1}{k_i} = \frac{1}{k_{i,1}} + \frac{1}{k_{i,2}}$$

## 7. CONCLUSIONS

This study will focus on deformation, failure processes and bending stiffness of rafter-tie beam connection and modern tenon (dovetail) joint as secondary beam-main beam connection (both joints are made by CNC wood-working machine). To characterize the behavior of the frameworks, different types of joints and geometries will be studied. In order to validate the results, it will be made comparison of analytical, numerical and of course experimental approaches. Comparison should bring out some new knowledge of understanding carpentry joints behaviour which is most important in the field of structural design and timber repair and their retention for next generation.

## 8. REFERENCES

- [1] M. Drdácý, F. Baroš, z. Sokol: *Experimentální výzkum styčniků historických dřevěných krovů*, Praha-UTAM, 1999, 69p.
- [2] M. Drdácý, F. Wald, J. Mareš, Z. Sokol: *Component Method for Historical Timber Joints*, The Paramount Role of Joints into Reliable Response of Structures, NATO Science series, Series II, Vol.4 (ed. C.C.Banitopoulos, F.Wald). Kluwer Academic Publishers, Dordrecht, 2000, pp. 417-425.
- [3] J. Bodig, B.A. Jayne: *Mechanics of Wood and Wood Composites*, Van Nostrand Reinhold Company, 135 West 50th Street, New York, 1982, 712p.
- [4] S. Thelandersson, H. J. Larsen: *Timber Engineering*, John Wiley & Sons Ltd, The Atrium, Southern Gate, Chichester, West Sussex, 2003, pp. 303-331.

## ACKNOWLEDGMENT

This research has been supported by research plan VZ1 JN MSM 210000001 „Functional qualification and optimization of building structures“.





Ivan D. PELESHKO<sup>1</sup>  
Vitalina V. YURCHENKO<sup>2</sup>  
Nikita A. BELIAEV<sup>3</sup>

## COMPUTER-AIDED DESIGN AND OPTIMIZATION OF STEEL STRUCTURAL SYSTEMS

### ABSTRACT

A new computer-aided methodology for design and optimization of steel structures based on hybrid genetic algorithm with gradient learning of the best individual has been reported. The optimum design problem is formulated as the structural-parametric mathematical programming task with Boolean, integer and real design variables. In this way, cross sectional sizes of structural members, node coordinates as well as topology parameters can be considered as design variables. The system of constraints includes load-carrying capacity and stiffness conditions for structural members and entire steel construction according to building standards and regulations. Architectural, technological and other requirements can be integrated to constraint system as well. Determination of purpose function takes into account design specifications and ability to formulate the analytical expression as function of design variables. Hybrid genetic algorithm based on the parallel operations of genetic operators and update gradient method was used for solving the structural-parametric optimization task. Proposed technique was realized with elaborated software. Numerical example with new optimal design decision of plane two-hinged transverse frame with lattice structural members demonstrates the effectiveness of the proposed optimization methodology.

**KEYWORDS:** structural optimization, steel constructions, steel transverse frames, computer-aided design, genetic algorithm, gradient method, finite element method, software

### 1. INTRODUCTION

Structural optimization has been an active research area for over one hundred years. The development of mathematical programming techniques as well as the finite element method made possible the emergence of structural optimization as a potential design tool. An optimal design of steel structural systems represents the purposeful searching the values of these system parameters which ensure the best objective function value. Usually, the optimization problem is formulated as the non-linear programming task which includes set of design variables, system of constraints and objective function.

<sup>1</sup> Associate Prof. PhD. Eng., Lviv Politechnic National University, Lviv, UKRAINE

<sup>2</sup> Associate Prof. PhD. Eng., Kyiv National University of Civil Engineering and Architecture, Kyiv, UKRAINE

<sup>3</sup> Master Student, Eng., Kyiv National University of Civil Engineering and Architecture, Kyiv, UKRAINE

If objective function and constraint functions of the mathematical model are continuously differentiable and defined in smooth domain of all admissible design parameters, then such optimization problem can be solved with gradient method successfully [8, 10]. In this context, searching of optimal values of design variables is performed when structural topology, support conditions, node connections and load pattern are prescribed and constants. Usually, such kind of problems is related to the *parametric optimization tasks*.

Today theory of optimum structural design is developed in the tideway of solution the structural topology optimization problem with variable design parameters [2, 7]. The set of design variables includes quantity of node, quantity and locations of bars together with variable node coordinates and cross-sectional sizes of the structural members. These kinds of problems are related to the *structural optimization tasks*, they have some particularities. On the one hand, design variables of continuous and discrete types present. On the other hand, quantity and behavior of the design variables as well as constraints and objective functions vary during structural transformation of the iterative searching process. Design domain is not smooth, separate sub-domains have a difference dimensionality or are created by difference set of the design variables.

Different variations of random search methods as well as homogenization methods [1] have been proposed in order to solve the structural optimization problems. In the performance of structural optimization tasks methods implemented goal seeking exhaustive of finite set of design decision alternatives have been preferred. One of these methods is *genetic algorithm* (GA) that reflects in a simplified way several processes of natural evolution [3, 5, 6, 9]. Synthesis of new topological design decisions is performed due to random variations of the initial topology or by excluding bars from the “ground” structure.

## 2. PROBLEM FORMULATION

We pose the structural optimization problem as the non-linear programming task in the following mathematical terms: to find these unknown parameter values:

$$\bar{x} = \{x_i \mid i = 1 \dots n\}, \quad (1)$$

which minimize an objective function:

$$f^* = f(\bar{x}^*) = \min_{\bar{x} \in \mathbf{D}} f(\bar{x}), \quad (2)$$

subject to:

$$\psi_\kappa(\bar{x}) = 0, \quad \kappa = 1 \dots n_{ec}; \quad (3)$$

$$\varphi_\eta(\bar{x}) \leq 0, \quad \eta = 1 \dots n_{ic}; \quad (4)$$

$$\bar{x}^L \leq \bar{x} \leq \bar{x}^U, \quad i = 1 \dots n; \quad (5)$$

were  $\bar{x}$  – the vector of design variables (variable structural parameters);  $n$  – quantity of variables;  $f$ ,  $\psi$ ,  $\varphi$  – functions of the vector argument;  $n_{ec}$  – amount of equality constraints  $\psi_\kappa(\bar{x})$ , which define hyperplanes of feasibility;  $n_{ic}$  – amount of inequality constraints  $\varphi_\eta(\bar{x})$ , which define regions of feasibility in the design space  $\mathbf{D}$ .

Unknown structural parameters Eqn. 1 give an indication of some properties of steel structures and structural members. The specific technical-and-economic index can serve the objective function Eqn. 2. We enter an equilibrium conditions for each case of structural loading into the system of constraints Eqn. 3. Beside from this, load-carrying ability (namely, stresses and buckling checks) as well as stiffness conditions for structural members and entire structure according to building regulations and requirements are included to the system of constraints Eqn. 4 – Eqn. 5. Architectural, technological, and other requirements can be also integrated to the constraint system.

### 3. PARAMETRIC OPTIMIZATION BASED ON UPDATE GRADIENT METHOD

We propose to solve the parametric optimization task of steel structural systems using update gradient method. This method bases on construction of the design decision sequence, which ensures the convergence to the optimum point  $\bar{x}^*$  with the minimal objective function value  $f^*$  (see Eqn. 2):

$$\bar{x}_{k+1} = \bar{x}_k + \Delta\bar{x}_k, \quad (6)$$

where  $\bar{x}_k = (x_1^k, x_2^k, \dots, x_n^k)^T$  – the current approximation of the task solution;  $\Delta\bar{x}_k = (\Delta x_1^k, \Delta x_2^k, \dots, \Delta x_n^k)^T$  – an increment vector for current design variables;  $k$  – step number. A start point  $\bar{x}_0$  of the iterative process is engineering assessment of the structural design decision.

Active constraints only are considered at the each searching iteration. The set of active constraint numbers  $\mathbf{A}$  at the current point  $\bar{x}_k$  can be determined as:

$$\mathbf{A} = \mathbf{I} \cup \mathbf{J}, \quad \mathbf{I} = \left\{ \kappa \mid \kappa = \overline{1, n_{ec}} \right\}, \quad \mathbf{J} = \left\{ \eta \mid \varphi_\eta(\bar{x}_k) \geq -\varepsilon, \eta = \overline{n_{ec} + 1, n_{ic}} \right\},$$

where  $\varepsilon$  – the small positive number.

The increment vector for current design variables  $\Delta\bar{x}_k$  can be calculated according to the following equation:

$$\Delta\bar{x}_k = \Delta\bar{x}_\perp^k + \Delta\bar{x}_\square^k, \quad (7)$$

where  $\Delta\bar{x}_\perp^k$  and  $\Delta\bar{x}_\square^k$  – vectors, which are determined subject to conditions of liquidation of constraint residuals and improvement of the purpose function value respectively.

Component  $\Delta\bar{x}_\perp^k$  can be determined using following formula:

$$\Delta\bar{x}_\perp^k = \mathbf{\Gamma} \times \bar{\mu}_\perp, \quad (8)$$

where  $\mathbf{\Gamma}$  – gradient matrix for the active constraints;  $\bar{\mu}_\perp$  – vector-column calculated below.

The values of constraint violations at the current point  $\bar{x}_k$  represent by the vector of residuals described below:

$$\vec{\phi} = \left( \psi_\kappa(\bar{x}) \mid \kappa \in \mathbf{I}; \varphi_\eta(\bar{x}) \mid \eta \in \mathbf{J} \mid \varphi_\eta(\bar{x}) > 0; 0 \mid \varphi_\eta(\bar{x}) \leq 0 \right)^T.$$

In order to liquidation the constraint violations presented by  $\vec{\phi}$  the component  $\Delta\bar{x}_\perp^k$  as a first approximation should satisfy Taylor's theorem [8] for the smooth multivariable function at the vicinity of the current point  $\bar{x}_k$  for all constraints from the set  $\mathbf{A}$ , namely:

$$-\vec{\phi} = \mathbf{\Gamma}^T \times \Delta\bar{x}_\perp^k. \quad (9)$$

With substitution of Eqn. 10 in Eqn. 11 we have obtained equation system for computing the vector-column  $\bar{\mu}_\perp$  such as presented below:

$$\mathbf{\Gamma}^T \times \mathbf{\Gamma} \times \bar{\mu}_\perp = -\vec{\phi}. \quad (10)$$

Component  $\Delta\bar{x}_\square^k$  can be calculated by the following formula:

$$\Delta\bar{x}_\square^k = \xi \bar{p} = \xi \times \left( \nabla \vec{f} - \mathbf{\Gamma} \times \bar{\mu}_\square \right), \quad (11)$$

where  $\nabla \vec{f}$  – vector of purpose function gradient at the current point  $\bar{x}_k$ ;  $\bar{p}$  – the purpose function gradient  $\nabla \vec{f}$  projection on the surface of active constraints at the current point  $\bar{x}_k$ ;  $\xi$  – step parameter;  $\bar{\mu}_\square$  – vector-column calculated approximately with least-squares technique

according to the correlation described below:

$$\mathbf{\Gamma} \times \bar{\mu}_{\square} \approx \nabla \bar{f}, \quad (12)$$

or by the following equation:

$$\mathbf{\Gamma}^T \times \mathbf{\Gamma} \times \bar{\mu}_{\square} = \mathbf{\Gamma}^T \times \nabla \bar{f}. \quad (13)$$

Using Eqn. 8 and Eqn. 11 the formula Eqn. 7 can be expressed as presented below:

$$\Delta \bar{x}_k = \mathbf{\Gamma} \times \bar{\mu}_{\perp} + \xi \times (\nabla \bar{f} - \mathbf{\Gamma} \times \bar{\mu}_{\square}), \quad (14)$$

$$\Delta \bar{x}_k = \xi \times \nabla \bar{f} + \mathbf{\Gamma} \times (\bar{\mu} - \xi \times \bar{\mu}_{\square}), \quad (15)$$

where  $\bar{\mu}_{\perp}$  and  $\bar{\mu}_{\square}$  are calculated according to Eqn. 10 and Eqn. 12 or Eqn. 13 respectively.

Modification of the gradient method which ensures the selection of linear-independent constraints with constant vector lengths of constraint and purpose function gradients has been proposed in [12, 13].

Parametric optimization methodology for steel structural systems based on gradient method can be described as presented below.

An algorithm for solving the parametric optimization task for steel structural systems includes the following steps.

- Step 1. Specification the start design decision and initial data* for calculating. Describing the set of design variables  $\bar{x}_k$ , where  $k$  – iteration number,  $k = 0$ , is performed. The initial data for the parametric optimization problem are structural topology, material characteristics of the structural members, types of bar cross-sections, support conditions, locations of hinges, pattern of the design load, pre-stressed diagram, deflection limits, optimality criteria and additional constraints.
- Step 2. Calculation of geometrical and effective lengths* (for buckling verifications) of the structural members using initial data. At the next iteration length values is corrected based on current values of the geometrical design variables.
- Step 3. Determination the cross-sectional characteristics* such us areas, moments of inertia, second moments of inertia, and so on, using current values of cross-sectional design variables.
- Step 4. Static analysis.* Using finite element method for each design load case combinations calculation the linear displacements for all structural nodes and stresses (for stresses verifications) for all design section of all structural members is performed.
- Step 5. Verification the constraints of the mathematical model and forming the set of active constraint numbers.* Checking that the design structure complies with requirements Eqs.(3)-(5) should be performed for all load case combinations in all design sections of the structural members. Then, it has to identify the active (breached) constraints and include the numbers of these constraints as components into the set of active constraint numbers.
- Step 6. Calculation the current purpose function value  $f(\bar{x}_k)$  and purpose function gradient  $\nabla \bar{f}(\bar{x}_k)$ ,* determination the desire purpose function increment  $\Delta f(\bar{x}_k)$ . The purpose function gradient  $\nabla \bar{f}(\bar{x}_k)$  can be calculated by numerical differentiation using the finite difference approximation. The desire purpose function increment  $\Delta f(\bar{x}_k)$  can be specified as about 5...25% from the purpose function current value  $f(\bar{x}_k)$ .
- Step 7. Formation the vector of residuals  $\bar{\phi}$  and the matrix of the active linear-independent constraints gradients  $\mathbf{\Gamma}$  with triangular structure.*

*Step 8. Calculating design variable increments and improved approximation of the optimum design decision.* Increment value  $\Delta\bar{x}_k$  is determined according to Eqn. 15, the next design decision  $\bar{x}_{k+1}$  – by Eqn. 6.

*Step 9. Verification the stop conditions for the iteration searching.* If the current design decision fulfils all constraints of the mathematical model with assumed precision, it can be go at the step 10. For other cases it has to return to the step 2 with  $k \leftarrow k + 1$ .

*Step 10. The optimal design decision is  $\bar{x}_k$  with the optimum purpose function value  $f(\bar{x}_k)$ .*

#### 4. STRUCTURAL OPTIMIZATION USING HYBRID GENETIC ALGORITHM

GA uses some coding the set of desirable parameters instead of these parameter values and so it is applied for solution of discrete optimization problem. With that, unknown parameters are specified on numerical sets as well as on finite sets of any type. Searching strategy in GA bases on computation and comparison the values of some estimate function in the design space points under consideration. At once requirements for continuity, unimodality and differentiability of this function are not raised. That is why it is possible to apply GA for wide range functions including ones without analytical description.

One of the directions improving the evolutionary optimization methods is the application of *hybrid genetic algorithm* that combines properties of genetic algorithms and other optimization methods. Usually, initial estimation located at the domain of extremum is found by genetic algorithm. Next, position of the extremum is improved by gradient method. In that case, the convergence of the iterative process accelerates and accuracy of received results enhances.

In order to solve the problem given by Eqn. 1 – Eqn. 5 genetic algorithm uses iterative direct search that modeling evolutionary process. Each  $k^{\text{th}}$  solution of the problem  $\bar{x}_k^{(t)}$  (individual) is represented by symbol string  $\mathbf{B}_k^{(t)}$  (chromosome), which consists of sub-strings  $\beta_{i,k}^{(t)}$  (genes), where  $t$  – step (generation) number. The function  $\chi(\mathbf{B}_k^{(t)})$  (individual fitness to environment) prescribed on the string set estimates each individual approximation to the optimum decision.

The basic execution cycle (generation) is presented below.

*Step 1. Initialization.*  $t = 0$ . The initial set (population) of symbol strings according to prescribed structure  $\mathbf{A}^{(t)} = \{ \mathbf{B}_k^{(t)} \mid k = \overline{1, \nu} \}$  is formed by random generation of  $\nu$  binary strings.

*Step 2. Individual fitness computation and definition of the best individual.* Calculation the values of fitness function  $\chi(\mathbf{B}_k^{(t)})$  for any individuals of current population  $\mathbf{A}^{(t)}$ . The best individual  $\mathbf{B}_k^{*(t)} \in \mathbf{A}^{(t)}$  (leader) with a better fitness function value is selected and stored.

*Step 3. Reproduction.* The reproduction group of individuals according to chosen selection scheme is selected from population  $\mathbf{A}^{(t)}$ . Then reproduction of “the offspring” with inherited ancestral features is executed. It consists of the choice of given couple of “ancestors” and construction of genetic codes of individuals-“the offspring” with predetermined probability  $p_c$  according to chosen crossover scheme based on genetic codes of individuals-“ancestors”.

*Step 4. Recombination.* There is a construction of genetic codes of individuals-“mutants” with predetermined probability  $p_m$  according to the chosen mutation scheme.

*Step 5. Adaptation of the best individual.* The best individual  $\mathbf{B}_k^{*(t)}$  (best design decision) is improved separately according to the gradient method presented above.

*Step 6. Selection.* There is a selection with replacement of all individuals of population  $\mathbf{A}^{(t)}$  for further genetic processing.

If preset amount of population modifications executed or other stop conditions fulfilled, then iterative searching (evolution) have to be stopped. For other case, it should be returned to step 2 with  $t \leftarrow t + 1$ .

In order to solve structural optimization problem with hybrid genetic algorithm the *coding technique* for design variables as well as describe *estimate function* of design decisions in terms of symbol strings have been developed [11, 12]. The coding technique is a rule of one-to-one mapping the set of possible alternatives of structural design decisions on finite set of symbol strings. The choice of coding technique for specific optimization problem defines efficiency of GA application in a great measure. Each problem class needs the development of coding technique and estimate function of coding designs according to problem features.

## 5. SOFTWARE OPTCAD FOR OPTIMAL DESIGN AND ANALYSIS OF STEEL STRUCTURAL SYSTEMS

Parametric and structural optimization methodologies presented above have been realized in software OptCAD ([www.optcad.com](http://www.optcad.com)). The OptCAD destination is computer-aided optimal design of steel structural systems. This software ensures the solving of the wide range problems, namely: (i) linear static system analysis; (ii) verification of the structural members and entire structure in conformity with building regulations and standard requirements; (iii) searching the values of unknown structural parameters, which ensure that the designed steel structure will comply with building requirements and described designer's criterions; (iv) parametric and structural optimization of steel structural systems by the determined purpose function.

Program interface allows performing problem formulation for optimum design of steel structural systems. Specialized OptCAD's windows ensure entering initial data used traditionally by CAD-system based on FE method analysis. The software OptCAD provides series of new features, which increase swiftness and quality of the optimal design process. With orientation on deciding of wide range problems for steel structural systems of different types OptCAD allows to take into account specific designing conditions which mirror structural particularities and designer's experience; to optimize structural parameters considering any criterion function with determined analytical expression; and to define optimal values for every variable structural parameters indicated by the designer as unknown.

Implementation of these features is derived from the development of *input language* for the design problem statement and using this language in software interface. The OptCAD ensures an input of analytical expressions according to syntax and semantics of the elaborated input language at the any components of the program interface where expected the entering of real number of data for structural analysis. Syntax of entry language includes: (i) names of standard set of arithmetical function; (ii) names of operators and programming functions; (iii) names of design variables; names of specific expressions described by user; (iv) names of special functions which return values of structural parameters.

The process of problem statement formulation is divided into stages according to sequence of input data using in analysis and optimization algorithms. After calculating of structure at each stage it is defined a series of enabled state variables, which may be used as input data for the next stages. Since the values of design variables are change on the each step of the iterative searching process, so recalculation of input expression using current values of

design variables and state variables is executed at the each modification of the design decision.

Using the names of the design variables and special functions as an input data in OptCAD's interface we ensure the access to the current values of structural state variables during design problem formulation. Software OptCAD is presented in details on the web-site: [www.optcad.com](http://www.optcad.com).

## 6. NUMERICAL EXAMPLES

Let consider the parametric optimization task for transverse two-hinged steel frames of steel warehouse framework. Building object is located in seaport Ust-Luga of Russian Federation and designed as repository for granulated sulfur with further shipment in merchant ship. The general building sizes are length 247,25 m and width 69,0 m. Steel framework of the building consists of transverse frames with span 69,0 m positioned along building length with bay 7,5 m. Transverse two-hinged steel frames consist of lattice structural members (columns and rafters) fabricated from tubes with steel grade St20 according to СНиП II-23-81\* [14]. There is a service platform at the level +28,25 m provided for supporting the crane-loader and conveyor (Fig. 1). The bearing constructions of this platform are suspended to the structural members of the transverse frames.

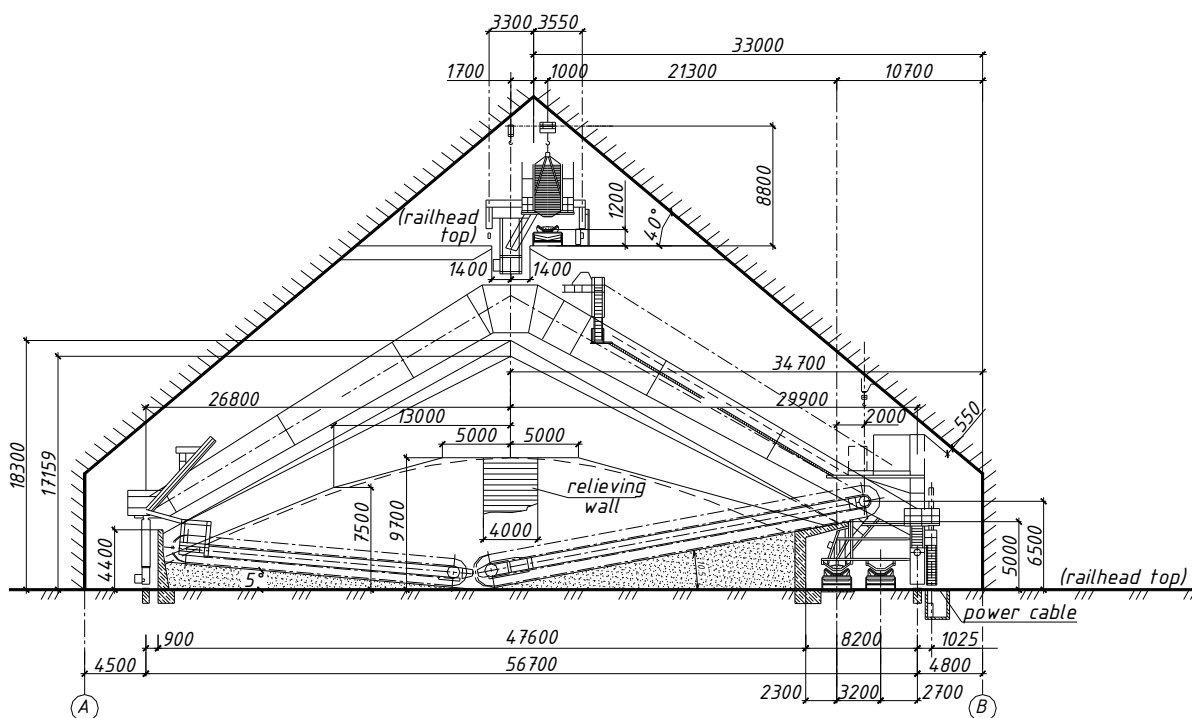


Fig. 1. Technological equipments and constraints that describe useful space in building

Parameters of the geometric scheme of the transverse frames and cross-sectional sizes of the structural members were considered as design variables. Variable parameters of the geometrical scheme were building height at the eave node  $H_{zdk}$  and at the ridge  $H_{zd}$ , distance between upper and lower chords of the lattice rafter at the eave node  $h_{op}$  and at the erection joints  $h_2$ ,  $h_4$ ,  $h_6$  i  $h_7$ , distance between chords of the lattice column at the eave  $b_{op}$  and parameter  $b_7$  (see Fig. 2). Start values of the design variables were accepted according to design decision of the steel framework developed by Open Join-Stock Company "V. Shymanovsky Ukrainian Research and Design Institute of Steel Construction", namely:

$$H_{zd} = 39,58 \text{ m}, H_{zdk} = 10,63 \text{ m}, h_2 = h_4 = h_6 = h_7 = h_{op} = b_{op} = 2,6 \text{ m}, b_7 = 0,55773 \text{ m}.$$

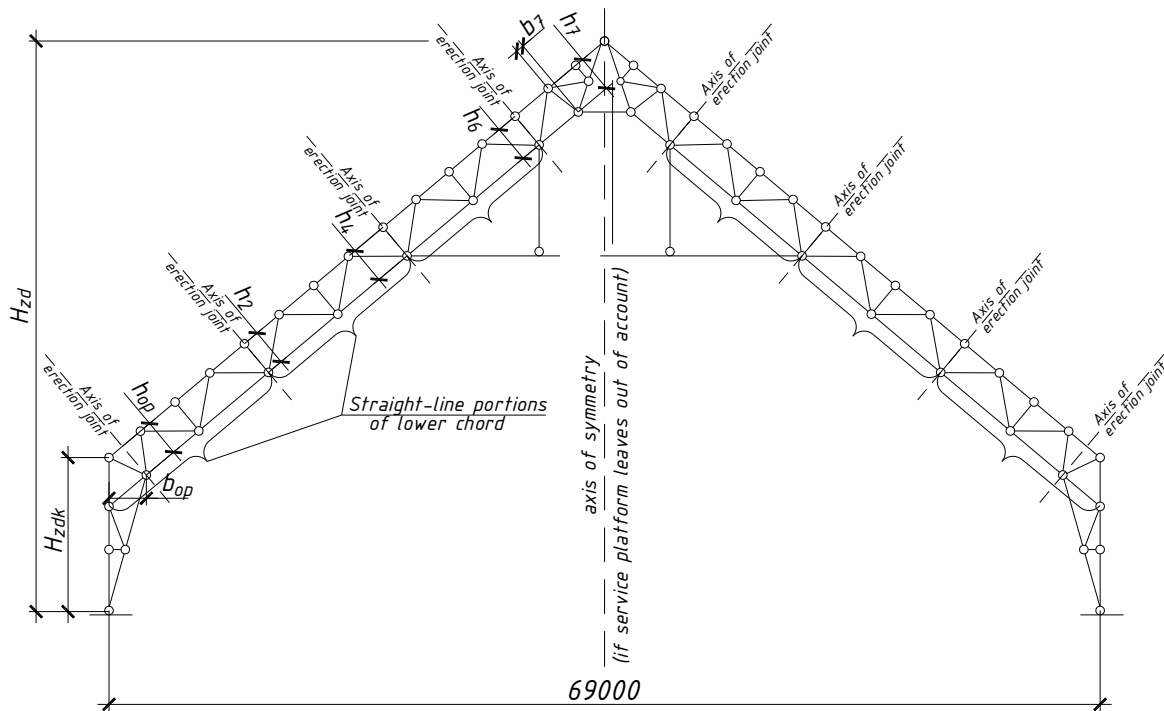


Fig. 2. The design scheme of the two-hinged transverse frame with specification of geometrical design variables

Geometrical scheme of the transverse frame was described using the set of nodes and bars with orientation on implementation of finite element method for linear static analysis. Node coordinates of the design scheme were determined in Cartesian coordinate system and presented as expressions in dependence of geometrical design variables.

During optimization process it was considered dead loads, live loads, tree types of snow loads and two types of wind load combined in 16 design load case combinations according to requirements of ДБН В.1.2-2:2006 [4]. All loads and effects on structure were presented as concentrated loads at the nodes and were determined analytically depending on variable parameters of the geometrical scheme.

Verifications of bearing capacity of structural members at the ultimate limit state as well as displacement checks at the serviceability limit state were included into the constraint system of mathematical model. So, it was considered stresses checks, overall and local buckling checks for structural members subject to central tension and compression.

The minimum weight of the transverse frame as well as the minimum cost on fabrication and erection were considered as the criterion of optimality. Task dimensions are: account of design variables is 50, account of problem constraints is 14000.

Optimization results received using software OptCAD are presented at the Table 1. Fig. 3 and Fig. 4 show optimal design decisions by the criterion of minimum structural weight as well as costs on fabrication and erection (project with start values of design variables indicates by red color, optimum project indicates by blue color).



Table 1. Optimal values of geometrical design variables

Design variable	Start value, m	Optimum values, m, by the criterion of minimum			
		weight		costs on fabrication and erection	
		when lower chord of lattice rafter is			
		straight-line	polygonal	straight-line	polygonal
$H_{zd}$	39,58	38,82	39,55	38,74	39,44
$H_{zdk}$	10,63	11,92	11,84	12,08	12,03
$h_2$	2,60	–	3,23	–	3,31
$h_4$	2,60	–	3,21	–	3,23
$h_6$	2,60	–	2,68	–	2,70
$h_7$	2,60	2,18	2,68	2,13	2,61
$b_7$	0,55773	1,00	0,56	1,05	0,63
$h_{op}$	2,60	3,61	3,72	3,73	3,87
$b_{op}$	2,60	3,08	3,02	3,02	2,95
<b>Weight, t</b>	<b>30,78</b>	<b>18,98</b>	<b>18,45</b>		
<b>Costs, UAH</b>	<b>786681</b>			<b>534647</b>	<b>524257</b>

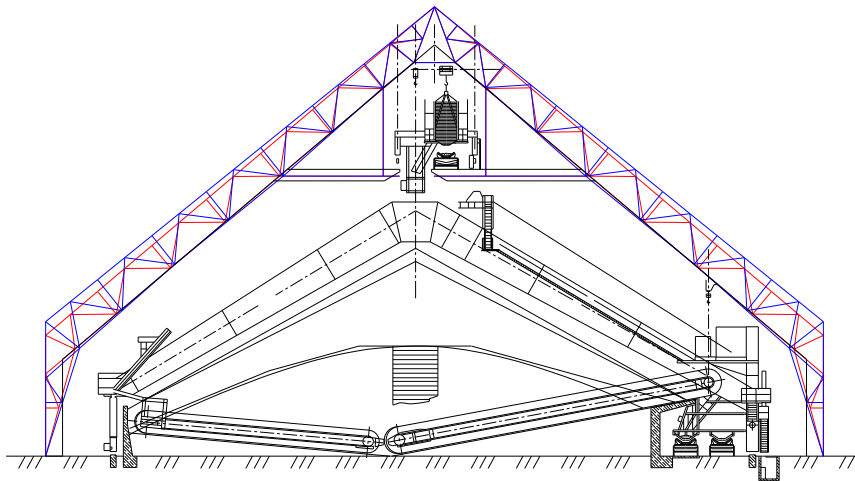


Fig. 3. The optimum design decision by the criterion of minimum structural weight when lower chord of rafter is straight-line

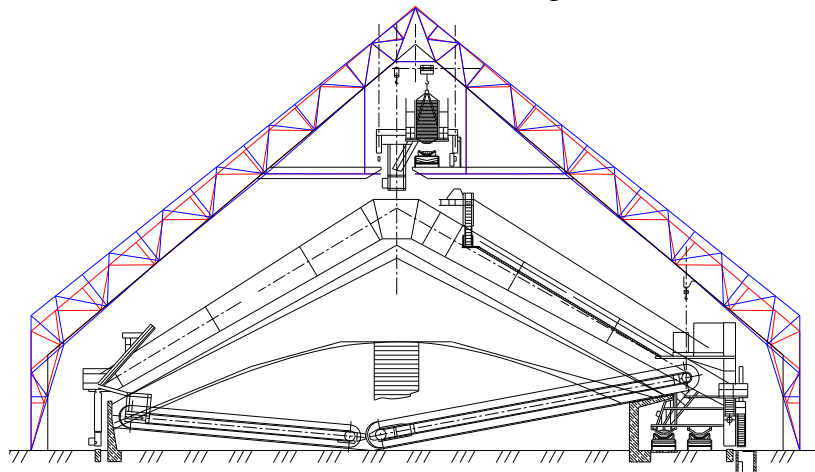


Fig. 4. The optimum design decision by the criterion of minimum cost on building and erection when lower chord of rafter is straight-line

## CONCLUSION

In this paper it was presented a computer-aided technique for design and optimization of steel structural systems. The body of mathematics combines finite element method for linear static structural analysis and hybrid genetic algorithm with gradient learning of the best individual for solving the structural-parametric optimization task.

The optimum design problem is formulated as the structural-parametric mathematical programming task with Boolean, integer and real design variables. In this way, cross-sectional sizes of structural members, node coordinates as well as topology parameters can be considered as design variables. The system of constraints includes load-carrying capacity and stiffness conditions for structural members and entire system according to building requirements and regulations. Parametric and structural optimization methodologies have been realized with elaborated software devoted to computer-aided optimal design of steel structural systems.

The parametric optimization task for plane transverse two-hinged steel frame with lattice structural members have been considered and solved. Parameters of the geometric scheme of the transverse frames and cross-sectional sizes of the structural members were considered as design variables. New optimal layouts of steel transverse frame by the criterion of minimum weight as well as minimum costs on fabrication and erection were presented.

## REFERENCES

- [1] Bendsøe M. P., Optimization of structural topology, shape and materials, Berlin, Springer-Verlag, 1995.
- [2] Czarniecki S., Multithreaded genetic program in truss shape optimization, Theoretical Foundations of Civil Engineering, VIII, 556-560, 2000.
- [3] Davis L., Smith D., Adaptive design for layout synthesis, Dallas, Texas Instruments, 1985.
- [4] ДБН В.1.2-2:2006. Loads and effects. Design requirements. – Kiev, MINBUD, 2006. (in Ukrainian)
- [5] Gen M., Cheng R., Genetic algorithms and engineering design, John Wiley & Sons, 1997.
- [6] Goldberg D. E., Genetic algorithms in search, optimization and machine learning, Reading, MA, Addison-Wesley, 1989.
- [7] Jenkins W. M., Towards structural optimization via the genetic algorithm, Computers and Structures, 40 (5), 1321-1327, 1991.
- [8] Haug A., Arora J., Applied Optimal Design: Mechanical Systems and Structures, Moscow, Mir, 1983 (in Russian).
- [9] Holland J. H., Adaptation in natural and artificial systems, Ann Arbor, University of Michigan Press, 1975.
- [10] Kirsch U., Optimum Structural Design, New York, McGraw-Hill, 1981.
- [11] Permyakov V. O., Yurchenko V. V., Peleshko I. D., An Optimum Structural Computer-Aided Design Using Hybrid Genetic Algorithm, Proceeding of the International Conference “Progress in Steel, Composite and Aluminium Structures”, Gizejowski, Kozłowski, Slecza & Ziolk (eds.), Taylor & Francis Group, London, 819-826, 2006.
- [12] Permyakov V. A., Perelmuter A. V., Yurchenko V. V. Optimal designing of steel structural systems. Kiev, Publisher “Steel”, 2008. (in Russian)
- [13] Peleshko I., Yurchenko V., An optimum structural computer-aided design using update gradient method, Modern Building Materials, Structures and Techniques: Proc. 8<sup>th</sup> Int. Conf., Vilnius, 2004.
- [14] СНиП II-23-81\*. Steel structures. – M.: 1996. – 96 p. (in Russian)

Zdzisław PISAREK<sup>1</sup>

## RESISTANCE AND STIFFNESS OF THE BEAM TO COLUMN JOINTS WITH ANGLE FLANGE CLEATS

### ABSTRACT

The method of calculation of the moment resistance and initial stiffness for bolted angle flange cleats connections has been presented. Calculation of this characteristic without computer use is rather troublesome. Simple formulae for calculation of the moment resistance and initial stiffness was developed and presented in this paper.

**KEYWORDS:** steel structures, semi-rigid joints, strength, stiffness, simplified formula.

### 1. INTRODUCTION

At the beginning of XX century one paid attention on inadequate to the reality the reflection of the behaviour of steel structures resulting from the usage of too simplified models of nodes (stiff and hinge). The lack of suitable tools and developed methods of analysis did not permit on the practical application of more advanced characteristics of joints. Designers, being based mainly on the intuition, constructed hinges, to provide the possibly good conformity with the static schema of the structure. Joints connected beam to column, assumed as stiff, was designed as welded with the use of strong stiffeners. To provide the freedom of the rotations in nodes for beams assumed as simply supported, joints were designed as so called “technical hinge”.

This situation was gradually changed with the development of production technology of the steel structures, with usage of the modern connectors, materials and uses in factories of modern lines to the automatic, digitally controlled processing, in the cut and hole drilling. This exerted the simplification of the elements and nodes solutions. For elements this concerned the more frequent usage of hot rolled sections, and also utilizations of the composite steel concrete constructions.

In joints was bounded for avoidance of solutions with stiffening, because it's required a manual welding of the stiffeners. Where it is possible, was bounded for the elimination of the whole welding, as the expensive process and unfavourably influencing on the structural steel.

In United States was widely used joints with use of the angle cleats connected beam flange to the column (Fig. 1a) or beam web to the column (Fig. 1b) more seldom the combination of these of two kinds of connections (Fig. 1c).

<sup>1</sup> Assistant Prof. PhD. Eng., Rzeszow University of Technology, Rzeszow, POLAND,

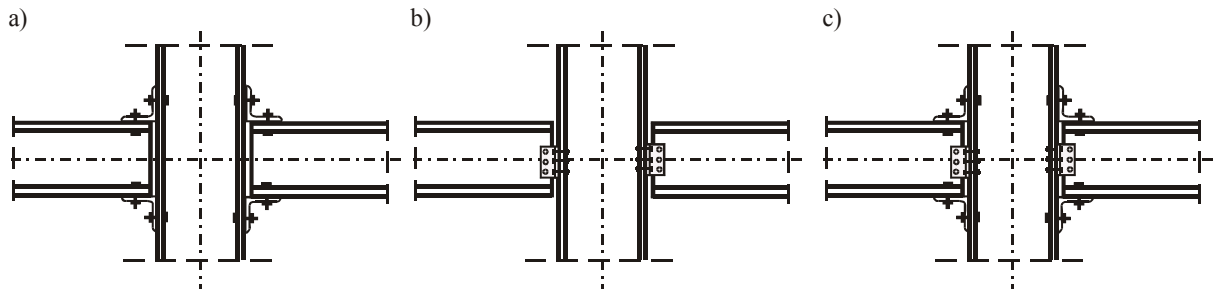


Fig. 1 Joints with the use of angle cleats.

Investigations of these types of the joints were presented in [1], [2], [3]. Totally to experimental research was subjected above 300 joints with the use of angle cleats connected beam web, and above 100 connections jointed beam flange to the column. Connections of these types are considered as typical flexible joints, achieved the strength capacity about 50% resistance of the attached beam. The growth of the stiffness of the connection is achieved by the enlargement of thickness of the angle flanges.

Joints with the use angle cleats connected beam flanges to the column became enough popular that the procedure of their calculation had been found in the standard [4].

## 2. MOMENT RESISTANCE AND STIFFNESS OF THE JOINT

In the analysis of the structure, the Standard [4] demands to take into account the influence of the resistance and the stiffness of joints. The analytical model for calculation characteristics of the joints, introduced in [4], is based on the component method. In this method, the whole connection is composed of basic components. Moment resistance of the joints is based on the lowest resistance of the joint components, and stiffness is depending on their deformations.

The moment resistance of the joint can be calculated as:

$$M_{j,Rd} = z \cdot F_{Rd} \quad (1)$$

where:  $z$  – lever arm, assumed as the distance from the centerline of the compression to the centerline of the bolt row in tension, and

$F_{Rd}$  – the lowest resistance of the joint components.

In beam to column connection with use angle flange cleats, the moment resistance depend on following components (see fig. 2):

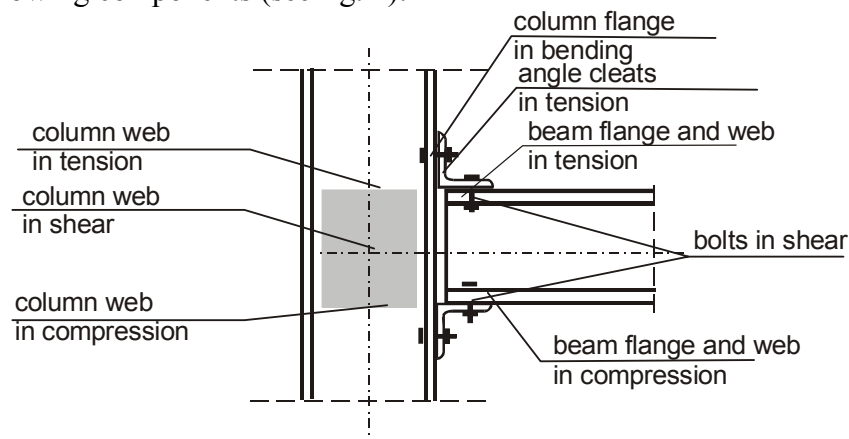


Fig. 2. Basic components in beam to column connection with angle flange cleats  
The stiffness of the joint with user angle flange cleats can be predicted from [4], as:

$$S_j = \frac{E \cdot z^2}{\mu \cdot \sum_i \frac{1}{k_i}} \quad (2)$$

where:  $E$  - the elastic modulus;  $z$  - the level arm;  $\mu$  - the stiffness ratio and  $k_i$  - the stiffness coefficient for basic joint component  $i$ .

In case of the beam to column connections with angle flange cleats, the following components should be taken into account:

- column web in shear  $k_1$ ,
- column web in compression  $k_2$ ,
- column web in tension  $k_3$ ,
- column flange in bending  $k_4$ ,
- angle cleat in tension  $k_6$ ,
- bolts in tension  $k_{10}$ ,
- bolts in shear  $k_{11}$ ,
- bolts in bearing  $k_{12}$ ,

### 3. WORKED EXAMPLE

For the performance of the procedure, a worked example was presented. This example illustrated beam to column joint with use of angle cleats (Fig. 3).

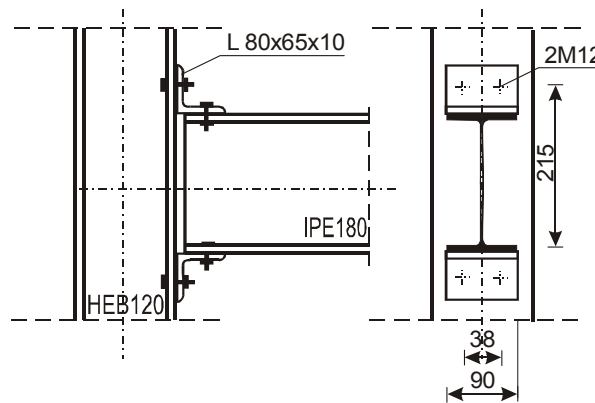


Fig. 3. Joint dimension for calculation example.

Basic data:

Steel grade S 275:  $f_y = 275 \text{ N/mm}^2$ ,  $f_u = 430 \text{ N/mm}^2$ ,  $\varepsilon = 0,92$

Beam IPE 180:  $W_{y,pl} = 166 \cdot 10^3 \text{ mm}^3$ ,  $A = 23,9 \cdot 10^2 \text{ mm}^2$ ,

$h_b = 180 \text{ mm}$ ,  $b_b = 91 \text{ mm}$ ,

$t_{fb} = 19,0 \text{ mm}$ ,  $t_{wb} = 12,0 \text{ mm}$ ,  $r_b = 24 \text{ mm}$ .

Column HEB 120:  $W_{y,pl} = 165 \cdot 10^3 \text{ mm}^3$ ,  $A = 34 \cdot 10^2 \text{ mm}^2$ ,

$h_c = 120 \text{ mm}$ ,  $b_c = 120 \text{ mm}$ ,

$t_{fc} = 11,0 \text{ mm}$ ,  $t_{wc} = 6,5 \text{ mm}$ ,  $r_c = 12 \text{ mm}$ .

Angle cleats L80x65x10:  $h_a = 65 \text{ mm}$ ,  $b_a = 80 \text{ mm}$ ,  $t_a = 10 \text{ mm}$ ,  $r_a = 8 \text{ mm}$ .

Bolts M12 class 5.8:  $A_b = 113 \cdot 10^2 \text{ mm}^2$ ,  $A_s = 84,3 \text{ mm}^2$

Beam and column sections are class 1.

- Column web panel in shear.

For single-sided joint, the design plastic shear resistance of unstiffened column web is obtained from:

$$V_{wp,Rd} = \frac{0,9 \cdot f_{y,wc} \cdot A_{vc}}{\sqrt{3} \cdot \gamma_{M0}} = \frac{0,9 \cdot 275 \cdot 1096}{\sqrt{3} \cdot 1,0} = 156612 \text{ N}$$

where:

$$A_{vc} = A - 2 \cdot b \cdot t_{fc} + (t_{wc} + 2 \cdot r_c) \cdot t_{fc} = 34 \cdot 10^2 - 2 \cdot 120 \cdot 11 + (6,5 + 2 \cdot 12) \cdot 11 = 1096 \text{ mm}^2$$

- Column web panel in compression.

$$F_{c,wc,Rd} = \frac{\omega \cdot k_{wc} \cdot b_{\text{eff},c,wc} \cdot t_{wc} \cdot f_{ywc}}{\gamma_{M0}}, \text{ and } F_{c,wc,Rd} \leq \frac{\omega \cdot k_{wc} \cdot \rho \cdot b_{\text{eff},c,wc} \cdot t_{wc} \cdot f_{ywc}}{\gamma_{M0}}$$

Effective width of column web in compression for bolted joints with angle flange cleats:

$$b_{\text{eff},c,wc} = 2 \cdot t_a + 6 \cdot r_a + 5 \cdot (t_{fc} + s) = 2 \cdot 10 + 6 \cdot 8 + 5 \cdot (11 + 12) = 183 \text{ mm}$$

Transformation parameter, for single-sided joint is equal  $\beta = 1,0$ , and reduction factor for  $\beta = 1$  is  $\omega = \omega_1$

$$\omega_1 = \frac{1}{\sqrt{1 + 1,3 \left( \frac{b_{\text{eff},c,wc} \cdot t_{wc}}{A_{vc}} \right)^2}} = \frac{1}{\sqrt{1 + 1,3 \left( \frac{183 \cdot 6,5}{1096} \right)^2}} = 0,628$$

If the maximum longitudinal compressive stress in column  $\sigma_{\text{com,Ed}}$  not exceed  $0,7 \cdot f_{ywc}$ , then reduction factor  $k_{wc}$  can be adopted as 1, then:

$$F_{c,wc,Rd} = \frac{0,628 \cdot 1,0 \cdot 183 \cdot 6,5 \cdot 275}{1,0} = 205427 \text{ N}.$$

The reduction factor for web panel buckling  $\rho$ , is depending on the web slenderness:

$$\bar{\lambda}_p = 0,932 \sqrt{\frac{b_{\text{eff},c,wc} \cdot d_{wc} \cdot f_{ywc}}{E \cdot t_{wc}^2}} = 0,932 \sqrt{\frac{183 \cdot 74 \cdot 275}{210 \cdot 10^3 \cdot 6,5^2}} = 0,604$$

where:

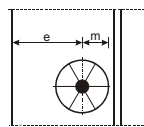
$$d_{wc} = h_c - 2 \cdot (t_{fc} + r_c) = 120 - 2 \cdot (11 + 12) = 74 \text{ mm}$$

if  $\bar{\lambda}_p \leq 0,72$  then  $\rho = 1$ , and finally:  $F_{c,wc,Rd} = 205427 \text{ N}$

- Column web panel in tension.

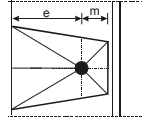
$$F_{t,wc,Rd} = \frac{\omega \cdot b_{\text{eff},t,wc} \cdot t_{wc} \cdot f_{ywc}}{\gamma_{M0}},$$

Where effective width of column web is taken as equal to the effective length of equivalent T-stub from:



- Circular patterns:

$$l_{\text{eff,cp}} = 2 \cdot \pi \cdot m = 2 \cdot \pi \cdot 6,2 = 39,0 \text{ mm}$$



- Non – circular patterns:  $l_{eff.nc} = 4 \cdot m + 1,25 \cdot e = 4 \cdot 6,2 + 1,25 \cdot 31 = 63,6 \text{ mm}$ ,

where  $m = (w - t_{wc} - 2 \cdot 0,8 \cdot r_c) / 2 = (38 - 6,5 - 2 \cdot 0,8 \cdot 12) / 2 = 6,2 \text{ mm}$ , and  $e = 41 \text{ mm}$

$$F_{t,wc,Rd} = \frac{0,628 \cdot 39 \cdot 6,5 \cdot 275}{1,0} = 43779 \text{ N}$$

• Beam flange and web in compression.

$$F_{c,fb,Rd} = \frac{M_{b,Rd}}{h_b - t_{tb}} = \frac{45,6 \cdot 10^6}{180 - 19,0} = 283230 \text{ N}$$

$$\text{with } M_{c,Rd} = M_{pl,Rd} = \frac{W_{pl} \cdot f_y}{\gamma_{M0}} = \frac{166 \cdot 10^3 \cdot 275}{1,0} = 45,6 \cdot 10^6 \text{ Nmm}$$

• Column flange in bending.

The resistance of the column flange in bending is taken as minimum values from three modes of failure.

$$\text{Bolt resistance } F_{t,Rd} = \frac{0,9 \cdot f_{ub} \cdot A_s}{\gamma_{M2}} = \frac{0,9 \cdot 500 \cdot 84,3}{1,25} = 30348 \text{ N}, \text{ and}$$

$$B_{p,Rd} = 0,6 \cdot \pi \cdot d_m \cdot t_p \cdot f_u / \gamma_{M2} = 0,6 \cdot \pi \cdot 18 \cdot 10 \cdot \frac{390}{1,25} = 138,431 \text{ N}$$

$$M_{pl.1,Rd} = 0,25 \cdot l_{eff.cp} \cdot t_{fc}^2 \cdot \frac{f_y}{\gamma_{M0}} = 0,25 \cdot 39,0 \cdot 11,0^2 \cdot \frac{275}{1,0} = 324431 \text{ Nmm}$$

$$M_{pl.2,Rd} = 0,25 \cdot l_{eff.nc} \cdot t_{fc}^2 \cdot \frac{f_y}{\gamma_{M0}} = 0,25 \cdot 63,6 \cdot 11,0^2 \cdot \frac{275}{1,0} = 529072 \text{ Nmm}$$

$$F_{T,fc,Rd} = \min \left\{ \begin{array}{l} \frac{4 \cdot M_{pl.1,Rd}}{m} = \frac{4 \cdot 324431}{6,2} = 209310 \\ \frac{2 \cdot M_{pl.2,Rd} + n \cdot \sum F_{t,Rd}}{m + n} = \frac{2 \cdot 529072 + 7,8 \cdot 2 \cdot 30348}{6,2 + 7,8} = 90092 = 60696 \text{ N} \\ \sum F_{t,Rd} = 2 \cdot 30348 = 60696 \end{array} \right.$$

• Angle cleats in tension.

The effective length of the angle flange cleats is taken as half of width of the cleats, then  $l_{eff} = 45 \text{ mm}$ , values  $m$  for large gap  $m = w_1 - 0,5 \cdot t_a = 35 - 0,5 \cdot 10 = 30 \text{ mm}$ , and  $e = 30 \text{ mm}$

$$M_{pl.a,Rd} = 0,25 \cdot l_{eff.cp} \cdot t_{fc}^2 \cdot \frac{f_y}{\gamma_{M0}} = 0,25 \cdot 45,0 \cdot 10,0^2 \cdot \frac{275}{1,0} = 309375 \text{ Nmm}$$

$$F_{T,a,Rd} = \min \left\{ \begin{array}{l} \frac{4 \cdot M_{pl.a,Rd}}{m} = \frac{4 \cdot 309375}{30} = 41250 \\ \frac{2 \cdot M_{pl.a,Rd} + n \cdot \sum F_{t,Rd}}{m + n} = \frac{2 \cdot 309375 + 30 \cdot 2 \cdot 30348}{30 + 30} = 40660 = 40660 \text{ N} \\ \sum F_{t,Rd} = 2 \cdot 30348 = 60696 \end{array} \right.$$

• Bolts in shear.

$$F_{v,Rd} = 2 \frac{\alpha_v f_{ub} A}{\gamma_{M2}} = 2 \frac{0,6 \cdot 500 \cdot 113}{1,25} = 54240N$$

- Bolts in bearing.

$$F_{b,Rd,1} = 2 \cdot \frac{k_1 \alpha_b f_u d t_1}{\gamma_{M2}} = 2 \cdot \frac{2,5 \cdot 0,895 \cdot 390 \cdot 12 \cdot 10}{1,25} = 167544N$$

$$\text{where } k_1 = \min \left\{ \begin{array}{l} 2,8 \frac{e_2}{d_0} - 1,7 = 2,8 \frac{26}{13} - 1,7 = 3,9 \\ 2,5 \end{array} \right. = 2,5$$

$$\alpha_b = \min \left\{ \begin{array}{l} \alpha_d = \frac{e_1}{3d_0} = \frac{35}{3 \cdot 13} = 0,895 \\ \frac{f_{ub}}{f_u} = \frac{500}{390} = 1,282 \\ 1,0 \end{array} \right. = 0,895$$

Finally, strength of components is a minimum value from above, then  $F_{T,Rd} = F_{T,a,Rd} = 40660N$ , and moment resistance of the joint:

$$M_{j,Rd} = z \cdot F_{Rd} = 215 \cdot 40660 = 8,74 \cdot 10^6 Nmm = 8,74kNm$$

Stiffness of the joint

- Column web panel in shear.

$$k_1 = \frac{0,38 \cdot A_{vc}}{\beta \cdot z} = \frac{0,38 \cdot 1096}{1 \cdot 215} = 1,937mm$$

- Column web panel in compression.

$$k_2 = \frac{0,7 \cdot b_{eff,c,wc} \cdot t_{wc}}{d_{wc}} = \frac{0,7 \cdot 183 \cdot 6,5}{74} = 11,252mm$$

- Column web panel in compression.

$$k_3 = \frac{0,7 \cdot b_{eff,t,wc} \cdot t_{wc}}{d_{wc}} = \frac{0,7 \cdot 39 \cdot 6,5}{74} = 2,398mm$$

- Column flange in bending.

$$k_4 = \frac{0,9 \cdot l_{eff} \cdot t_{fc}^3}{m^3} = \frac{0,9 \cdot 39 \cdot 11^3}{6,2^3} = 196mm$$

- Angle cleats in tension.

$$k_6 = \frac{0,9 \cdot l_{eff} \cdot t_a^3}{m^3} = \frac{0,9 \cdot 45 \cdot 10^3}{30^3} = 1,500mm$$

- Bolts in tension.



$$k_{10} = \frac{1,6 \cdot A_s}{L_b} = \frac{1,6 \cdot 84,3}{33} = 4,087 \text{ mm}$$

- Bolts in shear.

$$k_{11} = \frac{16 \cdot n_b \cdot d^2 \cdot f_{ub}}{E \cdot d_{M16}} = \frac{16 \cdot 1 \cdot 12^2 \cdot 500}{210 \cdot 10^3 \cdot 16} = 0,343 \text{ mm}$$

- Bolts in bearing.

$$k_{12} = \frac{24 \cdot n_b \cdot k_b \cdot k_t \cdot d \cdot f_u}{E} = \frac{24 \cdot 1 \cdot 1,23 \cdot 0,94 \cdot 12 \cdot 390}{210 \cdot 10^3} = 0,618 \text{ mm}$$

Finally stiffness of the joint is equal:

$$S_j = \frac{E \cdot z^2}{\mu \cdot \sum_i \frac{1}{k_i}} = \frac{210 \cdot 10^3 \cdot 215^2}{3,1 \cdot \left( \frac{1}{1,937} + \frac{1}{11,252} + \frac{1}{2,398} + \frac{1}{196} + \frac{1}{1,500} + \frac{1}{4,087} + \frac{2}{0,393} + \frac{4}{0,618} \right)} = 211 \text{ kNm/rad}$$

#### 4. PROPOSED ESTIMATION OF THE RESISTANCE AND STIFFNESS OF THE JOINT

As can be see in the example, the procedure of the calculation of characteristics of the connection is complicated. Developed design procedure shown that the moment resistance and initial stiffness are depended on several different parameters of both dependent as and independent in relation to himself. The influence of some of these parameters on the resistance and the stiffness of the connection are introduced on graphs (Fig. 4 – 13).

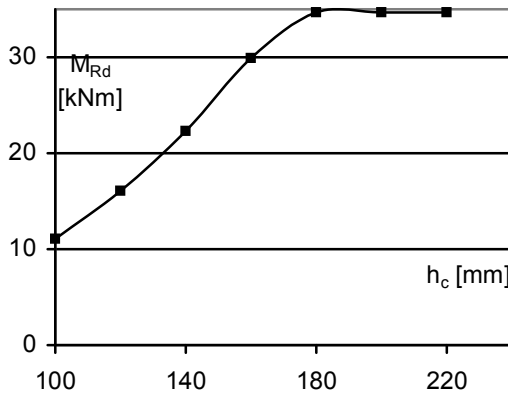


Fig.4. Influence of the column depth  $h_c$  on moment resistance of the joint.

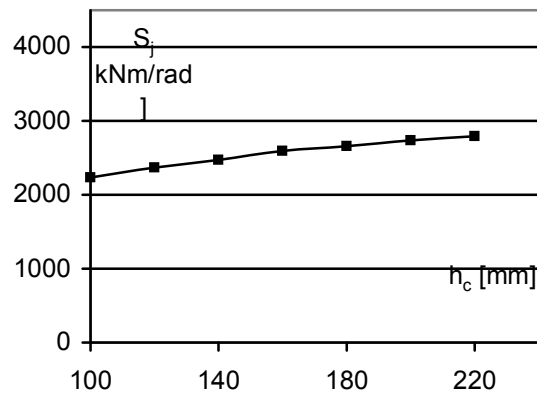


Fig.5. Influence of the column depth  $h_c$  on initial stiffness of the joint.

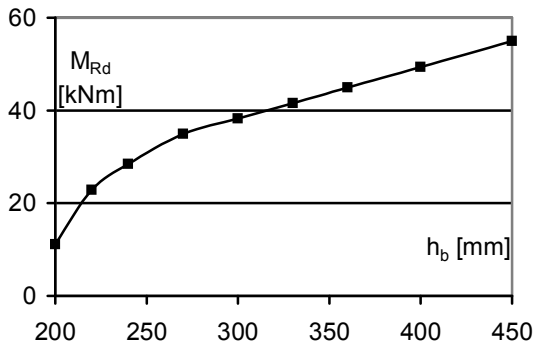


Fig.6. Influence of the beam height  $h_b$  on moment resistance of the joint.

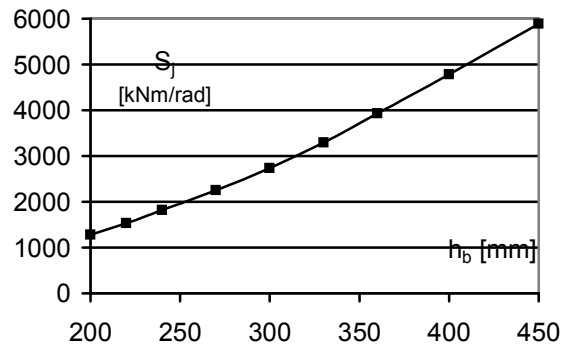


Fig.7. Influence of the beam height  $h_b$  on initial stiffness of the joint.

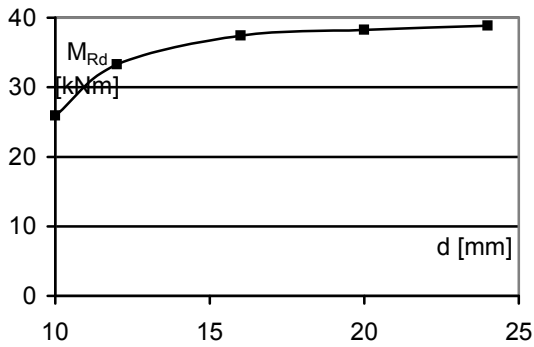


Fig.8. Influence of the bolt diameter  $d$  on moment resistance of the joint.

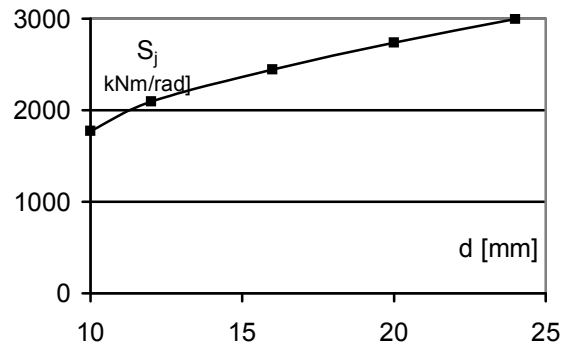


Fig.9. Influence of the bolt diameter  $d$  on initial stiffness of the joint.

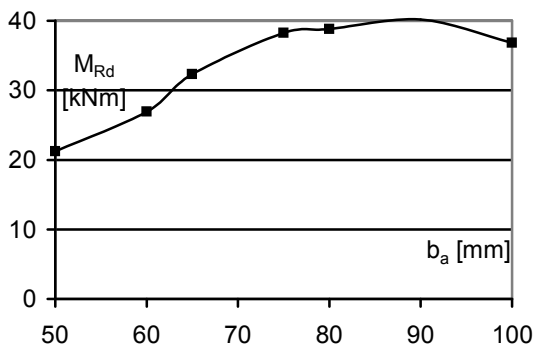


Fig.10. Influence of the angle flange width  $b_a$  on moment resistance of the joint.

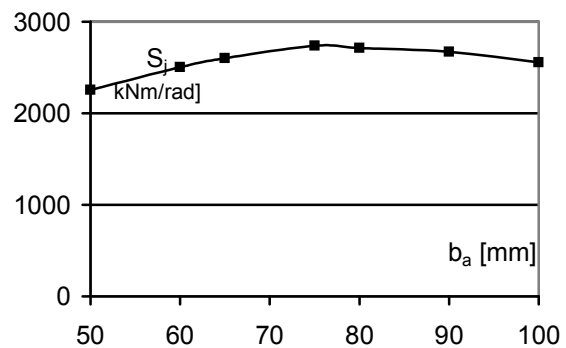


Fig.11. Influence of the angle flange width  $b_a$  on initial stiffness of the joint.

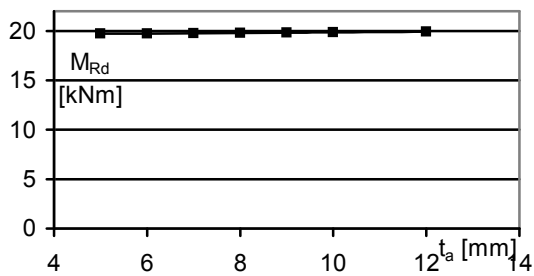


Fig.12. Influence of the angle flange thickness  $t_a$  on moment resistance of the joint.

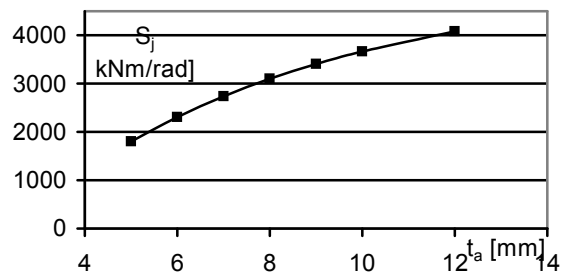


Fig.13. Influence of the angle flange thickness  $t_a$  on initial stiffness of the joint.

After analysing of several hundred different configurations of beam to column joints with use of angle flange cleats was ascertained that on the resistance and the stiffness the greatest influence had: the height of the beam  $h_b$ , the depth of the column  $h_c$ , the length of flange of the angle cleats, the diameter of the bolts  $d$ , and geometric dimensions which usually are variable dependent from the elements of the connection.

Constant values of the following parameters were established:

- steel grade for all elements S235,
- bolts grade 10.9,
- column with HEB - section,
- beam with IPE - section,
- angle flange cleats length is equal to width of column flange, and their thickness is means thickness of accepted angle section,
- the spacing of the bolts is depended on connected elements according to constructional recommendations ,
- gap  $g$  is equal 5 mm.

As variable parameters, the following joint properties were analyzed:

- beam height  $x_1 = h_b$  in range (200; 450) [mm],
- column depth  $x_2 = h_c$  in range (100; 300) [mm],
- length of flange of the angle cleats  $x_3 = b_a$  in range ( 60; 200) [mm], and
- bolt diameter  $x_4 = d$  in range ( 10; 24) [mm].

To finding of the approximation function of was applied the theory of the planning of the experiment [5], and the computer simulation. For determine of characteristics of the joints, was adopted a plan the experiment of Hartley PS/DS-P:Ha<sub>4</sub> based at the range of variation on the hypercube, with the arrangement showing in table 1.

Table 1. Planning of experiment for determination of the resistance and stiffness of the joint.

	$\hat{x}$				X				Unstiffened joint		Joint with stiffeners	
	$\hat{x}_1$	$\hat{x}_2$	$\hat{x}_3$	$\hat{x}_4$	$x_1$ : $h_b$	$x_2$ : $h_c$	$x_3$ : $b_a$	$x_4$ : $d$	$M_R$ [kN·m]	$S_{j.ini}$ [kN·m/mra d]	$M_R$ [kN·m]	$S_{j.ini}$ [kN·m/mrad]
1	+1	-1	-1	-1	450	100	60	10	17,92	2721	17,92	2930
2	-1	+1	-1	-1	200	300	60	10	9,95	652	9,95	719
3	-1	-1	+1	-1	200	100	200	10	8,72	1369	8,72	1476
4	+1	+1	+1	-1	450	300	200	10	39,21	6227	39,21	6573
5	+1	-1	-1	+1	450	100	60	24	6,13	4179	6,13	4696
6	-1	+1	-1	+1	200	300	60	24	5,09	1067	5,09	1259
7	-1	-1	+1	+1	200	100	200	24	8,72	3075	8,72	3679
8	+1	+1	+1	+1	450	300	200	24	181,79	15332	181,79	17610
9	-1	0	0	0	200	200	130	16	26,05	1947	26,05	2124
10	+1	0	0	0	450	200	130	16	60,81	8605	60,81	9588
11	0	-1	0	0	330	100	130	16	10,31	4164	10,31	4863
12	0	+1	0	0	330	300	130	16	73,29	5108	73,29	5490
13	0	0	-1	0	330	200	60	16	24,53	2290	24,53	2394
14	0	0	+1	0	330	200	200	16	58,10	5874	58,10	6487
15	0	0	0	-1	330	200	130	10	28,22	3005	28,22	3169
16	0	0	0	+1	330	200	130	24	36,59	6454	36,59	7262
17	0	0	0	0	330	200	130	16	46,39	4845	46,39	5287

After the achievement of calculations was observed that in the investigated range of joints, the stiffening of the column by stiffeners have not influence on the resistance of the joint, and only enlarges his stiffness. In case of two-sided joints, their resistance is such alone as the moment resistance of the cantilever joints. The stiffness of two-sided stiffened connections is such alone as stiffened cantilever joints. In case of two-sided not stiffened joints the stiffness is comparable with the arithmetic mean of the stiffness of cantilever stiffened and unstiffened.

After analyzing with the overlay SOLVER of several variants of the approximation function, the function giving the least square error was chose. The resistance of the bolted beam to column joint with the use of angle flange cleats can be obtain from:

$$M_{Rd} = 8,2572 \cdot 10^{-6} \cdot h_b^{1,172} \cdot h_c^{0,7736} \cdot b_a^{0,8754} \cdot d^{-0,1609} \quad (3)$$

The stiffness of the unstiffened connection can be obtained from:

$$S_{j,ini} = 0,001429 \cdot h_b^{1,5576} \cdot h_c^{0,1531} \cdot b_a^{0,7038} \cdot d^{0,6306} - 447 \quad (4)$$

However the stiffness of the stiffened connection can be obtain from equation:

$$S_{j,ini} = 0,000755 \cdot h_b^{1,6014} \cdot h_c^{0,1329} \cdot b_a^{0,7474} \cdot d^{0,7534} - 332 \quad (5)$$

where:  $M_{Rd}$  - in kNm,  $S_{j,ini}$  - in kNm/rad, and  $h_b, h_c, b_a, d$  - in mm.

## 5. SUMMARY

The knowledge of the moment resistance and the initial stiffness of the joint have a basic meaning in the initial stage of the designing, for choice of the suitable method of analysis of the construction. Proposed in this paper, an approximation formulas allowed on the preliminary estimation of the joint characteristics, without the necessity of the usage of arduousness calculations according to the procedure presented in [4].

Comparing results received according to the exact standard method, and calculations by means of simplified formulas, differences did not exceed a dozen or so percent.

For worked example introduced in the Section 3, from approximate formulas the moment resistance amounts 8,32 kNm, and the initial stiffness 217 kNm/rad .

## REFERENCES

- [1] Altmann R., Maquoi R., Jaspard J.P.: Experimental Study of the Non-Linear Behavior of Beam-to-Column Composite Joints. Journal of Constructional Steel Research, Vol. 18, 1991.
- [2] Azizinamini A., Bradburn J. H., Radziminski J. B.: Initial Stiffness of Semi-Rigid Steel Beam-to-Column Connections. Journal of Constructional Steel Research, Vol. 8, 1987.
- [3] Hotz R.: Traglastversuche für Stützen – Riegel – Verbindungen mit verbesserter Wirtschaftlichkeit. Der Stahlbau. Heft 11, 1983.
- [4] EN 1993-1-8: 2006 Eurocode 3: Design of steel structures - Part 1-8: Design of joints.
- [5] Polański Z.: Planowanie doświadczalne w technice. PWN Warszawa 1984. (in polish)

Adam W. REICHHART<sup>1</sup>

## ANALYSIS OF PROFILED SHEET SHELLS AS A SYSTEM OF FOLDS

### ABSTRACT

It is possible to shape shells of flat profiled sheets thanks to their high geometrical orthotropy. A general method of geometrical shaping of shells is presented in brief. The method can be applied to build any shells of flat profiled sheets. A computer programme enables the determination of shell generatrices and other shell lines necessary for the design of shells. The structural analysis of flat roofs made of profiled sheeting is normalised. According the standards, an analysis of sheets consists in verifying individual folds as sheeting members. In shells, the shape and dimensions of individual folds are longitudinally variable, and folds are inclined longitudinally and transversely. Research has shown that twist of folds does not have significant impact on their stiffness.

**KEYWORDS:** profiled sheet, shell, design, analysis, space structure.

### 1. INTRODUCTION

Profiled sheets are characterised by significant geometrical orthotropy. In flat profiled sheets longitudinal bend, compression or tension stiffness is several thousand times higher than its transversal twist, bend or compression stiffness. This makes it possible to shape shells by twisting or bending the sheets transversally. Sheets shaped in such a way may be connected to form a band, which in practice can become any geometrical oblique rectilinear shell, Fig.1.

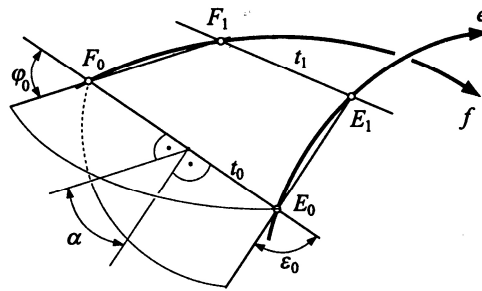


Fig.1. Suspended shell roof over a stage

To shape a spatial rectilinear shell a special method needs to be applied. The **method of shaping rectilinear shells of profiled metal sheets** consists in:

- (a) choosing a *fixing shape*  $[e, f, t_0]$ , where  $e, f$  are directrices of the shell (usually any of plane or spatial curves), and  $t_0$  is a chosen initial generatrix and
- (b) specifying the *structural condition*  $[SC]$  determining the position of the other generatrices in relation to the fixing shape.

The shaping of a shell, i.e. determination of its generatrices, is based on searching subsequent generatrices, especially the connection lines of the shell's sheets, Fig. 2.



SCHEME OF SHELL SHAPING ALGORITHM

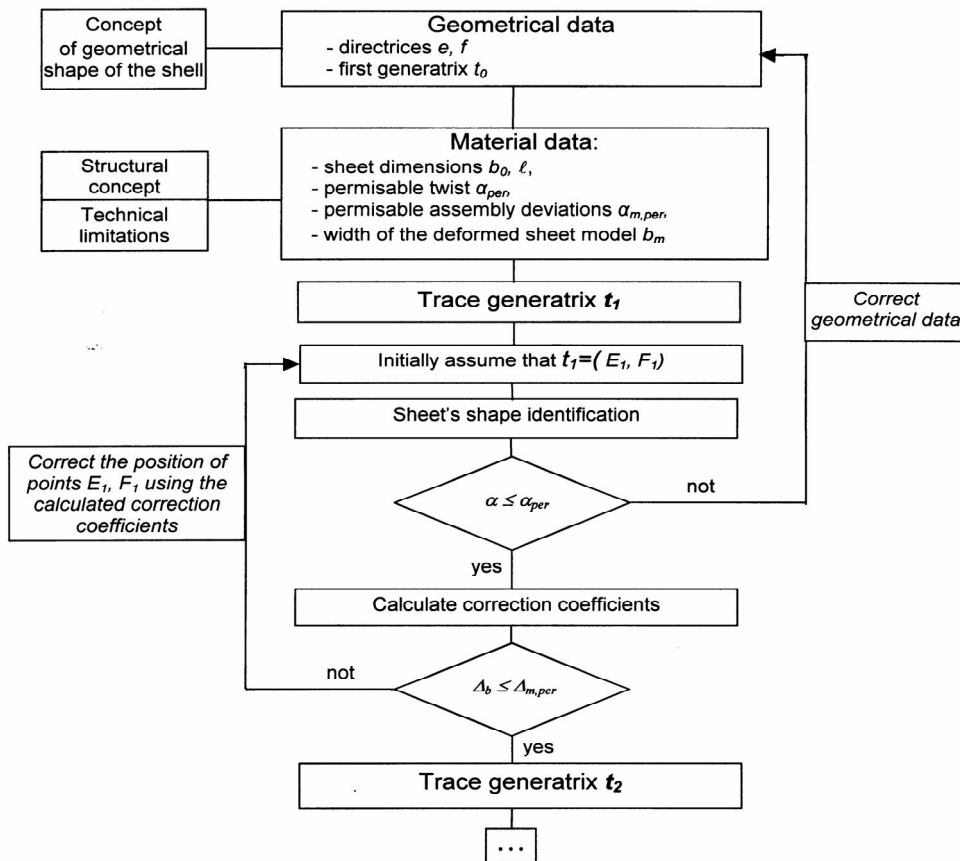


Fig. 2. Fixing shape  $[e, f, t_0]$  and the first sheet of shell built with the use of the computer programme

This method allows to shape any shell possible to be composed of flat profiled metal sheets. The geometrical shape of the surface can be obtained depending on the shape and mutual positioning of  $e$  and  $f$  and the position of generatrix  $t_0$ . The choice of the type of sheet

is related to the structural condition and the admissible magnitude of deformation. If the limits are exceeded, the geometrical assumptions have to be corrected.

This designing method provided a convenient basis to formulate a computer programme which is helpful not only at the stage of shell shaping but also during calculation and during the determination of dimensions of each profiled metal sheet and the supporting members of the shell, [1,2]. Fig. 2.

To fix the shape of the shell, it needs to be connected to bar members. In line with strength and structural requirements, the intended profiled sheet shell should be assigned a member grid not only to preserve its shape but also to bear the loads acting directly on the shell and to transfer them to other elements of the structure. Therefore, it may be assumed that a profiled sheet shell is a structure of shell-shaped and connected metal sheets and members of the shell to which the sheets are fixed, Fig.3.

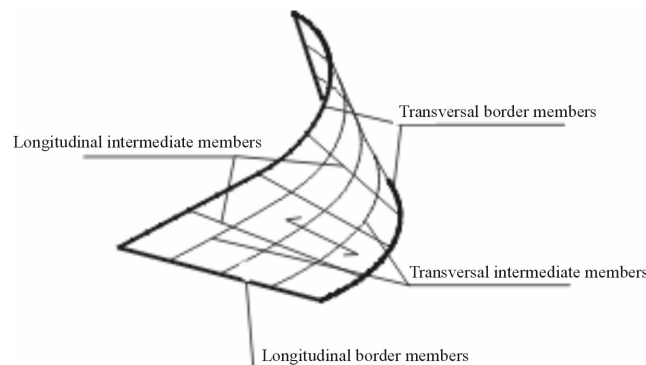


Fig.3. Members of a shell made of profiled sheets

The connections between the sheeting and the members in a shell are being named in line with the terminology used for profiled sheeting acting as a panel i.e.:

- *seam connection* – between sheets,
- *main connection* – between sheeting and transversal members,
- *intermediate connection* – between sheeting and longitudinal members (if needed).

The connections between sheets and members may be *direct connections* or *intermediate connections*. The connections with transversal members should be direct, Fig.4.

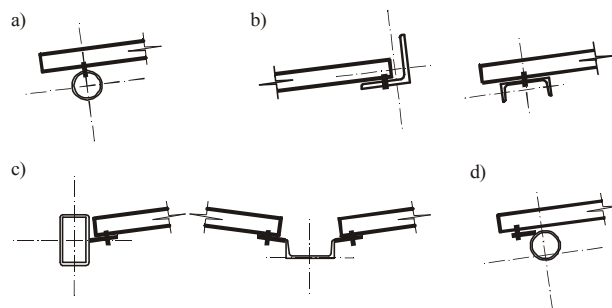


Fig. 4. Ways of supporting a profiled sheet shell on members

These are usually made in each trough of a fold. An intermediate connection between longitudinal members and the sheeting may be applied if the longitudinal members do not touch the sheeting. In such cases *shear connectors* should be used. Such a connection is important if in the shell there are forces parallel to longitudinal members, e.g. when the shell is being shorn.

## 2. BASIC PRINCIPLES OF ANALYSIS SHELLS OF PROFILED SHEETS

A strength analysis should be made separately for each type of shell elements taking into account interaction of the entire structure system. This approach allows to consider jointly the load capacity, stability and stiffness of the structure and their interactions.

### 2.1. Folds as shell members

In order to adapt flat roof analysis and design procedures for the purposes of designing shells of profiled sheeting, it has to be demonstrated that it is possible to treat a shell as a system of individual folds.

Research on flat sheets has shown a large difference in displacement of the loaded fold and the neighbouring unloaded folds. Significant orthotropy of profiled sheeting results in that the independence in load transfer by individual folds is similar in the shell to the one observed in flat roofs. Research has been made to determine the influence of twist angle on the behaviour of folds in a loaded shell. A set of three connected sheets twisted at different angles from 0 deg to 50 deg was examined (Fig. 5). The results have shown that deflection of a loaded fold is more than two times higher than the deflection of the neighbouring unloaded folds, however it does not depend on the twist angle [3].



Fig. 5. Test setup

As regards surface loads (e.g. snow loads), load values change on subsequent folds, but the differences in loads on neighbouring folds are insignificantly small and their effect on shell resistance is twice smaller so may be ignored. Thus, it may be assumed that it is correct to use the calculation of individual folds in shell resistance analysis.

### 2.2. Coordinate system of a fold

To enable the analysis of a single fold, an orthogonal coordinate system  $\{u, v, w\}_f$  related to it has been adopted with the  $w$  axis normal to the shell, the  $v$  straight axis identical to the indifferent axis of the fold<sup>1</sup> and the  $u$  curve axis perpendicular to the other axes of the system, [1]. Figure 6 shows this coordinate system with the origin in the middle of the fold's

<sup>1</sup> In the geometrical model of a shell, fold axis may be identified with the shell's generatrix.



length. In general, due to the slope of a shell, the fold (axis  $v$ ) is inclined to the level at angle  $\beta_f$ , Fig.6a, and the  $\{u,v,w\}_f$  system is twisted around the  $v$  axis with the  $w$  axis deflected from the vertical plane including the  $v$  axis at angle  $\delta_f$ , which is variable along the fold, Fig.6b. The total twist of the fold around the  $v$  axis equals  $\alpha_f = \alpha_l \cdot l$ , where  $\alpha_l$  is a unit twist angle of the fold, and  $l$  is its length.

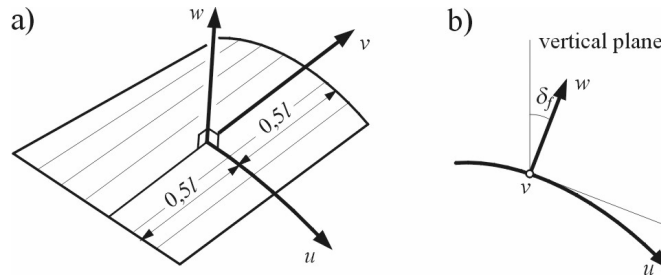


Fig. 6. Disposition of the fold's coordinate system towards the shell and the corresponding deviation of the  $w$  axis form the vertical plane including the  $v$  axis

The shape of a fold's cross-section has to be taken into account in resistance analysis of an individual fold. The shape varies along the fold since as a result of assembly deformation (torsion) sheet's width changes (only the width of individual flanges and webs is constant) and the fold is twisted and rotated due to the fact that the shell's slope varies along the width. However, the fold's cross-section remains symmetrical after bending or twisting, with the  $w$  axis being the symmetry axis. The other principal axis of the cross-section is the  $u$  axis. The fold is a thin-walled member with moments of inertia varying along the  $v$  axis. The fold edges are stiffened and elastically supported by the webs of the neighbouring folds.

Loading acts on shell surface and may be transferred to the supporting structure of profiled sheets via members laid transversally to folds or directly to the surface of the sheeting structure. In consequence, individual folds bear concentrated forces or continuous load respectively.

Continuous load on one fold  $q(v)$ , usually varying on its length, may be decomposed into  $q_u(v)$ ,  $q_v(v)$ ,  $q_w(v)$ . Such load usually results from self-weight, sheeting and installation weight and snow, whereas wind load acts along axis  $w$ , Fig.7. Loads  $q_u(v)$ ,  $q_v(v)$  are in general eccentric.

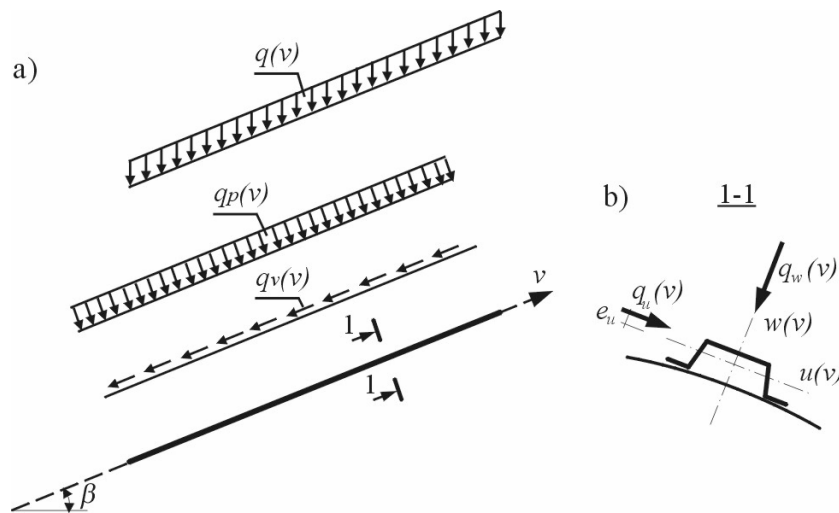


Fig. 7. Continuous load of a fold  $q(v)$  decomposed in the direction of axes of the  $\{u,v,w\}_f$  system into elementary loads acting along the main axes of the fold's cross-section. Values and directions of these loads vary along the fold's length.

### 2.3. Preliminary loading of a fold related to the shaping of a shell during assembly

The loading related to the shaping of a shell has to be taken into account regardless of the surface load. Individual folds of initially flat profiled sheets are twisted or bent transversally in a shell. As a result of connecting the neighbouring sheets their width changes. Thus, the transformation of individual folds from flat to shell form may be treated as a composition of free twisting of the fold along its longitudinal axis and changing of initially constant width  $b$  to varying width  $b_p(v, \alpha_l)$  of the fold in the shell, Fig.8.

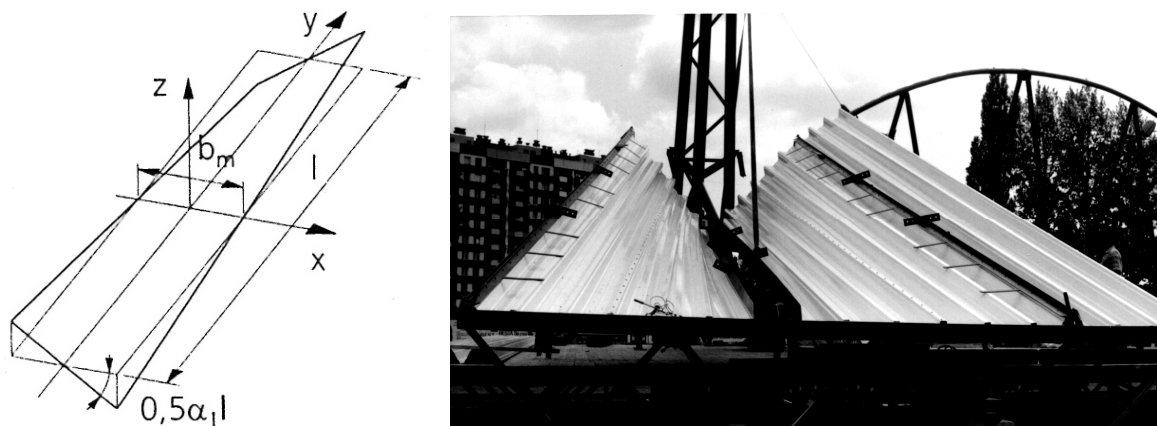


Fig. 8. Model of twisted sheet and shell with strongly twisted profiled sheets; shell members during assembly

In most shells, forces resulting from twist are small. However, transversal forces resulting from width change increase significantly with the increase of the twist angle; they vary along fold's length: they are greater at the supported area (tension) and lesser in the middle area (compression), [1]. Fold's width may be additionally changed by intentional perpendicular tension or compression; effects of those changes should be added to the effects of width change due to bending or twisting.

### 2.4. Loading implied by shell support conditions or by deflection of the shell as a membrane

Depending on the configuration of the whole  $\{u, v, w\}_f$  system and its boundary conditions, there are respective displacements and effort of perpendicular and parallel elements. They may cause mutual displacement of neighbouring folds in directions normal or tangent to the shell, [1].

Displacements of folds in the direction normal to the shell cause their deflection, which is analysed as in flat roofs. However, displacements of shell's members in the direction tangent to the shell cause deformation of the form of entire shell in a comparable manner as in flat roofs and thus result in mutual displacement  $\Delta_f$  of the neighbouring fixing points of the sheeting in the direction of its generatrices, Fig.9.

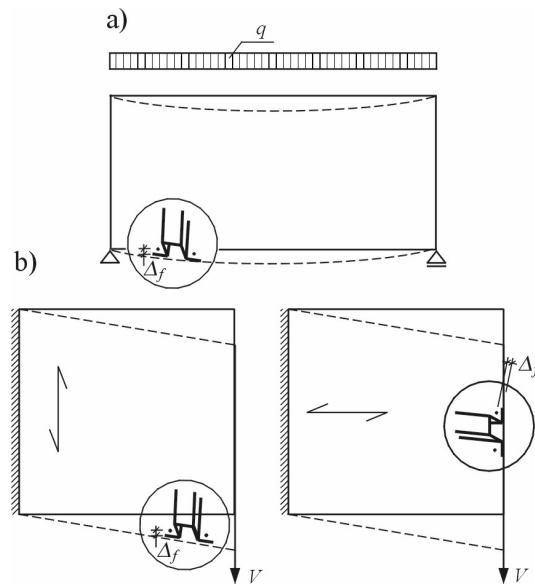


Fig. 9. Sheet deformation scheme in: a) freely supported roof, b) cantilever panel with different arrangement of sheets

The situation shown in the Figure 8a may occur in a sheeting shell structure from the Figure 10. However, possible displacements and their values may differ depending on the support of individual edge members of the shell or their stiffness, Fig. 10c, d, e.

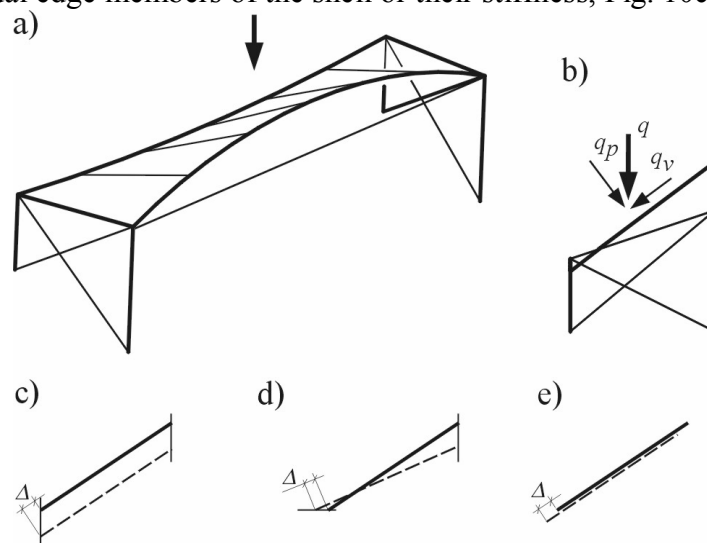


Fig. 10. Shell cover with a possibility of displacement against edge generatrices: a) structure scheme, b) vertical cross-section of the middle fold, c-e) examples of displacement of the middle fold of the shell

The deformation shown in Fig. 9b may also occur in a cantilever shell, Fig. 11. Fold displacements in part D represent such a deformation, whereas the displacements in part A are quite different.

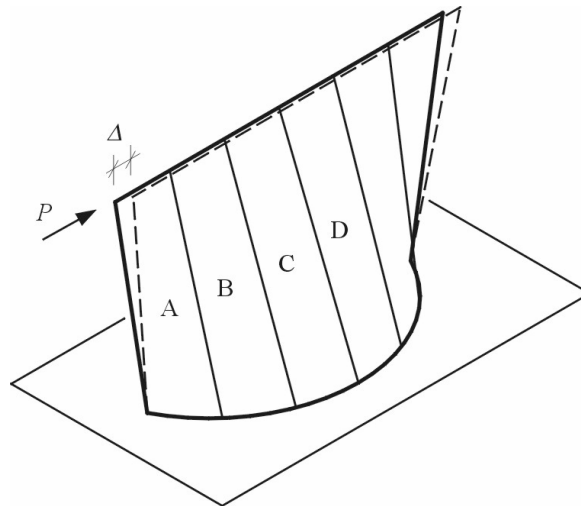


Fig. 11. Shear in a cantilever shell

Figure 12 presents schemes of two projections of a fold twisted by angle  $\alpha$  and fixed to perpendicular members in points AB, CD. In case of displacement of the perpendicular support line CD in its direction by value  $\Delta$ , the fold is subject to complex displacement against line AB. Displacement  $\Delta$  of the line CD against AB may be decomposed to displacement  $\Delta_{ob}(CD) = \Delta \cdot \sin(\alpha)$  causing a turn around AB and displacement  $\Delta_{sc}(CD) = \Delta \cdot \cos(\alpha)$  resulting in the fold's shear.

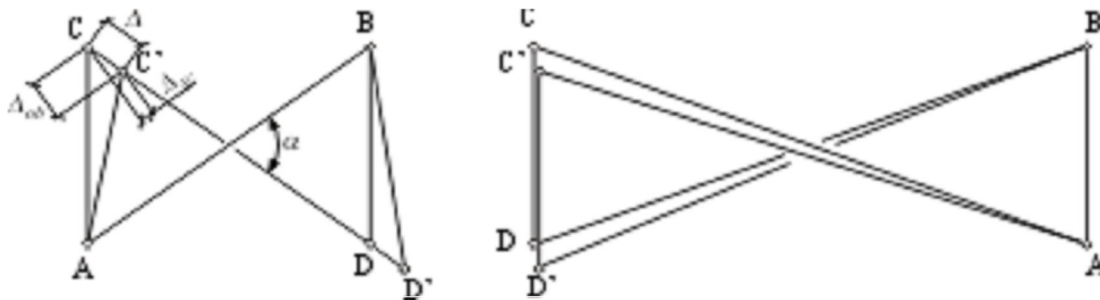


Fig. 12. Projections of a twisted fold before and after displacement of the support CD by the value  $\Delta$  and components of the displacement against the support AB

Component displacements causing the turn are comparable to deflections. Therefore, considering significant length of the sheet, they usually cause small forces along fold flanges. The principal resistance against shear is demonstrated by folds in parts C and D in Fig. 11.

## 2.5. Stability of a shell subject to shear

Large mutual displacements of shell members may result in shear buckling of the shell. Proper construction of shells must exclude such a situation as it may result in a sudden breakdown of the structure. Tangent displacements are counteracted by shear stiffness of folds and stiffness against profile distortion between the neighbouring fixing points, like in flat panels. The folds' counteraction, transmitted by connections to members, ensures shear rigidity of the shell. The described research on cylindrical, [4], and hyperbolic paraboloid, [5,6,7] has shown that their shear buckling resistance is greater than in flat panels. Strain in shorn shells is of the same kind as in flat roof panels whose shear resistance calculation is described in [8,9]. Extended research on shorn flat panels has proven their large rigidity and stiffness, [8,10,11]. Considering the research, in case of shells, it is allowed to apply formulas

for flat roofs to calculate the rigidity of shorn shells of profiled sheeting.

The author proposes rules for design using procedures of Eurocode 3 especially Part 1-3 [9] and European Recommendations for application of Stressed skin design [8], which enables to design rectilinear shells of flat profiled metal sheets.

### 3. SUMMARY

Shaping shells of profiled sheeting in line with the presented principles offers a vast array of new geometrical forms, Fig. 13.

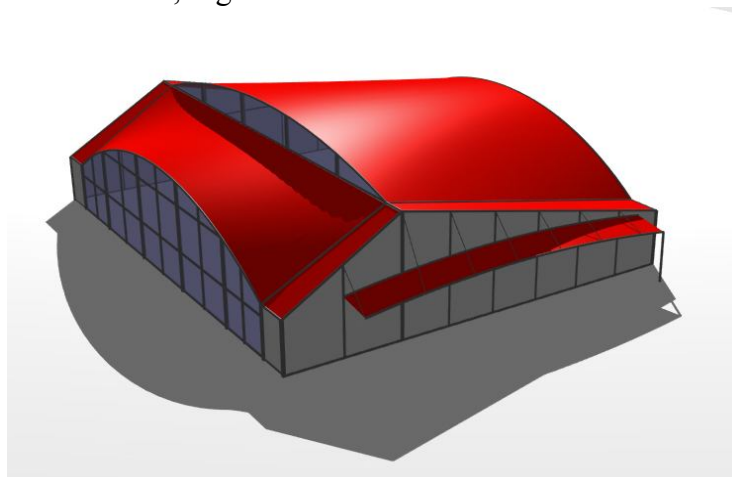


Fig. 13. Design of a sports hall of 2000 m<sup>2</sup>

Use of profiled sheets as construction material for covers offers several advantages. Thanks to the large range of profile heights the span between the supports may be up to about 10 m. Commercial length exceeds 20 m and the presented shaping method allows lengthening the sheets. Additionally, the technology of coating considerably extends the life of sheets.

The difficulty in shaping complex forms is reduced by the shell shaping computer programme providing results in text form (Excel) and graphic form (Autocad).

The possibilities of application of profiled sheet shells are large. Realisation of such structures is less complicated than in case of other spatial forms. It only requires the contractors to be trained before the assembly.

The presented new forms of shell structures are subject to further research conducted in Rzeszow University of Technology. The static analysis and resistance calculations in accordance with the presented rules can be aided by the computer programme. The approach presented herein covers all aspects of design which need to be analysed. In case of any matters which are not sufficiently examined the designer needs to rationally assess the security.

### 4. REFERENCES

- [1] Reichhart A.: Geometrical and structural shaping of shells made of profiled metal sheets (in Polish), Oficyna Wyd. Politechniki Rzeszowskiej, Rzeszów 2002.
- [2] Reichhart A.: Specificity of shells made of elastic deformed profiled metal sheets, Proc. of the 4th Int. Colloq. on Structural Morphology, Delft 2000.
- [3] Reichhart A., Dudziński P.: Influence of the torsion of sheets in a profiled sheets shell on the participation of folds in carrying concentrated load (in Polish), Proc. IX Intern. Scientific Conf. Nauk. Rzeszów-Lviv-Kosice 2004.
- [4] Abdel-Sayed G.: Critical shear loading of curved panels of corrugated sheets, Proc. ASCE,

- J. Eng. Mech. Div., 96 (EM6), Dec. 1970
- [5] Banavalkar P.V., Gergely P.: Analysis of thin steel hyperbolic paraboloid shells, Proc. ASCE, J. Struct. Div., 98 (ST 11) 1972
- [6] Fischer M.: Versuche zur Ermittlung des Tragverhaltens einer hyperbolischen Paraboloidschale aus einlagigen Trapezprofilblechen, Stahlbau, H. 4, 5, 1972.
- [7] Gergely P., Winter G.: Experimental investigation of thin-steel hyperbolic paraboloid structures, Proc. ASCE, J. Struct. Div., 98 (ST10) 1972
- [8] European Recommendations for the Application of the Metal sheeting Acting as a Diaphragm. Stressed Skin Design. ECCS Committee TC7, TWG 7.5, May 1995
- [9] EN 1993-1-3 Eurocode 3 – Design of steel structures – Part 1-3: General rules – Supplementary rules for cold-formed members and sheeting, Brussels 2006.
- [10] Easley J.T.: Buckling Formulas for Corrugated Metal Shear Diaphragms, J. Struct.Div., ASCE, July 1975.
- [11] Bródka J., Garncarek R., Miłaczewski K.: Corrugated sheets in steel construction (in Polish), Arkady, Warszawa 1999.

Dmitrijs SERDJUKS<sup>1</sup>  
Karlins ROCENS<sup>2</sup>  
Rajmondas OZOLINSH<sup>3</sup>

## EVALUATION OF CLADDING ELEMENT'S PRESTRESSING FOR SADDLE-SHAPED CABLE ROOF

### ABSTRACT

Prestressed cladding element for the long span saddle-shaped cable roofs was considered. Peculiarity of the prestressed cladding element is absence of rigid contour. The generally woven by the basket weave fabric from the Vectra (LCP) yarns, which is covered by the PolyTetraFluoroEthylene (PTFE) copolymer foil, steel cables and steel pipes were considered as the materials of covered fabric, load-bearing cables and central pillar, correspondingly.

The covered fabric is joined directly with the cables of saddle-shaped roof and the displacements of the cables have significant influence on the prestressing level of cladding element. Influence of the displacements of 50x50 m cable net of saddle-shaped roof on the prestressing level of cladding element was evaluated.

**KEYWORDS:** cable net, tensioned fabric, steel cables, vertical displacements.

### 1. INTRODUCTION

Cable roofs can be divided into the groups depending on the type of cladding. It can be rigid elements working at bending. Reinforced concrete slabs, profiled metal sheets, several types of composites that are the examples of rigid elements for cable roofs cladding. Such elements mainly are used for the permanent structures and are characterized by the comparably big materials consumption [1].

Tensioned fabric is other type of cladding for cable roofs and membrane structures, where high strength materials can be used in the full scale. Decreased materials consumption and dead weight in combination with the increased mobility are the most significant advantages of tensioned fabric as the cladding element material.

Probability of wave development at some parts of structure after design vertical load application is a serious problem for tensioned fabric claddings. Other parts of cladding can be over-strengthened in this case.

<sup>1</sup> Asoc.Prof. Dr.sc.ing., Riga Technical University, Riga, LATVIA,

<sup>2</sup> Prof. Dr.sc.ing., Riga Technical University, Riga, LATVIA,

<sup>3</sup> Prof. Dr.sc.ing., Riga Technical University, Riga, LATVIA.

Development of cladding element with the increased compliance and enough strength is probable way to fix the problem together with the cladding's prestressing. Combination of rigid and compliant elements also is possible.

Prestressed cladding element (Fig.1) is formed by the load-bearing cables, tensioned fabric and central pillar.

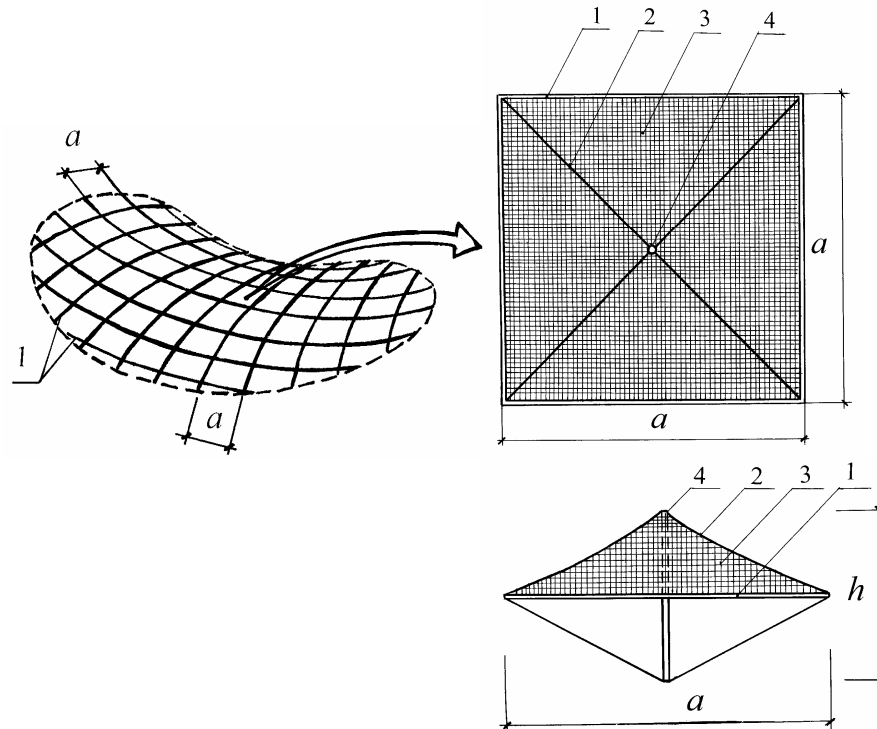


Fig.1. Prestressed element of cladding:

1– cables of the net; 2 – load-bearing cable; 3 – tensioned fabric; 4 – central pillar

The load-bearing cables and tensioned fabric are joined with cables of the net. The displacements of the cable net after application of design vertical load can seriously effect on the stress-strain state of the prestressed cladding element. This effect can be controlled by the choice of rational level of cladding element prestressing and it height. As a criteria of rationality are considered minimization of materials consumption and vertical displacements after application of design vertical load.

So, the aim of the paper is to evaluate the dependences of cladding element prestressing level and it height on the materials consumption and vertical displacements. Approach for prestressed cladding element designing also should be developed.

## 2. CHOICE OF MATERIALS FOR PRESTRESSED CLADDING ELEMENT

Tensioned fabric is significant unit of prestressed cladding element. In general, tensioned fabrics can be coated or uncoated. Uncoated fabrics have short service lives and it applications is limited by the temporary membrane and cable structures. Coating of fabrics gives the following benefits:

- protecting the yarns against different sources of damages (UV, abrasion, atmosphere);
- proofing the membrane against rainwater and atmospheric moisture;
- stabilizing what might otherwise be unstable fabric geometry;
- providing material to permit heat-sealed seams.

Coated fabrics can be divided into the following groups depending on the type of coatings [1]:



- PVC coatings;
- PTFE coatings;
- Silicone coatings.

PTFE coatings cause the biggest interest due to the row of advantages. Since PTFE upper limit of continuous service temperature is +260 °C it can be used in hot climatic zones. The lower limit of the continuous service temperature is -200 °C. Temperature variations have no influence on the lifespan. PTFE has a low thermal conductivity (0.25-0.50 W/Km) and good insulating properties. PTFE is under normal conditions inflammable, and is resistant against the strongest corrosive substances. PTFE is not soluble in most common solvents. Because of its hydrophobic properties, PTFE is an excellent protection for the textile reinforcement of the membrane. PTFE is totally resistant to UV and IR-radiation. PTFE membranes show no ageing or increased brittleness due to UV/IR radiation [2].

Almost all permanent fabric structures built today are entirely synthetic. The most common fibers used for the membranes and cable roofs are glass and polyester fibers. Special attention should be added to LCP (liquid crystal polymer based on aromatic polyester) yarns [1]. Using of other kinds of fibers is limited by the increased costs (carbon, Kevlar fibers), increased dead weight and possibility of corrosion (metal fibers) and relatively low modulus of elasticity (cotton, hempen fibers). But glass and polyester fibers possess a number of disadvantages: Glass fibers deteriorate when exposed to moisture and polyester degrades when exposed to sunlight. Fabrics can be divided into the following groups depending on the type of yarns [2]:

- organic (cotton, hempen);
- mineral (glass, carbon);
- metal (steel, copper, bronze);
- synthetic (polyamide, polyester, acryl, Kevlar).

Ethylene-TetraFluoroEthylene copolymer foils (ETFE) also took a special position between tensioned claddings. The main characteristics of fibers, which are initial components of tensioned fabrics, are given by [2-5] and shown in the Table 1.

Table 1. The main characteristics of fibers, which are initial components of tensioned fabrics

Materials	Density g/cm <sup>3</sup>	Strength in tension, MPa	Elongation at break, %	Modulus of elasticity, MPa
Steel	7.86	2200	1.1	210000
Bronze	8.50	320-1100	10-35	96000-120000
Aramid (Kevlar, Twaron)	1.45	till 2700	2.0-4.0	130000-150000
Carbon fibers (CFC, Celion, Carbolon, Thornel)	1.7-2.0	2000-3000	<1	200000-500000
Polyamides (Nylon, Perlon)	1.14	till 1000	15-20	5000-6000
Glass	2.55	till 3500	2.0-3.5	70000-90000
Vectra (LCP)	1.40	2850	3.3	65000
Polyesters (Trevira, Dacron, Diolen)	1.38-1.41	1000-1300	10-18	10000-15000
Ethylene and PoliTeratFluoroEthylene copolymer foils (ETFE, Tefzel, Dyneon)	1.70-1.76	48-234	45-650	900-3500

Vectra (LCP) yarns, as it is shown in the Table 1, take intermediate position between polyester and glass ones. It means that Vectra (LCP) yarns can be used as components of tensioned fabrics for membrane and cable structures. Practical absence of creep allows us to consider Vectra (LCP) yarns as a material for prestressed structures [2]. So, coated fabric on the base of Vectra (LCP) yarns and PTFE coating will be considered next.

Steel cable on the base of the wire with tensile strength in 1960 MPa and modulus of elasticity in  $1.7 \cdot 10^5$  MPa was considered as the material of load-bearing cables. Steel with the yield strength in 240 MPa was considered as the material of central pillar.

### 3. DESIGN OF PRESTRESSED CLADDING ELEMENT

#### 3.1. General approach

The design procedure of the prestressed cladding element can be divided into the following stages:

- development of the design scheme of prestressed cladding element;
- determination of loads, acting on the prestressed cladding element;
- previous evaluation of the prestressed cladding elements units cross-sections;
- analyze of the prestressed cladding element by the program „ANSYS/ED 5.5” for WINDOWS and correction of previously determined cross-sections of units.

The design scheme of prestressed cladding element is shown in the Fig. 2.

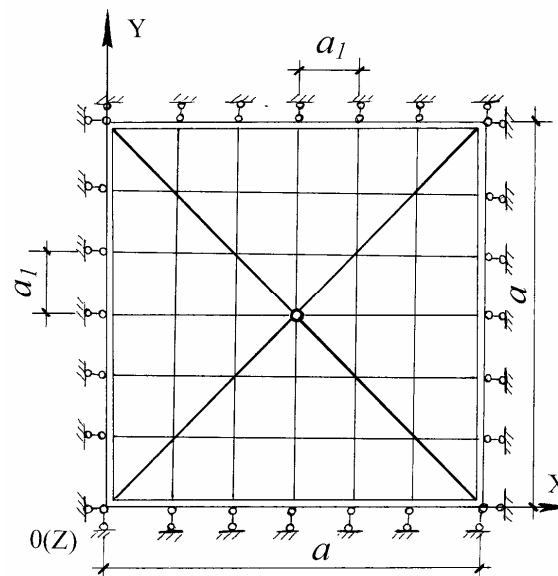


Fig. 2. Design scheme of prestressed cladding element:  $a$  – dimension of prestressed cladding element,  $a_1$  – distance between the conditional yarns in warp and weft directions

Following assumption are taken into account during formation of design scheme. Design vertical load is applied as the point wise forces to the nodes of the design scheme. Two variants of support point strengthening are possible. The first variant is related to the case, when cable net is enough rigid and displacements of support points of prestressed cladding element can be neglected. The second variant is related to the case, when cable net is compliant and displacements of support points of prestressed cladding element must be taken into account.

Tensioned coated fabric is considered as totality of yarns in warp and weft directions modeled by the universal nonlinear spatial cable finite element LINK 10 with specific bilinear stiffness matrix, which defines that the element works in tension only without bending stiffness [1]. The modulus of elasticity and tensile strength of yarns in warp and weft directions are determined basing on the properties of separate fiber.

### 3.2. Evaluation of mechanical properties of coated fabric

The modulus of elasticity and tensile strength of coated fabric on the base of Vectra (LCP) yarns and PTFE coating were evaluated basing on the assumption, that the properties are mainly determined by the characteristics of the base fabric.

Modulus of elasticity of tensioned fabric and the tensile strengths in warp and weft directions were considered as the main mechanical properties. Modulus of elasticity of tensioned fabric in warp and weft directions was evaluated by the following equations [6]:

$$E_{f,o} = E_1 \cos^4 \beta_o, \quad (1)$$

$$E_{f,y} = E_1 \cos^4 \beta_y, \quad (2)$$

where

$$\cos \beta_o = 1 - 0,001a_o,$$

$$\cos \beta_y = 1 - 0,001a_y.$$

Here  $E_{f,o}$ ;  $E_{f,y}$  - modules of elasticity of cladding element in warp and weft directions respectively;  $E_1$ - modulus of elasticity of separate yarn,  $\beta_o$ ,  $\beta_y$  – angles of yarns inclinations in warp and weft directions respectively,  $a_o$ ,  $a_y$ - shrinkage of fabric in warp and weft directions respectively.

The tensile strength of coated fabric was determined on the base of the scheme [6], which is shown in Fig. 3 for the basket weave case.

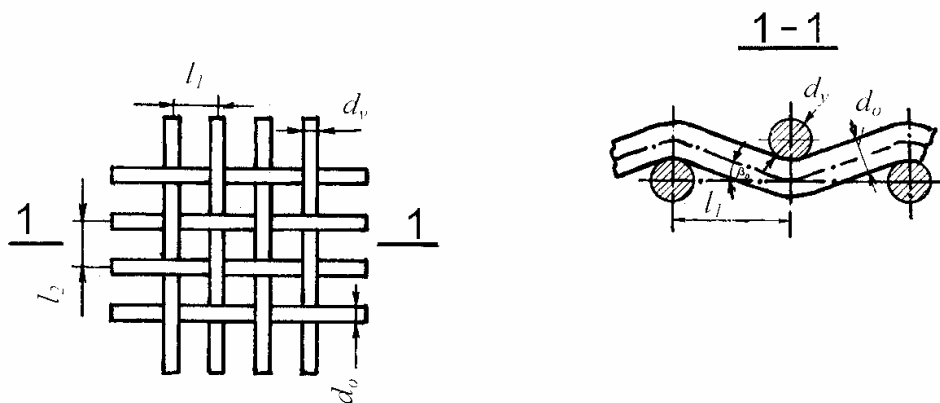


Fig. 3. Scheme of the basket weave fabric:  $\beta_o$ – angle of yarns inclination in warp direction;  $d_o$ – diameter of the yarns in warp direction;  $d_y$ – diameter of the yarns in weft direction;  $l_1$ – distance between the centres of the yarns in warp direction;  $l_2$ – distance between the centres of the yarns in weft direction.

Quasi instantaneous tensile strength of fabric in warp and weft directions (kN/m) was determined using the recommendations [7] depending on the breaking force of fabric in both

directions.

$$\tilde{N}_{f,o} = 0.5K_o n_o P_o, \quad (3)$$

$$\tilde{N}_{f,y} = 0.5K_y n_y P_y, \quad (4)$$

where

$$P_x = P_y = \eta_0 m_0 p_0 \left(1 + \frac{\nu}{\eta_0} \cos \beta_c \sin \beta_c\right),$$

$$\operatorname{tg} \beta_c = 0.67 \pi d_l t_l.$$

$\tilde{N}_{f,o}$  и  $\tilde{N}_{f,y}$  – tensile strength of fabric in warp and weft directions (kN/m);  $P_o$  and  $P_y$  – breaking force of yarns in warp and weft directions;  $K_o$  and  $K_y$  – coefficients of yarn strength using in warp and weft directions;  $n_o$ ,  $n_y$  – amount of yarns in warp and weft directions at 1 meter;  $\nu$  – friction coefficient of fiber;  $\eta_0$  – coefficient taking into account inhomogeneity of fiber loading in the yarn;  $m_0$  – amount of fibers in the cross-section of the yarn;  $p_0$  – breaking force of fiber;  $\beta_c$  – lay angle of a yarn;  $d_l$  – external diameter of the yarn;  $t_l$  – number of twists at one millimetre of the yarns length .

#### 4. EVALUATION OF CLADDING ELEMENT'S PRESTRESSING

The interaction between the materials consumption and maximum vertical displacements of the prestressed cladding element, from one side, and the level of prestressing and height of cladding element, from other, were obtained by the numerical experiment. Using a computer program “ANSYS/ED 5.5” for WINDOWS the numerical experiment was carried out. The numerical experiment was combined with the determination of tension forces, acting in the units of prestressed cladding element under the main load combination. The main load combination includes dead weight of cladding element and accidental snow load which is equal to 0.2 kPa. Level of prestressing for tensioned fabric changes within the limits from 0.2 to 0.6 from its load bearing capacity. The values of height of prestressed cladding element changes within the limits from 0.25 to 1 m. The dimension of considered prestressed cladding element was equal to 2.5 m. The materials consumption was determined as the dead weight of prestressed cladding element, related to the covered area.

The displacements of cable net of saddle – shaped roof were taken into account. The cable roof was 50x50 m in plan with the rational geometrical characteristics: the initial deflection of contour cables was 8.6 m, the initial deflection of suspension and stressing cables 20 m and the step in plan of the latter ones was 1.414 m [8].

The dependences of the materials consumption of the prestressed cladding element on the level of prestressing of tensioned fabric and height of cladding element are shown in Fig.4.

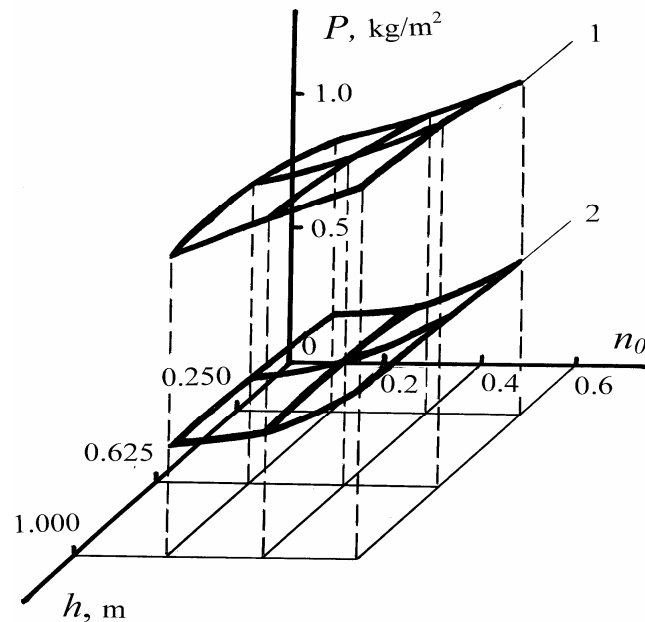


Fig. 4. The dependences of the height  $h$  of prestressed cladding element and level of it prestressing  $n_0$  on the materials consumption  $P$ : 1 - the displacements of cable net of saddle – shaped roof were taken into account; 2 - the displacements of cable net of saddle – shaped roof were not taken into account

The dependence 1 shows, that the material consumption of prestressed cladding element changes within the limits from 1.040 to 1.401  $\text{kg/m}^2$ , when the level of prestressing and values of height of prestressed cladding element changes within the limits from 0.2 to 0.6 and from 0.25 to 1 m, correspondingly. The displacements of cable net of saddle-shaped roof were taken into account. The materials consumption changes within the limits from 0.368 to 0.633  $\text{kg/m}^2$  in the case, when the displacements of cable net were neglected.

The dependences of the maximum vertical displacements of the prestressed cladding element on the level of prestressing of tensioned fabric and height of cladding element is shown in Figure 5. The displacements of cable net of saddle – shaped roof were neglected. The dependence shows, that the maximum vertical displacements of prestressed cladding element changes within the limits from 34.80 to 43.27 mm, when the level of prestressing for tensioned fabric heights of prestressed cladding element changes within the limits from 0.2 to 0.6 and from 0.25 to 1 m, correspondingly. The maximum vertical displacements of prestressed cladding element changes within the limits from 600 to 618 mm in the case, when the displacements of the cable net of saddle-shaped roof were taken into account.

It was shown, that the displacements of cable net of saddle-shaped cable roof has significant influence on the behaviours of prestressed cladding element. So, materials consumption grows from 2.21 to 2.83 times when the displacements of cable net of saddle – shaped roof were taken into account.

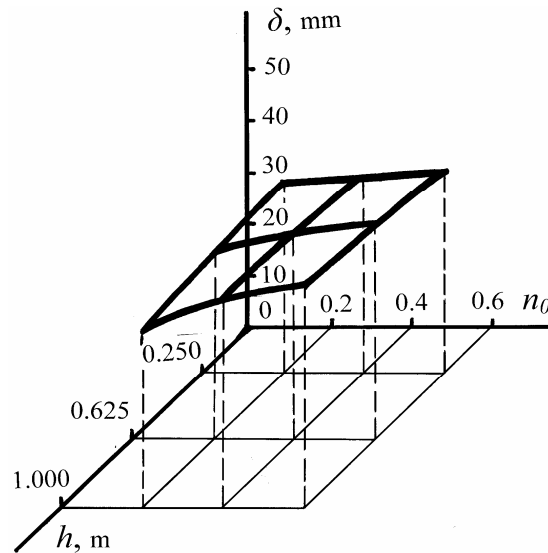


Fig. 5. The dependences of the maximum vertical displacements  $\delta$  of the prestressed cladding element on the level of prestressing  $n_0$  of tensioned fabric and height of cladding element  $h$

The dependences, which are shown in figures 4 and 5, were determined in the form of second power polynomial functions:

$$P(\delta) = b_0 + b_1 h + b_2 n_0 + b_{12} h n_0 + b_{11} h^2 + b_{22} n_0^2. \quad (5)$$

The coefficients of equation (5) were determined applying the method of experimental design (Table 2).

Table 2. Coefficients of the equation (5)

The dependences	Values of coefficients*					
	$b_0$	$b_1$	$b_2$	$b_{12}$	$b_{11}$	$b_{22}$
The dependence of the height $h$ of prestressed cladding element and level of it prestressing $n_0$ on the materials consumption $P$	<u>0.3523</u>	<u>-0.2636</u>	<u>0.3100</u>	<u>0.0867</u>	<u>0.4089</u>	<u>-0.2875</u>
	0.8518	0.0489	0.1367	0.1367	0.1671	-0.7875
The dependences of the maximum vertical displacements $\delta$ of the prestressed cladding element on the level of prestressing $n_0$ of tensioned fabric and height of cladding element $h$	0.0352	0.0035	0.0217	0.0217	0.0041	-0.0120

\*Values, given in the numerator, are obtained for the case, when the displacements of cable net of saddle-shaped roof were neglected.

The min values of prestressed cladding element materials consumption was obtained, when the level of prestressing for tensioned fabric was equal to 0.2 from it load bearing capacity and height was equal to 0.25 m.

## 5. CONCLUSIONS

Prestressed cladding element on the base of Vectra fabric, coated by the PTFE foil, steel cables and pillar was considered. Approach for the designing of prestressed cladding element for cable roof was suggested. Mechanical properties of prestressed fabric were evaluated, basing on the properties of separate yarn.

The dependences of 2.5x2.5 m cladding element prestressing level and height on it materials consumption and vertical displacements were evaluated. The displacements of the cable net of 50x50 m saddle-shaped roof were taken into account.

It was shown, that the maximum vertical displacements of prestressed cladding element changes within the limits from 34.80 to 43.27 mm, when the level of prestressing for tensioned fabric and heights of prestressed cladding element changes within the limits from 0.2 to 0.6 and from 0.25 to 1 m, correspondingly. The min value of prestressed cladding element materials consumption was obtained, when the level of prestressing for tensioned fabric was equal to 0.2 from it load bearing capacity and height was equal to 0.25 m.

## REFERENCES

- [1] Pakrastinsh L., Rocens K., Serdjuks D. *Evaluation of the Behavior of Tensioned Composite Cladding Element for Cable Roofs*. Architecture and Constructional Science. Sci. Proc. of Riga Technical University, Riga, Latvia, 2005.
- [2] Forster, B., Mollaert, M., *European Design Guide for Tensile Surface Structures*. Vrije Universiteit, Brussel, ©Tensinet, 2004.
- [3] Blum R., *Material Properties of Coated Fabrics for Textile Architecture*. Proc. of the symposium The Design of Membrane and Lightweight Structures, Vrije Universiteit Brussel, 2000.
- [4] Okais S.M., *Materials & Confection of Membranes and Existing Membrane Structures*. Proceedings of the symposium The Design of Membrane and Lightweight Structures, Vrije Universiteit, Brussel, 2000.
- [5] Houtman R., *There is no Material like Membrane Material*. Proc. of the Tensinet symposium designing Tensile Architecture. Vrije Universiteit, Brussel, 2003.
- [6] Koritskij K., *Engineering Design of Textile Materials*. Moscow, 1971, [In Russian].
- [7] Kumar K., Cochran, Ir.I.E., *Closed Form Analysis for Elastic Deformations of Multilayered Strands*, Journal of Applied Mechanics, ASME Vol.54, 1997.
- [8] Serdjuks D., Rocens K. *Decrease the Displacements of a Composite Saddle- Shaped Cable Roof*. Mech. Compos. Materials, Vol. 40, No5, 2004.





Slávka ŠIMKOVÁ<sup>1</sup>

## REINFORCED CONCRETE MEMBERS UNDER THE INFLUENCE OF ELEVATED TEMPERATURES

### ABSTRACT

The paper is focused on performed experiments and created solving model for determination of strain and state of stress of temperature loaded, symmetrically reinforced concrete element. The attention is also paid to comparison of experimental dependence and dependence resulting from the created mathematical model between length strain and tensile stress of reinforced concrete specimens, which were caused by force effects of steel reinforcement under the influence of elevated temperatures up to 100 °C. Calculations according to the created model fit well the processes running at the heating up to 60°C without taking into consideration thermal creep. Above the temperature of 60 °C, it is necessary to consider the influence of the thermal creep, which, as it is shown, is not negligible above the mentioned temperature also during its short term effect.

**KEYWORDS:** elevated temperature, thermal length strain, tensile stresses

### 1. INTRODUCTION

Elevated temperature could be a significant loading state of reinforced structural member. Even in statically determinate member, it can initiate state of stress due to different value of coefficient of thermal dilatation for concrete and steel or concrete shrinkage.

### 2. EXPERIMENTAL PROGRAM

The experiments which were focused on the influence of temperatures on the strains and stresses of reinforced concrete members, were carried out on unreinforced and symmetrically reinforced prisms with dimensions 100x100x400 mm. The average value of compressive strength after 28 days of curing was 54 MPa. The compressive strength of concrete was tested on cubes with the edge length of 150 mm.

The specimens were reinforced by the reinforcement ribbed bars of Grade 10 425(V) and the following steel ratios were observed:

- $\mu = 1,13\%$ ..... reinforcement: 4 $\Phi$ 6 mm (bars placed in the corners),
- $\mu = 2,01\%$ ..... reinforcement: 4 $\Phi$ 8 mm (bars placed in the corners),
- $\mu = 2,80\%$ ..... reinforcement: 4 $\Phi$ 8 mm + 1  $\Phi$ 8 mm ( 4bars placed in the corners, 1 bar in the centre of the section).

<sup>1</sup> Assistant Prof., PhD., Eng., Technical University of Košice, Košice, SLOVAK REPUBLIC

After finishing the curing, the specimens-prisms in the moist chamber were exposed to varied temperatures in four thermal cycles. Each thermal cycle represented the period of heating up to specified temperature, the maintenance of the temperature over a 24 hour period with the rate of heating 20°C per hour. Separate thermal levels were: 40, 60, 80 and 100°C. At each thermal level, the length strains were measured and modulus of elasticity was tested. To measure strains, a pair of indicators at both opposite sides was attached to each specimen.

### 3. MATHEMATICAL MODEL

#### 3.1. Elasticity modulus and length strains of unreinforced specimens

We need to know input functions to derivate relations for calculations of length strains and tensile stresses of reinforced specimens. For concrete, it is necessary to know the relations between elasticity modulus and temperature and the dependence of length strains of unreinforced specimens on temperature. Modulus of elasticity of steel is constant in observed temperature range.

At first, we were searching for approximating functions to experimental values of elasticity modulus and relative length strains of unreinforced specimens. Then, we used these at deriving formulas for calculation of relative length strains and tensile stresses of reinforced prisms in the dependence of temperature and ratio of reinforcement. The dependence between elasticity modulus of concrete and temperature (Fig. 1) is approximated by linear function in the form of:

$$E_c(T) = -0,175 T + 36,64 \quad [\text{MPa}] \quad (1)$$

The dependence between relative length strain and the temperature of unreinforced specimens is fully fit by polynomial of degree 2 in the entire observed temperature range (Fig. 2).

$$\varepsilon_c(T)_{,teor} = -4,6427 \cdot 10^{-5} T^2 + 1,29313 \cdot 10^{-2} T - 0,241397 \quad [\text{‰}] \quad (2)$$

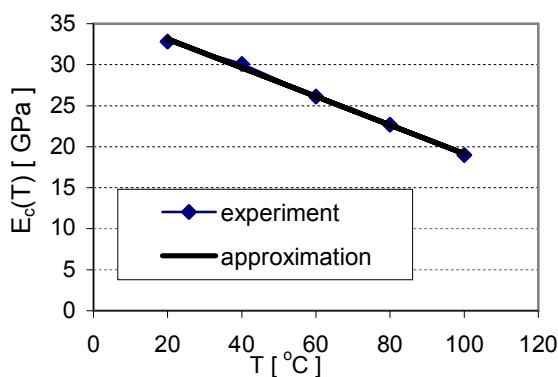


Fig. 1. Elasticity modulus of concrete

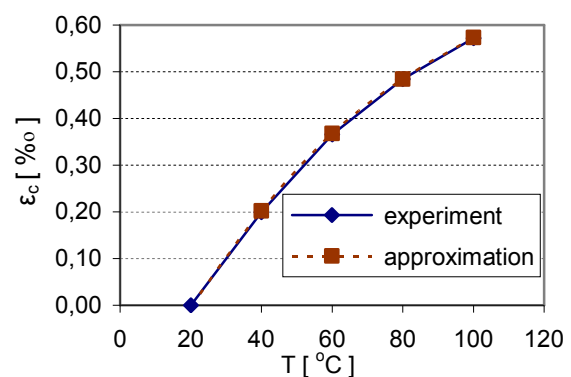


Fig. 2. Relative length strain of unreinforced specimens

#### 3.2. Coefficient of total length strain

For the purpose of next calculation, we defined the coefficient of total length strain  $\alpha_c(T)$ , which tangential values are obtained by derivative of function  $\varepsilon_{c,teor}(T)$ . This coefficient

contents thermal shrinkage and thermal length dilatation of concrete. Its equation is in form:

$$\alpha_c(T) = -9,2854 \cdot 10^{-5} T + 1,29313 \cdot 10^{-2} \quad (3)$$

### 3.3. Relative length strain and tensile stress of reinforced specimens

When deriving mathematical formulation for the calculation of resulting strains of reinforced prisms  $\varepsilon_v$  in the dependence of temperature and ratio of reinforcement, we started from elastic state and supposed there was a perfect cohesion between concrete and steel. We neglected the thermal creep of concrete under influence of stresses which rise as a consequence of reinforcement. The relaxation was also neglected.

The resulting relative length strain  $\varepsilon_v(T_1, T_2)$  of reinforced member - specimen, at heating from the temperature  $T_1$  to  $T_2$  is given by integral as follows:

$$\varepsilon_v(T_1, T_2) = \int_{T_1}^{T_2} \left\{ \alpha_c(T) + [\alpha_{sT} - \alpha_c(T)] \cdot \frac{\rho \cdot n(T)}{\rho \cdot n(T) + 1} \right\} dT \quad (4)$$

where:  $\rho$  is the degree of reinforcement and  $n$  is the ratio of elasticity modulus of steel  $E_s$  and concrete  $E_c$ .

The total length strains at separate thermal levels derived from experiments were compared to total length strains derived from created mathematical model [1].

A formula for the calculation of concrete tensile stress is derived in form:

$$\sigma_c(T_1, T_2) = \int_{T_1}^{T_2} \left\{ [\alpha_{sT} - \alpha_c(T_m)] \cdot \frac{\rho \cdot n(T)}{\rho \cdot n(T) + 1} \right\} dT \quad (5)$$

where:  $\alpha_c(T_m)$  is the coefficient of total length strain for temperature  $T_m = (T_1 + T_2)/2$

### 3.4. Stress-strain diagram in tension of steel- reinforced concrete specimens

For the particular degrees of reinforcement and observed temperature levels, the dependence between relative length strain  $\varepsilon_{cN}$  caused by force effects of the steel reinforcement and tensile stress in concrete  $\sigma_c$  (a part of stress-strain diagram in tension of reinforced specimens) was created. At the creating of stress-strain diagram resulting from the measured strains of the prisms, we started from the reasoning, which is obvious from the Fig. 3.

The figure contains:

$\varepsilon_{cN}$  - value of the relative concrete length strain influenced by the reinforcement,

$\varepsilon_{sN}$  - value of the restrained relative reinforcement length strain,

$\varepsilon_c$  - value of the unreinforced concrete relative length strain influenced by temperature,

$\varepsilon_{sT}$  - value of the relative length strain of non-concreted reinforcement influenced by its thermal length dilatation,

$\varepsilon_v$  - value of the total relative length strain of reinforced concrete influenced by temperature.

The tensile stress in concrete  $\sigma_c$  (Eq.6) in the stress-strain diagram, resulting from the experiment, was calculated by stress in reinforcement (as the elasticity modulus of reinforcement  $E_s$  is constant and Hooke's law is valid within the temperature range of 20-100°C).

$$\sigma_c = \varepsilon_{sN} \cdot E_s \cdot \mu \quad (6)$$

The elasticity modulus of concrete, also gained from the measured values of length strains of reinforced prisms  $\varepsilon_v$  and from the thermal length strains of non-concreted steel reinforcement is expressed as follows:

$$E_c = \sigma_c / \varepsilon_{sN} \quad (7)$$

At the temperatures of 80 and 100°C, so called effective elasticity modulus of concrete  $E_{cef}$  which contains, for instance thermal creep (respective influence of cracks), will be concerned.

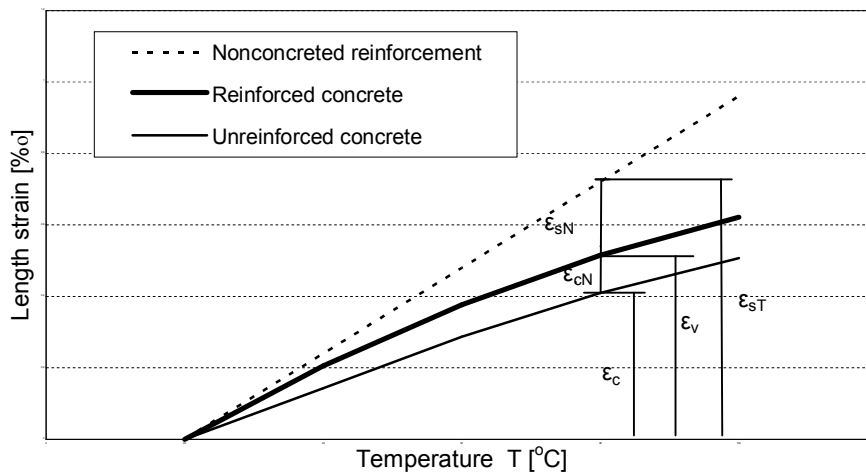


Fig. 3. Chart for the creating of stress-strain diagram in tension of reinforced specimens

By comparing the stress-strain diagrams of reinforced concrete specimens in tension resulting from the experiment and from the theoretical calculation according to the created mathematical model (Fig. 4, Fig. 5, Fig. 6), it was found that, up to 60°C, the values of relative length strain  $\varepsilon_{cN}$  and tensile stress  $\sigma_c$  are almost equal for observed degrees of reinforcement. Above this temperature, there are differences. One of the possible causes of differences might have been the neglect of the short-term concrete thermal creep from the tensile stress caused by thermal shrinkage and different thermal length dilatation of concrete and steel. The mentioned neglect of thermal short-term creep was in accordance with the Slovak standard STN 73 1230.

In work [2] following values of relative length strain caused by short-term thermal creep under the pressure of 5 MPa, namely on specimens of the same composition of concrete mixture and with the same dimensions which were used in our experimental program, are given:  $\varepsilon_{c,cr} = 0,163\text{‰}$  for  $T = 80\text{ °C}$  and  $\varepsilon_{c,cr} = 0,425\text{‰}$  for  $T = 100\text{ °C}$ . It is evident that these values are not negligible also under the short - term influence of temperatures. If we incline to contention of some authors [3], that thermal creep in tension rises initially quicker than the one in pressure, we should rightfully suppose that thermal creep in tension is not negligible under the 24 - hour influence of elevated temperatures, either.

Because there were no conditions, for the experiments of short-term creep in tension to be carried out (laboratory of our faculty is not equipped of necessary technology) we were searching the possibilities of approaching to experimental values of relative length strain  $\varepsilon_{cN}$  and tensile stresses  $\sigma_c$ . For this purpose, we have taken up simplifications as follows: linearity of creep was supposed and creep coefficient  $\phi$  was derived from the relation regarded for the

effective modulus of elasticity  $E_{cef}$  [4] (we supposed that mentioned relation applied for thermal creep in tension within thermal range of 20 – 100 °C).

From the formula for the effective modulus of elasticity, the coefficient of thermal creep is derived:

$$\varphi(T) = \frac{E_c(T) - E_{cef}(T)}{E_{cef}(T)} \quad (8)$$

where:

$\varphi(T)$  coefficient of thermal creep considered time invariant during short-term heating,

$E_c(T)$  elasticity modulus of concrete at given temperature according to (1).

The thermal creep length strain is expressed in form:

$$\varepsilon_{cN,cr} = \varphi(T) \cdot \varepsilon_{cN} \quad (9)$$

For the temperatures of 80 °C and 100 °C, the resulting relative length strain  $\varepsilon_{cNv}$  is obtained by the superposition of relative strains  $\varepsilon_{cN}$  and  $\varepsilon_{cN,cr}$ :

$$\varepsilon_{cNv} = \varepsilon_{cN} + \varepsilon_{cN,cr} \quad (10)$$

The influence of thermal creep on tensile stresses will be taken into consideration in the way that in relation (5), the values of  $E_{cef}(T)$  instead of  $E_c(T)$  will be put at temperatures of 80 °C and 100 °C. Fig. 4, Fig. 5 and Fig. 6 represent stress-strain diagrams of specimens in tension for the observed degrees of reinforcement:

- resulting from experiment,
- resulting from theory (mathematical model) without considering the thermal creep,
- resulting from theory (mathematical model) with considering the thermal creep at the temperatures of 80 °C and 100 °C.

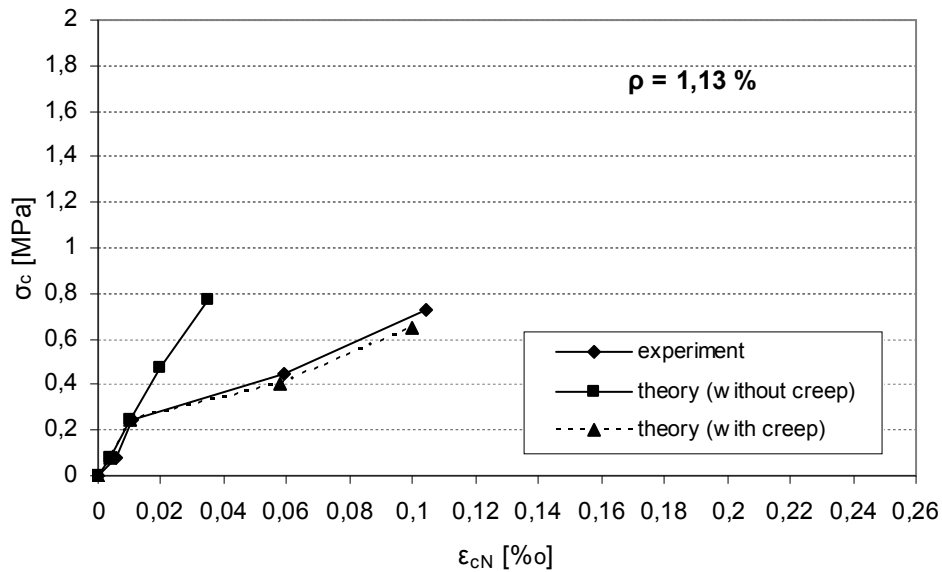


Fig. 4. Stress-strain diagram of reinforced specimens in tension,  $\rho = 1,13\%$

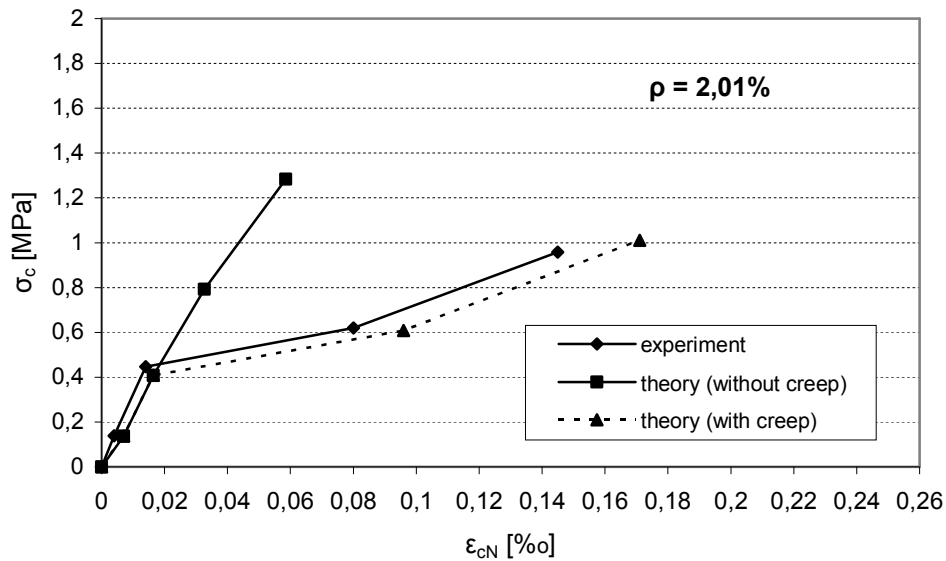


Fig. 5. Stress-strain diagram of reinforced specimens in tension,  $\rho = 2,01\%$

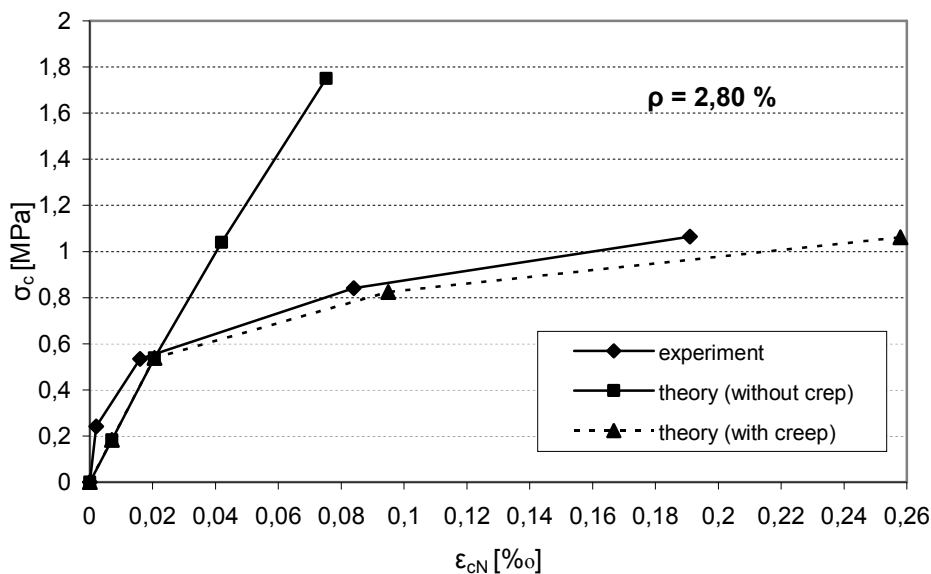


Fig. 6. Stress-strain diagram of reinforced specimens in tension,  $\rho = 2,80\%$

If the influence of thermal creep is considered in the calculation of relative length strain  $\epsilon_{cN}$  and tensile stress  $\sigma_c$  within the thermal range 80-100 °C, there are only small differences between the stress-strain diagrams in tension of steel-reinforced specimens obtained from theoretical calculation and from experiment. The higher difference of strain  $\epsilon_{cN}$  occurs only at the ratio of reinforcement 2,80%, namely at the temperature 100 °C – the value of  $\epsilon_{cN}$  is 24%. Only in the consequence of temperature attack, the tensile stress of 1,06 MPa was reached in the specimens with the highest ratio of reinforcement. This stress is also increased by tensile stresses influenced by shrinkage during curing period. Effective elasticity modulus of concrete, which was used in calculation of creep coefficient in tension  $\varphi(T)$ , probably contained also influence of cracks. Calculated value of  $\varphi(T)$  is not correct for the specimens with the ratio of reinforcement  $\rho = 2,80\%$  at the  $T = 100$  °C.

#### 4. EFFECTIVE MODULUS OF ELASTICITY

Every curve of stress-strain diagrams in tension as mentioned above (Fig. 4 Fig 5, Fig. 6) was plotted for given reinforcement ratio, but for different temperatures. It is possible, however, to use the other method, e.g. to create the stress-strain diagram of reinforced concrete specimens at given temperature. The loading regime is ordered by the amount of present reinforcement. The inclination of stress-strain diagram plotted in this way would correspond to the modulus of elasticity. If separate lines of mentioned diagrams are approximated by straight lines, than their inclination will represent the value of elasticity modulus of concrete. With the temperature rising, the inclination of line is decreasing, namely the elasticity modulus is decreasing (Fig. 7). It is evident from the Fig. 7 and Fig. 8, then the inclination of lines of reinforced specimen's stress-strain diagrams in tension, resulting from the experiment, is decreasing more rapidly above 60 °C than the lines of stress-strain diagrams resulting from theoretical calculation. The inclination of stress-strain diagram lines really correspond to the elasticity modulus of concrete in the whole observed temperature range. On the other hand, the decreasing of experimental lines inclination above 60 °C does not conform to real decreasing of elasticity modulus of concrete, but let's say, it is about effective elasticity modulus of concrete which contains thermal shrinkage respective micro- and macrocracks. There are elasticity modulus if values of  $\sigma_c$  and  $\epsilon_{cN}$  resulting from theoretical calculation are put into relation (7), or effective elasticity modulus if values resulting from experiment at the temperatures of 80 and 100 °C are put in mentioned relation (however for values up to 60 °C it is still elasticity modulus).

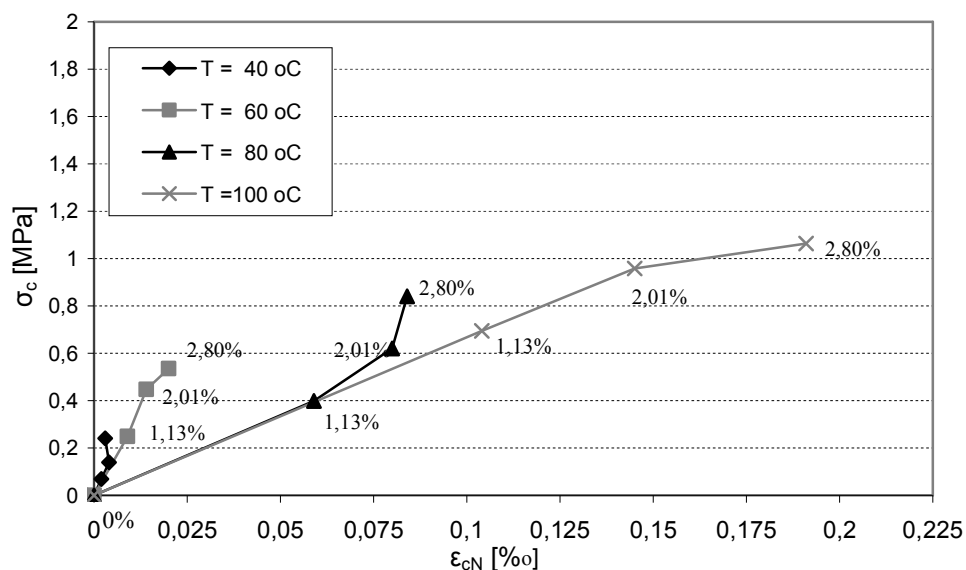


Fig. 7. Stress-strain diagrams of reinforced specimens in tension resulting from experiment,  $T = \text{const.}$

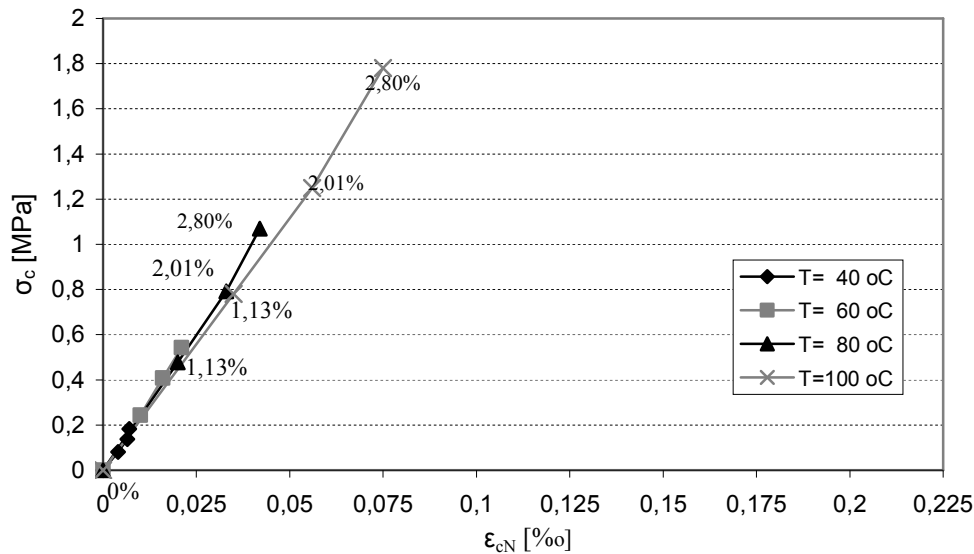


Fig. 8. Stress-strain diagrams of reinforced specimens in tension resulting from theoretical calculation,  $T = \text{const.}$

## 5. CONCLUSIONS

At elevated temperatures up to 100 °C, the thermal load of reinforced concrete members causes stresses and strains in concrete and steel which are consequences of a different thermal dilatation coefficient of both materials, of concrete thermal shrinkage and thermal creep. Thermal load is a non negligible factor for concrete in tension in which it influences the genesis and development of cracks.

Calculations according to the mentioned model with using of derivate input functions fit well the processes running at the heating up to 60°C without taking thermal creep into consideration. Above the temperature of 60°C, it is necessary to consider the influence of the thermal creep, which, as it is shown, is not negligible above the mentioned temperature also during its short-term effect.

From analysis of tensile stresses it follows that their values, mainly when they are added to tensile stresses by influence of shrinkage during the period of curing, can reach such high values at the temperature of 100°C, that in their stress-strain diagram, they are in the area of its peak while cracks can occur.

## REFERENCES

- [1] Šimková S., Priganc S., Fecko L.: Napätost' vystuženého betónového prvku pri zvýšených teplotách. In: Stavební obzor, roč. 14, 2005, č. 9, ISSN 1210 -04027, INDEX 47 755, s. 274 – 278
- [2] Jávor T. a kol.: Diagnostika, bezpečnosť a životnosť jadrových elektrární "kontajnerový projekt" (reg.č.PECO 936 302), Závěrečná správa úlohy so zreteľom na výsledky výskumu za r. 1997
- [3] Designing for Effects of Creep, Shrinkage, Temperature in Concrete Structures, American Concrete Institute, Detroit, Michigan, 1978, Publications SP-27
- [4] STN 73 1230: 1990 Navrhovanie betónových konštrukcií pre zvýšené a vyššie teploty, Vydavateľství ÚNM, Praha



Krystyna WRÓBEL<sup>1</sup>  
Wiesław KUBISZYN<sup>2</sup>

## **INFLUENCE OF CHANGE IN USE CONDITIONS ON AN INDUSTRIAL BUILDING SAFETY**

### **ABSTRACT**

The article describes the state of failure of a building for storing material to produce ceramic building elements. The hall belongs to the biggest brickyard in the Podkarpacie Region. The failure occurred in May 2008. Its direct cause was a sudden increase in the pressure exerted by a dump of clay stored directly at the retaining wall of the building. Due to its excessive height and faulty construction the dump lost stability and overloading the structure of the storage hall and consequently causing excessive deformation and damage to its structural and finishing elements.

The article presents the extent of the damage, the results of the strength – static analysis and the suggested necessary amount of work to restore the building to its former use.

**KEYWORDS:** industrial building, storage hall, reinforced concrete structure, retaining wall, loss of stability, failure.

### **1. INTRODUCTION**

Many industrial buildings built in the 60s and 70s show advanced degradation that has resulted from difficult use conditions, adverse weather, ageing and lack of maintenance and routine repair. Users often do not realize the danger posed by the bad state of the objects. Some additional loads to the building, regardless of their origin, may lead to a sudden state of failure.

The article describes the failure state of a store hall in the biggest brickyard in the Podkarpacie Region. The failure took place in May 2008. A too high and badly built clay dump located too close to the retaining wall lost its stability and, overloading the hall structure caused excessive deformation of the structural and finishing elements of the building.

### **2. DESCRIPTION OF THE STRUCTURE OF THE BUILDING**

It is a single-span, 18m×121.35m hall with dilatations every 30m. The building adjoins the material-pretreatment hall. The structural scheme of the building is shown in Fig. 1.

<sup>1</sup> Assistant Prof. PhD. Eng., Rzeszow University of Technology, Rzeszow, POLAND

<sup>2</sup> Assistant Prof. PhD. Eng., Rzeszow University of Technology, Rzeszow, POLAND

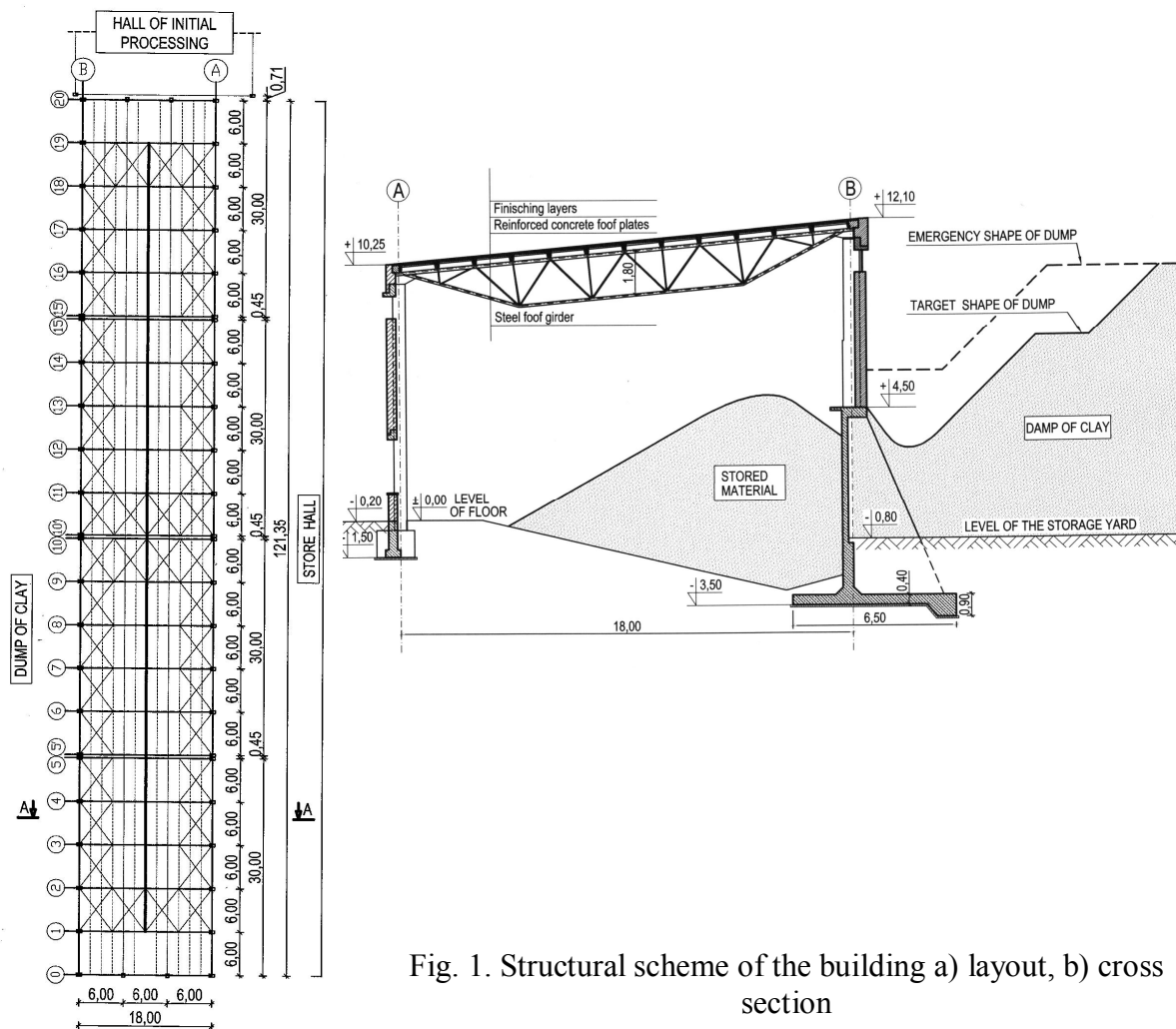


Fig. 1. Structural scheme of the building a) layout, b) cross section

The main transverse systems, spaced every 6m are:

- reinforced concrete bases of foundation in axis A and retaining wall in axis B,
- reinforced concrete, precast columns, in axis A and monolithic columns in axis B,
- steel roof girders with parallel chords sloping towards the level.

The lining of the building consists of: longitudinal walls in axes "A" and "B", made of various materials and capped with precast lintel - cornice elements; gable walls and precast roof plates.

### 3. CHANGES IN BUILDING LOADING AS IMMEDIATE CAUSE OF FAILURE STATE

The change in the shape of the dump directly behind the retaining wall in axis B, compared to its previous (after opening the brickyard) technologically faulty arrangement, brought about loss of stability of the slopes (Fig.2.). As a result, the structure of the building was overloaded in the pit area, almost along the whole length of the wall in axis "B". There followed damage and deformation of the structural and filling elements as well as the fittings causing immediate risk to the workers and the property.

The pressure of the clay on the structure of the building; i.e. retaining wall, main transverse systems, longitudinal brick wall built immediately on the retaining wall and stiff roof folded plate structure did the below described damage.

## 4. DESCRIPTION OF THE DAMAGE

The description and analysis of the state of repair of the structure focus on the damage following the excessive (failure threatening) loading effect of the dump.

### 4.1. Roof structure and covering

Five roof slabs totally slipped off the upper chord of the steel roof girder in axis 1 (Fig. 3) in 0 – 1 area. The girder displaced towards axis 2. Consequently, the roof covering as well as the roof finishing layers got damaged and sank (Fig. 4.). The covering developed folds in the dilatation area in axes 15-15' (Fig.5) and the whole roof plate structure displaced towards axis "A".



Fig. 2. Dump after losing slope stability



Fig. 3. View of roof slabs off the girder in axis 1



Fig. 4. View of roof slabs off the girder in axis 1



Fig. 5. Hollow in roof at slab slip-off

### 4.2. Gable walls

In axis "0" – the wall showed wide and hairline cracks (Fig. 6). Vertical and horizontal cracks appeared in the entrance gate area. (Fig. 7.).

In axis "20" – the ring beam over the roof of the preprocessing hall showed wide and thin cracks and displaced together with the whole roof plate structure towards axis "A" (Figs 8 and 9).

### 4.3. Outer longitudinal walls

In axis B – the longitudinal wall parts in dilatation 15-15' (Figs 10 and 11) shifted relative to each other and numerous cracks, deformations in edge areas as well as brick and

plaster loss could be seen.

In axis "A" – the wall suffered damage, the most extensive in peripheral areas and it displaced. Since there was no access to the wall, its full and accurate assessment was not possible. On the inner side there were cracks in the plane of contact of the stiff roof plate structure and the lintel element.



Fig.6. Separation of gable wall in axis "0" from longitudinal wall in axis "B"



Fig.7. Gable wall, corner A-0 – damage and separated strata along longitudinal wall

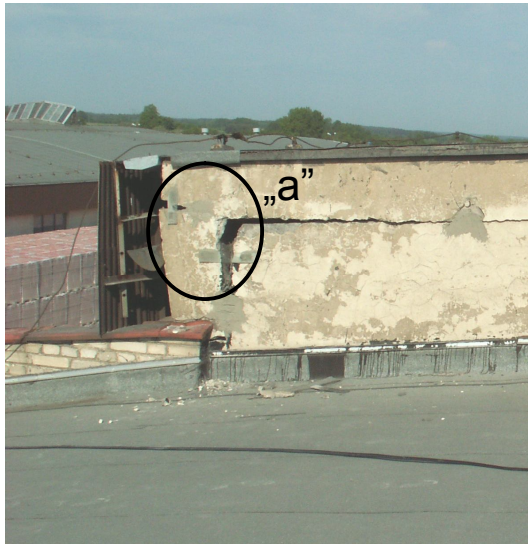


Fig.8. Damage to corner A-20 of gable wall



Fig.9. As in Fig.8. – detail "a"



Fig.10. Wall in axis “B”. Dilatation between axes 15 – 15’- general view



Fig.11. Detail “b” – wall parts displaced relative to each other

#### 4.4. Columns

In axis B most of the columns got damaged (thirteen out of twenty-one): B1, B3, B5, B5’, B8, B9, B10, B11, B15, B15’, B17, B18 and B19. Mostly the heads of the columns were damaged, whereas columns B1, B11 and B15’ suffered more extensive damage (Fig.12 and 13). In axis A column A-0 got damaged due to the roof plate structure displacement.



Fig.12. Head of column B1; axis “2” view



Fig.13. Head of column B5’- axis view



- target situation with considering how the dump shape will determine the way of picking up the material from the pit. The target shape of the dump is shown in Fig. 15.

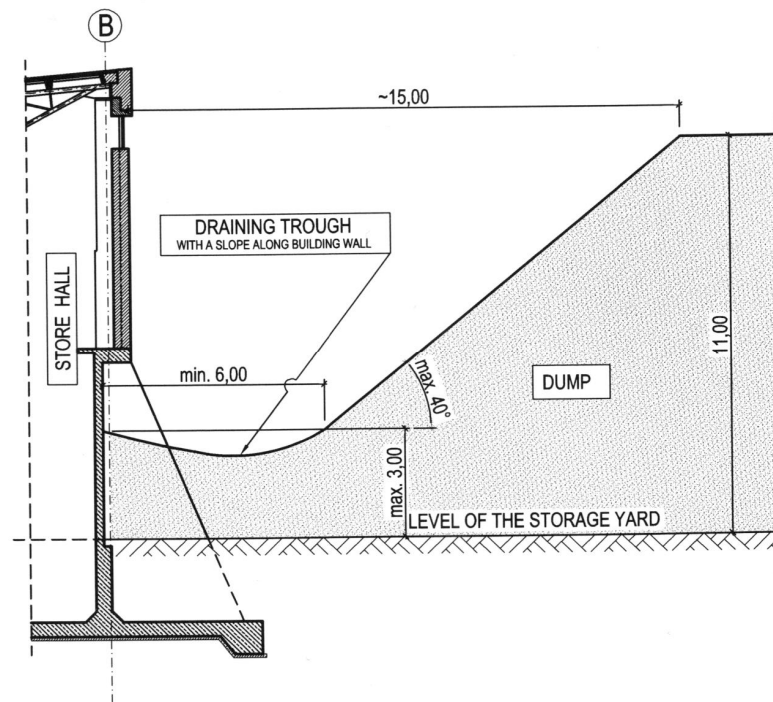


Fig.15. Target shape of the dump

## 6. SUGGESTED METHOD OF RESTORING USABILITY OF THE BUILDING

The necessary steps aimed at restoring the usability of the building were divided into two groups.

Range I – necessary strengthening work recommended and completed immediately after the failure to improve the retaining wall stability and relieve the longitudinal wall in axis B:

- filling all the boxes of the storage hall with material and picking it up over short sections
- reprofiling the shape of the dump following Fig.14., which gave a noticeable result reducing the deformation of the walls and columns.
- monitoring deformations by geodesic methods and by observation of the stuck monitoring seals.
- temporary stabilization of the roof slabs that got displaced – after the building deformations steadied (Fig.16.), which allowed getting rid of the feeling of direct threat to the user.

Range II – necessary work to be completed before the 2008/2009 winter time in order to remove the effects of the failure:

- strengthening the reinforced concrete columns with steel structures appropriately adjusted to the particular kind of the column damage as well as making extra supports for some girders. An example of the column strengthening is shown in Fig.17.
- repair of gable and longitudinal walls in edge areas at gable walls,
- repair of roof supporting structure – the girder in axis “1” (Fig.18.) and the roof slabs in area “0 – 1”,
- repair of the damaged roof covering and the finishing layers of the roof.





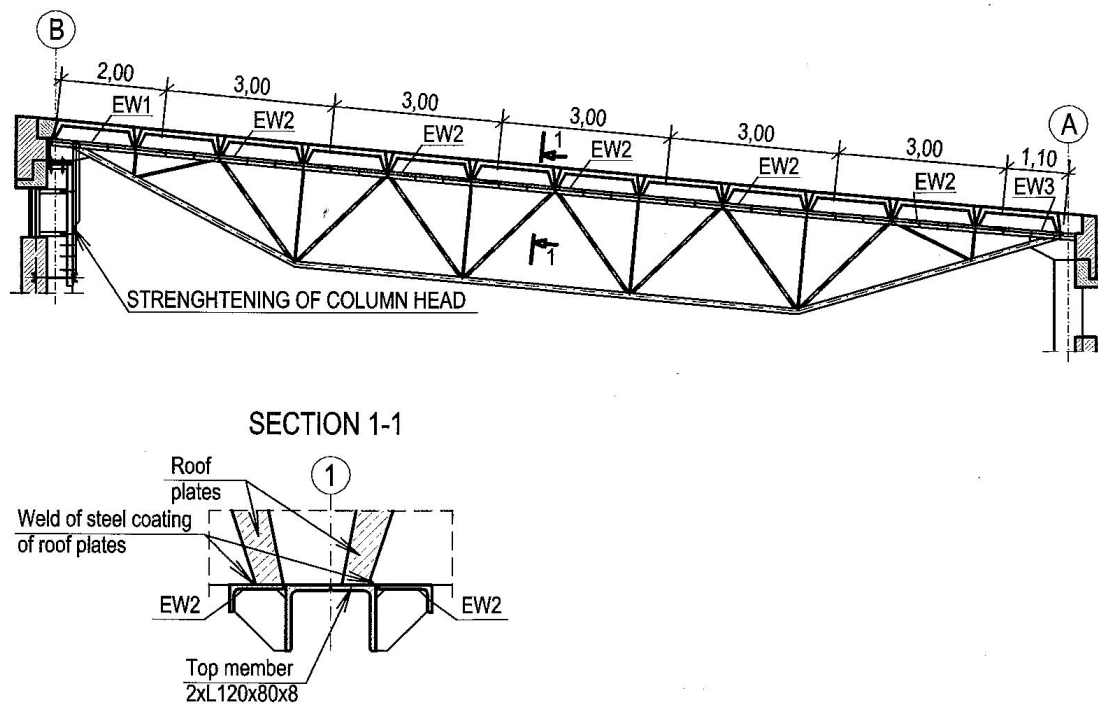


Fig.18. Repair of roof girder.

## 7. CONCLUSIONS

The immediate cause of the building failure was the improper location of the clay dump along the axis B wall of the material storage hall. The surface of the dump top was 2 – 3 meters above the top surface of the retaining wall. Moreover, the top surface of the dump had been shaped improperly – without slopes to enable rain water outflow. The right shape of the slopes protects the dump against getting soaked and unfavorable change of the clay parameters (regarding stability). What is more, the dump had been built of wet clay during rainfall. Technologically, those are impermissible errors which resulted in slope slides and a slump “in all directions”. This created extra, very strong lateral forces affecting the longitudinal building wall in axis B. The structure had not been designed to carry such heavy loads. All that saved the structure was the coincidence of two favorable factors:

- margins of safety following from the Limit State Method and the described spatial work of the store hall supporting structure,
- correct and timely preventive measures (stage I).

The resulting damage results mainly from exceeding the Usability Limit State whose symptoms were excessive horizontal displacements of the damaged main transverse carrying systems.

The group I work being done the building was temporarily passed as fit for use until 2008/2009 winter provided group II work had been completed. However, the completion of the latter has always been put off until a later date. That kind of practice evidences lack of the user’s responsibility for the technical state of the building as well as lack of imagination and a sense of real threat. Regrettably, similar situations are not uncommon.

The building also shows damage and loss due to its 30 year long use in unfavorable conditions specific for the storage of material to produce ceramic building elements (a mixture of clay, sand, sawdust and additives). Thus, another target, stage III., should be a major repair of the structure to eliminate the destruction. Repair and protection of structural elements should be a top priority, something that cannot be put off until tomorrow.

**REFERENCES**

- [1] PN-88/B-01807 Anticorrosive protection in building engineering. Concrete and reinforced concrete structures. Rules of structure diagnosis,
- [2] EN 206-1 Concrete: Specification, performance, production and conformity,
- [3] EN 1992 Eurocode 2: Design of concrete structures: September 2008,
- [4] Wróbel K., Kubiszyn W.: Technical estimation of store hall in the brickyard, Rzeszów, July 2008 r.,
- [5] Wróbel K., Kubiszyn W., Klich R.: Design of repair of store hall in the brickyard after damage. Rzeszów, September 2008.